ABSTRACT

AVCI, HUSEYIN. Unusual Formation of Precursors for Crystallization of Ultra-High Performance Polypropylene and Poly(ethylene terephthalate) Fibers by Utilization of Ecologically Friendly Horizontal Isothermal Bath. (Under the direction of Dr. Richard Kotek.)

The concept of production of new families of high performance polymers and engineering fibers has been reported many times in the technical literature. Such fibers have various end uses in industrial applications and exhibit the enhanced potential in the challenging areas such as ballistic, automotive, aerospace, bullet-proof vests, energy, and electronics. Since the first commercial synthesis of high polymers by Carothers and Hill, filament manufacturers have looked for ways to increase strength and fibers dimensional stability, thermal degradation resistance, etc., even at extreme conditions. Therefore, studies on the fine structure development and its relation with production conditions during the wet, dry, and melt spinning processes have received much attention by researchers to describe in detail the fundamental aspects of the fiber formation.

The production of ultra-high performance fibers at relatively high throughputs by a simple method using fiber-forming polymers via developing an ecologically friendly isothermal bath (ECOB) is the first aim of this study. In this case, polypropylene (PP) was chosen as a semi-crystalline thermoplastic polymer which is extensively used in industry and our daily lives. A unique, highly oriented precursor (f_a = 0.60), and yet noncrystallized, undrawn fibers were obtained with superior mechanical properties.

Fibrillated break, high crystalline and amorphous orientation factors of 0.95 and 0.87, respectively, demonstrate an unusual structural development after only 1.34 draw ratio for

the treated fibers. The second melting peak increased 9 ^{o}C for the treated fibers, which implies a higher level of molecular ordering and thermodynamically more stable phase. After hot drawing and 1.49 draw ratio, the fibers tenacity was close to 12 g/d, the initial modulus was higher than 150 g/d, and the ultimate elongation was at a break of about 20 %.

In the next phase of the research, the effects of horizontal isothermal bath (hIB)11 on the structural development and the production of ultra-high performance as-spun and drawn polypropylene (PP) filaments were investigated. Two different commercial fiber forming PP polymers were used with the melt flow rate of 4.1 and 36 g/10 min. The results demonstrate surprisingly different precursor morphologies for each type of polymer at their optimum process condition. Interestingly, the all treated fibers demonstrated the similar fiber performance having tenacity of about 7 g/d and modulus of 75 g/d for as-spun fibers. After fiber drawing with DR of 1.49, tenacity greater than 12 g/d and modulus higher than 190 g/d were observed. The mean value for the modulus after the drawing process for the high melt flow rate is about 196 g/d. The theoretical modulus of PP is 35–42 GPa[17], 275-330 g/d, which demonstrates the hIB fiber's modulus performance is approaching its theoretical maximum values.

A key aspect of the third section of this study was to obtain ultra-high performance poly(ethylene terephthalate) fibers (PET) by utilizing a low molecular weight polymer via hIB method. The resulted fibers showed the efficient polymer chain orientation and the highly crystalline and ordered structures. The highest tenacity of more than 8 and 10 g/d were observed for the as-spun and drawn fibers, respectively, after only 1.28 draw ratios. The significant effect of the temperature of hIB spinning system on the fibrillar structure and the

precursor's formation of the as-spun fibers was demonstrated. The melting temperature increased 8.51 ^{o}C from 254.05 to 262.56 ^{o}C when untreated and treated fibers are compared.

The most important contribution of this study is that all these various types of polymer precursors for crystallization with different molecular weights after the baths treatments were highly oriented, yet non-crystallized or just showed the initial stages of crystallization. By a subsequent hot drawing process with the low draw ratio (DR< 1.5), the treated fibers showed a well-developed chain orientation and highly crystallized structures with superior mechanical performance.

Unusual Formation of Precursors for Crystallization of Ultra-High Performance Polypropylene and Poly(ethylene terephthalate) Fibers by Utilization of Ecologically Friendly Horizontal Isothermal Bath

by
Huseyin Avci

A dissertation submitted to the Graduate Faculty of
North Carolina State University
in partial fulfillment of the
requirements for the Degree of
Doctor of Philosophy

Fiber and Polymer Science

Raleigh, North Carolina

2013

APPROVED BY:

Dr. Richard Kotek Chair of Advisory Committee	Dr. Samuel M. Hudson Committee Member
Dr. Xiangwu Zhang Committee Member	Dr. Julie Willoughby Committee Member

DEDICATION

My dissertation is dedicated to: My wife Zeynep Yurtseven Avci; my parents Huseyin and Hanim Avci; and my brother Mahmut Avci.

BIOGRAPHY

Huseyin Avci was born and raised in Turkey. He has lived with his parents, Huseyin and Hanim Avci; and five brothers in one of the most beautiful city of the Anatolia, the city of Malatya. In 2005, he received his Bachelor of Science in Textile Engineering from Dokuz Eylul University in Turkey with the second highest grade in the textile department. After graduation he worked as a Textile Engineer in Sanko Textile and a team leader of Gabardine's Product and Development in Calik Denim.

In 2008, he began pursuing a Master of Science degree in Textile Chemistry at North Carolina State University with Turkish Government scholarship. After graduation he married to Dr. Zeynep Hanim and then decided to start his Ph.D. degree in Fiber and Polymer Science at North Carolina State University under the supervision of Dr. Richard Kotek.

ACKNOWLEDGMENTS

I would like to express my sincere gratitude to many individuals at NC State University and elsewhere for their support and help during the long Ph.D. journey.

My special thanks go to my advisor Prof. Richard Kotek for his encouragement, guidance, patient and unconditional continuous support, and the freedom he gave me during my studies. I would like to extend my grateful to my committee's Prof. Samuel Hudson, Prof. Xiangwu Zhang, and Prof. Julie Willoughby for their assistance and enlightening.

I would like to specifically thank Prof. Jon Rust for motivating and encouraging me; and my acknowledgements go to Department of Textile Engineering, Chemistry, and Science and ATEX Technologies for the financial support during this research.

I also sincerely appreciate Brandi Keene, Joshua Yoon, Ramiz Boy, Yidan Zhu, and Chris Kelly for being great colleagues and contributions during my studies.

I would like to thank the Republic of Turkey Ministry of National Education for their financial support during my English educational course in Charlotte, NC and master's degree in NC State University and for providing me with the opportunity to study in the US.

I am grateful and also want to thank laboratory managers, and researchers in the Physical Textile Lab, Analytical Service Lab, and Analytical Instrumentation Facility: Mrs. Birgit Andersen, Mrs. Judy Elson, Mr. Jeff Krause, Mrs. Teresa White, Mr. Chuck Mooney, Mr. Roberto Garcia, Mr. Dzung Nguyen, and Mr. Tri Vu.

Finally and most importantly, I would like to thank to my wife, Zeynep Hanim; and my extended family and friends for their constant support, care and prayers not only during my Ph.D. study and also my whole life.

TABLE OF CONTENTS

LIST OF TABLES ..... **x**

LIST OF FIGURES ..... **xiii**

CHAPTER I **1**

1.1 Introduction 1

1.2 Background 4

1.2.1 Advances in the Production of High Performance Fibers 4

CHAPTER II **9**

2.1 Economic Relevance and Properties of Polypropylene Fibers 9

2.2.1 Molecular Weight (Mw) and Molecular Weight Distribution 14

2.2.2 Initial Morphology and Structure 17

2.3 Effects of Spinning Parameters on High Performance Polypropylene Fibers **20**

2.3.1 Rapid Quenching 20

2.3.2 Effecting of Various Drawing Parameters 23

i.Tensile drawing 24

ii.Zone drawing and zone annealing 30

iii.Constant load oven drawing 34

iv.Die drawing 39

v.Hot nip drawing 43

2.3.3 Gel Spinning Technique 44

2.4 New Generation of Reinforced Polypropylene Composites **50**

2.4.1 Liquid Crystal Polymer (LCPs) **51**

2.4.2 Nanoparticles-Reinforced Systems 58

2.4.2.1 Si-O anions-based nanoparticles 59

2.4.2.2 Titanium-based nanoparticles 64

CHAPTER III 70

3.1 Introduction **70**

3.2 High Tenacity, High Modulus Poly (ethylene terephthalate) (PET) Fibers **72**

3.3 A Recent Developments of New High Performance Poly(ethylene terephthalate) Technology: Liquid Isothermal Bath **75**

CHAPTER IV 87

4.1 Motivation **87**

4.2 Research Goals and Objectives 89

References **91**

CHAPTER V 100

Developing an Ecologically Friendly Isothermal Bath to Obtain a New Class High-Tenacity and High-Modulus Polypropylene Fibers 100

5.1 Abstract **101**

5.2 Introduction **102**

5.3 Experimental **106**

5.3.1 Materials and Production Methodology 106

5.3.2 Experiments and Characterization 108

5.4 Results and Discussion **112**

5.4.1 Tensile Properties of As-Spun and Drawn Filaments 112

5.4.2 SEM Analysis of As-Spun and Drawn Filaments 121
5.4.3 X-Ray Analysis of As-Spun and Drawn Fibers 125
5.4.4 Effect of ECOB on Thermal Properties of As-Spun and Drawn Filaments **135**
5.4.5 Effect of ECOB Temperature and Drawing on Birefringence of Fibers 140
5.5 Conclusions **145**
5.6 References **147**

CHAPTER VI 153

Effect of Molecular Weight and Liquid Type on Precursor Formation for Crystallization and Structural Development of Ultra High Performance Polypropylene Filaments 153

6.1 Abstract **154**
6.2 Introduction **155**
6.3 Experimental **159**
6.3.1 Materials and Production Methodology 159
6.3.2 Experiments and Characterization 161
6.4 Results and Discussion **165**
6.4.1 Mechanical Properties of As-Spun and Drawn Filaments 165
6.4.2 Scanning Electron Microscope Analysis 173
6.4.3 X-Ray Analysis of Untreated and Treated Fibers 179
6.4.4 Thermal Properties of Untreated and Treated Fibers 192
6.4.5 Effect of hIB on Birefringence of Treated Fibers 205
6.5 Conclusions **213**
6.6 References **216**

CHAPTER VII **222**

An Unusual Structure Development for High Performance Poly(ethylene terephthalate) Fibers using A Low Molecular Weight Polymer: Developing a Rare Formation of Precursor for Crystallization **222**

7.1 Abstract **223**

7.2 Introduction **224**

7.3 Experimental **229**

7.3.1 Materials and Production Methodology 229

7.3.2 Experiments and Characterization **231**

7.4 Results and Discussion **234**

7.4.1 Mechanical Properties of the PET Fibers Spun with and without hIB 234

7.4.2 Scanning Electron Microscopic Analysis 242

7.4.3 Wide Angle X-Ray Data Analysis 253

7.4.4 Differential Scanning Calorimetry Data Analysis 261

7.4.5 Birefringence and Density Data Analysis 269

7.5 Conclusions **279**

7.6 References **282**

LIST OF TABLES

Table 1. 1 Properties and applications of high-performance fibers[2]. 4

Table 2. 1 Physical properties of polypropylene filaments drawn in an oven at 130–135 ^{o}C[36]… 21
Table 2. 2 Tensile data of smectic fibrillar structure[38]. 22
Table 2. 3 Summary of optimum mechanical properties[41] 25
Table 2. 4 Tensile properties of original fiber, zone-drawn fibers, and zone-annealed fibers[46]. 32
Table 2. 5 Birefringence (Δt), orientation factors of crystallites and amorphous chains (f_c and f_a), and crystallinity (X_c) of original fiber, zone-drawn fibers, and zone-annealed fibers[46].... 33
Table 2. 6 Mechanical properties of PP fibers with different draw ratios in an oven at 130-135 ^{o}C[36]. 36
Table 2. 7 Physical properties of polypropylene filaments under different quenched conditions[36]. 38
Table 2. 8 Mechanical properties of Dyneema SK60, SK65, SK75, SK76[54]. 45

Table 3. 1 Properties and application of polyester fibers at 21 ^{o}C and 65 % relative humidity[69]. 71
Table 3. 2 Mechanical properties of fibers produced by the LIB method[10]. 79
Table 3. 3 Mechanical properties of PEN fibers spun with and without hIB at 4000 m/min[11]… 84

Table 5. 1 Technical data for Exxon and Total chip with their respective fibers[36, 37]..... 112
Table 5. 2 Spinning conditions of polypropylene fibers spun with/without ECOB. 113
Table 5. 3 Mechanical properties of polypropylene fibers spun with ECOB at 50 ^{o}C. 115
Table 5. 4 Mechanical properties of drawn PP fibers spun with and without ECOB at 150 ^{o}C draw temperature with 1.34 DR. 120

Table 5. 5 Degree of crystallinity, crystalline and amorphous orientation factor, and crystalline dimensions of PP as-spun fibers with and without ECOB. 129
Table 5. 6 Degree of crystallinity, crystalline and amorphous orientation factor, and crystalline dimensions of drawn PP spun fibers with and without ECOB under various draw ratios. 134
Table 5. 7 Thermal properties of polypropylene as-spun and drawn fibers with and without ECOB. 139

Table 6. 1 Mechanical properties of PP undrawn fibers spun with and without hIB. 166
Table 6. 2 Mechanical properties of draw PP fibers spun with and without hIB at different draw temperatures and ratios. 169
Table 6. 3 Spinning conditions of different molecular weight polypropylene fibers spun with and without hIB and ECOB. 180
Table 6. 4 Degree of crystallinity, crystalline and amorphous orientation factor, and crystalline dimensions of lower and higher molecular weight PP as-spun fibers with and without hIB. 186
Table 6. 5 Degree of crystallinity, crystalline and amorphous orientation factor, and crystalline dimensions of lower and higher molecular weight PP drawn fibers with and without hIB at 1.49 draw ratios. 191
Table 6. 6 Thermal properties of polypropylene (PP3155) as-spun and drawn fibers with and without hIB at various draw ratios. 196
Table 6. 7 Thermal properties of polypropylene (PP 3462) as-spun and drawn fibers with and without hIB at various draw ratios. 202

Table 7. 1 Spinning conditions of PET fibers spun with and without hIB. 235
Table 7. 2 Mechanical properties of PET as-spun fibers spun with and without hIB. 237
Table 7. 3 Fibril diameters for control and hIB treated fibers. 252
Table 7. 4 Degree of crystallinity and crystalline dimensions of PET as-spun fibers under various hIB temperatures. 257

Table 7. 5 Degree of crystallinity and crystalline dimensions of drawn PET spun fibers under various hIB temperatures. 260
Table 7. 6 Thermal properties of PET as-spun fibers spun with and without LIB*. 263
Table 7. 7 Thermal properties of drawn PET fibers spun with and without hIB*. 267
Table 7. 8 Thermal properties of as-spun and drawn PET fibers spun with hIB at 140 ^{o}C*….. 268
Table 7. 9 Volume fraction crystallinity of untreated and treated fibers by hIB before and after drawing process (draw ratio = 1.279). 278

LIST OF FIGURES

Figure 1. 1 Comparison of the theoretical crystalline lattice moduli of polymers with their maximum reported experimental fiber moduli[18] 2
Figure 1. 2 Chemical structure of high performance organic fibers. 6
Figure 1. 3 The step change in strength and stiffness from first generation to second generation manufactured fibers[1]. 7

Figure 2. 1 X-ray diffraction diagrams of isotactic polypropylene crystalline forms[16]. 12
Figure 2. 2 Effect of resin characteristics on the tensile strength of filaments spun at 210 °C[29] 16
Figure 2. 3 Elastic modulus vs. draw ratio as a function of draw temperature[41]. 25
Figure 2. 4 Tensile strength vs. draw ratio as a function of draw temperature[41]. 26
Figure 2. 5 Proposed morphology of natural drawn filament[41]. 27
Figure 2. 6 Proposed morphology of superdrawn filament illustrating concept of continuous crystal matrix[41] 28
Figure 2. 7 The change in structure during zone-drawing and zone-annealing[17]. 31
Figure 2. 8 Scheme of apparatus used for continuous vibrating zone-drawing (CVZD)[47].... 34
Figure 2. 9 A Schematic representative of melt spinning process of making high strength polypropylene fibers[48] 37
Figure 2. 10 Various types of solid phase deformation techniques[49] 40
Figure 2. 11 A Small representation of die drawing[17, 49]. 42
Figure 2. 12 A Schematic representation of the not nip devives[52] 43
Figure 2. 13 Stress–strain curves for gel spun-drawn polyethylene fibers. Draw ratios: (A):3, (B): 15, (C): 32[53]. 47
Figure 2. 14 Common additive types and geometries with their respective surface area-to-volume ratios[63]. 51
Figure 2. 15 Comparison of molecular chain structure of conventional polyester and liquid crystal polymer fibers[1]. 53

Figure 2. 16 Tensile strength vs. draw ratio of the blends of (a) highly, and (b) low viscous grade PP blended with different volume ratio of TLCP[58] 55
Figure 2. 17 Melting, first (o) and second (●) DSC scan, and cystallization (□) heats of PP vs. TLCP weight content[59]. 57
Figure 2. 18 SEM images of polypropylene (a, b), polypropylene with silica nanoparticles (c, d), and polypropylene with colloidal silica (e, f)[64]. 61
Figure 2. 19 A Schematic diagram of the pre-drawing method[65]. 62
Figure 2. 20 A Schematic representation of cross-sections of (a) polymer matrix with grafted nanoparticles before and after drawing, and (b) polymer matrix with untreated nanoparticles before and after drawing[65]. 64
Figure 2. 21 Comparison of tensile strength and elongation at break of polypropylene incorporated with TiO_2 vs. weight percent of TiO_2 with and without radiation treatment[66].. 67
Figure 2. 22 Photographs and SEM images of neat PP {colorless, (a)} fiber, and PP/TiO_2 {white (b)} nanocomposite fiber[61] 69

Figure 3. 1 Molecular structures of PET and PEN. 74
Figure 3. 2 Melt spinning of ultra-high oriented crystalline polyester filaments[9]. 76
Figure 3. 3 Schematic diagram of melt spinning via liquid isothermal bath at different LIB positions[10, 71]. 77
Figure 3. 4 (a) Volume fraction crystallinity, and (b) birefringence for as-spun and annealed PET filaments produced with and without LIB at different positions[71]. 81
Figure 3. 5 Schematic comparison of traditional spin-draw and hIB processes. 82
Figure 3. 6 SEM images of PEN fibers spun with hIB spinning system (a) undrawn zone, (b) transit zone between undrawn and drawn, and (c) drawn zone[11]. 85

Figure 5. 1 Melt spinning process with ECOB spinning system[33]. 107
Figure 5. 2 Effect of bath temperature on tenacity values of drawn fibers made ECOB spinning system with comparison of traditional spinning process under the same distance, 170 cm, between the spinneret and ECOB bath. 118
Figure 5. 3 SEM images of PP fibers spun with ECOB spinning system. 122
Figure 5. 4 SEM images of cross-section of drawn PP fibers..... 124
Figure 5. 5 Equatorial X-ray diffraction profiles of PP as-spun fibers spun with ECOB (ECOB1) and without ECOB (ECOB0). 126
Figure 5. 6 Azimuthal X-ray diffraction profiles of (110) planes of PP as-spun fibers spun with ECOB (ECOB1) and without ECOB (ECOB0). 127
Figure 5. 7 Equatorial X-ray diffraction profiles of drawn PP fibers spun with ECOB at the temperature of 50 ^{o}C..... 130
Figure 5. 8 Equatorial X-ray diffraction profiles of drawn PP fibers spun without ECOB at the temperature of 50 ^{o}C. 131
Figure 5. 9 Azimuthal X-ray diffraction profiles of (040) planes of drawn PP fibers spun with ECOB (ECOB1) and without ECOB (ECOB0). (Draw ratio = 1.487). 133
Figure 5. 10 DSC curves of polypropylene fibers spun without ECOB under various draw ratios..... 136
Figure 5. 11 DSC curves of polypropylene fibers spun with ECOB under various draw ratios..... 138
Figure 5. 12 The relation between birefringence of treated and untreated *i*-PP fibers at various ECOB temperatures..... 141
Figure 5. 13 The relation between birefringence and tenacity of treated and untreated *i*-PP fibers at various ECOB temperatures for undrawn and drawn fibers (Draw Ratio = 1.340). 142
Figure 5. 14 Microscope images of (a) untreated; and (b) treated fibers after drawing process (draw ratio = 1.487)..... 144

Figure 6. 1 Melt spinning process with ECOB spinning system[12]. 160
Figure 6. 2 SEM images of undrawn and drawn PP fibers (PP3155) spun with hIB (DR = 1.34). 174
Figure 6. 3 SEM images of cross section of undrawn and drawn PP fibers (PP3155) spun with hIB (DR = 1.34). 176
Figure 6. 4 SEM images of cross section of drawn PP fibers (PP 3462) spun with and without hIB (DR = 1.34). 178
Figure 6. 5 Equatorial X-ray diffraction profiles of PP as-spun fibers spun with and without hIB and ECOB by using different molecular weight polymers. 183
Figure 6. 6 Azimuthal X-ray diffraction profiles of undrawn lower (PP3155) and higher (PP 3462) molecular weight polypropylene fibers spun with and without hIB. 185
Figure 6. 7 Azimuthal X-ray diffraction profiles of drawn lower (PP3155) and higher (PP 3462) molecular weight polypropylene fibers spun with hIB at different draw ratios. 190
Figure 6. 8 DSC curves of polypropylene (PP3155) fibers spun without hIB at various draw ratios at the drawing temperature of 120 ^{o}C. 193
Figure 6. 9 DSC curves of polypropylene (PP3155) fibers spun with hIB at various draw ratios at the drawing temperature of 120 ^{o}C. 194
Figure 6. 10 DSC curves of polypropylene (PP 3462) fibers spun without hIB at various draw ratios at the drawing temperature of 120 ^{o}C. 197
Figure 6. 11 DSC curves of polypropylene (PP 3462) fibers spun with hIB at various draw ratios at the drawing temperature of 120 ^{o}C. 199
Figure 6. 12 The effect of liquid type and molecular weight of polypropylene on the DSC curves of the treated fibers after drawing at 1.49 draw ratios. 204
Figure 6. 13 The relation between birefringence of untreated and treated with hIB of *i*-PP fibers by using lower (PP3155) and higher (PP 3462) molecular weight polymers (draw ratio = 1.34). 208
Figure 6. 14 The relation between birefringence and tenacity of untreated and treated with hIB of *i*-PP fibers by using lower (PP3155) and higher (PP 3462) molecular weight polymers (draw ratio = 1.34). 210

Figure 6. 15 Microscope images of untreated, and treated fibers by using higher (PP 3462) and lower (PP3155) molecular weight polymer after the drawing of 1.49 draw ratios. 212

Figure 7. 1 Melt spinning process with hIB spinning system[28]. 230
Figure 7. 2 Comparison of the strength of drawn fibers at 1.279 DR with the drawing temperature of 220 ^{o}C at (a) 90, (b) 120 and (c) 150 cm production distance..... 239
Figure 7. 3 Low and high (letter with apostrophe) magnification of SEM images for PET as-spun fibers treated with hIB at (a) 60, (b) 100, (c) 125, and (d) 140 ^{o}C liquid temperatures….. 243
Figure 7. 4 SEM images of drawn PET fibers spun with hIB at the temperature of 125 ^{o}C….. 245
Figure 7. 5 SEM images of PET (0.97 dL/g) fibers spun with hIB for undrawn (left), and outside drawn zone (right) fibers. 246
Figure 7. 6 SEM Images of cross section of undrawn PET fibers spun with hIB spinning system at different liquid temperatures. 248
Figure 7. 7 SEM Images of cross section of drawn PET fibers spun with hIB spinning system at different liquid temperatures with control sample. 250
Figure 7. 8 Equatorial X-ray diffraction profiles of PET as-spun fibers spun without hIB spinning system. 254
Figure 7. 9 Equatorial X-ray diffraction profiles of PET as-spun fibers spun with hIB spinning system. 256
Figure 7. 10 Equatorial X-ray diffraction profiles of drawn PET fibers (a) spun without hIB, and (b) with hIB. 258
Figure 7. 11 DSC curves of PET as-spun fibers spun with and without hIB under different liquid temperatures..... 262
Figure 7. 12 DSC curves of drawn PET fibers spun (a) with and without hIB under different liquid temperatures, and (b) PET4 as-spun and drawn fibers spun with hIB at 140 ^{o}C at different production distance. 265

Figure 7. 13 The relation between birefringence of treated and untreated PET fibers at various hIB temperatures for undrawn and drawn fibers..... 270
Figure 7. 14 The relation between birefringence and tenacity of treated and untreated PET fibers at various hIB temperatures for undrawn and drawn fibers (draw ratio = 1.279) (Exponential (undrawn) $R^2 = 0.9703$, and Polynomial (drawn) $R^2 = 0.9998$). 272
Figure 7. 15 Fibers density of untreated and treated fibers by hIB before and after drawing process (draw ratio = 1.279). 275

CHAPTER I

1.1 Introduction

Improving properties of polymer fibers, for example mechanical, dimensional stability, thermal degradation, and other properties, and understanding a recent theoretical investigations on the solid mechanism of single crystal growth during the fiber formation leads to obtain fiber products with the unusual characteristics. Therefore, high performance fibers based materials are important industrial products and widely used in due to their versatility and outstanding tensile properties. They have found extensive use as fiber reinforcement and can be utilized in cords, ropes, fabrics, electronic packaging, sports equipment and fiber optics [1, 2].

Polypropylene fibers for the general textile uses have tenacities in the range of 4.5-6.0 g/den; however, the fibers with tenacity up to 9.0 g/den are produced with complex production drawing lines.

It is well know that the highest tenacity and elastic moduli reported for linear polymers are generally much lower than their theoretical values. Usually, crystal moduli are determined in the direction, parallel to the polymer chain axis via X-ray diffraction. The theoretical modulus of polypropylene is 35–42 GPa, 275-330 g/d, when measured by the X-ray technique with the theoretical strength of 3.9 GPa, 30 g/d, which is much higher as compared

to the maximum tenacity and modulus achieved through any of the existing research laboratory and industrial process[17]. However there are some exceptions for the tensile moduli of highly drawn fibers produced from ultrahigh molecular weight polyethylene (UHMW PE). Kevlar also showed the moduli close to the theoretical values[18]. Figure 1.1 demonstrates that most polymers, including those with rigid backbone chains, have much lower tensile moduli of those crystalline lattices in the chain direction.

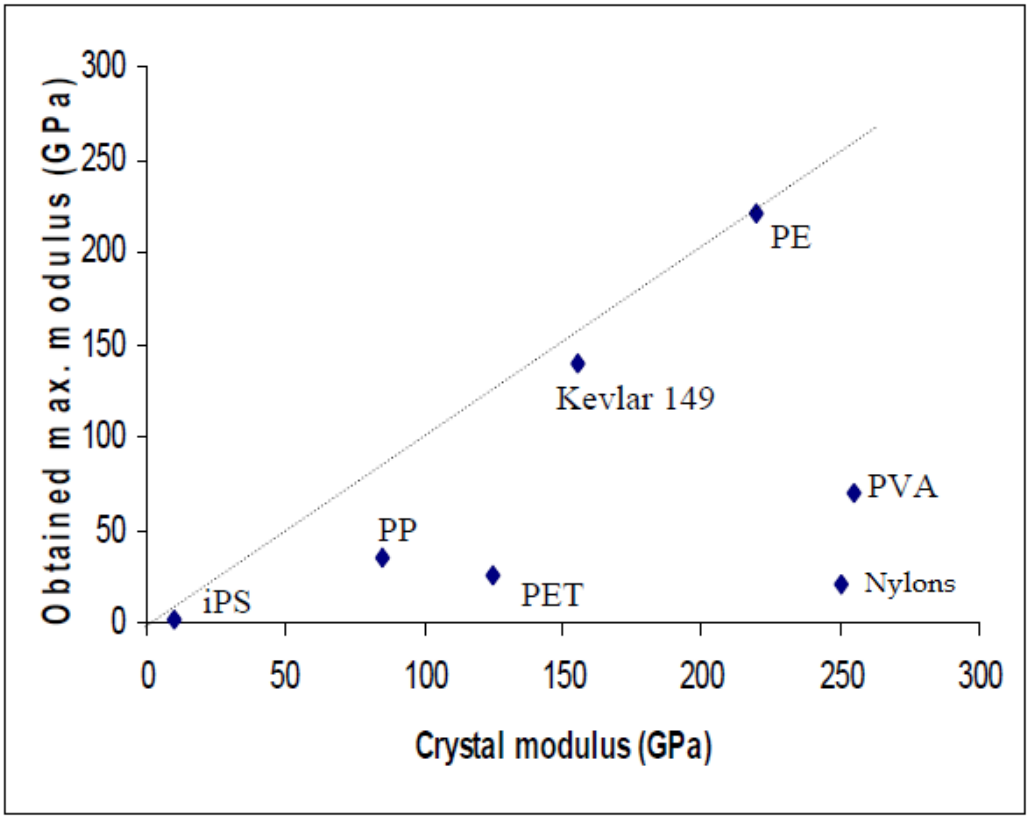

Figure 1. 1 Comparison of the theoretical crystalline lattice moduli of polymers with their maximum reported experimental fiber moduli[18].

After the discovery of the Ziegler-Natta catalysts in the 1950s, the linear polyethylene and stereoregular polypropylene became the important industrial polymers. Indeed, high-modulus and high-tenacity PP fibers are inert, hydrophobic and exhibit superior mechanical properties. However, a number of technical problems have to be solved to achieve such properties. Therefore, the first objective of our study is to develop an environmentally friendly method. Our research work has a great potential to produce a new class of high-tenacity and high-modulus polyolefin monofilament fiber, which has the highest tenacity and modulus values in the world, with the unique structural and morphological characteristics imparted by environmentally friendly technique (ECOB)'s novel fiber forming process.

Polyester fibers based on poly(ethylene terephthalate) (PET) is the largest volume synthetic fiber produced worldwide. It is well known that high molecular weight is essential for high-tenacity and high-modulus PET fibers. Another purpose of the present research is to develop and describe the production of high performance PET fibers from a low molecular weight PET with intrinsic viscosity (IV) of 0.65 dL/g. This production technology, a novel melt-spinning process modified with the liquid isothermal bath (hIB), was firstly developed by Dr. Cuculo and then modified from the vertical to the horizontal bath design[9,10,11]. In this case, the fibers were directed into a bath which was at least 30 ^{o}C above the glass transition temperature.

1.2 Background

1.2.1 Advances in the Production of High Performance Fibers

High performance fibers have been an important industrial product for many different applications. They have been developed and find extensive use in the markets as reinforcement fibers and also used in cords, ropes, fabrics, electronic packaging, sports equipments and fiber optics[1, 2]. Table 1.1 shows some important high performance fibers and their applications with mechanical properties[2].

Table 1. 1 Properties and applications of high-performance fibers[2].

Fiber	Young's Modulus (GPa)	Tensile Strength (GPa)	Diameter (μm)	Applications
Steel	200	2.8	90–400	Tire cords, piano wire
Ceramic (Al_2O_3-based, SiC-based)	350–380	1.7–5	10–20	Ceramic-matrix composites, high-temperature aerospace applications
Aramid	65–130	2.8–3.4	12	Body armor, bullet-proof vests, tire cords, sporting equipment, polymer-matrix composites
Nylon	6	1	20–40	Tire cords, polymer-matrix composites
Carbon	180–600	2.2–3.8	7–10	Automotive, aerospace, sporting equipment, polymer-matrix composites
Glass (silica-based)	70	1.8–3.4	8–14	Fiber optics, polymer-matrix composites

In the first half of the twentieth century nylon, polyester, acetate, etc. fibers were manufactured with outstanding technical properties and then started to be used widely in automobile tires as reinforcement instead of cotton and rayon[1]. In addition, nylon and polyester fibers have a certain degree of high strength and extension which cause a very high energy to break with good recovery properties. At this point, especially polyester is one of the most attractive candidates for high strength fibers that can be used in the ballistic applications and for making high-performance ropes. Structural perfection, for example straight, well aligned, stable, and densely-packed chains and a combination of extended chains with high crystal orientation cause high modulus and strength[3].

The second generation man-made fibers were produced from rigid and flexible polymers among the last of the twentieth century which show high performance and are named as high-modulus, high-tenacity (HM-HT) fibers with high thermal and chemical resistance[1]. Today, superior strength, stiffness and ballistic performance are defining characteristic of high-performance polymeric fibers. They are mainly divided in four groups[12]:

i. Polyaramids (Kevlar, Twaron, Technora, etc.).
ii. Highly oriented polyethylene (Spectra, Dyneema, etc.).
iii. Polybenzobisoxazole, PBO (Zylon, etc.).
iv. Polypyridobisimidazole, PIPD (M5).

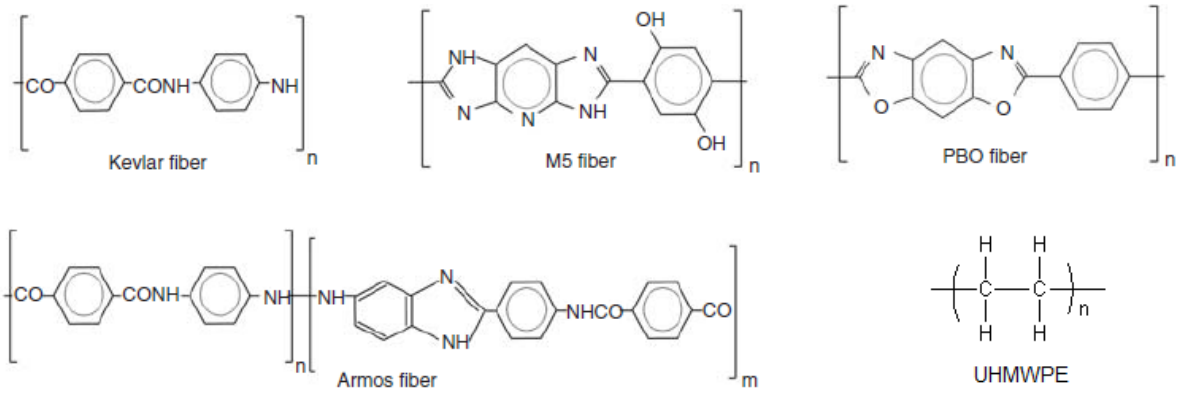

Figure 1. 2 Chemical structure of high performance organic fibers.

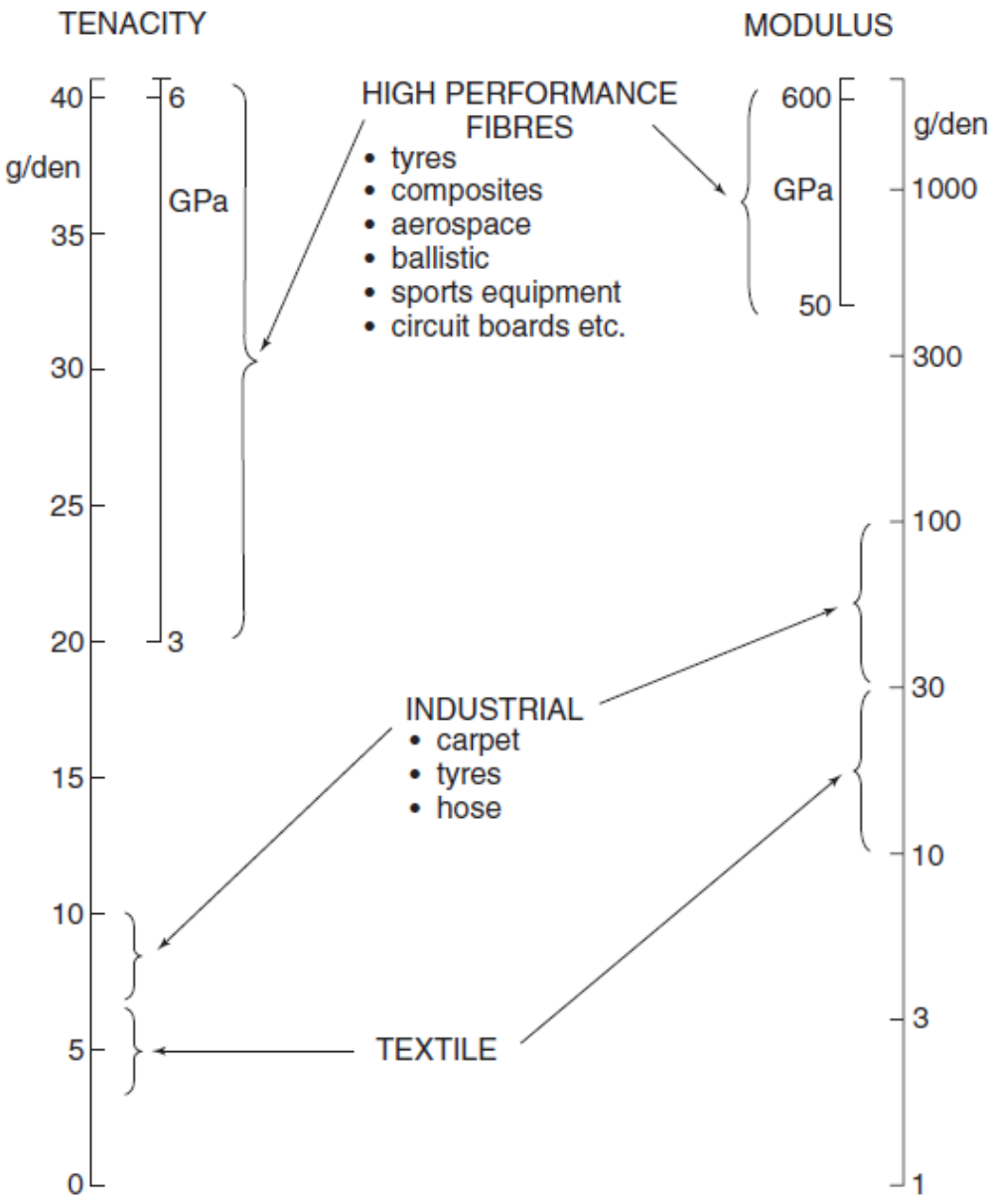

Figure 1. 3 The step change in strength and stiffness from first generation to second generation manufactured fibers[1].

These fibers, in tension, show rate-independent linear elastic materials and they are durable in transverse compression without a significant loss in their tensile load-carrying capacity even if being exposed large plastic deformation[12]. This behavior is a quite different than carbon and glass fibers. Kevlar, M5, and PBO have intrinsically rigid chain polymers, but ultrahigh molecular weight polyethylene has flexible polymer chains.

CHAPTER II

2.1 Economic Relevance and Properties of Polypropylene Fibers

Polypropylene (PP) is one of the most important and widely used thermoplastic polymers and it is extremely versatile as a fiber-forming material. In general, PP fibers and materials have relatively low cost, good mechanical strength, excellent chemical resistance, and reasonable thermal stability. In addition, the physical properties of PP can be tailored to meet the requirements with respect to processing and structure. Hence, a large variety of products, such as ropes, cords, nets, woven bags, tents, nonwoven fabrics, and reinforcing materials for various composites, medical care and building in different colors and with different stability are available today.

The global polyolefin fibers and thread market decreased in 2009 by 4.5%, to 5.72 million tons[24]. The routing of marketplace is changing to the monofilament form, such as ropes, cordage, and outdoor furniture webbing because of their higher strength, mildew resistance, and economics of polypropylene allowed it to replace other fiber products.

Molecular design and the morphological features are two crucial parameters to achieve the desired properties. Depending on the molecular design, which is associated with changing the average length of the molecular chains, can affect regularity of packing, and the chain stiffness. Moreover, the polymeric materials can partially crystallize, and forming a two

phase system where crystals are dispersed in an amorphous matrix. Crystallization and flow-induced orientation are commonly observed during the melt spinning depending on the melt temperature, take-up velocity, molecular weight, molecular weight distribution, and so on[19]. The crystallinity has many influences on mechanical to optical properties. The spun PP fiber is considered to have an amorphous phase and a crystalline phase where the crystals are dispersed in an amorphous matrix. The crystalline phase contains discrete lamellae or crystallites. The final behaviors of crystallization are affected by temperature and flow history. The crystallization rate and crystalline morphology can be dramatically changed by the flow. The spherulites are replaced by shish-kebabs when strongly exposed by flows, an extended chain fibrillar core, shish, with composite crystallites occurred instead of point nucleation which dressed with disk-like folded chain lamellae to the so-called kebabs [23].

According to the early concept of crystalline polymer morphology, the production of highly oriented materials would appear to be simple, the fringed micelle. On the contrary, nowadays, it has been accepted that polymers normally undergo chain-folding during crystallization, and microfibrils which consist of alternating chain-folded lamellae and amorphous regions that make the conventional fibers[17]. These lamellae are connected in the longitudinal direction by tie molecules that affect the strength and modulus. As has already been discussed, fibers usually have modulus and strength far below those theoretically predicted because of relatively a low number of tie molecules[17]. The detailed observation of deformation mechanism can give us some ideas about the fine structure of polymer fibers. Hence, measurement of degrees of crystallinity and orientation is the first step of the material

characterization. And it is one of the most important properties in determining the structure of the resulting fibers.

It is known that the linear chains can be highly oriented and yield a higher degree of crystallinity and a unique microstructure. The stereoregular placement of pendant methyl groups in isotactic-PP causes the facile packing and crystallization, however the atactic PP chains with their stereoregular distribution of methyl substituents, cannot pack tightly and crystallize so atactic-PP is an amorphous polymer. In addition, the random alignment and orientation for semicrystalline polymers lead to insufficient and lower strength and modulus values. Numerous studies show that *i*-PP has several polymorphs and it is very sensitive to the conditions of crystallization: the α-crystalline form (monoclinic), the β-crystalline form (hexagonal), (trigonal) or ɣ-phase, and mesomorphic or smectic form of iPP [20, 21, 22]. Figure 2.1 shows the X-ray diffraction diagrams of the various crystalline forms. The α-form *i*-PP has a monoclinic unit cell, and β-form *i*-PP is arranged in a hexagonal unit cell.

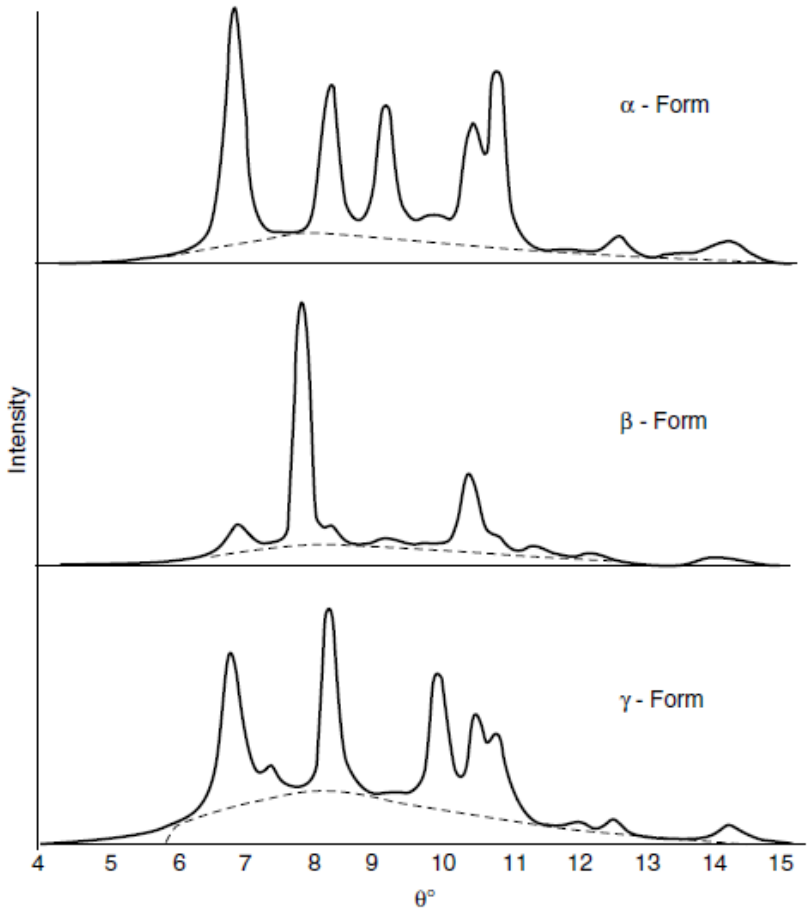

Figure 2. 1 X-ray diffraction diagrams of isotactic-polypropylene crystalline forms[16].

2.2 Relation Between Microstructure and High Performance Polypropylene Fibers

It has been observed that the properties of PP fibers are affected by various factors that come from polymer properties itself and external process conditions. Polymer properties include molecular weight, polydispersity, and the internal structure. Process conditions are: type of extrusion, extrusion temperature, extrusion velocity, airflow rate, take-up velocity, and temperature. Lewin[16] has divided these external methods in order to manufacture high performance fibers:

i. Very high degree and rapid quenching of extruding fiber and then drawing at low rates and high draw ratios;
ii. Slow, two-stage drawing of a conventionally produced fiber under carefully controlled temperatures;
iii. Hydrostatic extrusion;
iv. Inducing fibrillar crystal growth from dilute solutions;
v. Spinning a fiber in the form of a gel and then following by hot-thawing.

2.2.1 Molecular Weight (Mw) and Molecular Weight Distribution

Some researchers have studied the effect of molecular weight on the rheological and mechanical properties of PP fibers. It has been observed that a medium molecular weight polymer with a narrow molecular weight distribution was allowed to obtain high performance PP fibers[17]. And, till to a certain point of the molecular weight, the drawability increases with increasing molecular weight. In general, high molecular weight for the polymers is a crucial parameter to obtain high elongational viscosity and degree of crystallinity with high strength and modulus[17]. Kamezawa et al.[28] have concluded that the modulus also depends on molecular weight especially in the range of higher draw ratios. The formation and growth of the microcracks depends on the ends of extended chains, which occurred by unfolding polymer chains from the crystallites during drawing processes. Therefore, using a higher molecular weight, unfolding of chains during drawing becomes more difficult without formation of microcracks.

Isotactic polypropylene (*i*-PP) is one of the most important polymers which is extensively used in industries to manufacture bottles, films, fibers, and so forth. The mechanical properties and morphology of the product are strongly affected by its molecular weight and molecular weight distribution[17, 25-26]. The molecular weight distribution has influence on fiber properties and its spinning and drawing stages. The higher level of orientation and crystallinity for the fibers can be achieved from broad

molecular weight distributions than narrow distribution at the low take-up speed because of strain-induced crystallization which is mainly occurred by the high molecular weight tail[27]. However, the higher orientation levels are produced from narrow molecular weight distribution at high take-up speed[25]. A narrow molecular weight distribution is used to obtain higher tensile strength and a lower elongation at break. Moreover, Misra et al.[29] have studied and showed that increasing the weight-average molecular weight, decrease in melt flow ratio (MFR), leads to a higher crystallinity, birefringence, tensile strength, and tensile modulus. They concluded that the polymers with a higher polydispersity should be used to produce a higher crystallinity, tensile modulus, and elongation at break with lower birefringence and tensile strength. The higher crystallinity, tensile modulus, and lower birefringence are affected by elongational viscosity of the resin. In addition, in this case, stress-induced crystallization occurs in the spinline because high molecular weight tails in the distribution.

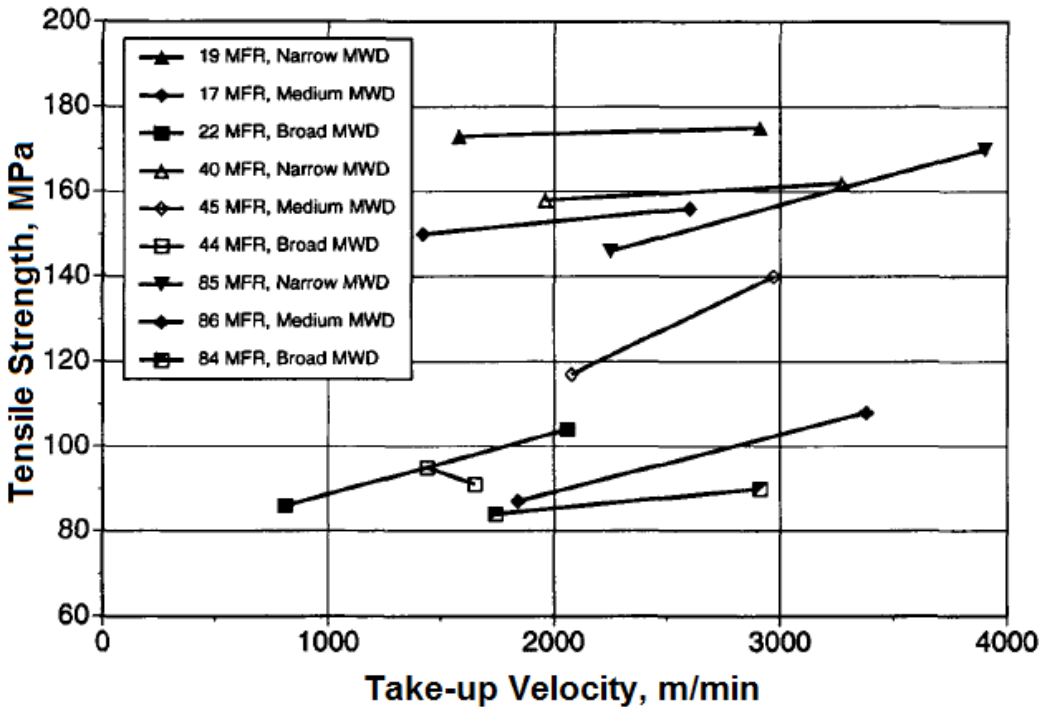

Figure 2. 2 Effect of resin characteristics on the tensile strength of filaments spun at 210 °C[29].

The gel spinning technique for the production of high-tenacity, high-modulus polypropylene fibers is another pathway to show importance of the molecular weight. Kavesh et al.[31] have produced stretched polypropylene fibers at between 8-13 g/d for tenacity with tensile modulus of between 160 to 220 g/d. The detailed information and process conditions are given in the next sections.

The difference of melt spinning behavior between metallocene-catalyzed isotactic polypropylene (m*i*-PP) and Ziegler–Natta-catalyzed isotactic polypropylene (Zn*i*-PP) have been investigated by Bond and Spruiell[30]. They have demonstrated that the narrow molecular weight distribution of metallocene resins was the primary factor that produced differences in the structure and properties of fibers spun from these polymer chips when compared with Ziegler–Natta catalyzed resins of similar weight average molecular weight or melt flow ratio (MFR). Although all the m*i*-PP resins had a very narrow molecular weight distribution, their relative differences are coming from a significant difference in their melt spinning behaviors.

2.2.2 Initial Morphology and Structure

The mechanical and morphological properties of PP fibers strongly depend on arrangement of the supramolecular structural elements such as smectic structure (paracrystallite), and the monoclinic form. Isotactic polypropylene is semicrystalline polymer that contains monoclinic α-form crystallites, β-crystalline form (hexagonal), (trigonal) or ϒ-phase, and mesomorphic or smectic meso-phase[32]. The crystallization temperature and the isotacticity are important parameters to form these structures. If the quenching is rapid from the melt to temperatures below the glass transition, a homogeneous perfectly amorphous glass cannot be formed to form ‘smectic’

structure[32]. Furthermore, α-crystallites and smectic mesophase are mainly created, however β-and ɣ-polymorphs are formed as minority components[17, 32]. Wang et al.[33] have pointed out that it is easier to achieve higher draw ratio for materials with paracrystalline structure and low crystallinity than with the monoclinic (α-crystallite) form. On the contrary, transformation from paracrystalline structure to α-monoclinic crystallites leads to a very high degree of modulus, yield stress, and a decrease in the natural draw ratio. Another study of Wang et al.[34] explained the structural analysis of as-spun fibers via WAXD: (i) the paracrystalline structures show a very low orientation with two broad reflections, (ii) the low orientation was also observed for the α-monoclinic structure, (iii) the distinct c+a axis orientation of crystallites and an oriented α-monoclinic structure can be observed. It is also important to consider the combination of these structures in as-spun fibers. The monoclinic structure in the filament needs more energy for deformation than a fiber of smectic structure under room and higher temperatures[17]. It was found that three-dimensional crystallite order with a large number of tie links require much more energy for deformation for monoclinic crystal than less-ordered smectic structure.

Chain entanglements are formed between lamellae in the gel-like spherulites but there are almost no chain connections between spherulites[35]. In gel-spun material, the higher degree of entanglement is one of the reasons to get a very high strength and modulus for undrawn materials. However, they can act like a cross-linking structure at a certain draw ratio, hence the drawability decreases[17]. The difference between

chain entanglement densities can cause to observe different strength and modulus versus draw ratios. At higher chain entanglement density, the drawing stress is affectively transferred to polymer chain throughout the chain entanglement points. Therefore, the higher degree of molecular orientation and the fibrillar crystallization can form by chain extension during the ultra-drawing process for ultra-high molecular-weight polyethylene gel-spun fibers[35].

2.3 Effects of Spinning Parameters on High Performance Polypropylene Fibers

Spinning conditions are the important parameters to be controlled in order to produce high-tenacity, high-modulus polypropylene fibers. Effect of each section in the production line should be well understood because it can cause dramatic change in mechanical and morphological properties.

2.3.1 Rapid Quenching

In the melting spinning, cooling of polymer moving jets can be accomplished by using air or a suitable liquid. Depending on the rate of cooling, the crystallization percentage can be controlled by increasing the cooling rate. Such condition inhibits crystallization of the polymers which gives more drawability for as-spun fibers[17].

Sheehan et al.[36] have produced high-tenacity PP filaments with the melt spinning technique by using highly isotactic polypropylene resin. They concluded that at a given drawn ratio, increasing molecular weight was leading to an increase in tenacity using polymer with the narrow molecular weight distribution. In this case water quench was used to manufacture undrawn filaments with paracrystalline structure which can be drawn easier than fibers having crystalline structure. The lower take-up speed was utilized to get a low orientation to obtain a pseudohexagonal or a smectic

structure instead of the usual monoclinic crystal form, and subsequently very high draw ratios were applied. Table 2.1 shows mechanical properties of some produced fibers.

Table 2. 1 Physical properties of polypropylene filaments drawn in an oven at 130–135 ^{o}C[36].

Draw ratio[a]	Denier	Tenacity (g/den)	Percent elongation	Modulus (g/den)
29	20.6	11.5	23	88
32	19.1	11.5	24	94
33	17.6	12.4	17	106
34	18.1	13.1	18	110

[a]Includes drawdown in spinning of 3X.

Yamada et al.[37] obtained high-modulus PP fibers using forced quenching in a zone drawing type apparatus from isotactic polypropylene. He argued that increasing draw ratio increases the fraction of taut tie molecules that results in an increase in orientation of amorphous chains. Therefore, higher modulus was observed. However, a very high draw ratio may have caused to observe aggregation of so many taut tie molecules in the amorphous region. Moreover, the taut-tie molecules gradually loosened with increasing annealing temperature above 310 K but the fraction of

unloosened taut tie molecules by annealing is larger at higher modulus than the lower modulus for each applied annealing temperature.

In addition, Noether[38] conducted a similar work as Sheehan and Cole[36] that produced a highly oriented smectic structure by applying a water quench and normal quench conditions during spin orientation. They investigated an increase in orientation and crystalline order; and the perfection of the monoclinic structure gradually developed using annealing method at various temperatures with 30 minutes for as-spun fibers. It can be seen in Table 2.2 that there was no any negative effect of annealing for very high performance fibers. The fibers maintained its strength of 5.7 g/d with annealing at 70 ^{o}C even if a very big change in crystallinity and morphology was observed for conventionally produced undrawn polypropylene fibers[16].

Table 2. 2 Tensile data of smectic fibrillar structure[38].

Annealing temperature (°C)	Denier	Tenacity (g/den)	Percent elongation	Modulus (g/den)
70	2.6	5.7	253	44
80	2.6	4.4	220	45
90	2.7	4.0	172	47
100	2.9	3.3	190	47
110	2.8	3.7	172	43
120	2.8	4.4	154	43
130	2.7	5.0	171	39

2.3.2 Effecting of Various Drawing Parameters

As is commonly known, high-tenacity and high-modulus PP fibers can be achieved by drawing processes. The drawing process depends upon polymer molecular weight, molecular weight distribution, initial morphology, drawing temperature and strain rate like take-up speed and draw ratio [17, 39]. It has been reported that sliding and deformation of tie chains occurred with the chains slip through crystals during the drawing of *i*-PP and also the lamellar disintegration is leading activation of constrained amorphous places[39]. Samuels et al.[40] conducted studies to observe a quantitative morphological description the uniaxial deformation of both melt cast sheet and melt spun filament. He concluded the location of the radii where a spherulite deformation occurs depended on the applied load and this deformation is divided in two stages. During the first stage, lamellar slip leading to *c*-axis orientation until obtaining fully oriented structure. Once this point is reached, the additional extension causes a new type of deformation mechanism which called crystal cleavage. At this point any further extension leads separation of lamellae in blocks and the helical chain axis of the noncrystalline molecules become more oriented to evolve into a fibrillar structure[40]. Any more deformation after this point causes to develop flaws and the sample breaks.

To achieve the greatest possible values of the tenacity and elastic modulus, researchers have been working on various deformation methods to increase the

orientation in amorphous regions and crystallinity percentage. Mukhopadhyay et al.[17] divided the drawing technique in five sub-categories:

i. Tensile drawing

In this method the produced filaments and other products are drawn at high temperature with a low strain rate to obtain a very high draw ratio. Taylor and Clark[41] manufactured 'superdrawn' polypropylene filaments in two-step discontinuous process at elevated temperatures. They used polypropylene with averaged molecular weight of 2.77×10^5 with the drawing rates were varied from 10 mm/min to 1 mm/min to obtain very high draw ratios of more than 25x by two-stage tensile drawing. They concluded the optimum draw temperature of 130 ^{o}C at which a linear relationship between the draw ratio and mechanical properties was observed. Table 2.3 shows the summary of optimum mechanical properties of fibers. In addition, Figure 2.3 and 2.4 show the elastic modulus and tensile strength as a function of draw ratio.

Table 2. 3 Summary of optimum mechanical properties[41].

Draw ration	Tensile modulus	Tensile strength	Elongation to break	Knot tenacity	Modulus loss after bend	Tensile strength loss after bend
	22.0 GPa	0.93 GPa		0.13 GPa		
27	$3x10^6$ psi	$1.3x10^5$ psi	7.8 %	$2x10^4$ psi	23 %	14 %
	240 gdtex	10 gdtex		1.4 gdtex		

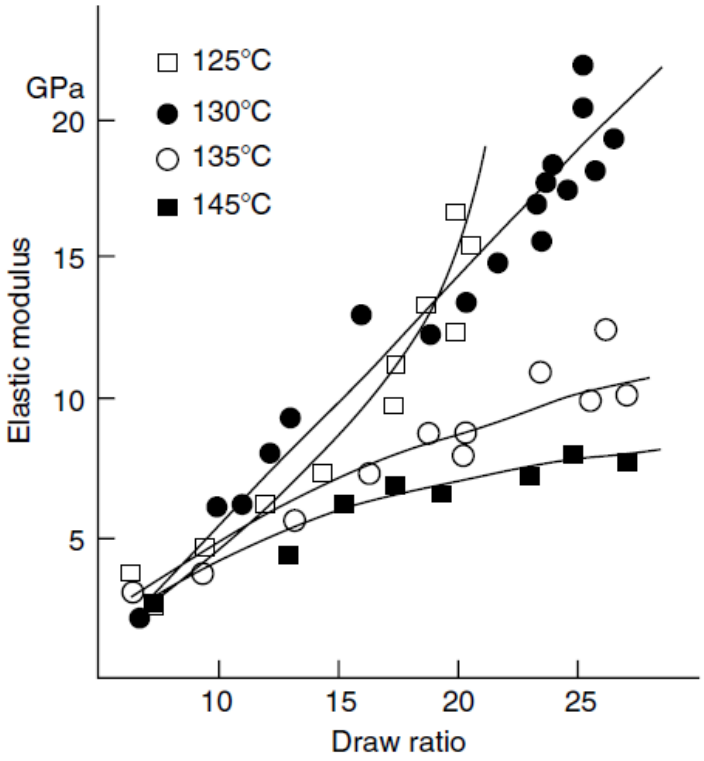

Figure 2. 3 Elastic modulus vs. draw ratio as a function of draw temperature[41].

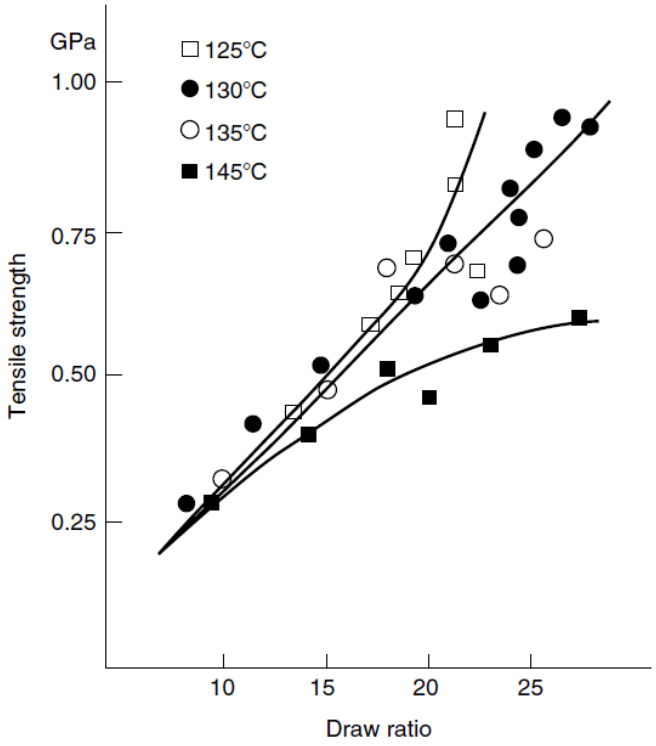

Figure 2. 4 Tensile strength vs. draw ratio as a function of draw temperature[41].

Taylor and Clark[41] mentioned the difference between the morphological changes during conventionally and 'superdrawn' drawn fibers. The undrawn crystalline polymer has folded-chain lamellae that were connected to a small fraction of tie molecules. These lamellae begin the form of folded chain blocks to lead occurrence of the microfibrils during the drawing process which is called the natural draw condition. As illustrated in Figure 2.5, the structure of the fibril is composed of alternating crystal blocks and amorphous layers. In general, the tie molecules which

connect chain-folded blocks in the longitudinal draw direction are mainly responsible the source of tensile strength and modulus[41].

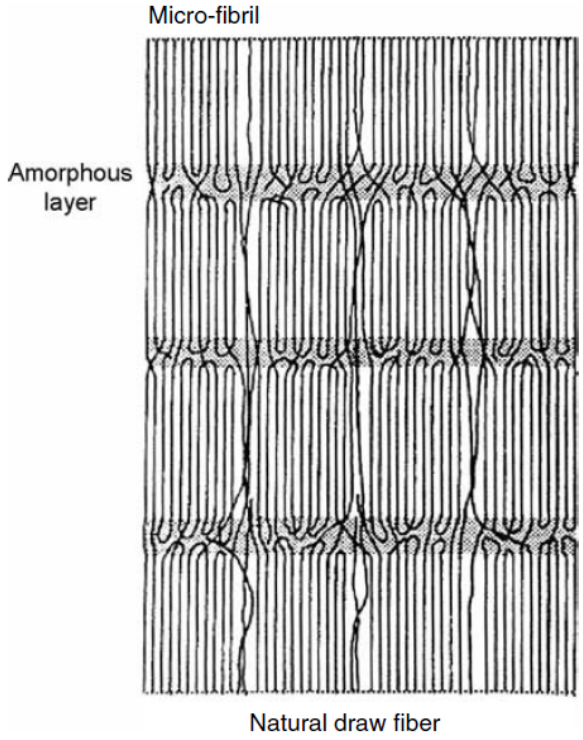

Figure 2. 5 Proposed morphology of natural drawn filament[41].

However, the proposed morphology of the 'superdrawn' fiber was the substantial increase in the number of tie molecules at the optimum temperature of 130 ^{o}C (see

Figure 2.6). Additional tie molecules were formed by unfolding of chains that were important parameters to explain this concept. In addition, sliding displacement of microfibrils is another mechanism to control the fluid flow behavior for drawing ratio[41].

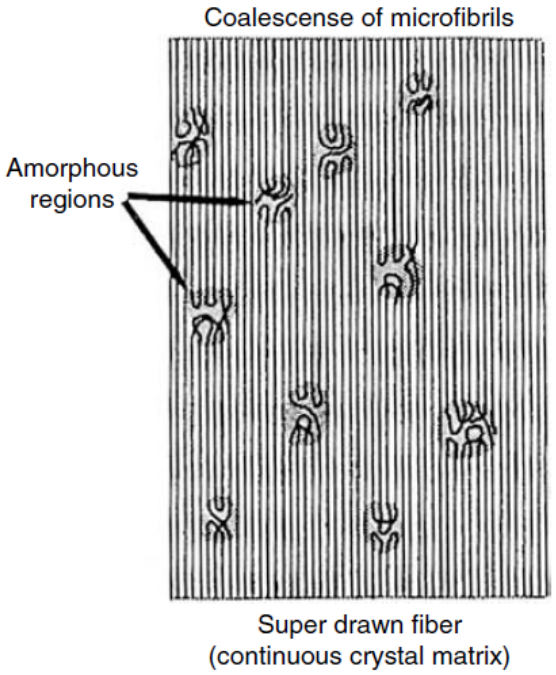

Figure 2. 6 Proposed morphology of superdrawn filament illustrating concept of continuous crystal matrix[41].

In addition, Cansfield et al.[42] worked on slow two-stage drawing of polypropylene with a series of molecular weight and molecular weight distribution polymers. The drawing was performed using Instron tensile testing equipment attached with an environmental chamber at crosshead speeds of 10 and 5 cm/min at different temperatures up to 30x draw ratios. They have pointed out the lower drawing temperatures, < 80 ^{o}C, do not have any effect to improve the mechanical properties of polypropylene films. Although, there was an approximately linear relationship between modulus and draw ratio were observed for the draw temperatures of 110, 130 and 150 ^{o}C with the maximum modulus value of 175 g/dtex.

De Candia et al.[43] have also studied the drawing of *i*-PP fibers at high temperature by two-stage isothermal drawing process. They obtained the ultra-drawing of isotactic polypropylene with draw ratio of more than 40x. They also concluded there was no any good improvement for the structure while any further drawing after a saturation value, which was 20x, was applied. A high degree of decreasing of the molecular mobility in the amorphous component was observed and explained by the cold drawing model. Another similar observation was a very weak or absent of β-transition and detectable α-transition in the drawn samples.

ii. Zone drawing and zone annealing

Many studies have been carried out on the development of high-tenacity, high-modulus PP fibers. A zone-drawing and zone-annealing method is one of the crucial techniques leading to manufacture high performance fibers. In general, this method is performed by a modified tensile tester which has a component with higher temperature to localize a part of spun fibers [17, 44]. For this purpose, the crosshead has a suitable size band heater. This method is different than traditional drawing systems because the heater is moving during the drawing hence the deformed region is heated with an appropriate rate. An advantage of zone drawing is to prevent the back folding of the drawn polymer chain and thermal degradation of fiber in a hot drawing technique[44]. This is achieved by the shifting heater ensemble along the fiber axis. The zone-drawing method has demonstrated beneficial effects when compared to hot-drawing experiments, for example, in general, micro-crystallite formation, back folding of molecular chains, and thermal degradation of the sample decreased[45].

In addition, Kunugi et al.[46] have reported the zone-annealing method consists of two stages of zone drawing: highly oriented amorphous filament, and zone annealing highly oriented crystalline fibers (see Figure 2.7). This study was carried out to obtain a very high degree of the molecular chains arrangement by the zone drawing and crystallize the fibers in a bundle state by the zone annealing process. A reconstructed tensile tester was used to manufacture excellent mechanical properties fibers from *i*-PP with the maximum values of 17.2×10^{10} dyne/cm^2, and 75.8 kg/mm^2 for Young's

modulus and tensile strength, respectively. As seen in Table 2.4, the zone annealing process caused to increase the fiber performance and decreased elongation at break (%) of fibers with contained numerous high-quality crystallites.

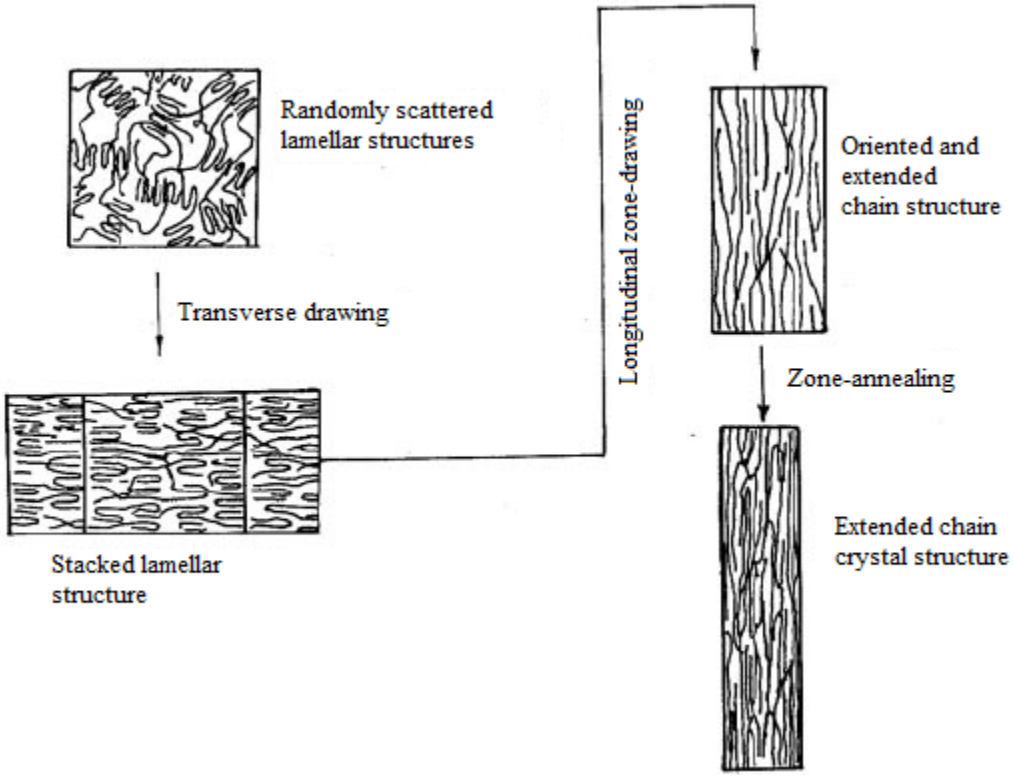

Figure 2. 7 The change in structure during zone-drawing and zone-annealing[17].

Table 2. 4 Tensile properties of original fiber, zone-drawn fibers, and zone-annealed fibers[46].

Sample		Young's modulus ($\times 10^{-10}$ dyn/cm^2)	Strength at break (kg/mm^2)	Elongation at break (%)
Original fiber		0.91	—	—
Zone-drawn fiber	1ZD[a]	3.82	38.1	36.3
	MZD[b]	5.57	46.2	29.8
Zone-annealed fiber	1ZD–1ZA[c]	12.60	59.5	8.7
	MZD–MZA[d]	17.20	75.8	8.8

1ZD: 1-step zone drawing.
MZD: multistep zone drawing.
1ZD-1ZA: 1-step zone annealing after 1ZD.
MZD-MZA: multistep zone annealing after MZD

Compared with the data between original, zone-drawn and zone-annealed fibers are shown in Table 2.5. It was found that the birefringence, orientation factors of crystallites and amorphous chains increased while compared with the original fiber. There is a tremendous increase for crystallites orientation factors but increased only slightly by zone annealing. Furthermore, the increment in the crystallinity increase was small and amorphous orientation factor increased with zone-annealed process. Therefore, it can be concluded that increasing amorphous chains orientation factor contributes greatly to the improvement in fiber performance. Authors also pointed out the large number of tie molecules is another reason to observe the excellent mechanical properties.

Table 2. 5 Birefringence (Δt), orientation factors of crystallites and amorphous chains (f_c and f_a), and crystallinity (X_c) of original fiber, zone-drawn fibers, and zone-annealed fibers[46].

Sample		$\Delta_t \times 10^3$	f_c	f_a	X_c
Original fiber		2.4	—	—	57.9
Zone-drawn fiber	1ZD[a]	30.4	0.970	0.605	54.8
	MZD[b]	31.5	0.985	0.634	59.5
Zone-annealed fiber	1ZD–1ZA[c]	34.0	0.988	0.825	62.2
	MZD–MZA[d]	36.9	0.990	0.957	65.6

1ZD: 1-step zone drawing.
MZD: multistep zone drawing.
1ZD-1ZA: 1-step zone annealing after 1ZD.
MZD-MZA: multistep zone annealing after MZD

In addition, Suzuki et al.[47] applied a continuous vibrating zone-drawing (CVZD) to isotactic polypropylene fibers to study fiber mechanical and structural properties. Therefore, a specially designed apparatus was manufactured to draw continuously fibers under vibration (please look Figure 2.8). As a result, improved mechanical properties of fibers were observed, for example, the degree of crystallinity of 62.4 % and the orientation factor of crystallites of 0.991 after the CVZD treatments in five steps at the drawing temperature of 150 °C with the frequency of 100 Hz. In this study an interesting phenomenon drew our attention that the vibration has affected more oriented molecular chains in the drawing direction, but inhibited the crystallization.

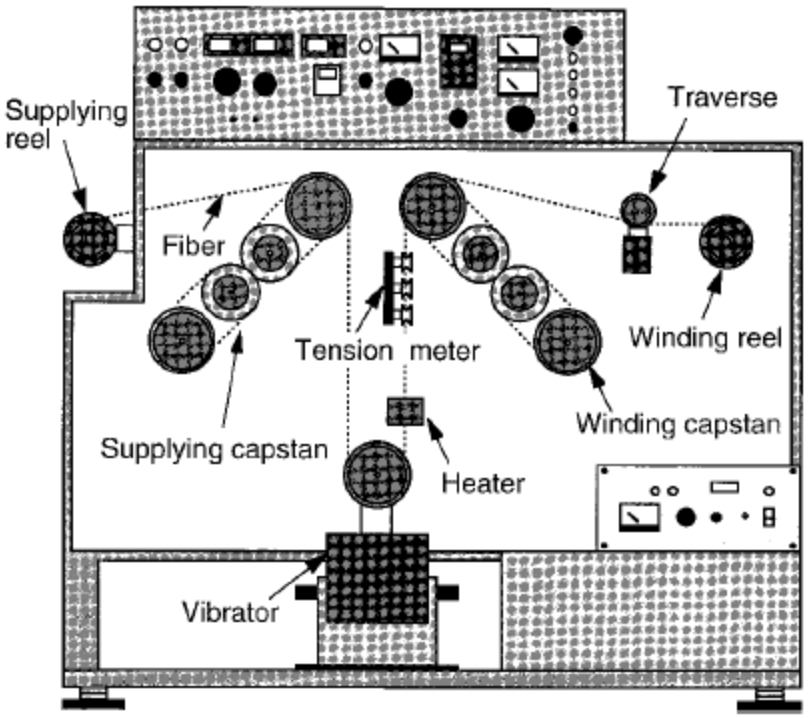

Figure 2. 8 Scheme of apparatus used for continuous vibrating zone-drawing (CVZD)[47].

iii. Constant load oven drawing

Sheehan et al.[36] manufactured 'super-tenacity' polypropylene filaments by a monofilament spinneret with drawing and annealing processes. Fibers were quenched with air, water bath and/or continuous drawing machine through a heated glycerine bath. Furthermore, a convection oven with a fixed load was used to draw

monofilaments that drawn under constant tension. The temperature of the oven was gradually increased to 130-135 ^{o}C, and then the drawing was performed under the same tension at the elevated temperature to obtain the final draw ratio. Lastly, the fibers were allowed to cool to room temperature and then the weight was removed. In this process, the fibers were not annealed. Table 2.6 shows physical properties of PP drawn filaments obtained at high drawn temperatures in the oven. It can be seen from Table 2.6 that increasing drawn ratio caused to observe high values for tenacity and modulus with lower elongation at break with the total draw ratios ranging from 29x to 34x. The maximum tenacity was observed at 34x draw ratios which gave the tenacity value of 13.1 g/d with modulus value of 110 g/d. They have found that increasing filaments temperature had a positive effect to increase the maximum draw ratios: (1) increasing the filament temperature increased the stretch ability during drawing, (2) the shrinkage decreased after drawing and increasing the rate of crystallization that stabilized the filaments in the stretched state.

Table 2. 6 Mechanical properties of PP fibers with different draw ratios in an oven at 130- 135 ^{o}C[36].

			Properties of drawn fibers		
Draw ratio, total	No. samples[b]	Denier	Tenacity, g./den.	Elongation at break, %	Modulus, g./den.
29	2	20.6	11.5	23	88
32	3	19.1	11.5	24	94
33	2	17.6	12.4	17	106
34	1	18.1	13.1	18	110

In addition, Chawla[48] has determined the difference between polyethylene, ultra-high molecular weight polyethylene (UHMWPE), and polypropylene fibers for the tenacity and modulus performances. In general, polypropylene does not show a very high modulus and crystallinity as polyethylene fibers that generally could have high modulus and crystallinity. This is because the side groups for polypropylene vs. highly linear polyethylene molecular chains. These bulky side groups prevent to manufacture an orderly arrangement of molecular chains and high degree of crystallinity[48]. Chawla[48] has suggested a schematic process to obtain high strength polypropylene fibers (see Figure 2.9). In this process, the melt temperature was set around 250 ^{o}C, and then the filaments quenched by a water-filled tank. The fibers were drawn in oven, followed by an annealing oven by draw rolls, and lastly to windup bobbins to obtain 9x or more draw ratios.

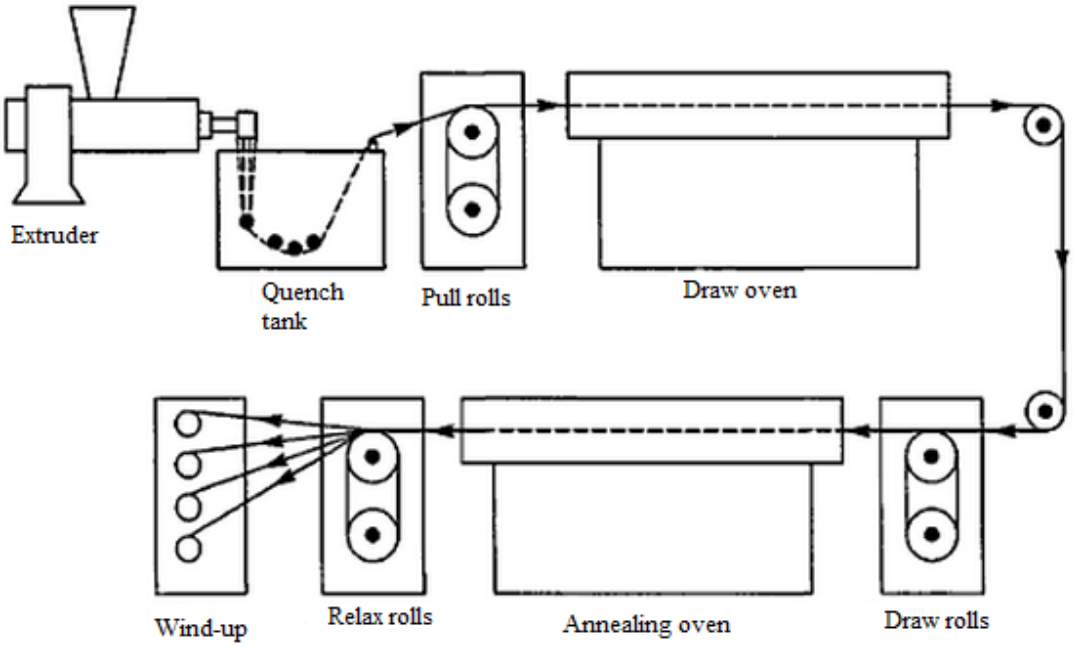

Figure 2. 9 A schematic representative of melt spinning process of making high strength polypropylene fibers[48].

The tenacity and modulus of filaments highly depend on the process parameters such as type of quench like water or air, drawing conditions for instance oven or roller system, and so forth. Sheehan et al.[36] have worked on effect of different quenching conditions to crystalline structure, crystallinity and tenacity for undrawn and drawn filaments (see Table 2.7). In extrusion method A, a highly isotactic polypropylene with a molecular weight of 110,000 was used, and then the filaments were hot drawn via a draw ratios of 8x and annealed. Filaments prepared by extrusion method C, a

highly isotactic polypropylene with a molecular weight of 405,000 and finally the fibers were cold drawn by a draw ratio of 5x without annealing process. As seen in Table 2.7, lower tenacities of the drawn filaments were observed when air quenching was used for the cooling system. This is because of partial orientation of the filaments attributed lower tenacities of drawn polypropylene filaments. On the other hand, if water bath was carried out for quench system for spinning filaments, unoriented paracrystalline structures were obtained with higher tenacity values.

Table 2. 7 Physical properties of polypropylene filaments under different quenched conditions[36].

Quenching conditions	Crystalline structure	Crystallinity of undrawn filaments, %	Tenacity of drawn filaments, g./den.
Extrusion method A			
Water bath, 50°C.	Unoriented paracrystalline	44	6.5
Air, 20°C.	Slightly oriented crystalline	54	4.8
Extrusion Method C			
Water bath, 10°C.	Unoriented paracrystalline	45	9.5
Air, 20°C.	Slightly oriented crystalline	62	5.5

iv. Die drawing

Many attempts have been reported to orient PP fibers or rods using solid phase deformation techniques for the production of ultrahigh tenacity and modulus oriented materials (Figure 2.10). Die-drawing has been explored as means of producing PP filaments or rods by drawing polymers through a conical die. In this case, researchers have tried to make an alternative technique instead of solvents based melt spinning and drawing under special conditions to produce high performance materials. Figure 2.11 explains the principle of die-drawing that the solid polymer is moved by applying a pulling force at the exit side of a converging die to steady drawing of the polymer through the die at some diameters[17,49]. The diameter and orientation were also affected by adjusting take-up mechanism with constant speed. The die should be maintained at a high temperature to achieve steady drawing of the polymer through the die.

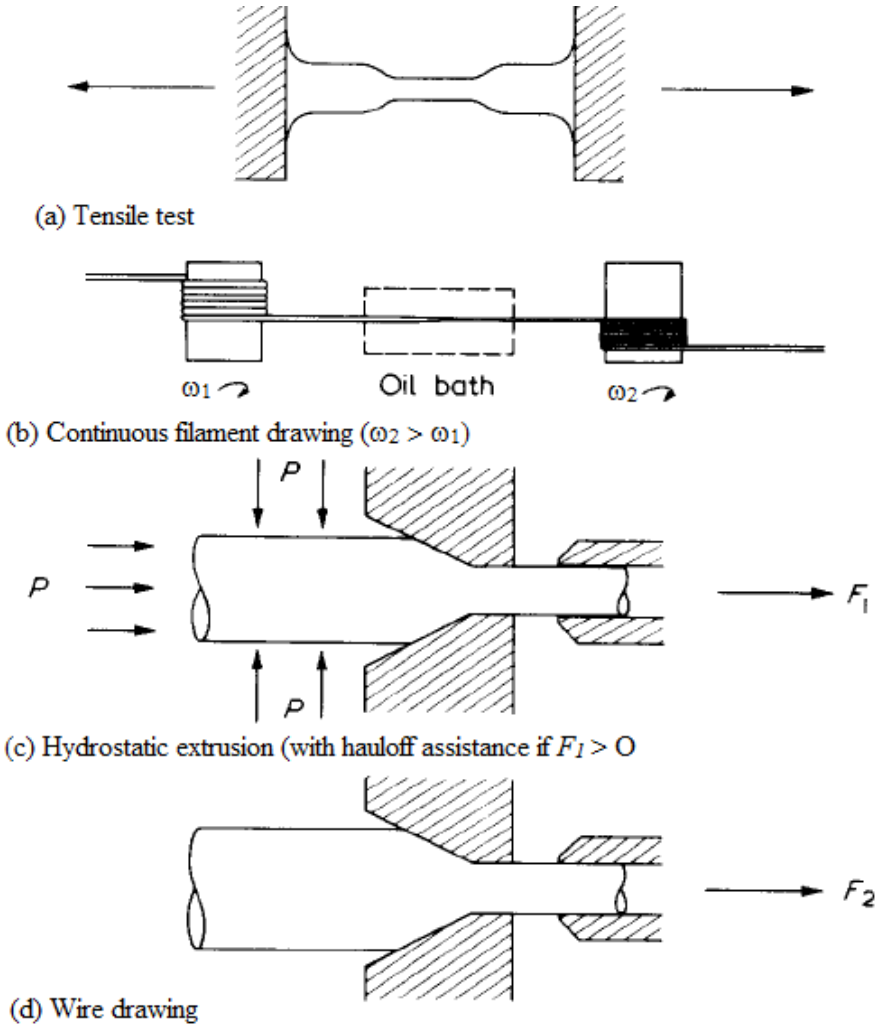

Figure 2. 10 Various types of solid phase deformation techniques[49].

Richardson et al.[50] have described the zones where deformation occurs and divided it in three sections. In the first drawing zone, the structure of conical die geometry should be designed to maintain convergent flow hence the uniform deformation can

be occurred under the same temperature of the isotropic billet and die structure. In the second drawing zone, isothermal tensile flow zone causes to alter a polymer by forcing it into a smaller size with deforming free of the die wall. In the third region, non-isothermal flow zone condition effects necking down phenomena after the die and finally the material progressively cools to form an approximate final cross-sectional size and shape.

Coates and Ward[49] have obtained ultra-oriented polypropylene rods by die-drawing at room temperature. The maximum Young's modulus was achieved about 20.6 GPa. They have also attributed the achievement of high production rates with the higher desired draw ratios. The researchers suggested to develop it into a continuous process because of the equipment design is relatively simple when compared to traditional extrusion process. In addition, monoaxial orientation can be observed in filament by die drawing process[17] with higher draw ratios. The higher draw ratios were observed with increasing shear deformations in the die by adding an elongational axial component. Shaw[51] has pointed out the die design with using effective external lubricants which prevented the distortion problems for the products and controlled axial extension rates.

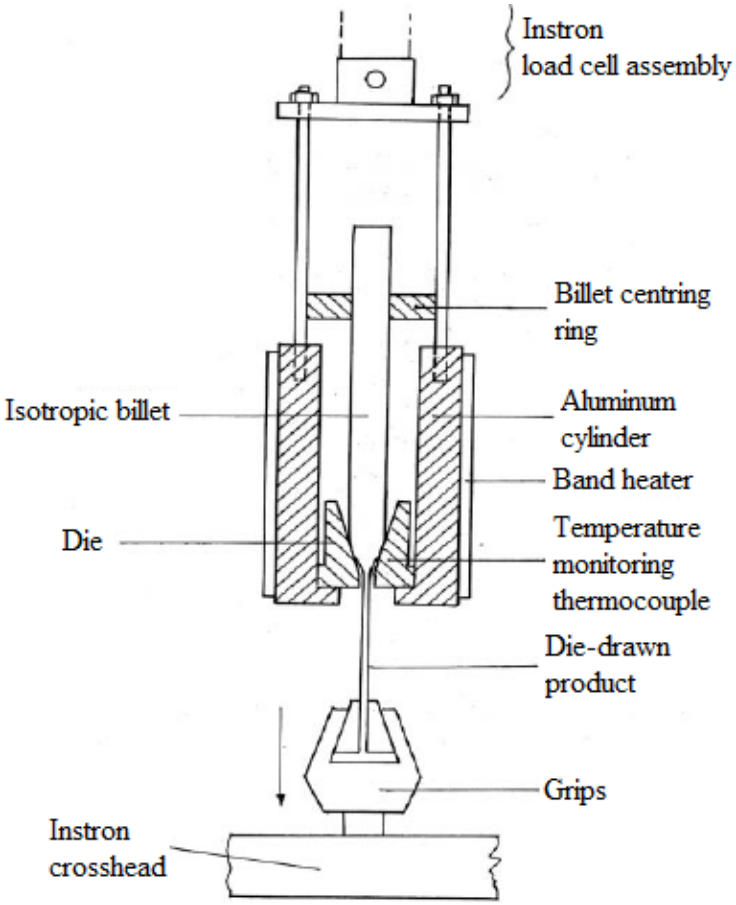

Figure 2. 11 A small representation of die drawing[17, 49].

v. Hot nip drawing

In this method, the extruded polypropylene sheet was mounted in specially designed grips[52]. A heating device with two sharp edges contacted the top of the sheet (Figure 2.12), and then the sheet was drawn at a constant rate of elongation by an Instron Tensile Tester.

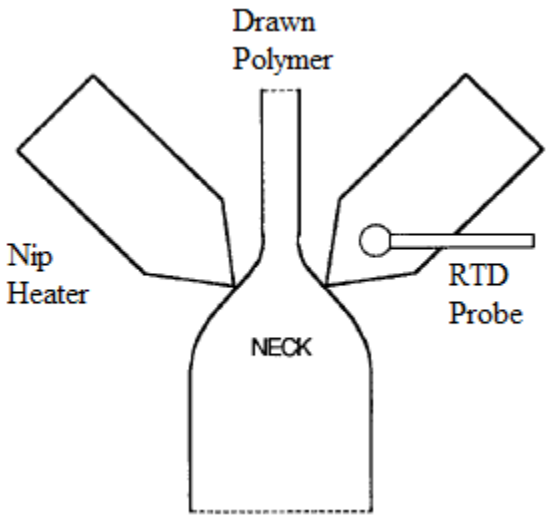

Figure 2. 12 A schematic representation of the not nip devives[52].

The drawing process can be repeated to obtain very high draw ratios. Additionally, a heating device should be mounted to the moving crosshead and the speed of crosshead need to be slow (1 cm/min) to avoid any breakage and failure[52].

Increasing draw ratio led to an increase in Young's modulus and tensile strength. Laughner et al.[52] observed the maximum modulus value of 13.2 GPa for a film via drawn two times with a draw ratio of 26x. In addition, only a single drawing he produced between 4.5-5.0 GPa for modulus value after a draw ratio of approximately 13x. After higher draw rations by the redraw process, more than 16x, fibrillation sometimes was observed. According to the researchers, highly oriented molecules in the draw direction caused to generate weak van der Waals interactions between aligned molecules which led to splitting.

2.3.3 Gel Spinning Technique

The creation of highly oriented polypropylene fibers with a very high degree of mechanical properties can take place in an extended state in gel spinning technique. In this method, ultra-high molecular weight polymers are used to manufacture fibers products. The main point of this technique is to reduce molecular entanglements in the gel and to obtain an efficient stretching of the polymer chains in the flow media.

Ultra-high molecular weight polyethylene fiber (UHMWPE) is produced through the solution/gel spinning technology with an ultra-high draw ratio to get minimal intermolecular entanglements. UHMWPE is synthesized from ethylene with

metallocene catalysis polymerization. This method has much more advantages than Ziegler-Natta technique because of getting much higher molecular weight.

HMWPE fibers show extraordinary physical and mechanical properties, for example, low specific weight, high modulus, high strength, high impact resistance, high cut and abrasion tolerance, excellent chemical resistance, and so forth[13]. Dyneema and Spectra are two popular brand names for the same-based polymer which are very strong fibers. These fibers are produced using gel spinning method through a spinneret to form very oriented filaments of UHMWPE. Table 2.8 demonstrates physical properties of Dyneema SK60, SK65, SK75, SK76[54].

Table 2. 8 Mechanical properties of Dyneema SK60, SK65, SK75, SK76[54].

	Physical Properties of Dyneema			
	SK 60	SK 65	SK 75	SK 76
Density (g/cc)	0.97	0.97	0.97	0.97
Strength				
Tenacity (N/tex)	2.8	3.1	3.5	3.7
Tenacity (g/den)	32	35	40	42
Tensile strength (GPa)	2.7	3.0	3.4	3.6
Modulus				
Specific modulus (N/tex)	91	97	110	120
Specific modulus (g/den)	1025	1100	1250	1350
Modulus (GPa)	89	95	107	116
Elongation (%)	3.5	3.6	3.8	3.8

Smith and Lemstra[53] revealed in one of the first publications on gel spinning method. They used high molecular weight polyethylene ($\bar{M}_w$= 1.5x10^6) with decalin solvent. Dilute and concentrated solutions were used to spin polyethylene monofilaments. 2 wt. % polyethylenes in decalin at 150 °C was prepared for the dilute solution method. Then, this highly viscous media was pumped at 130 ^{o}C through capillaries, and these liquid filaments were quenched in cold water which had almost all the decalin. Finally, these as-spun gel fibers were drawn at various draw ratios in hot-air oven at 120 ^{o}C with the strain rate of 1 s^{-1}. Figure 2.13 shows the stress & strain curve of solution spun/drawn polyethylene monofilaments. As seen, the drawing process increased the mechanical properties with 90 GPa for modulus, 3.0 GPa for strength were reported as the highest values after 32x draw ratios. They also demonstrated that decalin had a slight plasticizing effect to increase the attained draw ratio after removing the solvent in the drawing stage. However, they observed similar mechanical properties at the same draw ratio with and without solvent.

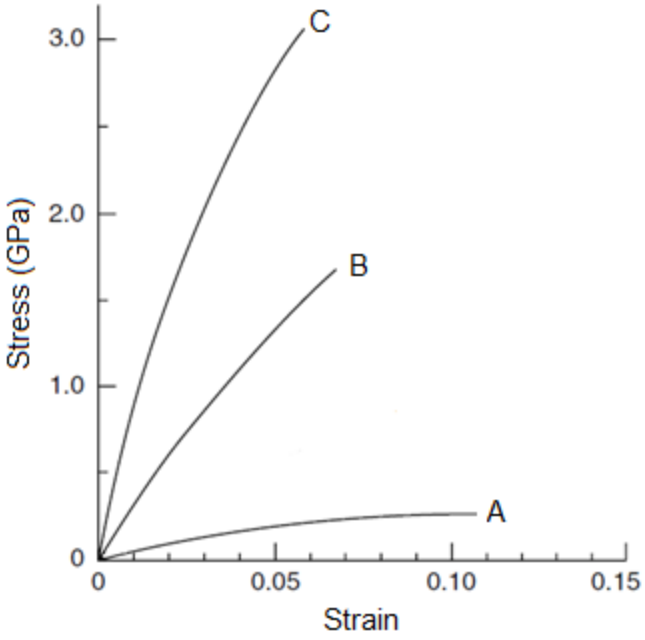

Figure 2. 13 Stress–strain curves for gel spun-drawn polyethylene fibers. Draw ratios: (A):3, (B): 15, (C): 32[53].

For concentrated solution, 10-50 wt. % of solvent, the fibers did not show the same drawability compared with the fibers spun from dilute solutions. The maximum draw ratio of 5x was observed at the draw temperature of 120 ^{o}C. This interesting phenomenon was explained as primarily due to occurrence of homogeneous and continuous structure of high molecular weight polyethylene in the dilute solution. Furthermore, a substantially smaller number of entanglements were formed when compared with the concentrated solution. This non-uniform structure with a very

large number of entanglements for concentrated solution caused to increase numerous defects which led to fracture upon drawing.

Isotactic polypropylene (*i*-PP) is another common polymer for producing high-performance fibers. It also has significantly higher melting temperature than polyethylene. Researchers have attempted to produce fibers of UHMW *i*-PP using the gel spinning technique. A high-molecular weight polypropylene has been used[55] to investigate gel-films formation by using 1 % polymer. The hot solutions of *i*-PP was quenched in decalin to -25 ^{o}C, and then left for a few hours. Ultra-drawn dried PP-gels with a draw ratio of 57x had a very close value for the theoretical modulus and strength of polypropylene. In addition, Kavesh et al.[56] disclosed in a US Patent production of high performance polyethylene and polypropylene fibers. The most preferable weight average molecular weight of polypropylene used in the process was around 2,000,000 (11 IV), IV represents the intrinsic viscosity of the polymer that was determined by decalin at 135 ^{o}C. A solution of ultrahigh molecular weight of polypropylene was obtained using a relatively nonvolatile solvent. Then, this solution was extruded through an aperture to produce an indefinite length of first gel after exposed to cooling process. The second step provided to form a second gel by the extraction of first gel into a volatile solvent and a low-porosity xerogel was manufactured after drying process of the second gel. Finally these first, second and/or a combination of gels were drawn to obtain high-tenacity and high-modulus polypropylene fibers. The drawing process could be applied after the first and second

gel formation by a single stage or more than two stages. In general, they applied two or more than two drawing stages with the last of the stages performed at a temperature between about 135-150 ^{o}C. A unique type of polypropylene fibers with the tenacity value of at least 8 g/d and a tensile modulus at least about 160 g/d were observed. These polypropylene fibers also demonstrated an elongation at break less than approximately 20 % and the main melting temperature of 160 ^{o}C with porosity less about 10 %.

Kristiansen et al.[57] have used a nucleating agent 1,3:2,4-bis(3,4-dimethyl-dibenzylidene) sorbitol (DMDBS) for the polymer solutions in order to increase gelation/crystallization of *i*-PP. This synergistic effect improved the rate of gelation of solutions of *i*-PP so it became more feasible for production processes in the industries. The modulus up to 35 GPa with the tensile strength value of about 1 GPa and melting temperatures observed up to 228 ^{o}C for gel-processing/drawing of *i*-PP. They, firstly, dissolved DMDBS in decalin at a temperature between 150 and 185 ^{o}C, and then allowed to cool down to the room temperature after homogeneous solutions were obtained. *i*-PP was mixed with this solution using an antioxidant in order to prevent degradation of the polymer. After the mixture degassed under the vacuum, it was heated to 160–175 ^{o}C under nitrogen and stirred until getting completely dissolved solution. The solvent evaporated at room temperature to obtain films of a typical thickness of about 0.2 mm. Subsequently, drawing process was applied in separate experiments from the polymer solution.

2.4 New Generation of Reinforced Polypropylene Composites

For scientists and engineers involved in the research and practice of fiber formation, new fiber technologies have been developed in order to improve the mechanical properties, spinnability, and molecular orientation by adding reinforcing additives into polymer materials. These reinforcing agents can be organic and inorganic particles with different geometries to be incorporated with thermoplastic polymers (see Figure 2.14). It should be noted that the surface area/volume is more dominated for the fiber and layered materials and more pronounced for nanomaterials[63]. The relation between the surface area-to-volume ratios is highly dependent, three orders of magnitude, to the changing materials diameter and layer thickness from the micrometer to nanometer range[63].

The fillers can be incorporated to thermoplastic polymers during the melting process via a single or twin screw mixer or extruder to prepare master-batch just prior to the extrusion process. In addition, post-processing of the composite, to give final structure, such as extrude molding, injection molding, melting spinning film blowing, and compression molding have a great influence for the final characteristics and degree of orientation of the fillers in the blends.

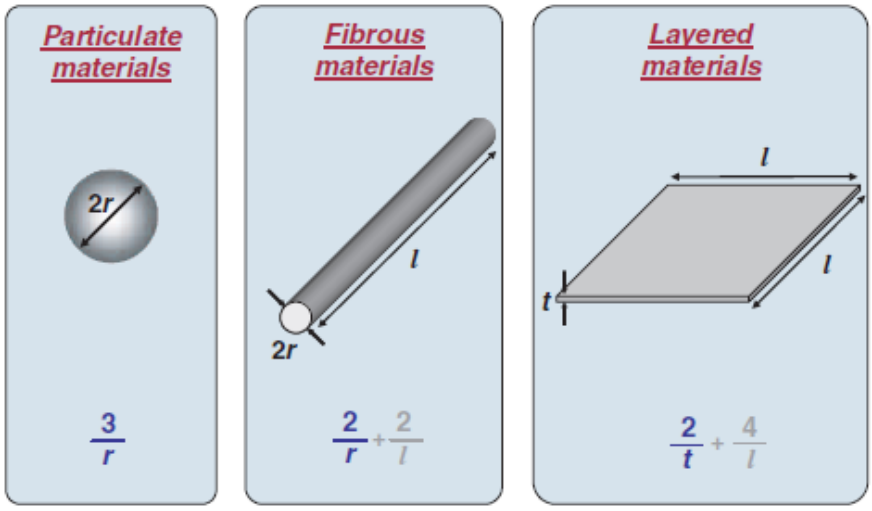

Figure 2. 14 Common additive types and geometries with their respective surface area-to-volume ratios[63].

2.4.1 Liquid Crystal Polymer (LCPs)

Liquid crystal polymers (LCPs) have received much attention in recent years as filler reinforcement for polypropylene[58-59]. Indeed, researchers have mainly worked to determine blend properties and appropriate conditions of thermotropic liquid crystalline polymer (TLCP) with polyamides, polycarbonate, poly(ethylene terephtalate), polystyrene, polypropylene, polyimide, polyetherimide**,** polysulfone, polyethersulfone, and so on [58, 60].

LCPs is a class of aromatic polyester polymers and is characterized by a high degree of aromaticity, planarity, and linearity in the chain backbone. Also, it shows a highly ordered structure (Figure 2.15) with extremely unreactive and inert in the both melt and solid states (orientation factor > 0.95). LCPs can be used as food containers, electrical components, gloves, inflatable structures, sports and medical products which requiring chemical inertness and high strength. 1,4-biphenyl, *p*-phenylene, and 2,6-naphthalyl moieties, which are most commonly used moieties, attached by ester or aramide linkages. Thermotropic LCPs are that the polymers forming liquid crystal phases in the melt; on the other hand, the polymers forming liquid crystalline phases in solution are defined as lyotropic[16].

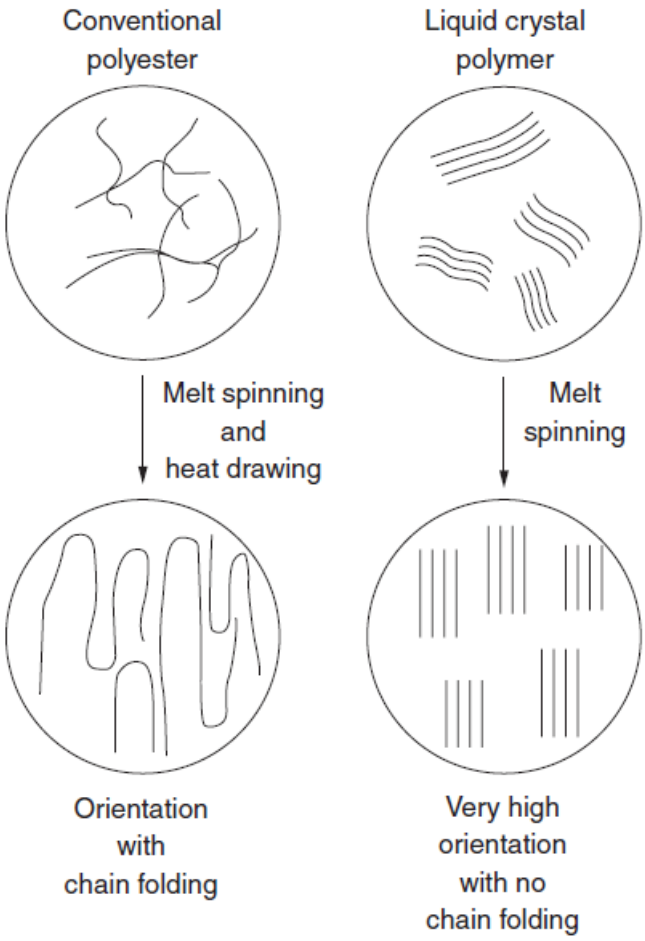

Figure 2. 15 Comparison of molecular chain structure of conventional polyester and liquid crystal polymer fibers[1].

LCP fibers are produced via melt spinning techniques that is similar to conventional polyester manufacturing, but wind-up speed is much lower and moderate drawn down processes can be applied while compared with PET fiber production[1, 16]. Vectran fiber

is one of the commercially available wholly aromatic polyester fiber and exhibits exceptional strength and rigidity.

Machiels et al.[58] worked on preparation, morphology, and mechanical properties of blends of TLCP with polypropylene. After using two different grades of polypropylene, blending with the low-viscosity PP resulted in continuous fiber/matrix morphology about 3 μm without any intermediate droplet / matrix morphology. In addition, blending with high-viscosity PP by single-screw extruder lead in large, to poorly dispersed, and poorly distributed TLCP. Therefore, they used second extrusion step to get enough level of mixing that directed to the skin-core morphologies because of fast breakup of the TLCP fibers with relatively high diameter of 7 μm depending on the draw ratios. For both low and high viscous grade PP blended with TLCP, drawing process was needed to achieve satisfactory mechanical properties. Tensile strength of the blends of high and low viscosity grade PP blended with different volume ratio of TLCP are shown in Figure 2.16. It can be seen that the tensile strength for both type of polypropylene increased with increasing the draw ratios. Highly viscosity grade PP blended with TLCP demonstrated higher tensile strength than low viscosity grade PP, and showed approximately 225 MPa with a draw ratio of close to 15x. For low viscosity grade PP blended fibers displayed the maximum value of about 130 MPa after a draw ratio of 12x according to the Figure 2.16.

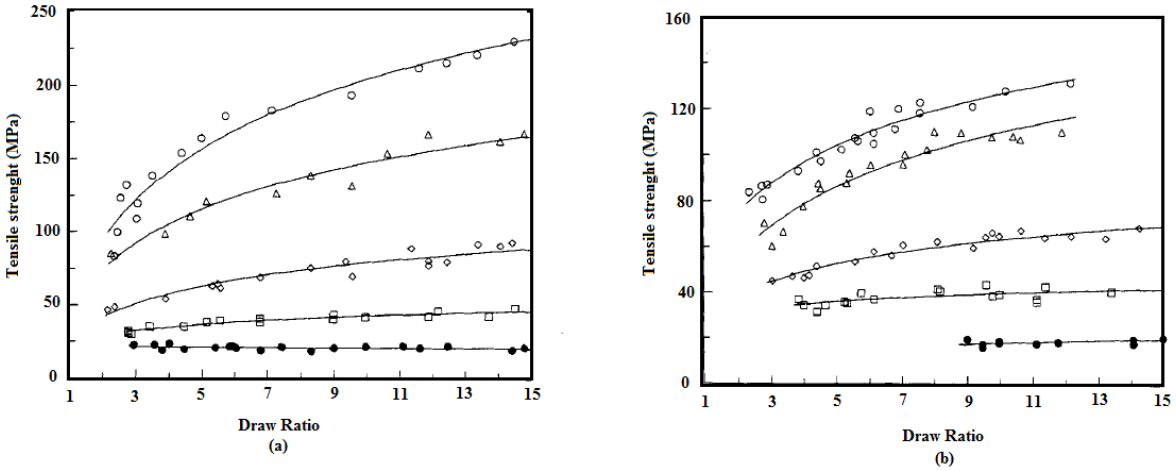

Figure 2. 16 Tensile strength vs. draw ratio of the blends of (a) highly, and (b) low viscous grade PP blended with different volume ratio of TLCP[58].

The modification of polypropylene by blending with thermotropic liquid crystal helped maximize the reinforcing potential of the TLCP. Therefore, many studies have been done in recent years. In 2000, Echevarria et al.[59] worked with the blends of polypropylene and thermotropic copolyester (Rodrun) by direct injection molding at different processing temperatures. For this study, they blended two grades of polypropylene melt flow index (MFI) of 17.8 and 0.8 g/10 min with Rodrun content of 40 % at desired weight ratios at process temperatures of 190, 220 and 250 °C. Before the injection molding, the Rodrun pellets were dried for 16 hours at 80 °C. Figure 2.17 shows the melting and crystallization heats of crystalline phase of the blends which produced at 190 ^{o}C. As seen, almost a linear relationship was observed

for melting and crystallization heat with increasing TLCP weight content. They have also monitored the similar behavior for low viscosity polypropylene blends. Melting and crystallization temperatures of polypropylene blends were almost same as those of pure PP that indicated full immiscibility and the lack of strong interactions between the phases formed during the production. In addition, the blend samples demonstrated core-skin morphology as Machiels et al.[58] observed for their samples. Using more viscous polypropylene for the blends led to Rodrun migration to the skin. The Young‘s modulus of the blends with different amount of the Rodrun content showed very low values corresponding to the rule of mixtures between the values of the pure PP and Rodrun (9.0 GPa) as monitored by Machiels et al.[58]. This may be due to a low degree of orientation of Rodrun in the blends compared to that of pure Rodrun. The blends showed the maximum modulus of 3.69 and 3.42 GPa at 220 and 250 ^{o}C process temperatures with 40 % of the Rodrun content for higher and lower polypropylene MFI, respectively with 2.4 and 1.5 % elongation at break. Moreover, polypropylene with MFI value of 17.8 g/10 min caused to form fibrillar morphology of the polypropylene blends at the skin. Hence it led to manufacture higher modulus and yield (or break) stresses, higher ductility and impact strength values than more viscous PP blends.

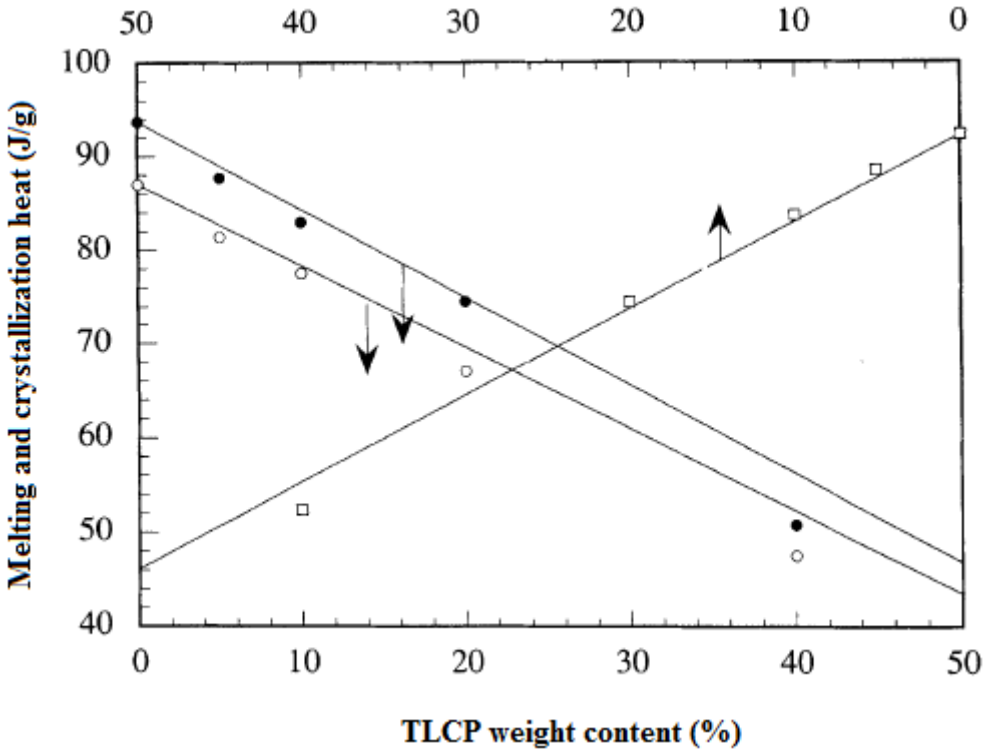

Figure 2. 17 Melting, first (o) and second (●) DSC scan, and crystallization (□) heats of PP vs. TLCP weight content[59].

Jin et al.[60] concluded that to obtain a very well-dispersed TLCP phases in the matrix polymer:

1. The optimum mixing temperature and shear rate should be determined in order to get TLCP perfectly dispersed in the matrix;

2. Using an elongating force to lead the TLCP's microdomains to form finer and continuous microfibers;
3. Governing process conditions is another crucial parameter to distribute TLCP microfibers to manufacture a maximum degree of orientation in the polymer matrix.

2.4.2 Nanoparticles-Reinforced Systems

The mixing process of two components is important to obtain uniform particle dispersion. In general, it is easy to produce the uniformly dispersed fillers in the matrix polymer when they can form a miscible blend and good filler-matrix adhesion after the mixing and post-treatments. If the components are immiscible and incompatible, it becomes harder to observe good dispersion which affects the morphology and final properties of the blend. In addition, it is important to evaluate the size of reinforcing fillers to obtain uniform distribution into polymer materials. For example, most micrometer-scaled additives can cause spinline failures because the sizes of individual and agglomeration can approach to the fiber diameter[61]. In order to prevent these kinds of problems and increase their effects, it is required to incorporate nano-reinforcements into polymer matrix. In general, the nanomaterials can be divided in five groups according to its geometrical structure: nanoparticles,

nanotubes, nanofibers, fullerenes, and nanowires with particle, layered, and fibrous type materials[63]. In fact reinforcement especially reinforcement of nanofillers could expand to the range of carbon black, silica nanoparticle, polyhedral oligomeric sislesquioxanes (POSS)[63]. These nanomaterials can be incorporated into fiber-forming polymers by three methods; namely, melt mixing, solution mixing, and in situ polymerization[61]. Nowadays, nanocomposites have been widely and successfully used in structural applications, for instance automotive parts, airplanes, constructions, flame-retardant materials, etc. Nanoparticles have extremely large aspect ratio with reduced thickness and larger total surface area per unit volume which induce to obtain maximized interaction between the nanofiller and matrix[61-62].

2.4.2.1 Si-O anions-based nanoparticles

Polypropylene nanocomposites, in particular, Si-O anions-based have attracted attention with the advantages of the nanoparticles imposing efficient impact on the physical properties of the composites. Polypropylene blended layered-silicate to obtain nanocomposites is one attractive system that can be used in engineering applications. Polymers having polar functional groups are important to improve adhesion between the layered-silicate reinforced surface and the polymer matrix. Furthermore poor dispersion and weak mechanical properties can be prevented by using surface treatment to increase hydrophilicity and modify the chemistry of the PP

matrix by adding polar groups[62]. Lee at al.[62] obtained and compared PP/layered-silicate nanocomposite fibers in the presence or absence of PP-based maleic anhydride compatibilizer. They observed improved tensile strength over the uncompatibilized composite because the compatibilizer modified the chemistry of the PP matrix by the attachment of polar groups. This modification led a more effective exfoliation of the particles.

Using different types of silica nanoparticles as fillers with various incorporating methods were reported by several researchers. Garcia et al.[64] reported using two different inorganic fillers: colloidal (sol) and powder silica nanoparticles with particle size $\leq$ 30 nm to obtain polypropylene-SiO_2 nanocomposites. The silica powder was mixed with polypropylene using a side feeder situated directly behind the melting zone at a twin-screw extruder. In addition, incorporation of the colloidal silica into polypropylene was obtained with designed a high-pressure reaction-zone for the twin-screw extruder for mixing the polymer and silica. Figure 2.18 demonstrates SEM images of morphology for fractured pure polypropylene (a, b), polypropylene with silica nanoparticles (c, d), and polypropylene with colloidal silica (e, f). They reported some micro-size agglomeration of silica (Figure 2.18c and 2.18d) and almost no visible particle agglomerates for colloidal silica (Figure 2.18e and 2.18f) at this magnification in the composites. Degree of crystallinity was observed with the values of 48, 50, and 45 % for pure polypropylene, polypropylene with silica nanoparticles, and polypropylene with colloidal silica, respectively. Regarding the mechanical performance measurements, there was no significant difference between the pure

polymer and composite samples for the yield stress. However elastic modulus increased from 1.2 to 1.5 and 1.6 GPa for polypropylene with silica nanoparticles, and polypropylene with colloidal silica, respectively. The influence of the filler particles on Izod impact strength was significant which improved approximately 68 % for the impact strength with addition of colloidal particles than the pure polymer matrix from 3.44 to 5.77 KJ/m^2.

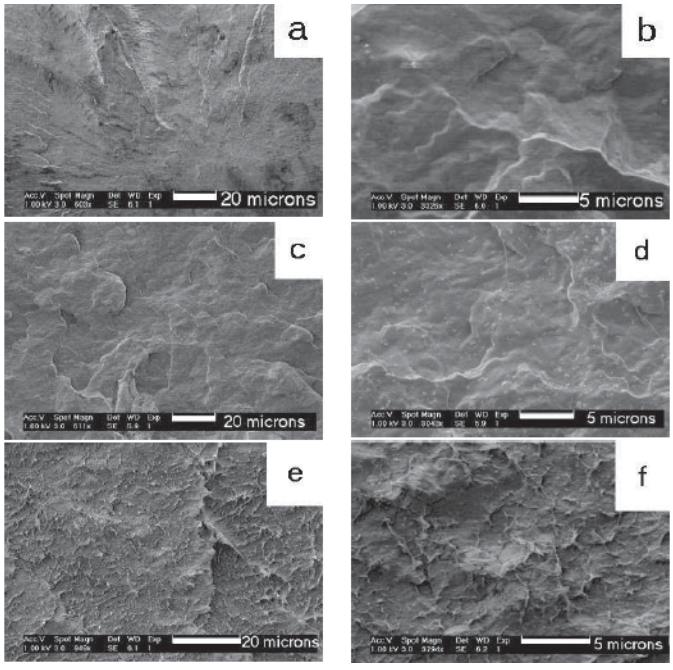

Figure 2. 18 SEM images of polypropylene (a, b), polypropylene with silica nanoparticles (c, d), and polypropylene with colloidal silica (e, f)[64].

In order to improve mechanical properties of PP fibers, a pre-drawing technique was used in Ruan et al.[65] study (please see Figure 2.19) to incorporate nanoparticles into polymer matrix. In this method, dried silica nanoparticles with monomer butyl acrylate and a certain amount of solvent were irradiated with ^{60}Co γ-ray in air at room temperature to obtain poly (butyl acrylate) (PBA) grafted nano-SiO_2. Therefore, this graft polymerization led to convert hydrophilic surfaces of nanoparticles into hydrophobic surfaces by forming grafted polymer chains covalently attached to the nanoparticles.

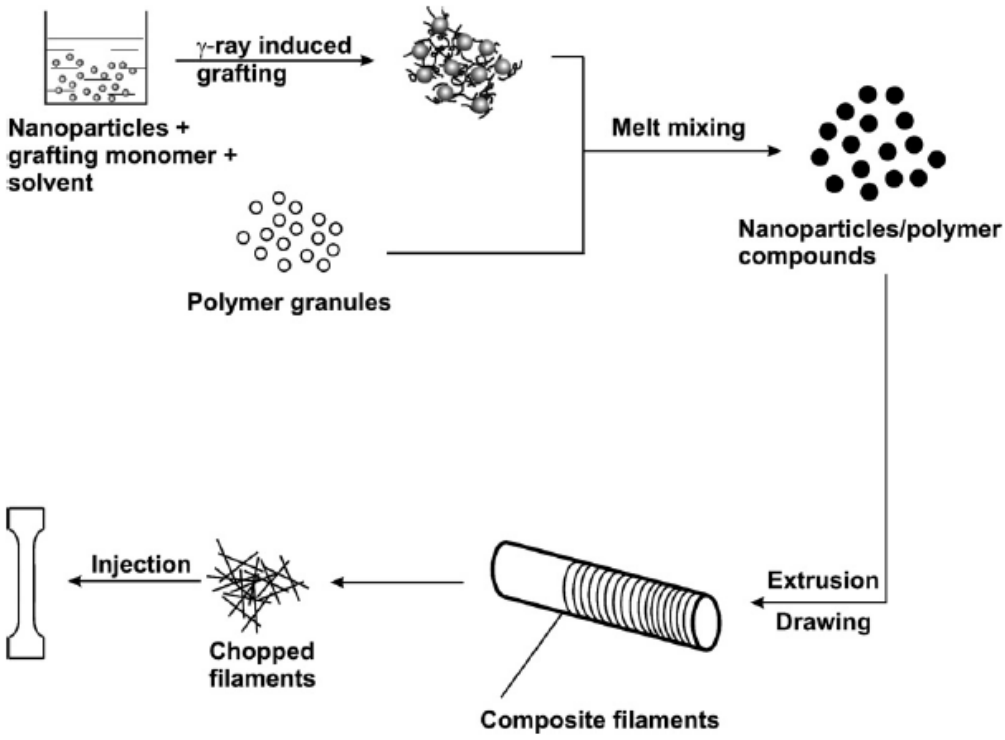

Figure 2. 19 A schematic diagram of the pre-drawing method[65].

Grafted polymers with covalently connected with silica nanoparticles and entangled with the surrounding polymer matrix extended and longitudinally aligned in fiber after drawing process are shown in Figure 2.20 (a). A high degree of dispersion of nanoparticles was prevented regarding to the entanglement between the grafted polymer and matrix which caused intimate filler/matrix interaction. Figure 2.20 (b) demonstrates polymer matrix with untreated nanoparticles before and after drawing. In this case, the agglomerated fillers stayed nearly undeformed before and after the drawing process that guided poor interfacial interaction and mechanical properties. Mechanical properties of PP nanocomposites made from the filaments showed that the tensile strength had similar performance for neat PP and PP-composite containing untreated silica nanoparticles after drawing value of 15x. On the contrary, notch impact strength increased from 1.34 ± 0.02 to 1.72 ± 0.02 kJ/m^2 for neat PP and PP-composite containing untreated silica nanoparticles, respectively. In contrast, using polymer matrix with grafted nanoparticles greatly affected the mechanical properties. The tensile and notch impact strength improved from 35.75 ± 0.77 to 38.10 ± 0.57 MPa and from 1.34 ± 0.02 to 4.09 ± 0.05 kJ/m^2 for neat PP and PP-matrix with grafted nanoparticles, respectively. The authors also reported that lower percent grafting of nanoparticles caused a higher degree of orientation of PP chains and higher concentration of β-crystal in PP-matrix during the filament process.

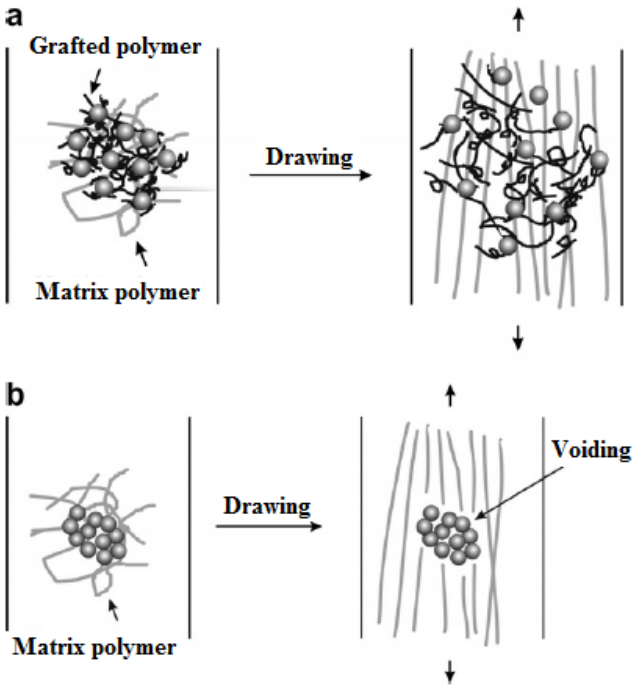

Figure 2. 20 A Schematic representation of cross-sections of (a) polymer matrix with grafted nanoparticles before and after drawing, and (b) polymer matrix with untreated nanoparticles before and after drawing[65].

2.4.2.2 Titanium-based nanoparticles

There is a large body of literature that discusses the mechanical, thermal, UV, electric and so forth property behavior of filled-polymer systems with titanium-based nanoparticles. The researchers have reported that the modulus of composite materials can be predicted because that is a bulk property and depends mainly on the geometry, modulus, particle size distribution, and concentration of the filler materials[66]. On the

other hand, it is hard to predict the tensile strength of the composite materials because local polymer–filler interactions are dominant factors with some other reasons which already mentioned. Two main types of tensile strength-filler concentration responses can be formed: the upper bound and lower bound[66]. In the upper bound response, a very strong interaction between the polymer and reinforcing agent can be observed, however weak, or almost no interaction between the polymer and additives forms in the lower bond response.

Madani[66] reported improved mechanical properties of polypropylene filled with surface-treated titanium dioxide nanoparticles. Furthermore, the author compared polypropylene composite materials loaded with a different amount of unmodified and modified nano-fillers. TiO_2 is widely used in industrial applications as filler and filler for white and colored polymer articles because they are chemically more stable than their metallic counterparts. In this work, TiO_2 was mixed with an acrylate monomer, trimethylolpropane triacrylate (TMPTA), after drying to obtain the surface-coated nanoparticles by removing the solvent. Subsequently these modified particles were irradiated with electron beam in the presence of air. Modified and unmodified fillers mixed with polypropylene by using tumble mixing, and followed by compounding this mixture on Brabender Plasticorder at temperature of 200 ^{o}C. As seen in Figure 2.21, treated nano-TiO_2 without radiation treatment had improved tensile performance of PP-composite materials and reached the maximum value of tenacity at the loading value of 15 wt. %. Moreover, the similar observation was monitored for untreated TiO_2-filled PP and all compositions showed higher tensile performance than

the virgin polypropylene. In the case of radiation treatment of modified TiO_2 which considerably improved in the strength of PP-based composites and demonstrated the maximum tensile strength around 5 wt. % with filler due to increased adhesion between filler and matrix. In order to keep these high strength values for the composites, we should obtain a high degree dispersion of filler and decrease the particle–particle interaction as possible.

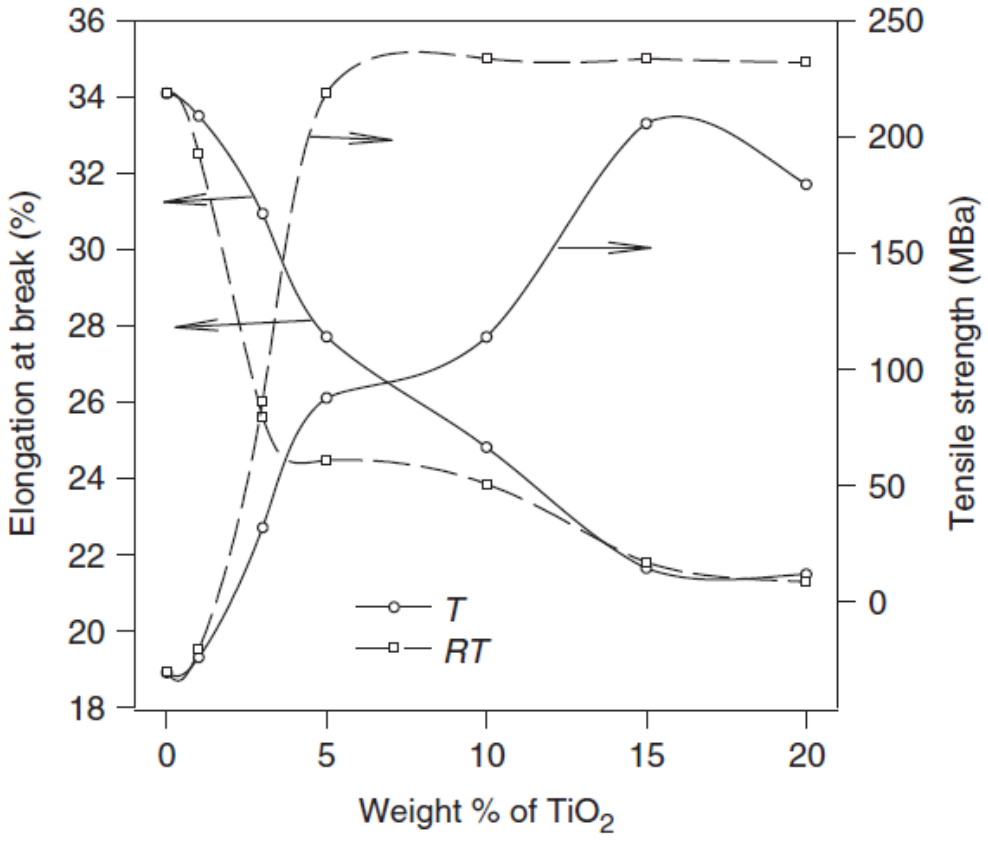

Figure 2. 21 Comparison of tensile strength and elongation at break of polypropylene incorporated with TiO_2 vs. weight percent of TiO_2 with and without radiation treatment[66].

There are some recent reports related to the improvement in the mechanical properties by using TiO_2 to produce PP/TiO_2 nanocomposite fibers. Especially direct incorporation of the reinforcing agent to polypropylene matrix by melt spinning technique takes the advantages of traditional polymer processing. Esthappan et al.[61] have investigated polypropylene/titanium dioxide composites by melt mixing

technique. The main purpose of that research study was to synthesize titanium dioxide nanoparticles, and then mixing with polypropylene matrix by melt spinning and then drawing. For this purpose they produced titanium dioxide nanoparticles by wet synthesis method using $TiCl_4$ and NaOH solution to water with stirring. Subsequently, different concentrations of the nanoparticles in PP-matrix were obtained as sheets after processing by mixing chamber and hydraulic press. The composite fibers were obtained using a small scale spinning machine after the sheets were cut into small pieces (Figure 2.22). As seen in Figure 2.22, PP/TiO_2 nanocomposite fiber was white in color with a smooth in appearance revealed by SEM images. The tenacity of the PP-based composite fibers increased with addition of titanium dioxide nanoparticles and showed a maximum value of 9 g/d with 3 wt% of TiO_2. The authors concluded the distribution and orientation of the reinforcing agents are main factors to manufacture high performance composite filaments. On the other hand, increasing the filler content led to decrease peak melting temperature of the nanocomposite fibers from 166.7 ^oC to 164.6 ^oC at 3 wt% TiO_2 filled that was determined by DSC at heating rate of 10 ^oC/min. Furthermore, the degree of crystallinity increased with an increasing the filler content and reached the maximum value at 1.5 wt. % TiO_2 filled-fiber and then decreased. This may be due to nano-TiO_2 played as an nucleating agent that results in a higher degree of crystallinity but at a higher filler content ($\geq$ 3 wt. %) the nanoparticles lead to more agglomeration to prevent the crystal growth to observe a lower degree of crystallinity[61].

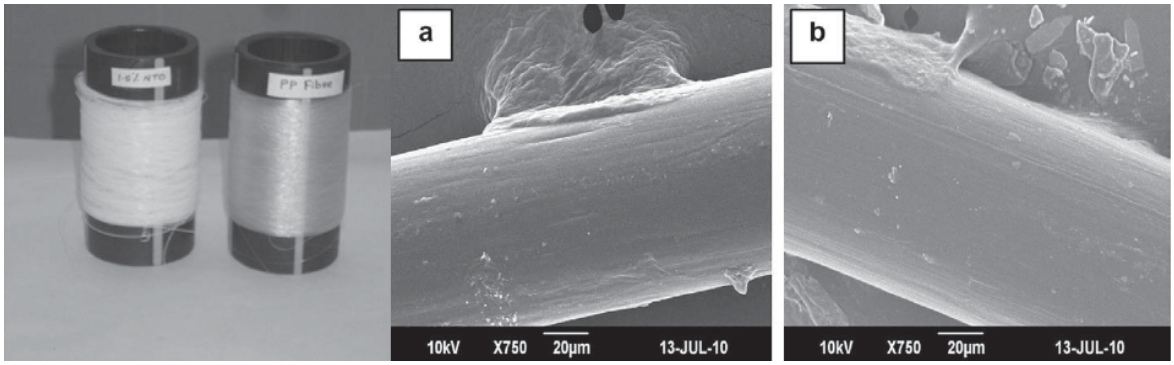

Figure 2. 22 Photographs and SEM images of neat PP {colorless, (a)} fiber, and PP/TiO_2 {white (b)} nanocomposite fiber[61].

In addition, many other studies have been done with using carbon black, carbon nanotubes, short carbon fibers, cenosphere, zeolites, etc. as additives for polypropylene to observe mechanical, crystallization and structural characteristic of the composite materials.

CHAPTER III

3.1 Introduction

Polyester filaments is one of the most universal and industrial fibers that has excellent basic properties with the advantage of physical and chemical stability, wear and corrosion resistance[68-69]. In general, polyester contains at least 85 % by weight of an ester of a substituted aromatic carboxylic acid in its main and long chain. In general, the polyester fibers characteristics[70]:

- Strength;
- Resistance to stretching and shrinking;
- Resistance to most chemicals;
- Quick drying;
- Crisp and resilient when wet or dry;
- Wrinkle resistance;
- Mildew resistance;
- Abrasion resistance;
- Retains heat-set pleats and crease;
- Easily washed.

As seen in Table 3.1, it is widely used as a synthetic filaments and staple fibers source in many applications for industrial purposes such as tire cord fabric, some high performance industrial fibers and sewing yarns, and so forth[69]. It also shows high performance in modulus and tenacity with low water absorption and minimal shrinkage when compared with other industrial filaments. Therefore the importance of polyester fiber in all type of end-use of polyester polymer increases every year and has reached about 60 % of the world's total polyester polymer as fiber consumption in 2010[68].

Table 3. 1 Properties and application of polyester fibers at 21 ^{o}C and 65 % relative humidity[69].

Property	Phys. Unit	Filaments		Staple fibers	
		Regular	High breaking strength	Regular	High breaking strength
Applications		Weaves, knits	Tire cord fabric, industrial yarns	Mixtures with wool or cotton	Industrial fibers, sewing yarns
Density	g cm^{-3}	1.38	1.39	1.38	1.39
Module, textile	N/tex	6.6–6.8	10.2–10.6	2.2–3.5	4.0–4.9
Breaking strength, textile	N/tex	0.35–0.5	0.62–0.85	0.35–0.47	0.48–0.61
Elongation at rupture	%	24–50	10–20	35–65	17–40
Elast. recovery after 5% elongation	%	88–93	90	75–85	75–85
Moisture regain	%	0.4	0.4	0.4	0.4

In general, standard polyester fiber is considered as poly(ethylene terephthalate) fibers, however poly(trimethylene terephthalate), poly(butylene terephthalate), poly(1,4-cyclohexylene dimethylene terephthalate) are other types of polyester with a small percentage of total production[69].

3.2 High Tenacity, High Modulus Poly (ethylene terephthalate) (PET) Fibers

Poly(ethylene terephthalate) is one of the most important thermoplastic polymer resin of the polyester family and commonly used in synthetic fibers, liquid containers, polymer-matrix composite, medical and other technical areas, and widely used in our daily lives.

The modulus and tenacity of the melt-spun PET fibers is below those of the desired fibers to achieve high performance products. To improve mechanical properties and dimensional stability of PET fibers with an oriented structure and appropriate high crystallinity, many different types of technique have been developed. They are, in general, two-step spin draw processes, 1 or 2 step drawing high-speed spinning, zone drawing / zone annealing, solid-state extrusion, solution spinning, microwave heating, and vibrational hot drawing[4-5]. In the commercial application, one step with high speed spinning process is looking more promising as a low cost reduction method but the fibers show limited mechanical properties. Hence, two-step spin-draw technique is widely utilized in order to produce high modulus and strength, also low break elongation of PET fibers[4, 6].

One of the most successful methods to produce high modulus and high strength PET fibers from ultrahigh molecular weight is solution spinning techniques. However, this method has some disadvantages[7, 8], such as using organic solvent which is mainly toxic and expensive, also a very high draw ratio is needed.

Poly(ethylene naphthalate) (PEN) fiber is one of the high performance polyester fibers and has superior mechanical and tensile properties, also dimensional stability. Furthermore, it shows excellent thermal and electric properties, chemical resistance, and outstanding gas barrier properties[15]. PEN is derived from ethylene glycol, and 2,6-naphthalenedicarboxylic acid via a transesterification reaction to get a mixture of oligomers, and then a polycondensation is carried out to produce the PEN pre-polymer under the reduced pressure with the polymerization catalyst[15].

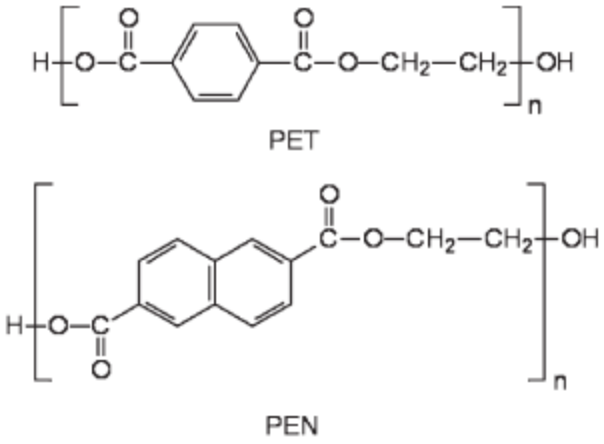

Figure 3. 1 Molecular structures of PET and PEN.

PEN fibers can be produced with the classical spin draw process, which consist of melt-extrusion, melt-spinning, and hot-drawing processes. On the other hand, high speed spinning process (higher than 4000 m/min) can be applied to obtain highly oriented and crystalline fibers in one step without the additional hot drawing process. Post-heat treatment is also carried out after spinning and drawing to improve the physical properties[15].

Morphology studies demonstrate that limited molecular orientation and crystallization is usually obtained by using the traditional melt-spinning process, which is one of the crucial problems to manufacture high performance fibers. Therefore, it is necessary to improve or modify the traditional melt-spinning process to produce filaments with high tenacity and crystallinity, low shrinkage and a high degree of orientation.

3.3 A Recent Developments of New High Performance Poly(ethylene terephthalate) Technology: Liquid Isothermal Bath

High modulus and high tenacity fibers offer an interesting arena to fiber manufacturers and scientists to create high performance products with high strength and greater stability. There are so many different types of methods available to produce high modulus and high strength PP and PET fibers as already been explained in the previous chapters.

In order to reduce production cost and improve the mechanical properties of PET fibers, in the 1990s, a novel melt-spinning process with the liquid isothermal bath (LIB) was developed to manufacture high performance PET fibers[9, 10]. A highly oriented, crystalline and modulus fiber with high tenacity was able to be produced by the LIB process. Dr. Cuculo et al.[9] developed a new method which related to a melt-spinning process to obtain a very high degree of orientation, high crystallinity, low shrinkage, and high tenacity. A melt spun PET fibers were directed into a liquid bath which was at least 30 ^{o}C above the glass transition temperature. After withdrawing the fibers, they were wound up at speed between 3000-7000 m/min (Figure 3.2). The filament could be obtained with high tenacity of 7-9 g/denier and a break elongation of 14-30 %.

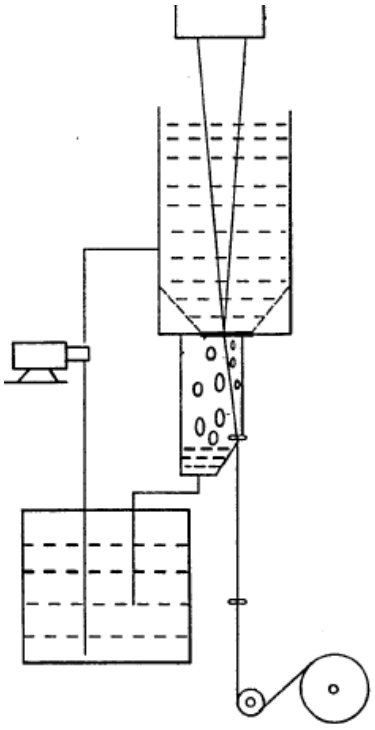

Figure 3. 2 Melt spinning of ultra-high oriented crystalline polyester filaments[9].

Afterwards, this method has been developed[10] for the synthetic melt spun fibers that were extruded into a liquid isothermal bath, and then a very low draw ratio was carried out after withdrawing the filaments from the bath (see Figure 3.3).

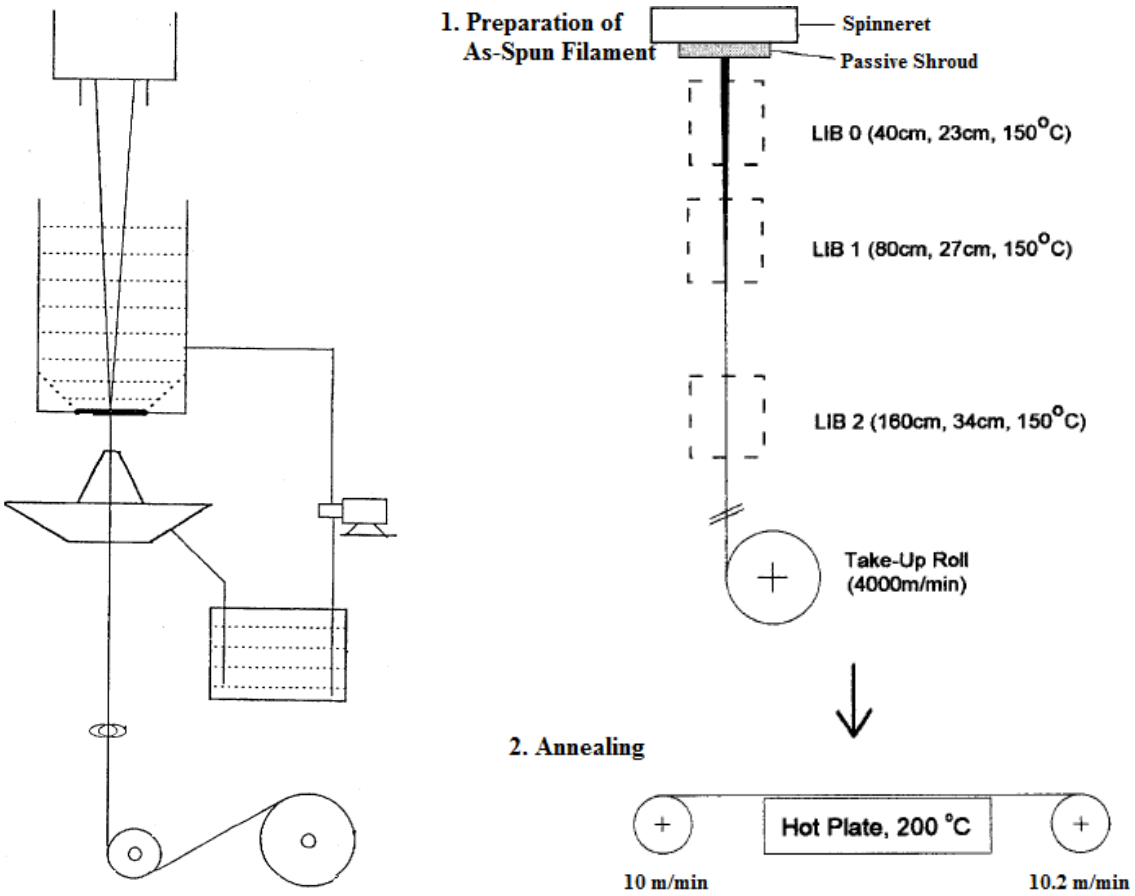

Figure 3. 3 Schematic diagram of melt spinning via liquid isothermal bath at different LIB positions[10, 71].

In a traditional melt spinning and drawn processes; the molten polymers are forced via spinning pumps through spinnerets to form filaments and then the molten filaments are cooled to achieve solidified filaments which have low crystallinity, orientation and inferior

mechanical properties. They are stretched or drawn in one or more steps to obtain a higher orientation of the polymer chains along the fiber axis but during this process low dimensional stability also can be occurred. For the melt spinning that was modified by liquid isothermal bath, the superior mechanical properties, excellent dimensional stability and controlled threadline dynamics can be manufactured with drawing (max DR of 1.5) and annealing processes. Table 3.2 shows the mechanical properties of fibers produced with and without LIB technique. It is clear that using LIB technology led to a tremendous improvement for tenacity and modulus values for PET fibers. For example, the fiber tenacity increased from 4.1 to 9.6 g/d by ca. 134 % with increasing the modulus value from 62.5 to 139.4 g/d by ca.123 % for as-spun fibers by using LIB technology. They also have higher tenacity and modulus performance against conventional commercial tire cords: 10.3 vs. 9.5 g/d for tenacity and 140.9 g/d vs. 96.1 g/d for the modulus.

Table 3. 2 Mechanical properties of fibers produced by the lib method[10].

	Tenacity (gpd)	Elonga-tion (%)	Modulus (gpd)	LASE-5% (gpd)	BOS (%)	Thermal Shrinkage (%)
As-spun LIB1	8.3	14.8	128.8	3.64	11.5	15.6
LIB1/DA*: DR = 1.1	9.1	10.7	138.9	5.49	—	—
LIB1/DA*: DR = 1.2	10.0	9.8	147.5	5.78	—	5.0
As-spun LIB2	9.6	10.5	139.4	5.07	10.0	15.2
LIB2/DA*: DR = 1.1	10.3	8.7	140.9	5.48	—	4.9
Unperturbed	4.1	67.5	62.5	1.23	3.0	3.5
Unperturbed*	5.7	16.1	116.8	3.13	—	3.3
DA, DR = 1.5						
Commercial 1	9.5	16.6	96.1	2.94	—	13.75
Commercial 2	7.4	16.5	87.9	3.31	—	6

DA = Drawn and annealed, DR = Draw ratio, BOS = Boil-off shrinkage
LIB 1 = Take-up speed of 3500 m/min, spinning denier 6 dpf (denier per filament), LIB depth 45 cm,
LIB 2 = Take-up speed of 5000 m/min, spinning denier 4.5 dpf, LIB depth 30 cm,
Unperturbed = Conventional spinning process, take-up speed 5000 m/min, spinning denier 4.5 dpf,
Commercial 1 = Conventional commercial tire cord,
Commercial 2 = Low shrinkage tire cord.
***Post Treated**

Numerous attempts have been made to observe as-spun, drawn and annealed PET filaments using the liquid isothermal bath modified spinning process[8-11, 71]. In general, Cuculo et al. have used high molecular weight PET chip (the intrinsic viscosity of the virgin chip of 0.97 dL/g) to manufacture all of the as-spun, drawn and annealed filaments. In one of their study, they examined the effect of LIB position on the spinning process to look at the structure and properties of as-spun and annealed filaments[71]. As seen in Figure 3.3, the effects of three

different LIB positions were observed: LIB0 was closest to the spinneret and LIB2 was farthest from the spinneret with the distance from the spinneret to the bottom of the bath of 40 and 160 cm, respectively. The depth of the liquid, (1,2-propanediol), was adjusted to 23 and 34 cm with the liquid temperature of 150 ^{o}C for all cases for LIB0 and LIB2, respectively, and a control sample (no LIB) was also produced. Subsequently, all produced filaments were annealed (Figure 3.3) with using a hot plate at the temperature of 200 ^{o}C. Figure 3.4 shows volume fraction of crystallinity and birefringence of LIB fibers at different LIB positions. Among these three LIB-treated samples through the annealing process, they had low volume fraction crystallinity than the control filaments after LIB and annealing treatment. The annealing process experienced a comparable increase in crystallinity for all samples. On the other hands, the LIB1 and LIB2 fibers showed higher birefringence than LIB0 and no LIB fibers before and after the annealing processes. These as-spun fibers showed similar or lower degree of crystallinity and highly oriented amorphous phase with lower degree of crystal growth after spun by LIB spinning system. These structural features were also confirmed by WAXS patterns. The authors hypothesized that very high level of threadline stress prevented local mobility of the constituent chains which lead to an increase in the overall orientation and hindered the growth of crystallites.

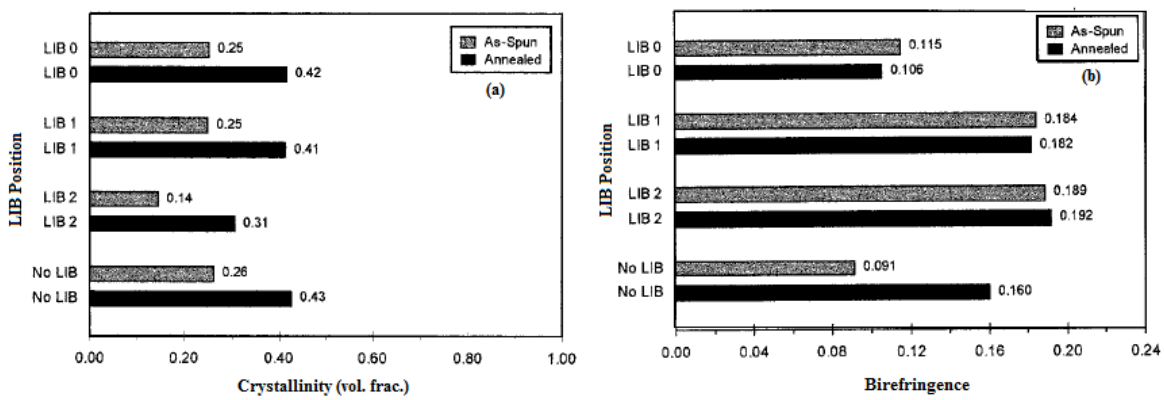

Figure 3. 4 (a) Volume fraction crystallinity, and (b) birefringence for as-spun and annealed PET filaments produced with and without LIB at different positions[71].

In addition, the as-spun no LIB filaments before and after annealing process demonstrated the lowest tenacity and modulus value of 3.45 and 5.57 g/d for tenacity, and 52.4 and 102.9 g/d for initial modulus, respectively. LIB technology that improved significantly the tenacity and modulus value from 3.45 to 8.39 g/d and from 52.4 to 114.8 g/d, respectively.

Finally a novel horizontal liquid isothermal bath (hIB) (Figure 3.4) has been developed to manufacture filaments with improved properties by the well-controlled generation of the precursor morphology, which is related to the crystallization, using the conventional melt-spinning processes[11]. It was then modified to not use only for laboratory scale work but also in the industry because of the feasibility, less capital equipment and energy sources.

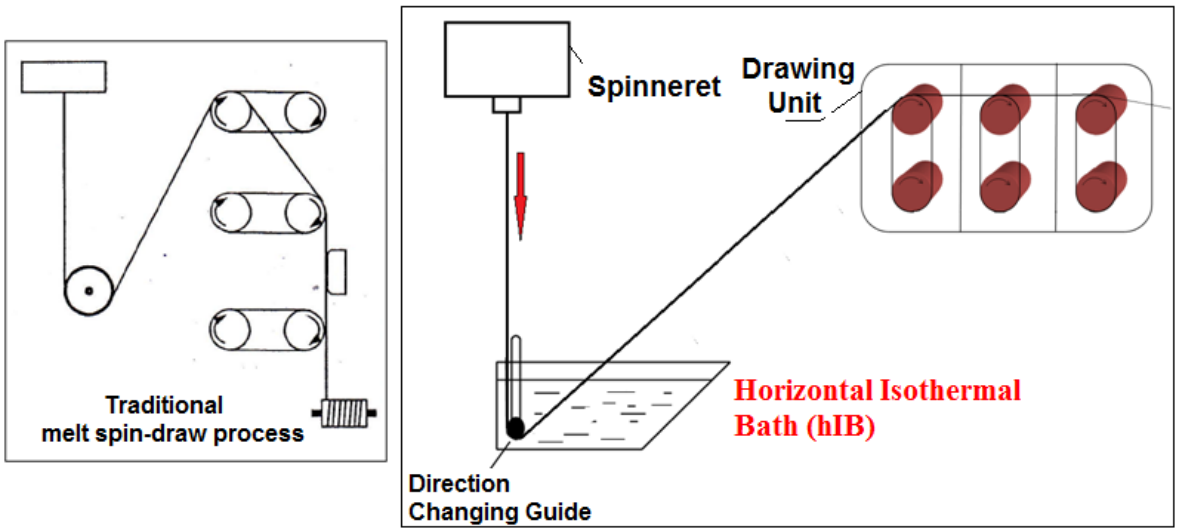

Figure 3. 5 Schematic comparison of traditional spin-draw and hIB processes.

One of the major problems of traditional melt-spinning process is that crystallization occurs during the spinning and drawing processes, that reduces chain mobility and molecular orientation, hence limited fiber properties are obtained. In addition, the precursor for crystallization is observed during drawing of the polyester samples, which temperature is close to the glass transition temperature (Tg), at a high strain and stain rate[11]. Hence, from the viewpoint of the transformation in the threadline, it is a fundamental point to extend the lifetime of the precursor to get high performance filament.

In the hIB system in which thermoplastic polymers can be used, the filaments are produced by melt-spinning technique into a liquid isothermal bath which has a higher temperature than glass transition temperature of the polymer[9, 10, 11]. Therefore, the polymer molecules get a

more chance to more thoroughly extend, orient and order during the mobile molten state. As a result, a very high degree of oriented crystalline synthetic filaments with high mechanical properties can be produced after very low draw ratios.

A number of experiments was attempted to investigate correlation between the fibers structural development and the production parameters for this technology by changing:

- the position of the hIB device,
- the liquid temperature,
- the liquid depth,
- the distance between the spinneret and the hIB device,
- take-up speed.

It has been found that the mechanical properties of the hIB-spun filaments, at a very low draw ratio, 1.28 DR, with the hot-drawn process that resulted in a dramatic increase in the tenacity. The fiber tenacity of 11.39 g/d was observed and the fiber modulus reached 134.9 g/d with the take-up speed of 3000 m/min at 7.78 for the fiber denier.

On the other hand, Chen et al.[11] studied various conditions to explore in detail physical properties of poly(ethylene naphthalate) (PEN) fibers. They demonstrated the fiber tenacity was much more affected by a take-up speed and liquid temperature. The fiber tenacity

increased with increasing take-up speed from 800 to 3000 m/min. In this work, the optimum process conditions were determined that the hIB device was placed 110 cm below the spinneret, and the liquid (at 135 ^{o}C) depth fixed at 25 cm with 4000 m/min take-up speed.

Table 3. 3 Mechanical properties of PEN fibers spun with and without hIB at 4000 m/min[11].

Fiber Sample		**Tenacity (g/d)**	**Modulus (g/d)**	**Elongation (%)**
Undrawn	no hIB	5.35	126.2	11.7
	hIB	7.27	114.5	12.8
Drawn	no hIB	7.31	173.0	8.7
(DR=1.40)				
	hIB	10.75	216.7	7.6

It can be seen from Table 3.3, tenacity of PEN fibers spun with hIB at 1.40 draw ratio showed more than 40 % higher value than that of the fibers without hIB. In general, this tenacity value is observed between 5-7 draw ratios for traditional melt–spinning technique. For the undrawn fibers with hIB, the modulus value was lower and the percent elongation at break value was higher than that of without hIB technology. Tenacity values for hIB as-spun fibers were increased by ca. 35.9 % from 5.35 g/d to 7.27 g/d. After the drawing, the

modulus increased from 173.0 g/d to 216.7 g/d by ca. 25.3% and the elongation at break decreased from 8.7 to 7.6 by ca. 12.6 % for no hIB and hIB fibers, respectively.

White color of the hIB fiber, which was related to the very unique morphology, was observed under certain conditions of time, tension and temperature. The distance between the hIB bath and spinneret, liquid depth and liquid temperature are important parameters for these certain conditions to obtain this unique morphology for the fibers. This color faded as well as the fibers lost wrinkling structure during hot drawing and gained a fibrillar structure with a high crystallinity (see Figure 3.6).

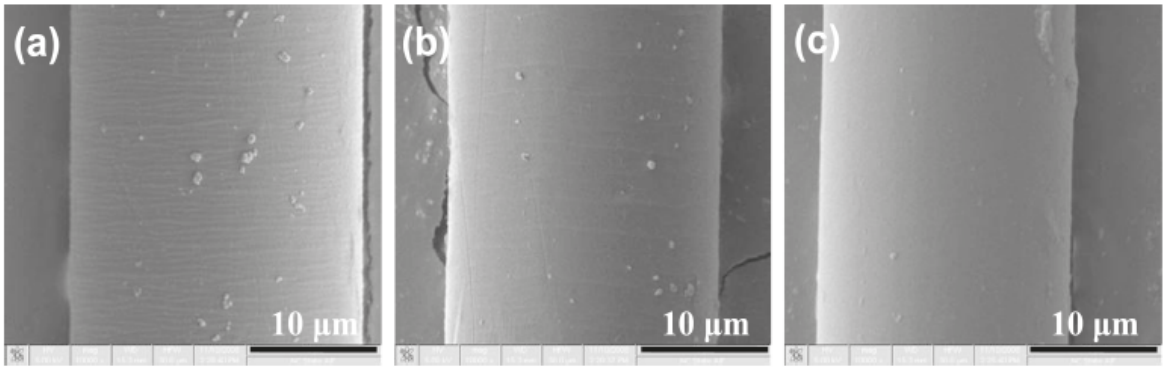

Figure 3. 6 SEM images of PEN fibers spun with hIB spinning system (a) undrawn zone, (b) transit zone between undrawn and drawn, and (c) drawn zone[11].

To investigate this phenomenon, three zones along the fiber were observed during drawing process by the heating tube. Undrawn zone is outside the tube, drawn zone is in the tube. It can be easily realized that the undrawn zone has some banded morphology which is a precursor for crystallization occurring or "mesophase", which has a high molecular orientation and low crystallinity[11]. Therefore, in the transit and drawn zone these periodic and compact bands start to disappear, hence a very high molecular orientation and a highly crystallized fibrillar structure were formed.

CHAPTER IV

4.1 Motivation

Melt-spinning, wet-solution spinning, dry-solution spinning, and gel spinning are the main methods to fabricate fibers from polymer materials. Depending on polymer type and applications, the polymers can be melted if they are thermoplastic, if not they may be dissolved in solvents or chemically treated to form soluble or thermoplastic derivatives to form the fluid state. This thick and viscous liquid is then forced through the tiny holes of a device called a spinneret to obtain a solidified filament. Indeed numerous advances have been made in the development and production of high performance fibers by these techniques. On the other hand, there are some disadvantages of these techniques that should be pointed out.

In the melt spinning technique the molten polymer without decomposition is directly extruded thorough the spinneret, and then solidified in a cooling chamber. Using separate drawing steps is one of the major disadvantages of the production of high performance filaments. Owing to this, an expensive capital investment, larger production area, more energy and labor are needed. In addition, higher molecular weight polymers should be used, therefore higher temperature above their melting point sometimes leads degradation and decomposition of the polymers which are also expensive. Most of the times, the end product shows poor and inadequate structural development which leads to limited fiber

applications[72]. The control of long production line is very critical for uniformity and it may cause higher amount of waste.

Wet spinning method is another technique that requires that the fiber forming polymer dissolves in a suitable solvent system. This polymer solution is then extruded through a spinneret that is submerged in a chemical bath with a reasonable temperature and pH to be coagulated and solidified. The production speed is low and sometimes more than one baths are required in order to remove the impurities and solvent from the polymer. It is a quite expensive method because of using solvent, chemical and capital investment. Using solvent and chemical with their recovery are crucial and need much more attention and sometimes become a problem for human health and environments[72, 73]. One of another important challenge is the control of filament cross-section because of inward and outward mass transfer process[72].

In the dry-solution spinning process, the filament forming polymers dissolve in volatile solvents and then the polymer solutions go through the spinnerets into a hot air stream, or inert gas, or air. The fibers solidify after removing the solvents in these streams. In this technique[72, 73], suitable volatile solvents should be used with a well-designed solvent recovery systems. The recovery systems should work very well and effectively to remove inflammable, flammable and toxic solvent vapors. The production rate is relatively low and sometimes an additional post treatment is needed to remove the residuals. The design of spinneret holes and diffusion with evaporation rate of solvents should be optimized to manufacture uniform outward mass transfer which sometimes leads to disrupt a circular

cross-section of the filaments. The environments and human health are two important issues and should be considered during the production.

4.2 Research Goals and Objectives

Understanding relationship between the production method and fiber properties is an important milestone to design and improve the production line. In addition, any type of new design should also be simple, cost effective, and have a less environmentally harmful impact than the existing methods. In this regards, the melt-spinning process with liquid isothermal bath (LIB) is looking promising to obtain high performance fibers [4, 6, 9-11, 71]. Eventually, the vertical liquid bath has been modified to a novel horizontal liquid isothermal bath (hIB)[11] which is cost-efficient, safer, easier, and also can be used in industrial spinning lines.

The first objective of this study is to develop of method for environmentally friendly, cost-efficient with high throughputs to produce a new type of high-tenacity and high-modulus polypropylene filaments. Isotactic polypropylene (*i*-PP) resin will be used for this purpose. It is well known that *i*-PP is one of the most crucial polymers which are extensively used in industries and research purposes. Our goal is to study isotactic polypropylene under influence of environmentally friendly liquid and spinning conditions to observe possible polymorphic transformations that will be supported with structural and morphological

analysis, and performance studies. During our studies and investigation, we obtained a new class of high-tenacity and high-modulus polyolefin monofilament fiber with unique structural and morphological characteristics imparted by environmentally friendly technique (ECOB)'s novel fiber forming process. The second aim involves using the existing hIB technology to obtain high performance polypropylene fibers and compare the structural and performance properties with ECOB technology. Production of high performance polypropylene fibers spun with hIB method will be a first time study in this area.

In industry, high performance poly(ethylene terephthalate) (PET) fibers are produced from polymer chips having IV close to or higher than 1 dL/g by using the traditional melt spinning methods with very high draw ratios. In this study, hIB spinning technique was used with low molecular weight PET chips to manufacture superior fiber properties by applying a draw ratio lower than 1.3. The third purpose of this study will focus on to demonstrate, for the first time, the production of high performance PET fibers from a standard molecular weight PET chip with hIB technology.

References

1. Hearle J. W. S. (2001). *High Performance Fibres*. Boca Raton, FL: Woodhead Publishing.

2. Kerr, M., Chawla, N., & Chawla K., K. (2005). The cyclic fatigue of high performance fibers. *JOM*, 67–70.

3. Kotek, R. (2008). Recent advances in polymer fibers. *Polymer Reviews*, 48, 221–229.

4. Wu, G., Zhou, Q., Chen, J. Y., Hotter, J. F., Tucker, P. A., & Cuculo J. A. (1995). The effect of a liquid isothermal bath in the threadline on the structure and properties of poly(ethylene terephthalate) fibers. *Journal of Applied Polymer Science,* 55, 1275-1289.

5. Hobbs, T., & Lesser, A. J. (2000). Preparation of high performance poly(ethylene terephthalate) fibers: two-stage drawing using high pressure CO_2. *Polymer*, 41, 6223–6230.

6. Wu, G., Jiang, J. D., Tucker, P. A., & Cuculo J. A. (1996). Oriented noncrystalline structure in PET fibers prepared with threadline modification process. *Journal of Polymer Science: Part B: Polymer Physics*, 34(12), 2035-2047.

7. Ito, M., Takahashi, K., & Kanamoto, T (1990). Preparation of high-modulus and high- strength fibers from high molecular weight poly (ethylene terephthalate). *Journal of Applied Polymer Science,* 40, 1257-1263.

8. Wu, G, & Cuculo, J. A. (1995). Preparation of high performance pet fiber by solution spinning technique. *Journal of Applied Polymer Science,* 56, 869-875.

9. Cuculo J. A. et al. (1992). US patent: US005149480A. Melt spinning of ultra-oriented crystalline polyester filaments.

10. Cuculo J. A. et al. (1998). US patent: US005733653A. Ultra-oriented crystalline filaments and method of making same.

11. Chen, P., Afshari, M., Cuculo, J. A., & Kotek R. (2009). Direct formation and characterization of a unique precursor morphology in the melt-spinning of polyesters. *Macromolecules,* 42, 5437–5441.

12. Grujicic, M., Bell, W. C., Arakere, G., He, T., Xie, X., & Cheeseman B. A. (2010). Development of a meso-scale material model for ballistic fabric and its use in flexible-armor protection systems. *JMEPEG,* 19, 22–39.

13. Xu, T., & Farris, R. J. (2007). Comparative studies of ultra high molecular weight polyethylene fiber reinforced composites. *Polymer Engineering and Science*, 47(10), 544–1553.

14. Polyester fiber. As viewed on line at (April 4th 2012):

http://www.fibersource.com/f-tutor/polyester.htm

15. Chen, P., & Kotek, R. (2008). Advances in the production of poly (ethylene naphthalate) fibers. *Polymer Reviews,* 48, 392–421.

16. Lewin M. (2007). *Handbook of Fiber Chemistry*. Baco Raton, FL: CRC Press. 2007; 3rd Ed.

17. Mukhopadhyay, S., Deopura, B. L., & Alagirusamy, R. (2004). Production and properties of high-modulus–high-tenacity polypropylene filaments. *Journal of Industrial Textiles*, 33(4), 245-268.

18. Porter, R. S., & Wang, L. (1995). Uniaxial extension and order development in flexible chain polymers. *Journal of Macromolecular Science, Part C: Polymer Reviews,* 35(1), 63-115.

19. Li, Z., Na, B., Tian, N., Lv, R., & Zou S. (2012). Enhanced molecular orientation and strain hardening in melt-spun isotactic polypropylene monofilaments through partial melting recrystallization. *Journal of Applied Polymer Science,* 123, 995–999.

20. Gomez, M. A., Tanaka, H., & Tonelli A. E. (1987). High-resolution solid-state 13C nuclear magnetic resonance study of isotactic polypropylene polymorphs. *Polymer*, 28, 2227-2232.

21. Colombe, G., Gree, S., Lhost, O., Dupire, M., Rosenthal, M., & Ivanov, A. D. (2011). Correlation between mechanical properties and orientation of the crystalline and mesomorphic phases in isotactic polypropylene fibers. *Polymer,* 52(24), 1-14.

22. Kotek, J., Raab, M., Baldrian, J., & Grellmann, W. (2002). The Effect of specific β-nucleation on morphology and mechanical behavior of isotactic polypropylene. *Journal of Applied Polymer Science*, 85, 1174- 1184.

23. Balzano, L., Rastogi, S., & Peters, G. W. M. (2009). Crystallization and precursors during fast short-term shear. *Macromolecules*, 42, 2088-2092.

24. Yakushenok, G. N., Genis, A. V., Machalaba, N. N., & Fetisova, A. A. (2011). Current state and outlook of global chemical fibre and thread market development. *Fibre Chemistry,* 43(1), 10-17.

25. Shahi, Z. T. M., & Mojtahedi, M. R. M. (2010). Effect of blending two fiber-grade polypropylenes with different molecular weight distributions on the physical and structural properties of melt-spun filament yarns. *Journal of the Textile Institute*, 101(6), 547-555.

26. Sakurai, T., Nozue, Y., Kasahara, T., Mizunuma, K., Yamaguchi, N., Tashiro, K., & Amemiya, Y. (2005). Structural deformation behavior of isotactic polypropylene with molecular characteristis during hot drawing process. *Polymer,* 46(20), 8846–8858.

27. Andreassen, E., & Myher, O. J. (1993). Infrared spectroscopy measurements of residual stresses in polypropylene fibers. *Journal of Applied Polymer Science,* 50, 1715–1721.

28. Kamezawa, M., Yamada, K., & Takayanagi, M. (1979). Preparation of ultrahigh modulus isotactic polypropylene by means of zone drawing. *Journal of Applied Polymer Science,* 24, 1227-1236.

29. Misra, S., Lu, F. M., Spruiell, J. E., & Richeson, G. C. (1995). Influence of molecular weight distribution on the structure and properties of melt-spun polypropylene filaments. *Journal of Applied Polymer Science,* 56, 1761–1779.

30. Bond, E. B., & Spruiell, J. E. (2001). Melt spinning of metallocene catalyzed polypropylenes. I. On-line measurements and their interpretation. *Journal of Applied Polymer Science,* 82, 3223–3236.

31. Kavesh et al. (1983). US Patent: 4,413,110. High tenacity, high modulus polyethylene and polypropylene fibers and intermediates therefore.

32. Iijima, M., & Strobl, G. (2000). Isothermal crystallization and melting of isotactic polypropylene analyzed by time- and temperature-dependent small-angle x-ray scattering experiments. *Macromolecules*, 33, 5204-5214.

33. Wang, I. C., Dobb, M. G., & Tomka, J. G. (1996). Polypropylene fibres: exploration of conditions resulting in high tenacity. *Journal of the Textile Institute,* 87, 1-12.

34. Wang, I. C., Dobb, M. G., & Tomka, J. G. (1995). Polypropylene fibres: an industrially feasible pathway to high tenacity. . *Journal of the Textile Institute,* 86, 383-392.

35. Ohta, T., Takada, A., Yamamura, T., Kawaguchi, A., & Murakami S. (1995). The ultra-drawing behaviour of ultra-high molecular- weight polyethylene: comparison of

the gel-like spherulite pressing method and the gel-casting method. *Polymer*, 36, 2181-2187.

36. Sheehan, W. C., & Cole, T. B. (1964). Production of super-tenacity polypropylene filaments. *Journal of Applied Polymer Science,* 8, 2359-2388.

37. Yamada, K., Kamezawa, M., & Takayanagi, M. (1981). Relationship between orientation of amorphous chains and modulus in highly oriented polypropylene. *Journal of Applied Polymer Science,* 26, 49-60.

38. Noether, H. D. (1979). Morphology and mechanical properties of some spin oriented polypropylene fibres. *Progress in Colloid and Polymer Science,* 66, 109-112.

39. Mukhopadhyay, S., Deopura, B. L., & Alagirusamy R. (2006). Effect of drawing different mfi polypropylene filaments on a gradient heater. *AUTEX Research Journal*, 6(3), 136-141.

40. Samuels, R. J. (1968). Quantitative characterization of deformation in drawn polypropylene films. *Journal of Polymer Science Part A*, 6, 1101-1139.

41. Taylor, W. N., & Clark, E. S. (1978). Superdrawn filaments of polypropylene. *Polymer Engineering & Science*, 18(6), 518-526.

42. Cansfield, D. L. M., Capaccio, G., & Ward, I. M. (1976). The preparation of ultra-high modulus polypropylene films and fibres. *Polymer Engineering & Science*, 16(11), 721-724.

43. De Candia, F., Romano, G., Baranov, A.O. & Prut, E. V. (1992). Dynamic-mechanical behavior of highly drawn isotactic polypropylene. *Journal of Applied Polymer Science*, 46, 1799-1806.

44. Ohta, T. (1983). Review on processing ultra high tenacity fibers from flexible polymer. *Polymer Engineering and Science*, 23(13), 697-703.

45. Lyoo, W. S., Lee, H. S., Ji, B. C., Han, S. S., Koo, K., Kim, S. S., Kim, J. H., Lee, J. S., Son, T. W., & Yoon, W. S.(2001). Effect of zone drawing on the structure and properties of melt-spun poly(trimethylene terephthalate) fiber. *Journal of Applied Polymer Science*, 81, 3471–3480.

46. Kunugi, T., Ito, T., Hashimoto, M., & Ooishi M. (1983). Preparation of high-modulus and high-strength isotactic polypropylene fiber by zone- annealing method. *Journal of Applied Polymer Science*, 28, 179-189.

47. Suzuki A., Sugimura T., & Kunugi T. O. (2001). Mechanical properties and superstructure of isotactic polypropylene fibers prepared by continuous vibrating zone-drawing. *Journal of Applied Polymer Science*, 81, 600–608.

48. Chawla, K. K. (2005). *Fibrous Materials*. Cambridge: Cambridge University Press, Technology & Engineering.

49. Coates, P. D., & Ward, I. M. (1979). Drawing of polymers through a conical die. *Polymer*, 20, 1553-1560.

50. Richardson, A., Ania, F., Rueda, D. R., Ward, I. M., & Balta, F .J. C. (1985). The production and properties of poly(aryletherketone) (PEEK) rods oriented by drawing through a conical die. *Polymer Engineering & Science,* 25, 355–361.

51. Shaw, M. T. (1975). Flow of polymer melts through a well-lubricated, conical die. *Journal of Applied Polymer Science*, 19, 2811-2816.

52. Laughner, M. P., & Harrison, I. R. (1988). Hot nip drawing: a rapid method of producing high modulus polypropylene films. *Journal of Applied Polymer Science*, 36, 899-905.

53. Smith, P., & Lemstra, P. J. (1979). Ultrahigh-strength polyethylene filaments by solution spinning/drawing, 2a influence of solvent on the drawability. *Makromol Chem*, 180, 2983-2986.

54. Afshari, M., Sikkema, D. J., Lee, K., & Bogle M. (2008). High performance fibers based on rigid and flexible polymers. *Polymer Reviews*, 48, 230–274.

55. Cebe, P., & Grub, D. B. (1985). Gel-drawn fibres of poly(vinyl alcohol). *Journal of Materials Science,* 20, 4465-4478.

56. Kavesh et al. (1983). US Patent: 4,413,110. High tenacity, high modulus polyethylene and polypropylene fibers and intermediates therefore.

57. Kristiansen, M., Tervoort, T., & Smith, P. (2003). Synergistic gelation of solutions of isotactic polypropylene and bis-(3,4-dimethyl benzylidene) sorbitol and its use in gel-processing. *Polymer*, 44, 5885–5891.

58. Machiels, A. G. C., Denys, K. F. J., Van Dam, J., & De Boer A. P. (1997). Effect of processing history on the morphology and properties of polypropylene/thermotropic liquid crystalline polymer blends. *Polymer Engineering and Science*, 37(1), 59-72.

59. Echevarria, G. G., Eguiazabal, J. I., & Nazabal, J. (2000). Morphology and mechanical properties of direct injection molded polypropylene thermotropic copolyester blends. *Polymer Composites*, 27(6), 864-871.

60. Jin, X., & Li, W. (1995). Correlation of mechanical properties with morphology, rheology, and processing parameters for thermotropic liquid crystalline polymer-containing blends. *Journal of Macromolecular Science - Reviews in Macromolecular Chemistry & Physics*, 35(1), 1-13.

61. Esthappan, S. K., Kuttappan, S. K., & Joseph, R. (2012). Thermal and mechanical properties of polypropylene/titanium dioxide nanocomposite fibers. *Materials and Design,* 37, 537–542

62. Lee, H. S., & Ryoun, Y. J. (2008). Properties of polypropylene/layered silicate nanocomposites and melt-spun fibers. *Journal of Applied Polymer Science*. 109, 1221-1231.

63. Hussain, F., Hojjati, M., Okamoto, M., & Gorga, R. E. (2006). Polymer-matrix nanocomposites, processing, manufacturing, and application: An Overview. *Journal of Composite Materials*. 40(17), 1511–1565

64. Garcia, M., Van, V. G., Jain, S., Schrauwen, B. A., Sarkissov, A., & Van, Z. W. E. (2004). Polypropylene/SiO2 nanocomposites with improved mechanical properties. *Advanced Materials Science*. 6, 169–175.

65. Ruan, W. H., Mai, Y. L., Wang, X. H., Rong, M. Z., & Zhang, M. Q. (2007). Effects of processing conditions on properties of nano-SiO2/polypropylene composites fabricated by pre-drawing technique. *Composites Science and Technology*. 67, 2747–2756.

66. Madani M. (2010). Mechanical properties of polypropylene filled with electron beam modified surface-treated titanium dioxide nanoparticles. *Journal of Reinforced Plastics and Composites*. 29(13), 1999-2014.

67. Selvina, T. P., Kuruvillab, J., & Sabua, T. (2004). Mechanical properties of titanium dioxide-filled polystyrene microcomposites. *Materials Letters.* 58, 281– 289.

68. Lina, W., Yanwei, Wang, Z. D., Xuelian, X., Wentao, L., Suqin, H., & Chengshen, Z. (2011). Discussion on production of flat cross-section industry polyester filament. *Advanced Materials Research.* 332-334, 526-529.

69. Eyerer, P. (2010). *Polymers - Opportunities and Risks I: General and Environmental Aspects: Chances and Risks (The Handbook of Environmental Chemistry).* Berlin Heidelberg: Springer-Verlag Publishing.

70. Polyester fiber. As viewed on line at (April 4th, 2012):

http://www.fibersource.com/f-tutor/polyester.htm

71. Hotter, J. F., Cuculo, J. A., Tucker, P. A., & Annis B. K. (1998). Effect of liquid isothermal bath position in modified poly (ethylene terephthalate) PET melt spinning process on properties and structure of as-spun and annealed filaments. *Journal of Applied Polymer Science*. 69, 2051–2068.

72. Mishra, S. P. (2000). *A Text Book of Fibre Science and Technology*. New Delhi: Age International.

73. Types of Spinning (Man-Made Fibers). As viewed on line at (April 5th 2012): http://textileengineerr.blogspot.com/2010/10/types-of-spinning-man-made-fibers.html

CHAPTER V

Developing an Ecologically Friendly Isothermal Bath to Obtain a New Class High-Tenacity and High-Modulus Polypropylene Fibers

Keywords: Ecologically friendly bath, high performance, high throughputs, a new family polypropylene fiber.

To be submitted to *Journal of Materials Science*

5.1 Abstract

A number of production methods have been developed for high performance fibers; however, most processes use toxic solvents or generate a lot of by-products. Our research resulted in the development of a new family of high performance polypropylene (PP) fibers by utilizing simple, ecologically friendly bath (ECOB). Various commodity polymers can be used with ECOB melt spinning system at high throughputs and performance benefits. The treated as-spun PP fibers had highly oriented, but not crystalline precursor morphology with f_a up to 0.6 generating superior mechanical properties. After drawing at DR of 1.49 at 120 ^{o}C highly oriented crystalline and amorphous phases were achieved for the drawn fibers with the f_c and f_a value of 0.95 and 0.87, respectively. This fine structure for the ECOB treated fibers resulted in the tenacity close to 12 g/d, initial modulus higher than 150 g/d, and ultimate elongation at break of 20 %. The polymer melting point of new fibrillar PP fibers increased by 9 ^{o}C.

5.2 Introduction

High performance polypropylene fibers are extensively used in industry and many daily applications such as sport and specialty fabrics, cords, packaging, ropes[1, 2], geotextiles, automotives, etc. So far considerable research has been performed to improve mechanical properties of PP fibers by utilizing melt spinning, wet, dry, and gel spinning techniques. Understanding the mechanism of single crystal growth, degree of molecular orientation in amorphous regions, and the formation of crystallization precursor is very essential for the production of these fibers with the wide range of properties.

The theoretical strength and the modulus for polypropylene are 3.9 GPa and 35–42 GPa respectively[3]. However, commercial textiles PP fibers have much lower tenacity in the range from 4.5 to 6 g/d. Technical fibers with the highest tenacity value around 9 g/d must be drawn with complex production lines and/or by using chemical treatments during the manufacturing process. These facts clearly document that there is still a big gap between theoretical and mechanical properties of PP fibers attainable by using the current spinning technologies. Our research team took this as a challenging opportunity to develop new sophisticated processes.

It is known that the linear chains can be highly oriented in the fibers and yield a higher degree of crystallinity and a unique microstructure. The stereoregular placement of pendant methyl groups in isotactic-PP (*i*-PP) causes the facile packing and crystallization. However, the atactic PP chains with their random distribution of methyl substituents cannot pack tightly and crystallize. In addition, the random alignment and orientation for semicrystalline polymers lead to insufficient and lower strength and modulus values. *i*-PP shows a variety of

crystalline forms which are monoclinic α-crystallites, hexagonal β-structures, orthorhombic γ-polymorphs and 'smectic' meso-phase[17]. These different types of crystalline structures can be observed at different process conditions with each type having unique characteristics. For example α-crystalline form is thermodynamically stable but β-crystalline form is thermodynamically metastable[4, 5, 6].

The as-spun PP filament is considered as a semicrystalline fiber in which crystals are dispersed in an amorphous matrix. The traditional melt spinning technology is widely accepted and used by industry because it is simple, and do not require any mass transfer or adding chemical complexities. The crystallization and orientation for crystals and amorphous regions mainly depend on molecular weight, molecular weight distribution, take-up velocity, melt temperature, drawing temperature and ratios[7]. However, in the melt spinning and drawing process the crystallization is limited by the poor mobility of polymer chains in the solid state with the lower degree of molecular orientation. Hence, fibers may lack desired properties. Microfibrils consist of alternating folded-chain lamellae and amorphous regions between these lamellae, which make continuous structure within conventional fibers[17]. Tie molecules connect these lamellae in the longitudinal direction which mainly affect fibers modulus and strength.

Numerous studies showed that there is a strong relationship between the structural development and spinning conditions of the melt spinning process. For example, (i) increasing the cooling rate and rapid quenching for extruding fibers and then drawing at slow rates with high draw ratios (DR) or (ii) slow two-stage drawing process are two important

methods of manufacturing high performance fibers[8]. Sheehan et al.[9] used water for quenching with a lower take-up speed to obtain paracrystalline structure, hence the fibers drawn more easily than the fibers having well developed crystalline structure. After drawing at 130–135 ^{o}C in oven with 35 draw ratio, the filaments showed more than tenacity value of 13 g/d.

It is well known that molecular weight (MW) and molecular weight distribution (MWD) have a great influence on polymer elongational viscosity, degree of crystallinity, strength, modulus, and elongation at break[3, 10-11]. Researchers worked on the effect of MW and MWD on fiber performance by correlating them with the process conditions[3, 10, 41]. Spruiell and Richeson[12] observed that higher MW with narrow MWD leads to a higher tensile strength of spun filament.

Taylor and Clark[13] proposed production of 'superdrawn' polypropylene filaments in two-step discontinuous process at elevated temperatures. The optimum draw temperature was determined as 130 ^{o}C and the fibers were drawn 10 mm/min to 1 mm/min to obtain very high draw ratios of more than 25x by two-stage tensile drawing. The resulting fibers showed higher number of tie molecules by forming unfolding of chains. At a very high draw ratio spherulite deformation is divided into two stages i.) lamellar slip leading to *c*-axis orientation until obtaining fully oriented structure, and ii.) the additional extension causes a new type of deformation mechanism which is called crystal cleavage that leads the formation of the fibrillar structure[14].

To obtain the nearest possible performance to the theoretical values of the tenacity and elastic modulus, researchers have been working on various deformation methods to increase the orientation in amorphous regions and crystallinity percentage. A zone-drawing and zone-annealing method[3, 15], continuous vibrating zone-drawing (CVZD)[16], constant load oven drawing[17-18], die drawing[3, 19-20], hot nip drawing[21], gel spinning technique[22-23], adding reinforcing agents[24-29] are some important techniques to improve mechanical properties and dimensional stabilities of PP fibers. On the other hand, many of these methods have not been commercialized because they have some disadvantages. For instance, these methods, in general, need larger production areas, require waste recovery system, high energy consumption, and the use of solvents. The techniques can be discontinuous and quite expensive. Moreover the control of filament cross-section, higher amount of waste, very low production rate, and the issue of giving harm to the environment and human health are some other important concerns.

The key aspect of our research is the use of melt-spinning combined with the wet spinning[30-32]. The goal was to design an ecologically friendly bath (ECOB) producing highly oriented and noncrystalline precursor before the drawing process. Some of the important features of this eco-friendly method in simplicity, industrial applicability and cost effectiveness. Moreover, the method utilizes a lower molecular weight making it more practical. After drawing with a very low draw ratio (DR<1.5) the efficient polymer chain orientation can be achieved with highly crystalline and ordered structure for *i*-PP fibers.

5.3 Experimental

5.3.1 Materials and Production Methodology

Exxon fiber forming polypropylene PP3155 with density of 0.900 g/cm^3 and Total PP 3462 having density of 0.905 g/cm^3 were used in this study. PP fibers were produced via a Fourne single-screw extruder which had a single-hole with hyperbolic spinneret of 0.6 mm exit diameter. The take-up speeds were fixed around 3000 m/min for PP fibers during the collection of all control, without treatment and ECOB **(**ecological bath consisting of a nontoxic fluid) treated filaments.

The PP as-spun fibers with and without ECOB were then drawn by using a modified Instron tensile testing machine with 60 cm long heating tube. The draw speed was adjusted to 50 mm/min, and the draw temperature was between 120 and 150 ^{o}C for PP fibers. The production distance and ECOB depth are represented in Figure 5.1.

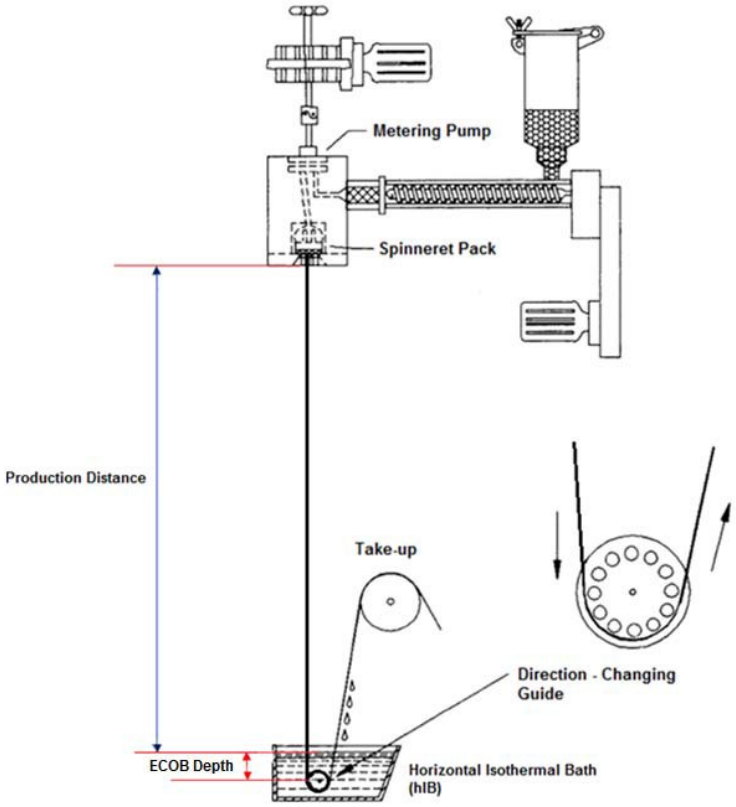

Figure 5. 1 Melt spinning process with ECOB spinning system[33].

5.3.2 Experiments and Characterization

Deniers of the monofilaments were determined using Vibromat ME Tester by measuring its resonant frequency. Tensile testing of individual filaments was carried out subsequently. The fiber modulus and tenacity (gf/denier), and also strain at break were investigated using a MTS Q-test/5 universal testing machine using TestWorks 4EM V4.11B software according to ASTM D3822. Gauge length of 25.4 mm and the constant cross-head speed of 15 mm/min were utilized. 5 pounds load cell was applied for PP drawn fibers with ECOB, and sometimes 50 g load cell used for PP as-spun and drawn fibers produced without ECOB spinning system.

The morphology, microstructure and fibers images were obtained using field emission scanning electron microscopy (SEM). In order to examine the fiber cross-section, the filaments were fractured after immersing in liquid nitrogen. The cross-section as well as sample surfaces were observed using JEOL 6400 which is a Cold Field Emission Scanning Electron high resolution microscope. Fibers were coated with a layer of Au/Pd with 0.5-30keV accelerating voltage.

Wide-angle X-ray diffraction (WAXD) measurements were performed using Rigaku SmartLab X-ray Diffractometer (XRD) equipped with $CuK\alpha$ radiation source, λ=1.542 Å, generated at 40 kV and 44 mA. The diffracting intensities were recorded every 0.02^{o} from 2θ scans in the range 5 – 30^{o} for PP. Crystallites sizes were calculated using the Scherrer equation (1) [34]:

$$L_{hkl} = \frac{K\lambda}{\beta cos\Theta} \quad (1)$$

where β is the peak half width, K is taken to be unity, λ is the radiation wavelength (1.542 Å), and ɵ is the Bragg angle.

The crystalline orientation factor (f_c) can be calculated using equation 2 [33, 45]:

$$f_c = \frac{(3\times < \cos^2 \varphi_{c,z} > -1)}{2} \quad (2)$$

$$< cos^2 \varphi_{(110)or(040),z} >= \frac{\int_0^{\pi/2} I(\varphi) sin\varphi cos^2\varphi \, d\varphi}{\int_0^{\pi/2} I(\varphi) sin\varphi \, d\varphi} \quad (3)$$

$$< cos^2 \varphi_{(c,z)} >= 1 - 1.099 < cos^2 \varphi_{(110),z} > -0.901 < cos^2 \varphi_{(040),z} > \quad (4)$$

where $\varphi_{c,z}$ is the angle between the *c* crystallographic axis and the fiber axis. The azimuthal intensity distributions for the (110) and (040) planes reflections were used in order to determine crystalline orientation factor (f_c).

The amorphous orientation factor, f_a, was determined by using the Stein and Norris equation (5) in which the overall measured fiber birefringence (Δn) was also used[33]. In addition, the calculated density[46] of the all fibers can be determined by using its degree of crystallinity from the DSC heating scan.

$$f_a = \frac{\Delta n - \chi f_c \Delta n_0^c}{(1-\chi)\Delta n_0^c} \qquad (5)$$

where Δn_0^c and Δn_0^a represent the intrinsic birefringence of the crystalline and the amorphous regions with the value of 0.0291 and 0.06, respectively[47].

A Perkin Elmer Diamond DSC Model 7 with Pyris software version 5 was used to observe thermal traces of ECOB treated (T) and untreated (U) fibers. A 3-5 mg polymer sample was encapsulated in a non-volatile aluminum pan and then heated at the heating rate of 20 ^{o}C /min under a flow of nitrogen gas to 200 ^{o}C. The degree of crystallinity of PP fibers was calculated from equation (6)

$$\text{Degree of crystallinity (\%)} = \frac{\Delta H_f x 100}{\Delta H_f^0} \qquad (6)$$

where ΔH_f is the heat of fusion of PP fibers. ΔH_f^0 is heat of fusion of 100 % crystalline PP which is 209 J/g[35].

A Nikon polarizing microscope was used in order to determine fibers birefringence by using a series of mineral oil refractive index liquids. The birefringence value (eq (7)) was determined after the mean value of at least three individual sample measurements[34].

$$\Delta n = n_{II} - n_{\perp} \qquad (7)$$

where n_{II} and $n_{\perp}$ are parallel and perpendicular refractive index of the sample, respectively.

5.4 Results and Discussion

5.4.1 Tensile Properties of As-Spun and Drawn Filaments

Although Exxon PP3155 type chips, (Table 5.1), were first used to develop good mechanical properties, there were some spinning problems. This high melt flow rate polymer was not very suitable to be used with various ECOB liquids, bath temperature, ECOB depth, and so on to explore the superior fiber mechanical properties in more details. Total PP 3462 chips had lower melt flow rate and gave us much better spinning performance.

Table 5. 1 Technical data for Exxon and Total chip with their respective fibers[36, 37].

Polymer type	Melt flow rate (g/10 min.)	Density (g/cm^3)	Tenacity (g/d)	Elongation at break (%)
Exxon PP3155	36	0.900	3.1	150
Total PP 3462	4.1	0.905	5.8	28

* DR of 6.

One of the most attractive mechanical properties of PP fibers spun with ECOB is their ultra-high tenacity and high-modulus. Table 5.2 demonstrates the spinning conditions of PP fibers spun with and without ECOB technology. It appears that our novel manufacturing method can be applied to produce high tenacity and high modulus PP fibers. The take-up

speed velocity was set around 3000 m/min with three different liquid temperatures, 50, 75 and 95 ^{o}C, and three different production distances between the spinneret and bath, namely 90, 130 and 170 cm to observe the effect of different process parameters on the fiber properties.

Table 5. 2 Spinning conditions of polypropylene fibers spun with/without ECOB.

Sample ID	Take-up speed (m/min)	Liquid temp. (^{o}C)	Liquid depth (cm)	Distance (cm)	Denier
ECOB000	2891			90	8.47±0.28
ECOB00	2891	Control (Untreated)		130	7.94±0.20
ECOB0	2891			170	11.07±0.78
ECOB111	2933			90	11.42±0.36
ECOB11	2933	50	20	130	11.37±0.16
ECOB1	2921			170	11.35±0.18
ECOBE*	**2909**	**50**	**20**	**170**	**10.60±0.14**
ECOB222	2916			90	11.28±0.29
ECOB22	2916	75	20	130	12.26±0.22
ECOB2	2916			170	11.13±0.33
ECOB333	2908			90	11.58±0.19
ECOB33	2908	95	20	130	11.20±0.18
ECOB3	2908			170	11.07±0.29

*Exxon PP3155

As shown in Table 5.3, at the ECOB temperature of 50 ^{o}C the treated as-spun fiber had not only slightly higher strength but also much higher initial modulus than the control fibers spun with traditional method. It should be pointed out that the fibers produced from 90 and 130 cm production distance could not reach 11 denier for control samples because of the quench and the cooling rate prior to fiber solidification. The tenacity and modulus increased respectively by ca. 12.10, 13.04, and 17.50 % for 90, 130 and 170 cm production distance when compared with to their respective as-spun control fibers (Table 5.3). The highest increase for modulus at the same distance of 170 cm by ca. 89.66 % from 36.57±6.28 to 69.36±3.92 g/d was observed. The corresponding changes in tenacity were from 5.03±0.09 to 5.91±0.08 g/d. Furthermore, elongation at break for the control fibers (see Table 5.3) were 121.31±7.30, 172.64±14.19, 213.90±15.13 % and decreased dramatically to 50.41±4.25, 64.47±2.67, and 64.81±3.35 % for ECOB fibers spun at 90, 130 and 170 cm distance, respectively. It is also interesting to note that the ECOB fibers produced from Exxon PP3155 chips showed slightly higher tenacity of 6.21±0.12 g/d, and modulus value of 81.42±3.82, when compared to the corresponding ECOB fibers produced from Total PP3462.

Table 5. 3 Mechanical properties of polypropylene fibers spun with ECOB at 50 °C.

Sample ID	Denier	Tenacity (g/d)	Modulus (g/d)	Elongation (%)
ECOB000	8.47±0.28	4.71±0.08	53.91±2.81	121.31±7.30
ECOB00	7.94±0.20	5.14±0.14	44.43±3.18	172.64±14.19
ECOB0	11.07±0.78	5.03±0.09	36.57±6.28	213.90±15.13
ECOB111	11.42±0.36	5.28±0.10	67.35±4.49	50.41±4.25
ECOB11	11.37±0.16	5.81±0.08	66.29±3.28	64.47±2.67
ECOB1	11.35±0.18	5.91±0.08	69.36±3.92	64.81±3.35
ECOBE*	*10.60±0.14*	*6.21±0.12*	*81.42±3.82*	*34.92±1.90*

*Exxon PP3155

The mechanical properties of the ECOB fibers manufactured at 75 and 95 °C also were studied to see the effect of bath temperature. There was no significant difference in tenacity and modulus values for the ECOB temperature of 50, 75 and 95 °C. A trend among the as-spun ECOB samples demonstrates that increasing the production distance leads to an increase in the mean value of tenacity, even if modulus are almost the same. The highest tenacity value of 5.99±0.07 g/d with the modulus value of 72.63±3.22 g/d was observed for ECOB treated fibers at the temperature of 75 °C with production distance of 170 cm. It is believed that using roller system between take-up mechanism and ECOB bath improved uniformity of fibers which lead to a higher fiber strength.

A tremendous increase of modulus and tenacity was observed for PP drawn fibers spun (1.34 draw ratio) with ECOB technology. Table 5.4 shows that tenacity values for the ECOB drawn fibers are between 8.85±0.46 and 11.11±0.39 g/d with the modulus values range 85.31±5.93 g/d to 139.97±10.19 g/d. Moreover, the elongations at break of the filaments varied from 20.78±2.26 to 34.55±3.71 %.

The adjusted zone temperature and melt flow rate of Total PP3462 (Table 5.1) were higher than Exxon PP3155. Hence, the draw temperature was set to 150 ^{o}C for polypropylene fibers with and 120 ^{o}C to polypropylene fibers without ECOB spinning system.

At 50 ^{o}C ECOB temperature, tenacity and modulus gradually increased from 9.86±0.38 to 11.11±0.39 g/d and 109.76±5.68 to 139.97±10.19 g/d, respectively for drawn treated fibers. The elongation at break remained nearly the same for the production distance of 90 and 130 cm which is about 22 %, however for the production distance of 170 cm it is around 27 %. The tenacity values decreased from 11.11±0.39 g/d to 10.52±0.32, yet the modulus values were almost the same when the drawing temperature was adjusted at 120 ^{o}C instead of 150 ^{o}C.

At 75 ^{o}C ECOB temperature, the highest tenacity and modulus were obtained from 170 cm distance, which are 10.89±0.67 and 124.12±11.06 g/d, respectively, after drawing 1.34 DR at 150 ^{o}C with the elongation of 23.18±3.02%. In every case, increasing production distance between the spinneret and bath to 130 and 170 cm (see Table 5.4), lead to an increase in the mean value of tenacities for ECOB fibers.

Associated with the ECOB temperature at 95 ^{o}C, an interesting data should be pointed out. Fiber tenacities were very close to each other when standard deviation is considered.

Apparently, the production distance was not a significant factor when a high ECOB temperature was used. As seen in Table 5.4 the highest tenacity value of 10.53±0.25 g/d at 95 ^{o}C was lower than that one for the other treated fibers. In addition, these fibers had the highest modulus value of 107.70±7.80 g/d and slightly higher elongation at break, around 30 %.

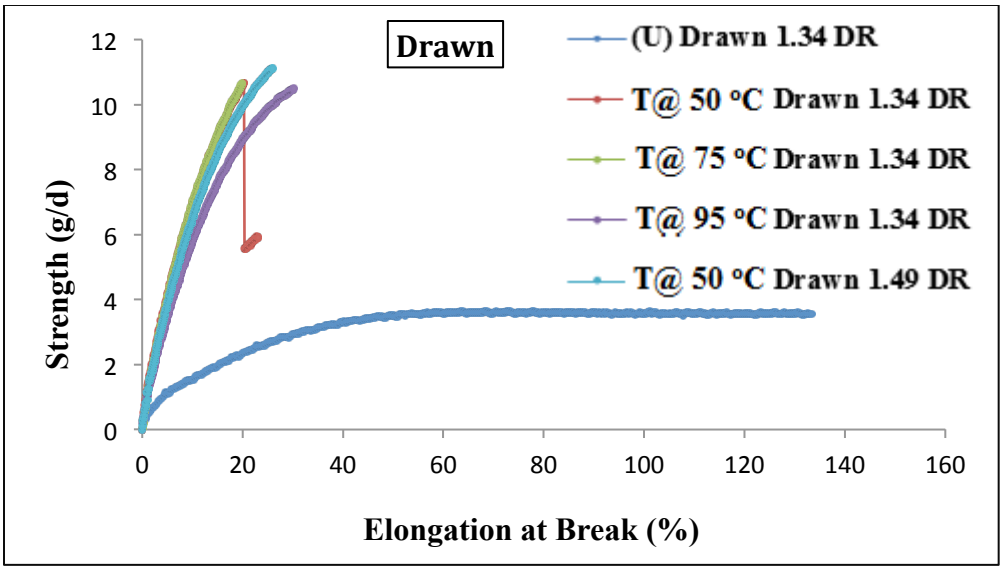

Figure 5. 2 Effect of bath temperature on tenacity values of drawn fibers made ECOB spinning system with comparison of traditional spinning process under the same distance, 170 cm, between the spinneret and ECOB bath.

Another interesting phenomenon drew our attention when Figure 5.2 was carefully examined. The drawn fibers spun with ECOB spinning system at the bath temperature of 50 ^{o}C with 170 cm production distance showed different stress-strain curve than others. When tensile tests were performed, the drawn monofilament did not break completely at the highest breaking load value but completely broke in two steps. This may be due to the difference between fiber core and sheath or microfibrillar structures, which form during the ECOB system and did not fracture at the same time. In-depth observational study was carried out to explain this phenomenon in the next sections.

Examination of drawn fibers with DR of 1.49 showed that the ECOB spinning system offers outstanding performance for PP fibers with tenacity value close to 12 g/d (~ 1.26 GPa) and more than 152 g/d (> 16 GPa) for modulus value. This performance is not possible with existing traditional high speed spinning and drawing technologies.

Table 5. 4 Mechanical properties of drawn PP fibers spun with and without ECOB at 150 ^{o}C draw temperature with 1.34 DR.

Sample ID	Denier	Tenacity (g/d)	Modulus (g/d)	Elongation (%)
ECOB000	6.40±0.91	5.85±1.60	65.09±20.91	85.55±36.11
ECOB00	6.47±0.62	5.74±1.44	64.63±16.58	88.88±43.04
ECOB0	8.30±0.49	3.64±0.25	32.38±4.75	137.98±20.49
ECOB111	7.26±0.36	9.86±0.38	109.76±5.68	21.60±1.25
ECOB11	7.99±0.62	10.20±0.42	111.14±7.38	22.95±1.66
ECOB1	***6.63±0.57***	***11.11±0.39***	***139.97±10.19***	***27.01±2.95***
ECOBE*	7.81±0.36	10.52±0.32	135.50±7.76	29.35±3.02
ECOB222	7.26±0.41	8.85±0.46	101.83±5.17	20.78±2.26
ECOB22	7.03±0.45	10.31±0.41	118.09±7.15	23.04±2.71
ECOB2	6.53±0.47	10.89±0.67	124.12±11.06	23.18±3.02
ECOB333	7.64±0.28	10.06±0.26	85.31±5.93	34.55±3.71
ECOB33	7.51±0.34	10.16±0.39	89.95±6.86	30.95±4.38
ECOB3	7.58±0.95	10.53±0.25	107.70±7.80	29.91±3.17

5.4.2 SEM Analysis of As-Spun and Drawn Filaments

One of the most important characteristic of hIB polyester fibers is the banded morphology that is a precursor for crystallization of PEN filaments under various spinning conditions[32]. During the drawing process, the fibers were marked with the three zones along the axial fiber direction. An unheated zone was outside of the tube; the second was the transit zone between the outside and inside drawn zones on the lower edge of the tube end. Finally the third one was the drawn zone in the tube, where the fiber was fully heated and drawn.

Figure 5.3 shows the surface of drawn ECOB1 polypropylene (DR = 1.34 at 120 ^{o}C draw temperature) fiber spun with ECOB technology. Interestingly, there was no any banded structure on the ECOB fiber surface. This behavior may be explained by the facile packing of pendant methyl groups in isotactic-PP during the crystallization process. Therefore, the difference between the skin and the core structure for the molecular orientation and the birefringence of the treated fibers were not significant for the formation of the banded structure[48]. It is also important to mention that the formation of this morphology is maybe related to a specific liquid type used in ECOB technology and for that reason it did not properly develop.

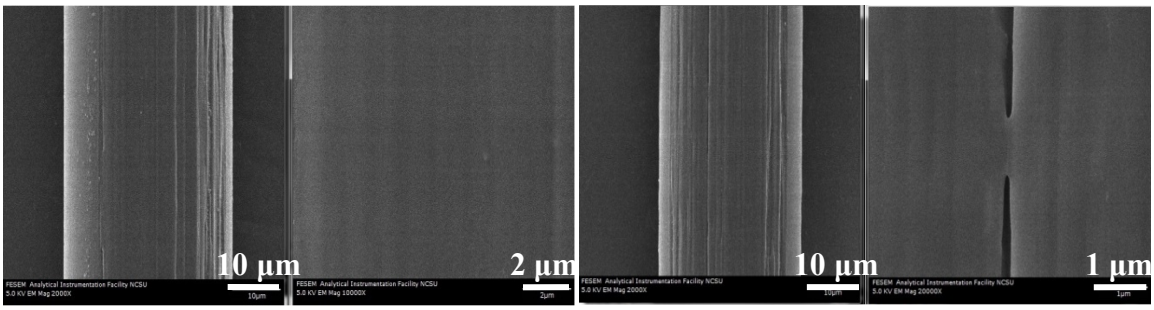

Outside Drawn Zone Transit Drawn Zone

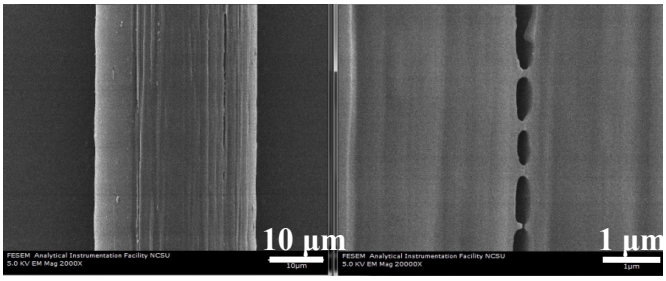

Inside Drawn Zone

Figure 5. 3 SEM images of PP fibers spun with ECOB spinning system.

Fibrillated break is one of the characteristics of Kevlar aramid fibers and also can be seen for UHMPE, aromatic copolyesters, PBO and PIPD fibers by long axial splitting mechanism[38]. These fibers are typically examples of highly oriented, highly crystalline, chain extended, high-modulus and tenacity filaments. For further investigation, the fiber samples were broken in liquid nitrogen, and the cross section was observed using field emission scanning electron microscope to study the inner morphology. As seen in Figure 5.4, ECOB treated fibers consist of microfibrils formed along the longitudinal axis to the fiber axis.

This is a unique property developed by the ECOB technology in which highly oriented crystalline and amorphous regions lead to form the microfibrillar structures. Figure 5.3 (inside drawn zone) and 4 demonstrate that the existence of microfibrillar structure for treated fibers may be a dominant factor to observe the two steps break (Figure 5.2) during the tensile test. Such a behavior was also confirmed during the fiber tensile tests. Uneven, fiber breaks often can be seen with the naked eyes confirming the fibrillar fine structures.

It is also believed that the treated fibers show separation of lamellae in blocks and the helical chain axis of the noncrystalline molecules became more oriented. Fiber became more oriented to evolve into the fibrillar structure[14] after drawing process with increase in the fraction of taut tie molecules in amorphous regions which lead to a higher orientation. Therefore any more deformation at this point, after a very low degree of draw ratio, could develop flaws causing the sample breaks.

Fibers spun without ECOB spinning system

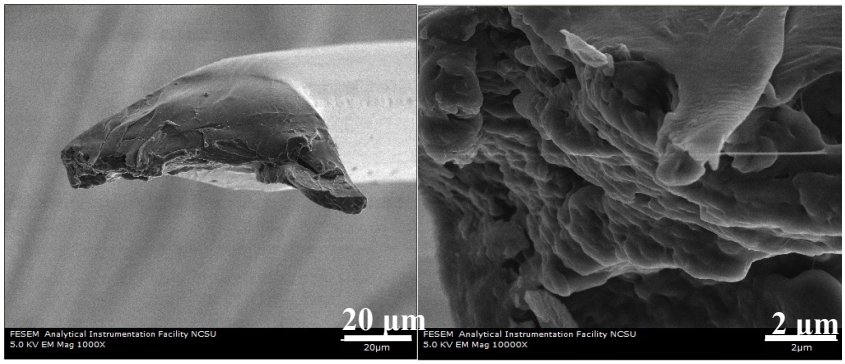

Fibers spun with ECOB spinning system

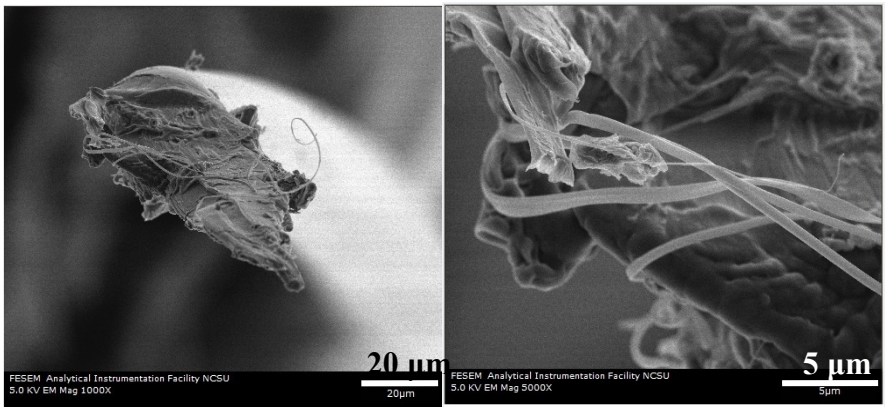

Figure 5. 4 SEM images of cross-section of drawn PP fibers.

5.4.3 X-Ray Analysis of As-Spun and Drawn Fibers

As seen in Figure 5.5, the significant effect of the ECOB spinning system on fiber crystallinity was observed. This is quite surprising for ECOB treated as-spun fibers in which the fibers show high tenacity and high modulus performance. Even if the treated fibers were produced at high speed spinning method, the crystal growth was efficiently suppressed by the liquid. ECOB treated as-spun filaments did not exhibit any distinct crystal peaks but the control fibers (untreated) had crystal peaks. Moreover, the ECOB fibers show much higher mechanical performance (Table 5.3). It indicates a highly oriented amorphous phase and a very low crystallinity were formed during the production as shown in Figure 5.5, 5.6 and Table 5.5.

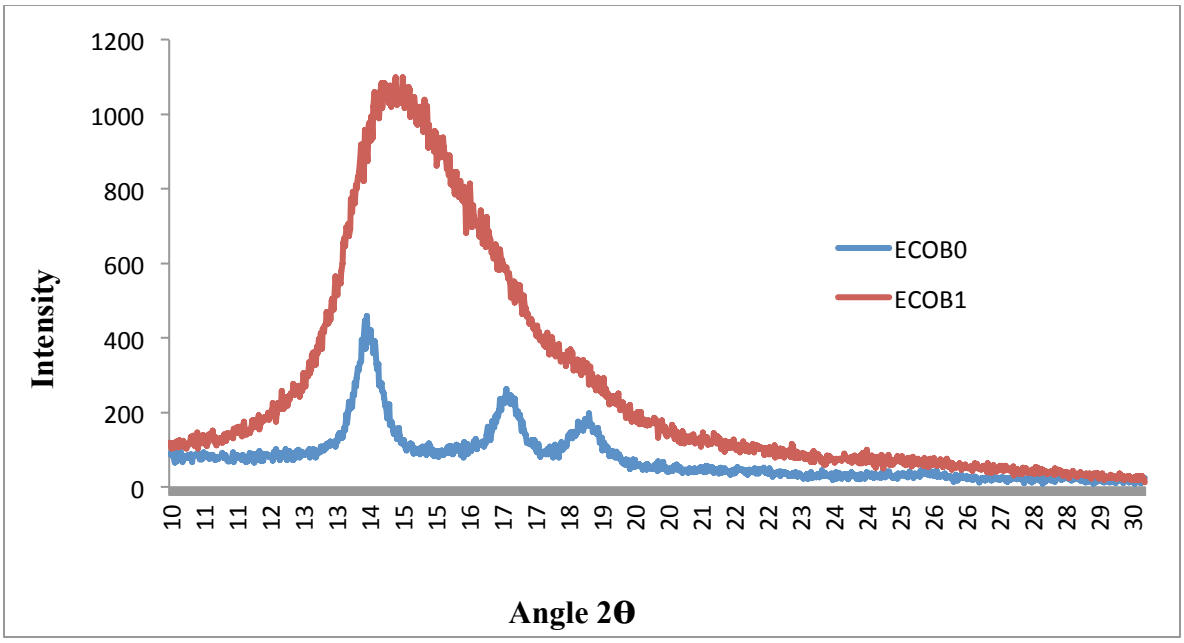

Figure 5. 5 Equatorial X-ray diffraction profiles of PP as-spun fibers spun with ECOB (ECOB1) and without ECOB (ECOB0).

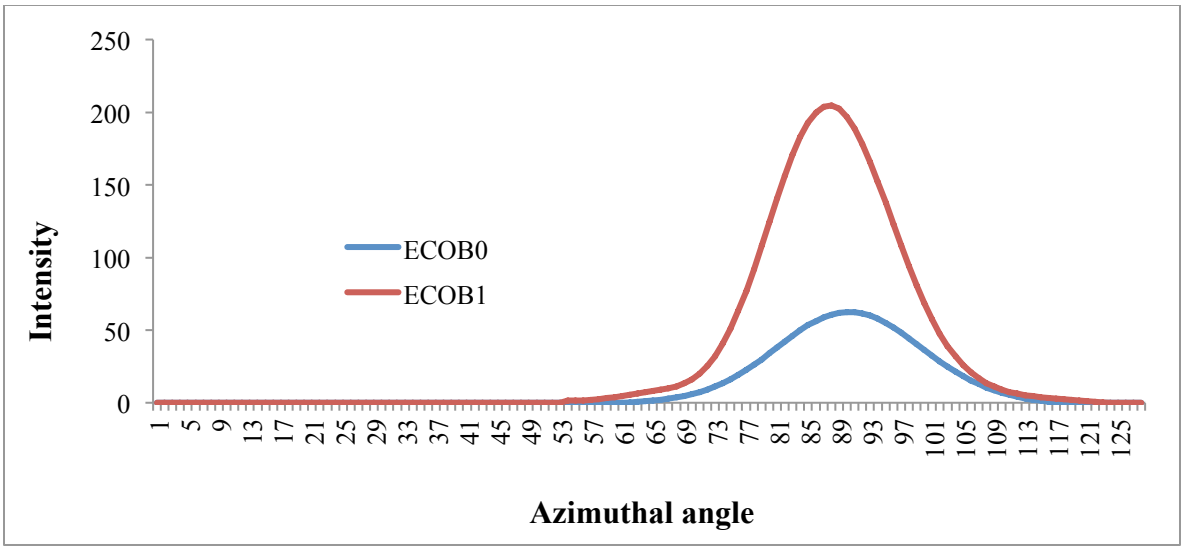

Figure 5. 6 Azimuthal X-ray diffraction profiles of (110) planes of PP as-spun fibers spun with ECOB (ECOB1) and without ECOB (ECOB0).

The degree of crystallinity decreased from 44.16 to 7.58 % when the ECOB spinning system was used at temperature of 50 ºC as seen in Table 5.5. Moreover Figure 5.5 and 5.6 demonstrate (110), (040), and (130) planes which are the principal reflections of the α-crystalline form (monoclinic) of *i*-PP. As can be seen from these Figures and Table 5.5, the crystallinity of ECOB treated fibers is much lower and showed a broad equatorial reflection than that one for the ordinary PP fibers. The crystallite size of treated fibers is quite small, while its amorphous orientation is much higher than the ordinary polypropylene fibers. The treated fibers demonstrated poorly developed crystallites, because crystal growth of these fibers were significantly suppressed, which lead to smaller apparent crystal sizes than the control fibers.

The crystalline orientation factors of 0.93 and 0.92 were comparable for both fibers (see Table 5.5). Even though the orientation in the crystalline phase of semicrystalline polymers has a great influence on fiber's tensile properties, the amorphous phase orientation is much dominant parameter. The amorphous orientation factor increased from 0.26 to 0.60 by ca. 131 % for treated fibers which plays a major role in determining fiber performance.

The bath effect is clear and obvious in obtaining highly oriented and yet noncrystallized molecular chains for as-spun fibers. The influence of the drag force and temperature on the fibers during the traveling through the liquid in the millisecond time period is undoubtedly significant. The growth of crystallites can be prevented because of the high threadline tension which restricts the motion of neighboring chain segments to form three dimensional structure[34]. In addition, the fibers probably had poorly developed unoriented structure during the moving between the spinneret and bath. A highly oriented precursor that was nearly completely amorphous was likely formed during the milisecond interaction of fiber and the hot liquid in the ECOB bath[34].

Table 5. 5 Degree of crystallinity, crystalline and amorphous orientation factor, and crystalline dimensions of PP as-spun fibers with and without ECOB.

				Crystallite size (Å)		
ECOB Temperature (^oC)	**Crystallinity (%)**	f_c	f_a	L_{110}	L_{040}	L_{130}
-	44.16	0.92	0.26	146	146	116
50	7.58	0.93	0.60	35	24	34

In contrast, after the drawing process with the temperature of hot plate of 120 ^oC and drawing speed of 50 mm/min, sharp and strong diffraction peaks were observed as seen in Figure 5.7 for ECOB treated fibers. This significant difference occurred after applying just DR of 1.340. The apparent crystal sizes and degree of crystallinity of fibers increased for both ECOB and without ECOB fibers while compared with all untreated and treated as-spun fibers. In addition, the degree of crystallinity of fibers spun ECOB were greater than that of fibers without ECOB treatment for different draw ratios. A degree of crystallinity increased from 49.90 to 52.25 % and from 51.38 to 58.48 % at draw ratio of 1.340 and 1.487, respectively, with using ECOB spinning system. For the untreated control fibers the degree of crystallinity increased from 44.16 to 49.90 and 51.38 % with increasing draw ratios from 1.340 to 1.487 DR, respectively.

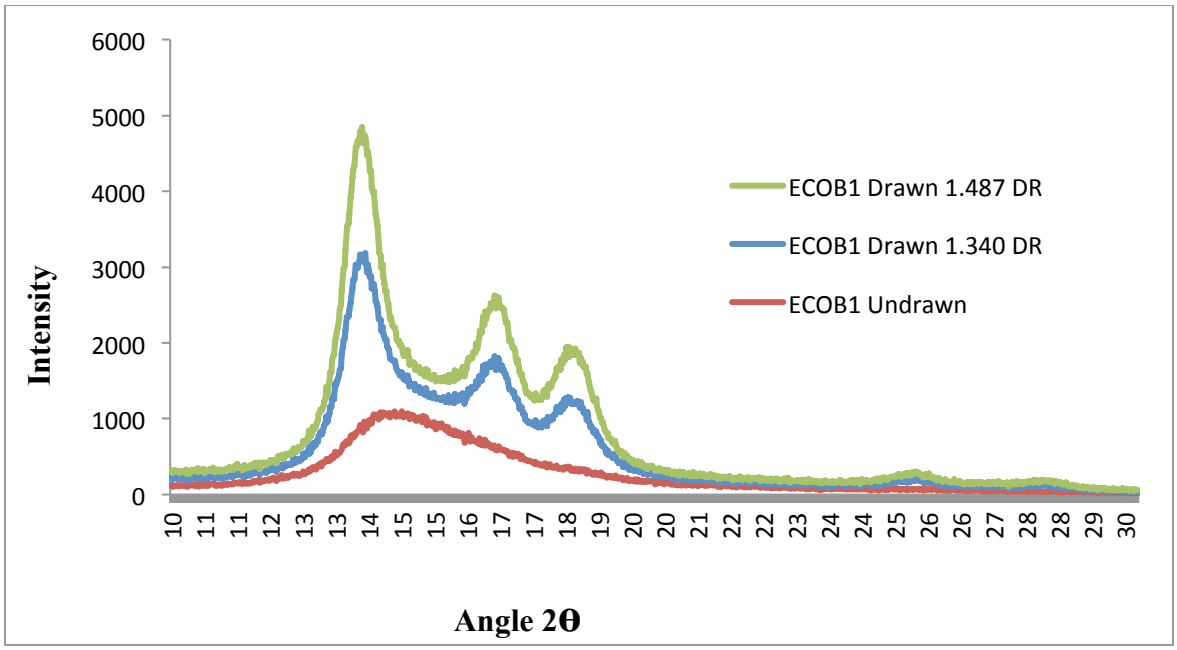

Figure 5. 7 Equatorial X-ray diffraction profiles of drawn PP fibers spun with ECOB at the temperature of 50 ^{o}C.

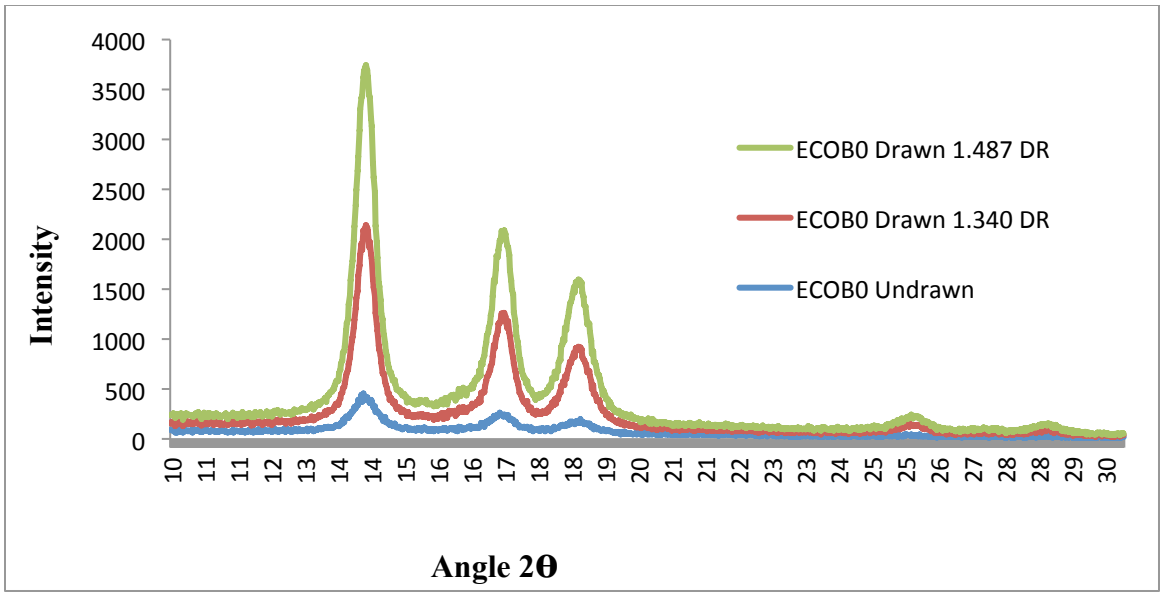

Figure 5. 8 Equatorial X-ray diffraction profiles of drawn PP fibers spun without ECOB at the temperature of 50 ^{o}C.

Tables 5.5 and 5.6 show that crystallites size increased with an increasing draw ratio for fibers spun with and without ECOB spinning system. However, fibers spun with ECOB have smaller crystallite size when compared with the control untreated fibers. This can be clearly seen by comparing Figure 5.7 and Figure 5.8. The small crystal dimensions for fibers spun with ECOB imply that the number of crystals is greater than that of fibers spun without ECOB process at similar degree of crystallinity. It is a quite interesting occurrence that should be investigated. Increasing degree of crystallinity with a decreasing crystallite size was observed, after UHMWPE was irradiated with gamma-rays and/or irradiated with other high-energy electron beams[39]. Such a phenomenon can be explained by the occurrence of

recrystallization process with the taut-tie chain scission leading to an increase of crystal perfection, and induction of the secondary crystallization with an increase in the polymer melting point. In addition, this recrystallization process might slightly decrease the crystalline orientation function because of the local stress relaxation and growing of new crystal lamellae at a slow rate[39, 40]. Even if the drawing process significantly improved the degree of crystallinity, it might not show the similar effect on the crystallite sizes because the treated undrawn fibers already had very small crystallite sizes. This could be another reason to observe the lower crystallite sizes than those of untreated drawn fibers. Moreover, an appropriate annealing process can be applied to the drawn fibers in order to obtain larger crystallite size which may lead to an increase in the fiber performance.

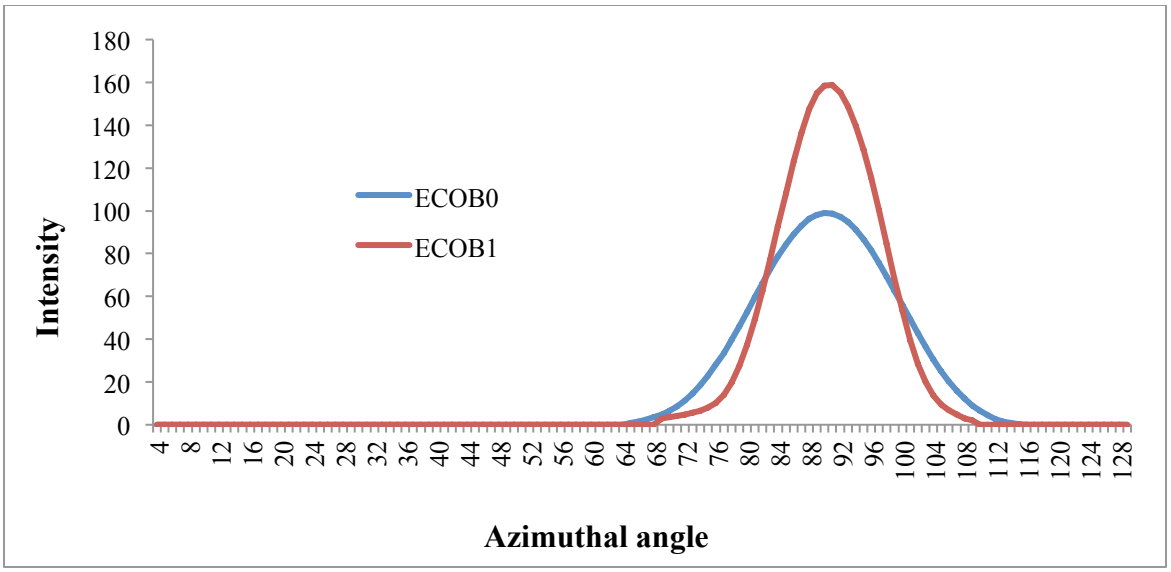

Figure 5. 9 Azimuthal X-ray diffraction profiles of (040) planes of drawn PP fibers spun with ECOB (ECOB1) and without ECOB (ECOB0). (Draw ratio = 1.487).

The azimuthal scan for drawn treated (ECOB1) and untreated (ECOB0) fibers after just DR of 1.487 for a characterization of chain orientation is shown in Figure 5.9. The treated fibers demonstrate sharp and strong peak in the azimuthal scan that indicates a well-developed chain orientation, whereas the untreated ones show a broader peak. The calculated values of the crystalline orientation for as-spun and drawn untreated PP were very similar (Table 5.6), which indicates PP crystallites remained almost the same orientation relative to the fiber axis. The greatest improvement in orientation of PP crystallites was observed for treated ones with the values of 0.95 after the drawing process (Table 5.6). Apparently, crystallites of the treated fibers were almost perfectly aligned along the fiber axis.

There was a significant change in both treated and untreated fibers for amorphous orientation factor after the fibers went through the stretching stage. Applying heat and axial fiber drawing ratios allowed to achieve increased molecular motion and forced the molecules to align in the draw direction in the amorphous phase. It was found that there was a significant fraction of oriented amorphous phase in the stretched treated fibers that showed ca. 78 % higher value than that of the ordinary fibers with the value of 0.87 (Table 5.6). The occurrence of high degree of preferential orientation with respect to the fiber axis caused the molecules of ECOB fibers efficiently packed together.

Table 5. 6 Degree of crystallinity, crystalline and amorphous orientation factor, and crystalline dimensions of drawn PP spun fibers with and without ECOB under various draw ratios.

					Crystallite size (Å)		
ECOB Temperature (^{o}C)	**Draw Ratio**	**Crystallinity (%)**	f_c	f_a	L_{110}	L_{040}	L_{130}
-	1.340	49.90			169	151	123
-	1.487	51.38	0.91	0.49	179	167	138
50	1.340	52.25			103	89	86
50	1.487	58.48	0.95	0.87	111	94	88

5.4.4 Effect of ECOB on Thermal Properties of As-Spun and Drawn Filaments

DSC thermograms for as-spun and drawn *i*-PP filaments are shown in Figure 5.10 and 5.11. The curves exhibit the double melting endotherms that can be observed for *i*- PP samples. In general, the second peak is formed after melting crystals and the subsequent recrystallization. The first peak can be seen in the range from 150 and 170 ^{o}C and is attributed to formation of a less ordered (α_1) crystalline form in the unoriented spherulites that had folded chain crystal lamellae[41, 42]. The original fibrillar crystals melt during this first melting peak. The second melting peak would be in the range of 170 and 185 ^{o}C when the melting of oriented crystals had occurred. They are thermodynamically more stable and had more ordered (α_2) monoclinic crystal phase which contributes to obtain a higher degree of crystallinity.

As shown in Figure 5.10 and Table 5.7, the temperatures for first melting peaks are similar, around 159 ^{o}C, for undrawn and drawn control fibers. Even the draw ratio increased from 1.340 DR to 1.487 DR, the peak temperature is slightly changed from 159.66 to 158.97 ^{o}C. On the other hand, the second melting peaks were seen in the range from 165.83 to 169.20 ^{o}C after applying drawing process and increasing draw ratios. At the draw ratio of 1.487, the second peak became more distinct in which the crystalline structure was formed in more ordered form. As we indicated before, after drawing process, the degree of crystallinity increased from 39.71 to 47.32 % with increasing draw ratios for the untreated fibers.

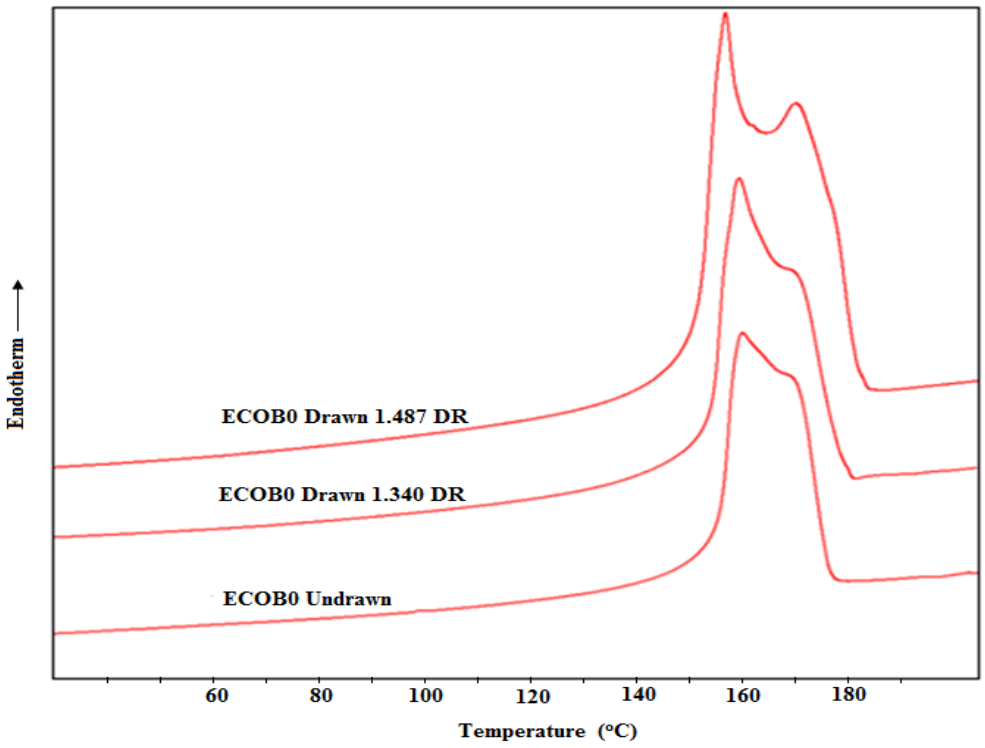

Figure 5. 10 DSC curves of polypropylene fibers spun without ECOB under various draw ratios.

Figure 5.11 shows DSC heating curves of polypropylene fibers spun with ECOB under various draw ratios. It is clearly seen that the thermal traces of ECOB treated fibers are significantly different than ones for the untreated, control fibers when compared with Figure 5.10. Unlike DSC curves of polypropylene fibers spun without ECOB under various draw ratios, the curves for ECOB treated *i*-PP fibers scan appears to display more complex

melting endotherms. The similar behavior was observed for Innegra PP fiber[42]. It is clear that the ECOB as-spun fibers had a small melting peak at 159.66 ^{o}C (Figure 5.11). This peak shifted between 170-175 ^{o}C for drawn ECOB fibers at 1.340 DR. Finally, the high melting peak was observed at 178.10 ^{o}C for drawn ECOB fibers at 1.487 DR. Some different type of crystals probably formed as they melted at a higher temperature. This unusual phenomenon was also observed during X-ray analysis. After drawing process higher degree of crystallinity with smaller crystallite size were investigated for ECOB treated filaments when compared with untreated fibers (Table 5.6).

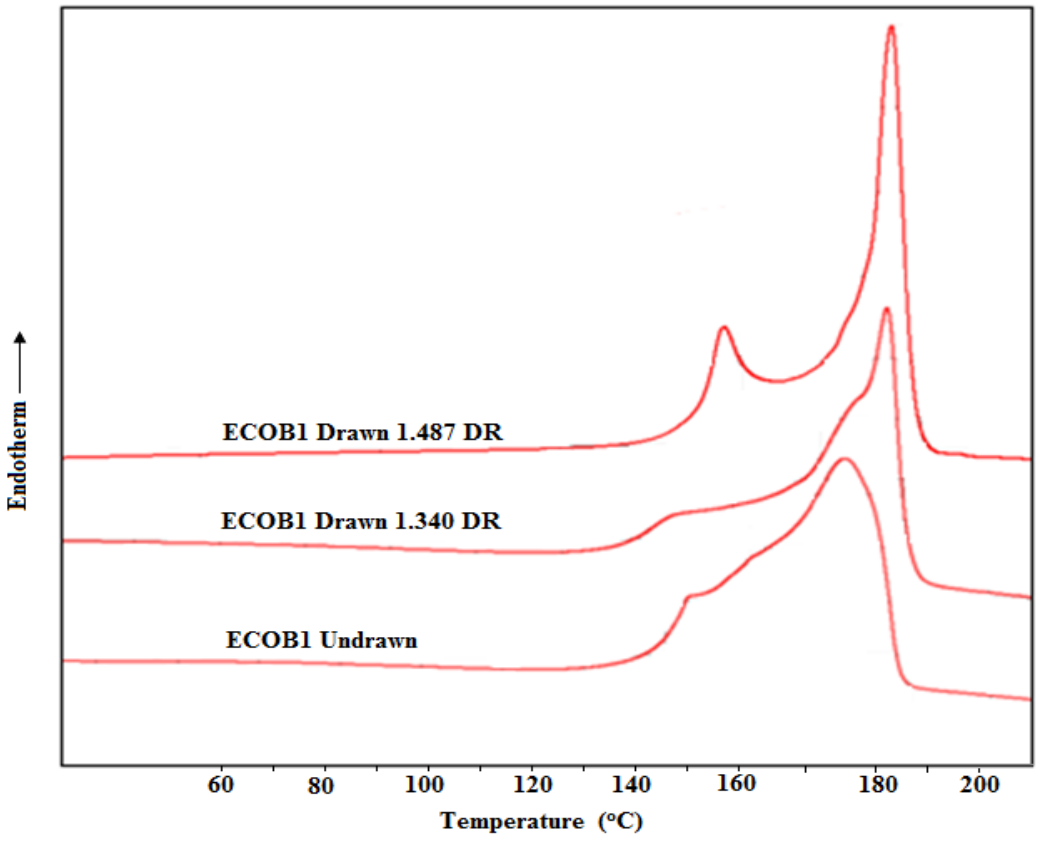

Figure 5. 11 DSC curves of polypropylene fibers spun with ECOB under various draw ratios.

The most prominent features of DSC traces for ECOB treated fibers is the second peak melting temperature and a higher heat of fusion of *i*-PP fibers as seen in Table 5.7. At 1.487 DR, the low temperature melting peak became more pronounced and shifted to a higher temperature for treated fibers, however for control fibers the second peak appeared clearly at 1.487 DR. In addition, after drawing process (1.487 DR), treated fibers showed 8.9 ^{o}C higher melting temperature than untreated fibers for second melting peak and 6.88 %

higher crystallinity as well. Table 5.7 revealed that the degree of crystallinity increased from 42.97 to 54.20 % with an increasing draw ratio to 1.487 for treated fibers. A higher melting peak temperature and the degree of crystallinity at higher draw ratios indicates an increased level of molecular ordering and thermodynamically more stable phase for the treated fibers.

Table 5. 7 Thermal properties of polypropylene as-spun and drawn fibers with and without ECOB.

Sample ID	**Onset Melting Point (^{o}C)**	**Peak Melting Point (^{o}C) (1^{st} peak)**	**(2^{nd} peak)**	**ΔH^{o}_{f} (J/g)**	**Crystallinity (%)**
ECOB0	155.72	159.40	165.83	83.004	39.71
ECOB1	149.41	152.92	172.04	89.802	42.97
ECOB0 Drawn 1.340 DR	155.11	159.66	166.96	95.000	45.45
ECOB1 Drawn 1.340 DR	149.70	153.21	178.10	101.077	48.36
ECOB0 Drawn 1.487 DR	154.70	158.97	169.20	98.910	47.32
ECOB1 Drawn 1.487 DR	154.57	158.08	178.10	113.277	54.20

5.4.5 Effect of ECOB Temperature and Drawing on Birefringence of Fibers

One of the most structural features of fibers is the axial and overall orientation of macromolecules that consequently lead to the fiber anisotropy when polymer molecules are more aligned in the parallel rather than perpendicular direction. It is clear from the literature that draw ratio and drawing velocity have significant effects on birefringence of *i*-PP filaments. The enhanced fiber birefringence is a result of a higher molecular orientation, and leads definitely to improved fiber mechanical properties.

The relationship between birefringence of untreated and treated *i*-PP fibers by ECOB spinning system is displayed in Figure 5.12. It is obvious that using ECOB system had a great positive influence on birefringence of treated fibers even if they were collected at the similar take speed without drawing process. The fibers birefringence improved by ca. 65 % from 0.020 to 0.033 by using ECOB. As mentioned previously the unique combination of properties such as a lower crystallinity and crystallite size, a lower elongation at break, a higher modulus and tenacity indicate the treated fibers had much higher amorphous orientation or were more ordered than untreated fibers. Furthermore, there was no significant birefringence difference between treated fibers at various temperatures as seen in Figure 5.12 for as-spun fibers. As it would be expected, the birefringence of fibers increased after drawing process as shown in Figure 5.12. The highest value of 0.039 was observed for treated fibers while untreated one remained at 0.027.

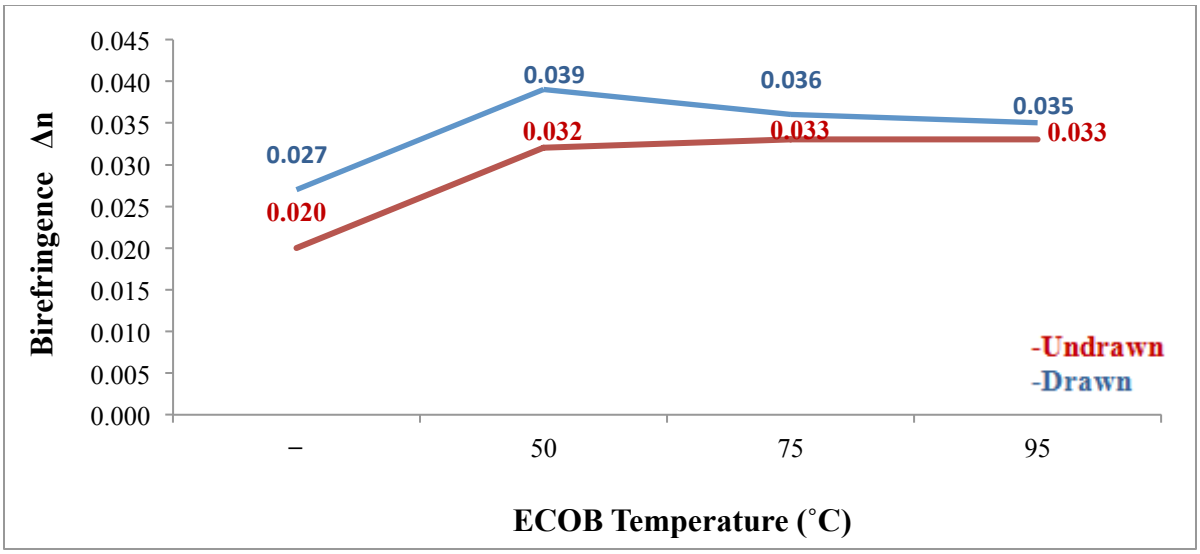

Figure 5. 12 The relation between birefringence of treated and untreated *i*-PP fibers at various ECOB temperatures.

Figure 5.13 shows the relationship between tenacity and birefringence for undrawn and drawn fibers. Although after the drawing process with 1.340 DR, the birefringence increased by ca. 22 % from 0.032 to 0.039, the tenacity increased by ca. 88 % from 5.91 g/d to 11.11 g/d. This tremendous increase in tenacity is caused by an increase in the degree of crystallinity (please look at Tables 5.5 and 5.6) for ECOB treated fibers. Normally much higher draw ratios are necessary to obtain these values in the traditional melt spin-draw processes. Before and after drawing process, the birefringence and tenacity values for treated fibers were very close to each other when standard deviation is considered. However, it should be noted that the drawing process for untreated, control fibers failed at 120 ^{o}C for most of the time. This is

due to that the untreated fibers had the poor thermal stability at elevated temperature. The SEM images of drawn untreated fibers also demonstrated a high level of surface deterioration. As a result, lower tenacity even lower than those for the undrawn fibers performance was observed for control fibers after the drawing process.

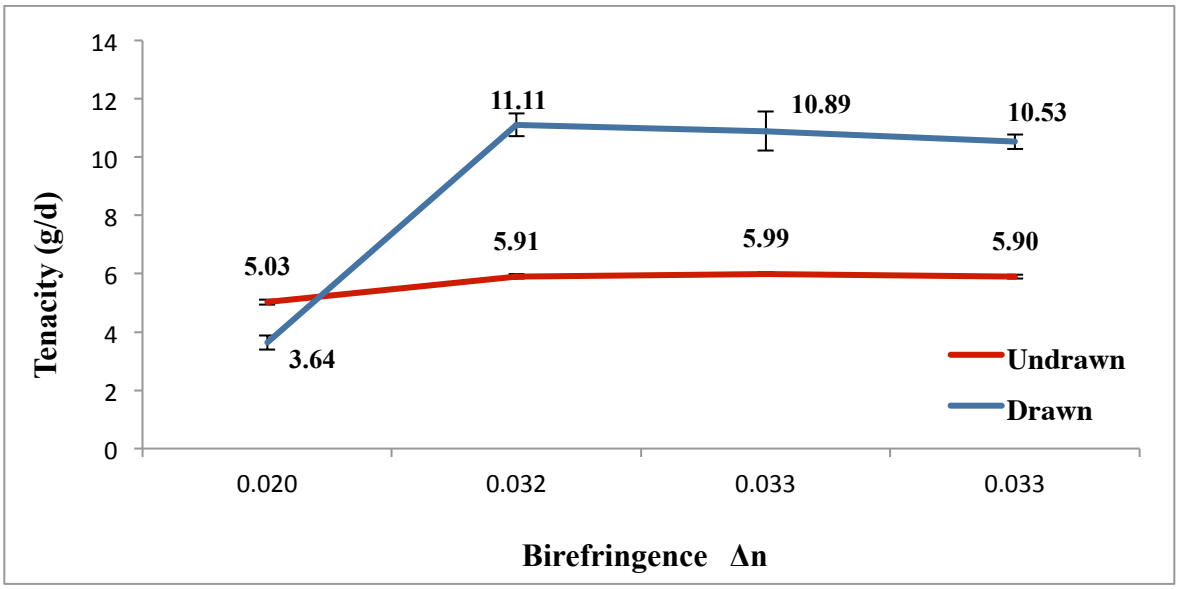

Figure 5. 13 The relation between birefringence and tenacity of treated and untreated *i*-PP fibers at various ECOB temperatures for undrawn and drawn fibers (Draw Ratio = 1.340).

Another interesting phenomenon drew our attention when control and treated drawn fibers (1.487 DR) were examined by a Nikon Eclipse polarizing microscope with water

immersion as shown in Figure 5.14. Treated fibers were white in color with outstanding performance while untreated ones were transparent when viewed with the naked eyes. One possible explanation can be the existence of void structure which are transversely stacked and axially attenuated for these dark transverse lines[43]. SEM images (Figure 5.3) shows some micron size voids which especially existed along fiber axis, however voids structures were not observed for ultra-high performance *i*-PP fibers that were produced by traditional liquid isothermal bath. Interestingly these dark banded structures were not observed for drawn untreated fibers. The similar observation was pointed out for etched Kevlar fibers[44]. Hence it is strongly believed that the transverse structure is not only because of void structure but also can be a result of a different type of morphological structures. It is also possible that highly oriented PP microfibrils consisting of alternating folded-chain lamellae and amorphous regions between these lamellae caused this behavior. Such unexpected trend will be investigated in more detail in another study of production of high performance *i*-PP fibers by horizontal isothermal bath (hIB).

Figure 5. 14 Microscope images of (a) untreated; and (b) treated fibers after drawing process (draw ratio = 1.487).

5.5 Conclusions

ECOB technology was successfully incorporated to production line to produce melt-spun PP filaments by the subsequent drawing to produce ultra-high performance fibers. A highly oriented amorphous phase with a very low degree of crystallinity and smaller crystallite size were developed for as-spun fibers by ECOB technology. As a result of a hot drawing at low draw ratios, a highly oriented crystalline phase was achieved, which yielded significantly improved fiber properties. The mean value of fiber tenacities of 11.67 g/d with modulus value of 152.36 g/d were obtained for PP drawn fibers at just 1.487 draw ratios. This value is much higher as compared to the maximum tenacity achieved by any of the existing melt spinning methods. After drawing process, tenacity and modulus increased by ca. 220.6 and 370.5 % for ECOB treated fibers when compared with the fibers which produced without ECOB technology for the similar production parameters. Moreover, the elongation at break decreased by ca. 84.8 % for the treated fibers.

A combination of results of tensile tests, WAXD, DSC, and SEM for the treated fibers showed that a unique precursor morphology with superior mechanical properties were obtained by utilizing ECOB spinning system. This study contributes a further understanding of structure development under simple, cost effective, ecologically friendly conditions. The treated filaments have similar mechanical performance for a certain fiber diameter in the wide liquid temperature ranges.

After drawing process, treated fibers showed smaller crystallite size that under proper annealing conditions can be increased resulting in improved mechanical properties.

The ECOB spinning system demonstrates the capability of manufacturing high performance filaments in industrial scale with smaller production area and much less capital investment than any traditional system.

The comparison of ECOB technology with hIB spinning system[32] for production of high performance *i*-PP fibers by using a lower molecular weight resin will be investigated in subsequent study.

5.6 References

1. Hearle J. W. S. (2001). *High Performance Fibres*. Boca Raton, FL: Woodhead Publishing.

2. Kerr, M., Chawla, N., & Chawla K., K. (2005). The cyclic fatigue of high performance fibers. *JOM*, 67–70.

3. Mukhopadhyay, S., Deopura, B. L., & Alagirusamy, R. (2004). Production and properties of high-modulus–high-tenacity polypropylene filaments. *Journal of Industrial Textiles*, 33(4), 245-268.

4. Huo, H., Jiang, S., An L., & Jiachun, F. (2004). Influence of shear on crystallization behavior of the β phase in isotactic polypropylene with β-nucleating agent. *Macromolecules*, 37, 2478-2483.

5. Arvidson, S. A., Khan, S. A., & Gorga, R. E. (2010). Mesomorphic-r-monoclinic phase transition in isotactic polypropylene: a study of processing effects on structure and mechanical properties. *Macromolecules*, 43, 2916–2924.

6. Karacan, I., & Benli, H. (2011). The influence of annealing treatment on the molecular structure and the mechanical properties of isotactic polypropylene fibers. *Journal of Applied Polymer Science*, 122, 3322–3338.

7. Li, Z., Na, B., Tian, N., Lv, R., & Zou S. (2012). Enhanced molecular orientation and strain hardening in melt-spun isotactic polypropylene monofilaments through partial melting recrystallization. *Journal of Applied Polymer Science,* 123, 995–999.

8. Lewin M. (2007). *Handbook of Fiber Chemistry*. Baco Raton, FL: CRC Press. 2007; 3rd Ed.

9. Sheehan, W. C., & Cole, T. B. (1964). Production of super-tenacity polypropylene filaments. *Journal of Applied Polymer Science,* 8, 2359-2388.

10. Shahi, Z. T. M., & Mojtahedi, M. R. M. (2010). Effect of blending two fiber-grade polypropylenes with different molecular weight distributions on the physical and structural properties of melt-spun filament yarns. *Journal of the Textile Institute*, 101(6), 547-555.

11. Sakurai, T., Nozue, Y., Kasahara, T., Mizunuma, K., Yamaguchi, N., Tashiro, K., & Amemiya, Y. (2005). Structural deformation behavior of isotactic polypropylene with molecular characteristic during hot drawing process. *Polymer,* 46(20), 8846–8858.

12. Misra, S., Lu, F. M., Spruiell, J. E., & Richeson, G. C. (1995). Influence of molecular weight distribution on the structure and properties of melt-spun polypropylene filaments. *Journal of Applied Polymer Science,* 56, 1761–1779.

13. Taylor, W. N., & Clark, E. S. (1978). Superdrawn filaments of polypropylene. *Polymer Engineering & Science*, 18(6), 518-526.

14. Ohta, T. (1983). Review on processing ultra high tenacity fibers from flexible polymer. *Polymer Engineering and Science*, 23(13), 697-703.

15. Samuels, R. J. (1968). Quantitative characterization of deformation in drawn polypropylene films. *Journal of Polymer Science Part A*, 6, 1101-1139.

16. Suzuki A., Sugimura T., & Kunugi T. O. (2001). Mechanical properties and superstructure of isotactic polypropylene fibers prepared by continuous vibrating zone-drawing. *Journal of Applied Polymer Science*, 81, 600–608.

17. Sheehan, W. C., & Cole, T. B. (1964). Production of super-tenacity polypropylene filaments. *Journal of Applied Polymer Science,* 8, 2359-2388.

18. Chawla, K. K. (2005). *Fibrous Materials*. Cambridge: Cambridge University Press, Technology & Engineering.

19. Coates, P. D., & Ward, I. M. (1979). Drawing of polymers through a conical die. *Polymer*, 20, 1553-1560.

20. Cebe, P., & Grub, D. B. (1985). Gel-drawn fibres of poly(vinyl alcohol). *Journal of Materials Science,* 20, 4465-4478.

21. Shaw, M. T. (1975). Flow of polymer melts through a well-lubricated, conical die. *Journal of Applied Polymer Science*, 19, 2811-2816.

22. Laughner, M. P., & Harrison, I. R. (1988). Hot nip drawing: a rapid method of producing high modulus polypropylene films. *Journal of Applied Polymer Science*, 36, 899-905.

23. Kristiansen, M., Tervoort, T., & Smith, P. (2003). Synergistic gelation of solutions of isotactic polypropylene and bis-(3,4-dimethyl benzylidene) sorbitol and its use in gel-processing. *Polymer*, 44, 5885–5891.

24. Machiels, A. G. C., Denys, K. F. J., Van Dam, J., & De Boer A. P. (1997). Effect of processing history on the morphology and properties of polypropylene/thermotropic liquid crystalline polymer blends. *Polymer Engineering and Science*, 37(1), 59-72.

25. Echevarria, G. G., Eguiazabal, J. I., & Nazabal, J. (2000). Morphology and mechanical properties of direct injection molded polypropylene thermotropic copolyester blends. *Polymer Composites*, 27(6), 864-871.

26. Hwan, L. S., & Ryoun, Y. J. (2008). Properties of polypropylene/layeredsilicate nanocomposites and melt-spun fibers. *Journal of Applied Polymer Science*. 109, 1221-1231.

27. Ruan, W. H., Mai, Y. L., Wang, X. H., Rong, M. Z., & Zhang, M. Q. (2007). Effects of processing conditions on properties of nano-SiO2/polypropylene composites fabricated by pre-drawing technique. *Composites Science and Technology*. 67, 2747–2756.

28. Garcia, M., Van, V. G., Jain, S., Schrauwen, B. A., Sarkissov, A., & Van, Z. W. E. (2004). Polypropylene/SiO2 nanocomposites with improved mechanical properties. *Advanced Materials Science*. 6, 169–175.

29. Madani M. (2010). Mechanical properties of polypropylene filled with electron beam modified surface-treated titanium dioxide nanoparticles. *Journal of Reinforced Plastics and Composites*. 29(13), 1999-2014.

30. Cuculo J. A. et al. (1992). US patent: US005149480A. Melt spinning of ultra-oriented crystalline polyester filaments.

31. Cuculo J. A. et al. (1998). US patent: US005733653A. Ultra-oriented crystalline filaments and method of making same.

32. Chen, P., Afshari, M., Cuculo, J. A., & Kotek R. (2009). Direct formation and characterization of a unique precursor morphology in the melt-spinning of polyesters. *Macromolecules,* 42, 5437–5441.

33. Lin, C. Y., Tucker, P. A., & Cuculo, John, A. (1992). Poly(ethylene terephthalate) melt spinning via controlled threadline dynamics. *Journal of Applied Polymer Science*, 46, 531-552.

34. Hotter, J. F., Cuculo, J. A., Tucker, P. A., & Annis B. K. (1998). Effect of liquid isothermal bath position in modified poly (ethylene terephthalate) PET melt spinning process on properties and structure of as-spun and annealed filaments. *Journal of Applied Polymer Science*. 69, 2051–2068.

35. Brandrup J., & Immergut E. H. (1999). *Polymer Handbook*. New York: Willey 2nd Ed.

36. Exxon MobilPP3155 Homopolymer Grade [homepage on the Internet, June 17th 2011]. Available from:

http://www.matweb.com/search/datasheet.aspx?matguid=d32d7bd5f1ed4c1dbd86e2b7f6b63297

37. Total Polypropylene 3462 [homepage on the Internet, June 17th 2011]. Available from: http://www.lonestarchemical.com/datasheets/polypropylene/72-total-polypropylene-3462

38. Elices, M., & Llorca J. (2002). *Fiber Fracture*. Oxford UK: Elsevier Science Ltd.

39. Zhang, H., Shi, M., Zhang, J., & Wang, S. (2003). Effects of sunshine UV irradiation on the tensile properties and structure of ultrahigh molecular weight polyethylene fiber. *Journal of Applied Polymer Science*. 89, 2757–2763.

40. Tretinnikov, O. N., Ogata, S., & Ikada Y. (1998). Surface crosslinking of polyethylene by electron beam irradiation in air. *Polymer*. 39(24), 6115–6120.

41. Somani, R. H., Yang, L., Sics, I., Hsiao, B. S., Pogodina, N., Winter, H. H., Agarwal, P., Fruitwala, H., & Tsou A. Orientation-induced crystallization in isotactic polypropylene melt by step-shear deformation. As viewed on line at (August 7th, 2012): *http://rheology.tripod.com/z09.13.pdf*

42. Unique Microstructural Features of Innegra™ High Modulus Polypropylene Fibers. A Report to Innegrity LLC Submitted by David R. Salem (2008). As viewed on line at (March 28th, 2012): http://wikinnegra.com/Wiki%20Pages/Unique%20Microstructural%20Features%20of%20Innegra%20High%20Modulus%20Polypropylene%20Fibers.aspx

43. Farrow, B., & Ford, J. E. (1964). Transverse markings in strained fibres. *Nature*. 201 (4951), 183-184.

44. Shahin, M. M. (2003). Optical microscopy study on poly(p-phenylene terephthalamide) fibers. *Journal of Applied Polymer Science*. 90, 360–369.

45. Bhuvanesh, Y. C., Gupta, V. B. (1995). Interaction between viscoelastic and structural relaxation in drawn polypropylene yarn. *Polymer*. 36(19), 3669-3674.

46. Lin, K. Y., Xanthos, M., & Sirkar, K. K. (2009). Novel polypropylene microporous membranes via spherulitic deformation – Processing perspectives. *Polymer*. 50, 4671–4682.

47. Samuels, R. J. (1968). Quantitative characterization of deformation in drawn polypropylene films. *Journal of Polymer Science Part A-2: Polymer Physics*. 6(6), 1101–1139.

48. Takeuchi, Y., Shuto, Y., & Yamamoto, F. Band pattern development in shear-oriented thermotropic copolyester extrudates. *Polymer*, 29, 605-612.

CHAPTER VI

Effect of Molecular Weight and Liquid Type on Precursor Formation for Crystallization and Structural Development of Ultra High Performance Polypropylene Filaments

Keywords: horizontal isothermal bath, ultra-high performance, polypropylene, precursor, highly oriented, improved thermal properties.

6.1 Abstract

A detailed experimental study has been conducted to investigate the effects of horizontal isothermal bath (hIB) on the production of ultra-high performance as-spun and drawn polypropylene (PP) filaments. Even though there are many published studies regarding the effect of the liquid isothermal bath (LIB) on as-spun and drawn polyester fibers properties, in this study, the effect of liquid on structural development of PP fibers were investigated for the first time. Two different commercial fiber forming PP polymers were used with the melt flow rate of 4.1 and 36 g/10 min. The results indicate that the optimum process condition depends on molecular weight of polymer. Interestingly, the fibers showed different precursor morphology for different molecular weight at each optimum process condition. However, these two sets of filaments demonstrated similar fiber tenacity and modulus of about 7 g/d, and 75 g/d, respectively, for as-spun and more than 12 g/d for tenacity and more than 190 g/d for modulus values of drawn fibers after just 1.49 draw ratios (DR). The mean value for the modulus after the drawing process for the high melt flow rate was about 196 g/d. The theoretical modulus of PP is 35–42 GPa[19], 275-330 g/d, shows the hIB fiber's modulus performance is approaching its theoretical maximum values. Moreover, ultra-high performance fibers demonstrated greatly improved thermal properties, degree of crystallinity, crystalline and amorphous orientation factors, and the formation of fibrillar structures. The hIB spinning system was found to play an important role to obtain highly oriented and predominantly amorphous structure for as-spun fibers and a well-defined, highly oriented crystalline fibrillar and amorphous structure after drawing process with the draw ratios lower than 1.5.

6.2 Introduction

Physical properties of polymers are intimately related to their microstructures. Polymer microstructure is affected by bonding and arrangements of atoms and groups, directions and types of monomer insertion, stereochemical attachments of side-chains, and so on. For example, polypropylene (PP) molecules consist of long backbone carbon–carbon chain structure with incorporated methyl group (CH_3) to the main chain. Stereosequence of attached side-chains is the main factor to obtain different tacticities, such as isotactic, syndiotactic, and atactic. Isotactic PP (*i*-PP) is mostly used polymer in which all methyl groups are on the same side of the main chain. Therefore *i*-PP is able to crystallize because of the polymer chains can be packed efficiently to form a semi-crystalline structure, whereas the random arrangement of methyl groups leads to formation of atactic PP that is an amorphous polymer. *i*-PP is a useful semi-crystalline thermoplastic polymer and finds many applications in the industry and our daily lives. In general, PP is accepted as the second most important polymer of worldwide with the expectation of revenues more than US$145 billion in 2019[1].

Crystals and amorphous matrix form a two phase system for semi-crystalline polymers. The degree of crystallinity has important effect on material mechanical and thermal properties. Therefore, many authors have worked on the formation of precursors of crystallization. For example, studies on *i*-PP with small- and wide X-ray scattering showed that a shear-induced precursor structure of a network of oriented phase was formed prior to the crystallization occurrence in situ in melt at 165 ^{o}C[2]. In addition, Kumaraswamy et al.[3] combined the birefringence measurements and wide-angle X-ray diffraction to observe a formation of an

oriented precursor of the shish-kebab structure after short shearing of polydisperse *i*-PP in situ. The lifetime for this precursor decreased with an increase of the temperature. Temperature and flow have an important influence on crystallization rate and crystallization morphology. Flow can start to improve the local orientations to enhance the nucleation rate, which increase the crystallization rate[4]. In addition, the crystalline morphology can be significantly changed by the flow[5]. Seki et al.[5] also observed the absolute effects of long chains on the crystallization kinetics and crystalline morphology with the blending of two different molecular weights of *i*-PP at a certain blending ratio. On the other hand, the temperature and cooling rate can alter the nucleation rate, crystallinity and spherulite sizes[6, 7]. Coppola et al.[4] have demonstrated faster crystallization rate by increasing the chain orientation at the lower temperature at a given shear rate. The crystalline phase contains discrete lamellae or crystallites. Shish-kebab structure can be formed if flow is strong enough; in this case, the long central fiber core is called shish, and composite crystallites occurred instead of point nucleation which dressed with periodically aligned disk-like folded chain lamellae to the so-called kebabs[8, 9, 10]. Different theories can be found for the formation of the shish-kebab structures. One explanation can be that the shish is developed after crystallization of totally stretched polymer chains, and the growing of the folded chain lamella crystals outward from the aligned cylindrical core causes the kebabs[9] to form. A high enough chain extension and orientation are required in order to nucleate the shish-kebabs[11].

i-PP has monoclinic α-crystallites, hexagonal β-structures, orthorhombic γ-polymorphs and a 'smectic' meso-phase[21]. These polymorphs are very sensitive to the conditions of crystallization. In the published literatures, the α-crystalline form (monoclinic)

is thermodynamically stable and can be observed during the melt spinning process with slow cooling and isothermal crystallization[39, 40]. It is also commonly observed in industrial productions and processes.

The characteristic peak of β-crystalline form (hexagonal) is located at 2ɵ = 16°, which is thermodynamically metastable and hard to observe during the common melt spinning process conditions. It might be observed with high undercooling or pressures during the melt spinning, or through some special laboratory conditions, such as through the temperature gradient method, using available nucleating agent, or the flow-induced crystallization method[39, 40]. Improved elongation at break and impact strength are two important characteristic of β-crystalline form[39]. Mesomorphic or smectic form (2ɵ =16° and 22°) of *i*-PP shows an intermediate characteristic performance between the crystalline and amorphous phase[41].

The aim of the present study is to investigate possible polymorphic transformations with support by structural and morphological analysis, and performance studies of isotactic polypropylene under influence of horizontal isothermal bath (hIB)[20, 42, 43] on the production of ultra-high performance as-spun and drawn filaments. This study also provides the structural properties and differences of the hIB fibers which were produced from two different molecular weights polymers. The generation of the precursor morphology for the crystallization of different molecular weight polymers is investigated under the effects of liquid temperatures, production distance, liquid depths and take-up speeds. All hIB fibers are

compared to the untreated fibers in order to differentiate the structural development and performances.

6.3 Experimental

6.3.1 Materials and Production Methodology

Fiber forming polypropylene (PP 3462 and PP3155) with the melt flow rate of 4.1 and 36 g/10 min, respectively, and the density of about 0.9 g/cm^3 were used in this study[44, 45]. PP treated and untreated fibers were produced via a Fourne single-screw extruder which had a single-hole with hyperbolic spinneret with 0.6 mm exit diameter. The take-up speeds were adjusted between 2500 and 2750 m/min depending on the polymer type and process conditions during the collection of all control, without treatment, hIB treated filaments.

The spun-fibers with and without hIB were then drawn by using a modified Instron tensile testing machine with a 60 cm long heating tube. The draw speed was adjusted to 50 mm/min, and the draw temperatures were 90, 120 and 150 ^{o}C for PP fibers to determine the most appropriate drawing temperature. The production distance and hIB depth are represented in Figure 6.1. These parameters are used during the production of fibers spun with hIB spinning technology.

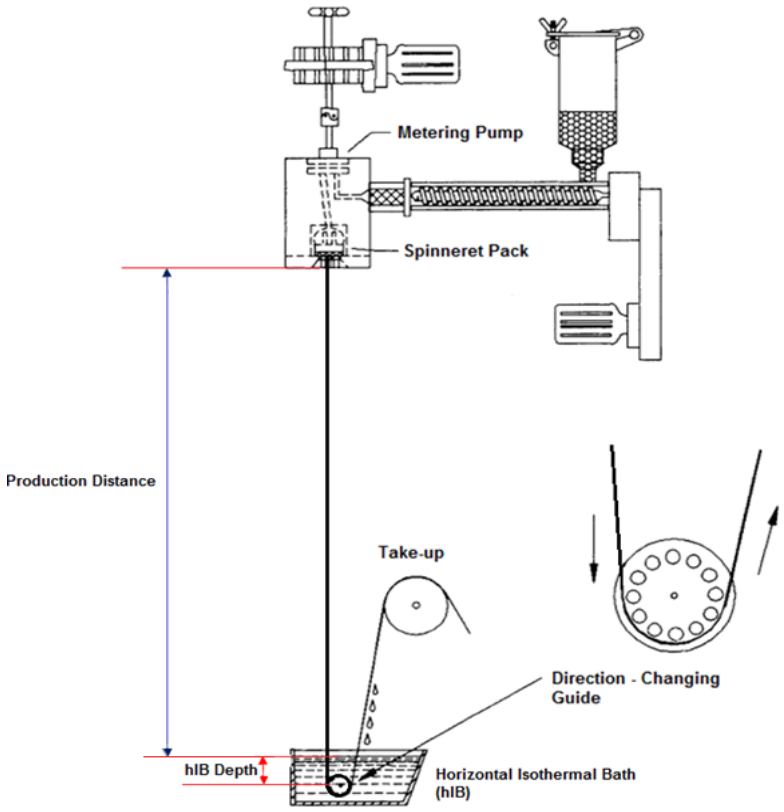

Figure 6. 1 Melt spinning process with ECOB spinning system[12].

6.3.2 Experiments and Characterization

Vibromat ME Tester equipment was used in order to determine the denier of monofilaments by resonant frequency and tensile testing of individual filaments was carried out subsequently.

An MTS Q-test/5 universal testing machine with TestWorks 4EM V4.11B software according to ASTM D3822 was performed to test the fiber modulus and tenacity (gf/denier), and also percentage strain at break (%). A gauge length of 25.4 mm and a constant cross-head speed of 15 mm/min were fixed. 5 pounds and 50 g load cells were used for all PP undrawn and drawn fibers with/without hIB.

A JEOL 6400 of a Cold Field Emission Scanning Electron microscope (SEM) was used to investigate the surface and cross-section morphology and microstructure. In order to examine the fiber cross-section, the filaments were put into liquid nitrogen and then broken apart in this liquid. The cross-section as well as the surface of the samples was observed at a high resolution after sample was coated with a layer of Au/Pd with 0.5-30keV accelerating voltage.

Wide-angle X-ray diffraction (WAXD) measurements were performed using Rigaku SmartLab X-ray Diffractometer (XRD) equipped with CuK_α radiation source, λ=1.542 Å, generated at 40 kV and 44 mA. The diffracting intensities were recorded every 0.02^o from 2θ

scans in the range 5 – 30° for PP. Crystallites sizes were calculated using the Scherrer equation[13]:

$$L_{hkl} = \frac{K\lambda}{\beta cos\Theta} \quad (1)$$

where β is the peak half width, K is taken to be unity, λ is the radiation wavelength (1.542 Å), and ϴ is the Bragg angle.

The crystalline orientation factor (f_c) can be calculated[14, 15]:

$$f_c = \frac{(3\times < \cos^2 \varphi_{c,z} > -1)}{2} \quad (2)$$

$$< cos^2 \varphi_{(110)or(040),z} >= \frac{\int_0^{\pi/2} I(\varphi) sin\varphi cos^2\varphi \, d\varphi}{\int_0^{\pi/2} I(\varphi) sin\varphi \, d\varphi} \quad (3)$$

$$< cos^2\varphi_{(c,z)} >= 1 - 1.099 < cos^2\varphi_{(110),z} > -0.901 < cos^2\varphi_{(040),z} > \quad (4)$$

where $\varphi_{c,z}$ is the angle between the *c* crystallographic axis and the fiber axis. The azimuthal intensity distributions for the (110) and (040) planes reflections were used in order to determine crystalline orientation factor (f_c).

The amorphous orientation factor, f_a, was determined by using the equation (5), which was developed by Stein and Norris, in which the overall measured fiber birefringence (Δn) was also used[14]. In addition, the calculated density[16] of the all fibers can be determined by using its fractional crystallinity, as obtained from the DSC heating scan.

$$f_a = \frac{\Delta n - \chi f_c \Delta n_0^c}{(1-\chi)\Delta n_0^c} \quad (5)$$

where Δn_0^c and Δn_0^a represent the intrinsic birefringence of the crystalline and the amorphous regions with the value of 0.0291 and 0.06, respectively[17].

A Perkin Elmer Diamond DSC Model 7 with Pyris software version 5 was used to observe thermal traces of ECOB treated and untreated fibers. 3-5 mg of the samples were encapsulated in a non-volatile aluminum pan and then heated at a heating rate of

20 ^{o}C/ min under a flow of nitrogen gas to 200 ^{o}C. The degree of crystallinity of PP fibers was calculated:

$$\text{Degree of crystallinity (\%)} = \frac{\Delta H_f x 100}{\Delta H_f^0} \quad (6)$$

where ΔHf is the heat of fusion of PP fibers. ΔH_f^0 is heat of fusion of 100 % crystalline PP which is 209 J/g[18].

Fibers birefringence was determined by using a Nikon polarizing microscope with a series of mineral oil refractive index liquids. The birefringence value (eq (7)) was obtained after the mean value of at least three individual sample measurements[13].

$$\Delta n = n_{II} - n_{\perp} \quad (7)$$

where n_{II} and $n_{\perp}$ are the parallel and perpendicular refractive index of the sample, respectively.

6.4 Results and Discussion

6.4.1 Mechanical Properties of As-Spun and Drawn Filaments

hIB spinning system was used with the expectation of highly oriented polymers to obtain samples with mechanical properties that would even approach their theoretical values of strength and modulus. It is also known that the random alignment and orientation for semicrystalline polymers lead to insufficient and lower strength and modulus. Therefore, mechanical properties of PP fibers spun with and without hIB were studied under different process conditions in order to compare with the mechanical properties. The main point of research was to start working with lower molecular weight polypropylene (PP3155 with melt flow rate of 36 g/10 min) at 90 ^{o}C liquid temperature and 170 cm of production distance with the liquid depth of 8 cm at about the take-up speed of 2500 m/min. Table 6.1 shows a comparison of mechanical properties of hIB and control (no hIB) undrawn fibers for different deniers. The as-spun, no hIB filament had the lowest tenacity in all the samples at the mean value of 4.84 g/d. It is of interest to note that the hIB process has the capability of producing high-performance, as-spun PP fibers according to the data in Table 6.1. Tenacity and modulus values are highly variable for different denier PP treated fibers. The highest tenacity is about 7.52 g/d with the modulus value of 75.51 for 12.74 denier for the undrawn filament. The denier range 5.00 to 12.74 did not create a significant change for the tenacity and modulus values for the treated fibers as seen in Table 6.1. However, the percent elongation at break was lower by about 50 % for 8.50 denier when compared to their respective treated fibers. In

addition, the tenacity and modulus increased by ca. 55 % and 177 %, respectively, when compared to its respective control sample from 4.84 g/d to 7.52 for tenacity and from 27.26 g/d to 75.51 g/d for modulus performances.

Table 6. 1 Mechanical properties of PP undrawn fibers spun with and without hIB.

Sample ID	Denier	Tenacity (g/d)	Modulus (g/d)	Elongation (%)
PPE4	5.00±0.10	7.14±0.20	77.67±6.44	60.52±5.36
PPE3	8.50±0.26	6.37±0.15	81.12±7.53	49.59±5.21
PPE2	9.48±0.23	6.90±0.18	71.64±7.73	70.56±8.29
PPE1	12.74±0.43	7.52±0.20	75.51±8.11	70.77±5.15
PPE0*	13.25±0.28	4.84±0.19	27.26±3.30	111.74±9.09

PPE0 represents untreated, control, fibers.

PPE1 sample was selected for further comparison and investigation of the effects of drawing temperatures and drawing ratios as documented in Table 6.2. Notice that an increasing of draw ratios (DR) from 1.20 to 1.34 lead to the superior mechanical properties and excellent tenacity values for 12.74 denier of the hIB as-spun PP fibers. The mean values of denier and elongation at break gradually dropped off and the tenacity with the modulus increased by

increasing draw ratios from 1.20 to 1.34. The highest tenacity and modulus were observed at the highest draw ratio of 1.34 at the value of 11.50 and 143.42 g/d, respectively, at the drawing temperature of 120 ^{o}C. Tenacity and initial modulus of the drawn hIB fibers both dramatically increased relative to their respective control drawn fibers by the improvement of ca. 53 and 131 %, respectively.

It is well known that drawing is generally done between the glass transition and melting temperatures of the fibers. Large temperature ranges have been employed for the drawing process to achieve high-modulus and high-tenacity fibers. The optimum temperature to draw the samples of the maximum modulus can be between 120 and 130 ^{o}C because the crystallite relaxation temperature of isotactic PP is around 117 ^{o}C[19]. In addition, it should not exceed the softening point (around 150 ^{o}C) of polypropylene fibers. Also, the lower value of tenacity and modulus were observed beyond 130 ^{o}C because the material became rubbery. A lower modulus value of, as expected, 119.81 g/d, was observed at 150 ^{o}C than 143.42 g/d at the drawing temperature of 120 ^{o}C. The best drawing condition, as explained in the literature, can be considered at the drawing temperature of 120 ^{o}C for both the tenacity and modulus performance, while the standard deviation is considered as seen in Table 6.2, even if the tenacity value at 150 ^{o}C was slightly higher. The as-spun fibers were not drawn and broke at the drawing temperature of 170 and 180 ^{o}C because these temperatures were very close or higher than the melting temperature of PP. In another case, after hot drawing, the white color of the treated fibers was observed at 90 ^{o}C and the color in fibers faded at 120 and 150 ^{o}C.

The similar behavior was investigated for PEN fibers and was an indication of a highly crystallized fibrillar structure[20].

The highest tenacity and modulus were obtained after 1.49 DR and 120 ^{o}C drawing temperature at the value of 12.21±0.30 and 196.66±22.40 g/d, respectively, with the elongation at break of 16.15±3.21 % for 7.19±0.71 denier filament. The theoretical modulus of PP is 35–42 GPa, 275-330 g/d, when measured by the X-ray techniques with the theoretical strength of 3.9 GPa, 30 g/d[19]. In this case especially, our modulus value approached its theoretical performance although a very low molecular weight polymer was used. Furthermore, during the drawing process, the color of fibers started to look white after 1.34 DR, and any more deformation after 1.49 DR caused it to develop flaws and the sample breaks. It is a strong evidence of oriented and fibrillar structures[17].

Table 6. 2 Mechanical properties of drawn PP fibers spun with and without hIB at different draw temperatures and ratios.

Sample ID	Draw Temp. (°C)	Draw Ratio	Denier	Tenacity (g/d)	Modulus (g/d)	Elongation (%)
PPE0	120	1.34	9.18±0.32	7.58±0.34	62.20±4.24	45.63±7.71
PPE1	120	**1.20**	8.96±0.23	9.61±0.33	105.93±6.72	36.53±3.06
PPE1	120	**1.25**	8.82±0.73	10.47±0.32	113.80±11.26	30.68±2.15
PPE1	120	**1.30**	8.43±0.56	11.01±0.38	127.90±9.50	28.09±3.19
PPE1	**90**	1.34	7.69±0.19	11.17±0.22	131.77±8.60	27.16±1.48
PPE1	**120**	1.34	7.45±0.30	11.50±0.32	143.42±10.25	24.00±1.89
PPE1	**150**	1.34	6.80±0.37	11.71±0.35	119.81±7.55	27.60±2.99

The starting point of the spinning conditions design for Total PP 3462 was set according to the experiments with Exxon PP3155. In addition to 90 °C, the liquid temperature was adjusted to 60 and 120 °C with 8 cm liquid depth and the take-up speed of about 2500 m/min. This is due to the fact that the lower melt flow rate for the polymer (g/10 min) gives more opportunity to study different liquid temperatures and other working conditions. However, desired fiber tenacity was not observed at these process conditions at three production distances, namely 90, 130 and 170 cm. The highest tenacity value of 6.52±0.07 g/d with the

modulus value of 71.16±3.92 g/d and the elongation at break of 151.46±9.77 % were observed for the liquid temperature of 120 ^{o}C at 8 cm depth. It should be noted that the bath temperature of 60 ^{o}C produced the similar tenacity and modulus with lower elongation at break of about 90 %. Higher elongation at break is one of the disadvantages of desired precursor morphology, which was also confirmed during the tensile test measurements, even if the increasing of the take-up speed to 3000 m/min for 120 ^{o}C liquid temperature did not much affect the fiber performance.

A number of trials at the liquid temperature of 90 ^{o}C were carried out. For instance, the liquid depth of 15 and 20 cm and the take up speed till 2750 m/min did not significantly improve the mechanical properties of as-spun treated fibers. The highest tenacity of 6.89±0.10 g/d was observed at 20 cm and 2750 m/min for the liquid depth and take-up velocity, respectively.

It is necessary to maintain a sufficiently high tension and liquid temperature with a suitable time to obtain stretched molecular chains and highly ordered structure. The optimized process conditions for Total PP 3462 polymer was obtained by placing the hIB device 170 cm below the spinneret, the liquid temperature of 60 ^{o}C and the liquid depth of 15 cm while using a take-up speed of 2500 m/min. These fibers spun with hIB demonstrated very unique mechanical properties, such as the tenacity value coming close to 7 g/d with the modulus performance of about 80 g/d at elongation at break range 55-60 %. As demonstrated for the highest performance PET fibers which were observed at lower distance of 90 cm for hIB spinning system, in the case of as-spun PP fibers spun with hIB, the highest mean value for

tenacity and modulus obtained at the highest production distance of 170 cm. It is known that the quenching rate (the rate of cooling to solidify the fiber) for PP and PET is different, and it affects the fiber properties. After molten state polymer emerged from the spinneret, PP fiber needs about double the time for PET fibers to solidify at the same conditions. It is might be a reason to work at different production distances for different types of polymers, as the fibers should have a certain degree of solidification before they reach the bath. It is also strongly related to glass transition temperature of the polymers.

After sample drawing to the draw ratio of 1.34 and 1.49 at the drawing temperature of 120 ^{o}C, fiber tenacity and modulus were significantly increased up to approximately 11.82 g/d and 12.30 g/d for tenacity, and 142.17 g/d and 192.05 g/d for modulus, respectively. Their elongations at breaks (%) were between 16 to 28 % for drawn fibers. Sheehan et al.[21] have produced high-tenacity PP filaments after drawing process by using a polymer with a melt flow rate of 0.61 g/10 min via quenched with water. The fiber's tenacity of 13.1 g/d and 110 g/d for modulus were observed after 34 draw ratio, which was drawn in an oven at 130–135 ^{o}C. hIB as-spun and drawn fibers results indicate the morphology was significantly improved, particularly in the modulus performance with a simple processing setup, as compared with Sheehan's work.

It is also very interesting to note that after the drawing process at 1.49 DR, the fibers for PP3155 and PP 3462 polymers showed almost the same tenacity and modulus performance at their optimum process condition, even though the PP3155 polymer has about 10 times higher

melt flow rate (g/10 min) than that of the PP3462. The possible reasons for this phenomenon with structural differences are provided in the next sections.

6.4.2 Scanning Electron Microscope Analysis

Undrawn as well as drawn fibers with and without hIB treatments were observed by SEM. Figure 6.2 shows SEM images of undrawn and drawn treated fibers. There was not any dramatic change on the fiber surface morphology after hIB treatment before and after drawing. In addition, treated fibers kept their uniformity along the axis with defect free morphology. Many researchers have worked on surface morphological features for polypropylene fibers during the melt-spinning process. As-spun PP fibers demonstrated spherulitic surface morphology and they gradually did transform to fibrils during the stretching process, as observed with atomic force microscopy[22]. The deformation of the original spherulites and then the orientation of lamellar stacks into different sizes of fibrils from nano- to micrometer scale can be observed during this stage. The processing conditions have a great influence on the final morphology.

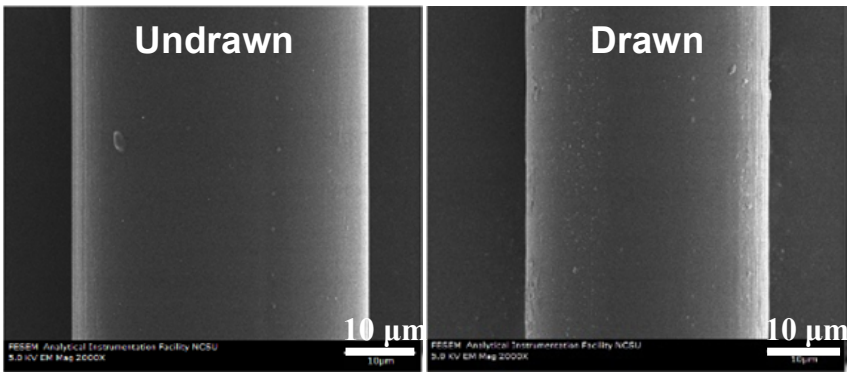

Figure 6. 2 SEM images of undrawn and drawn PP fibers (PP3155) spun with hIB (DR = 1.34).

As seen in Figure 6.3, unexpectedly, different sizes of diameters fibrillar structures were investigated for undrawn fibers after treatment with hIB process. It indicates that the transformation of the spherulitic morphology into the fibrillar morphology was probably initiated by the liquid bath via a high level of threadline tension and liquid temperature. It should be noted that the liquid bath is the key factor affecting the induced structure of the PP fibers. After drawing just 1.34 draw ratios, long axial splits type of fracture were observed for treated fibers. This type of break is generally observed for highly oriented and highly crystalline linear polymers, such as the para-aramid Kevlar and ultra-high molecular weight polyethylene (Spectra)[23] fibers; increasing shear stress with the load that leads eventually to pass the transverse cohesive forces between the chains and molecules to form an axial crack. The crack can be propagated along the axis of highly oriented molecules and fibrils and, if the

crack is slightly off axis, it will fuse with other cracks and eventually reach the outer edge of the fiber to form rupture[23], as demonstrated in Figure 6.3 for the drawn treated fibers. In addition, width of fibrillar structure from tens of nanometers to hundreds of nanometers is another strong evidence of highly oriented and highly crystalline morphology for drawn treated fibers. During the transformation of spherulitic morphology into a fibrillar morphology, where the orientation of the chains in the crystalline regions becomes parallel to the fiber axis and drawing direction, the lamellar crystals can be destroyed and re-formed. Drawing temperature and ratios for the re-crystallization of the lamellar crystals lead to a different thickness for the fibrillar structure[24].

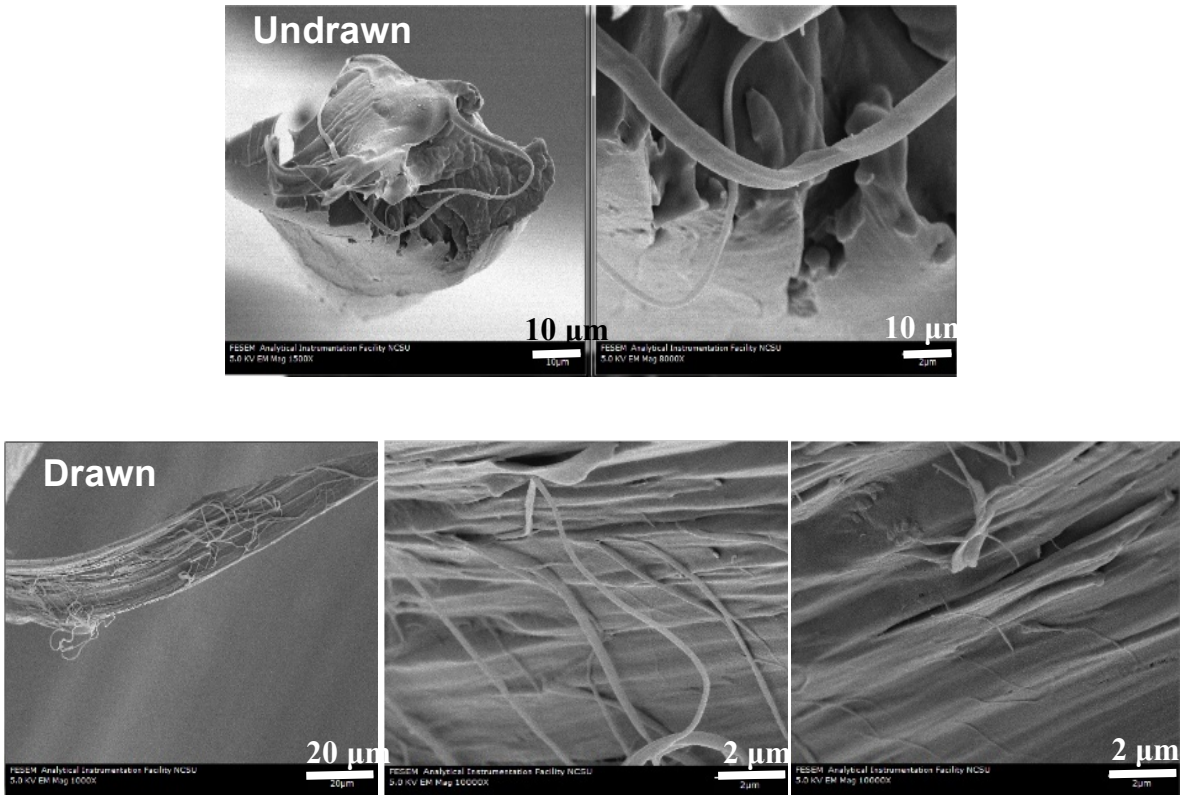

Figure 6. 3 SEM images of cross section of undrawn and drawn PP fibers (PP3155) spun with hIB (DR = 1.34).

The fiber surface morphology of a higher molecular weight PP (PP 3462) fibers were also smooth and uniform, and no significant changes were observed as demonstrated for lower molecular weight PP (PP3155) fibers. Interestingly, the fibrillar structure was not observed for treated undrawn fibers, even if some fibrils existed for treated undrawn lower molecular weight PP (PP3155) fibers (Figure 6.3). It might be explained that the level of entanglements,

intermolecular forces, and crystal slip with re-crystallization mechanism for formation of fibrillar structure was not probably the same as for the higher molecular weight polypropylene. It is also known that the higher molecular weight polymers have a higher level of entanglements. Therefore, threadline tension induced by the liquid drag could lead to the formation of highly oriented structure with not enough separation of lamellae in blocks to evolve into a fibrillar structure[17]. On the other hand, the treated fibers demonstrated nano- and microfibrils structures by long axial splits facture mechanism after a little hot drawing by transforming highly ordered structure into fibrillar crystals, as seen in Figure 6.4. Formation of fibrillar structure is also another evidence of a very highly oriented structure for treated undrawn fibers, as only 1.34 draw ratios was applied to the fibers during the drawing process. Moreover, the fracture mechanism of treated drawn lower and higher molecular weight PP fibers is clearly different when Figure 6.3 and 6.4 carefully are compared. The fracture mechanism of lower molecular weight drawn treated PP fibers (PP3155) is closer to Kevlar and Spectra than those of higher molecular weight drawn treated PP fibers (PP 3462). It suggests the hIB spinning system is more beneficial for lower molecular weight polypropylene as we concluded also for PET fibers in the term of fine structural development. The comparison of mechanical performance of lower and higher molecular weight drawn treated PP fibers at the same draw ratio of 1.49 showed almost the same performance, although there was about ten times the difference for melt flow rate between the polymers. This comparison also confirms that the level of mechanical performance improvement for lower molecular weight polymer is higher than that of the higher molecular weight one.

On the contrary, untreated control fibers exhibited poorly developed structure without any fibrils, both for undrawn and drawn fibers, by failing a ductile fracture mechanism (see Figure 6.4). This is a very important disadvantage of conventionally formed polypropylene fibers which show a limited mechanical property.

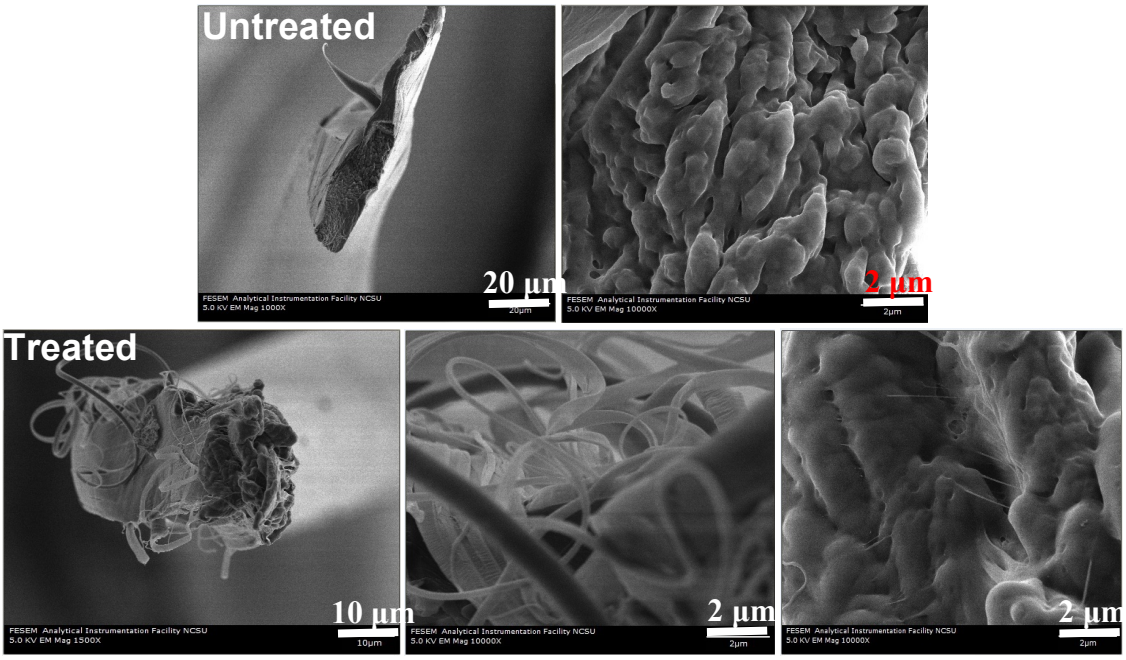

Figure 6. 4 SEM images of cross section of drawn PP fibers (PP 3462) spun with and without hIB (DR = 1.34).

6.4.3 X-Ray Analysis of Untreated and Treated Fibers

Crystallization during the high speed spinning is highly influenced by the spinning speed which can be explained by the effects of stress-induced crystallization[25]. The crystallinity and crystal orientation increase by increasing a take-up velocity and drawing ratio. In addition, wide-angle X-ray diffraction (WAXD) is one of the routine methods to characterize the structure and morphology of the oriented polymers. Table 6.3 illustrates spinning conditions of different molecular weight polypropylene fibers spun with the hIB and ECOB spinning system by using PP3155 and PP 3462 polymer types. In this regard, ECOB untreated and treated fibers are considered to compare the effect of liquid on fiber crystallization by using PP 3462 polymer type. This comparison is carried out for undrawn fibers with their optimum process conditions because the unique precursor morphology for crystallization is observed after just treatment with the liquid baths. The detailed effects of ECOB spinning system on the fiber properties are investigated in a different chapter.

Table 6. 3 Spinning conditions of different molecular weight polypropylene fibers spun with and without hIB and ECOB.

Sample	Take-up speed (m/min)	Liquid temp. (^{o}C)	Liquid depth (cm)	Distance (cm)
PP3155 (U)	2583			170
PP3155 (T)	2625	90	8	170
PP 3462 (U)	2580			170
PP 3462 (T)	2583	60	15	170
ECOB (U)	2891			170
ECOB (T)	2921	50	20	170

*U represents untreated and T is abbreviation for treated fibers.

A tremendous influence of the temperature of hIB and ECOB spinning system on fiber crystallinity was observed, especially by utilizing higher molecular weight polymer, as demonstrated in Figure 6.5. *i*-PP has several polymorphs and it is very sensitive to the conditions of crystallization. Figure 6.5 shows three strong peaks located on the equator as indexed as the (110), (040) and (130) planes reflections, respectively. These planes are the principal reflections of the α-crystals (monoclinic) of *i*-PP.

The liquid baths probably inhibited the growth of crystallites by increasing the spinline stress as the fibers went through the baths[13, 26]. Possibly, it prevented the motion of the neighboring chain segments and restricted three-dimensional arrangements for crystallization. Moreover, a

poorly oriented and nearly amorphous phase with pre-solidified fibers was formed between the spinneret and liquid tank. The existence of temperature and drag force in the liquid may have improved the orientation without any dramatic effect on crystallization because of a very short time interaction - about a millisecond - between fibers and liquid. However, lower molecular weight treated as-spun PP fibers (PP3155) demonstrated a quite different behavior for crystallization. The diffraction scans became better resolved as shown in Figure 6.5. The lower level of entanglements and less intermolecular forces for lower molecular weight polymers probably lead to an increase in interactions between the liquid and fibers. Therefore, relatively higher molecular mobility promoted the crystallization growth that lead to highly developed crystalline structures or just induced a new morphology. From this perspective, the higher level of crystallinity with highly oriented structures and some fibrils were observed only for lower molecular weight in undrawn treated PP fibers.

The comparison of the diffraction patterns for undrawn treated fibers demonstrated a strong relationship between distinct crystal peaks and mechanical properties (Figure 6.5). The formation of the well-resolved crystalline peaks increased the mechanical properties and the intensity for the diffraction profile. Increasing intensity while observing distinct crystalline peaks probably improved fibers tenacities from 5.91, to 6.91 and to 7.52 g/d for ECOB and hIB treated HMW, and hIB treated LMW fibers, respectively. The ranges for tenacity for fibers are exactly the same as the intensity and crystalline formation, as seen in Figure 6.5. Amorphous phase orientation factor increased from 0.60 to 0.71 by changing spinning system from ECOB to hIB with increasing the intensity and revealing poorly-formed crystal peaks

for the HMW polymer. It can be concluded that the amorphous phase orientation factor of 0.71 is an important threshold for the crystallization induced by the orientation mechanism. As predicted, f_a decreased to 0.63 when LMW polymer was used by hIB spinning system because of the crystallization process, even though it showed the highest tenacity and intensity for X-ray diffraction.

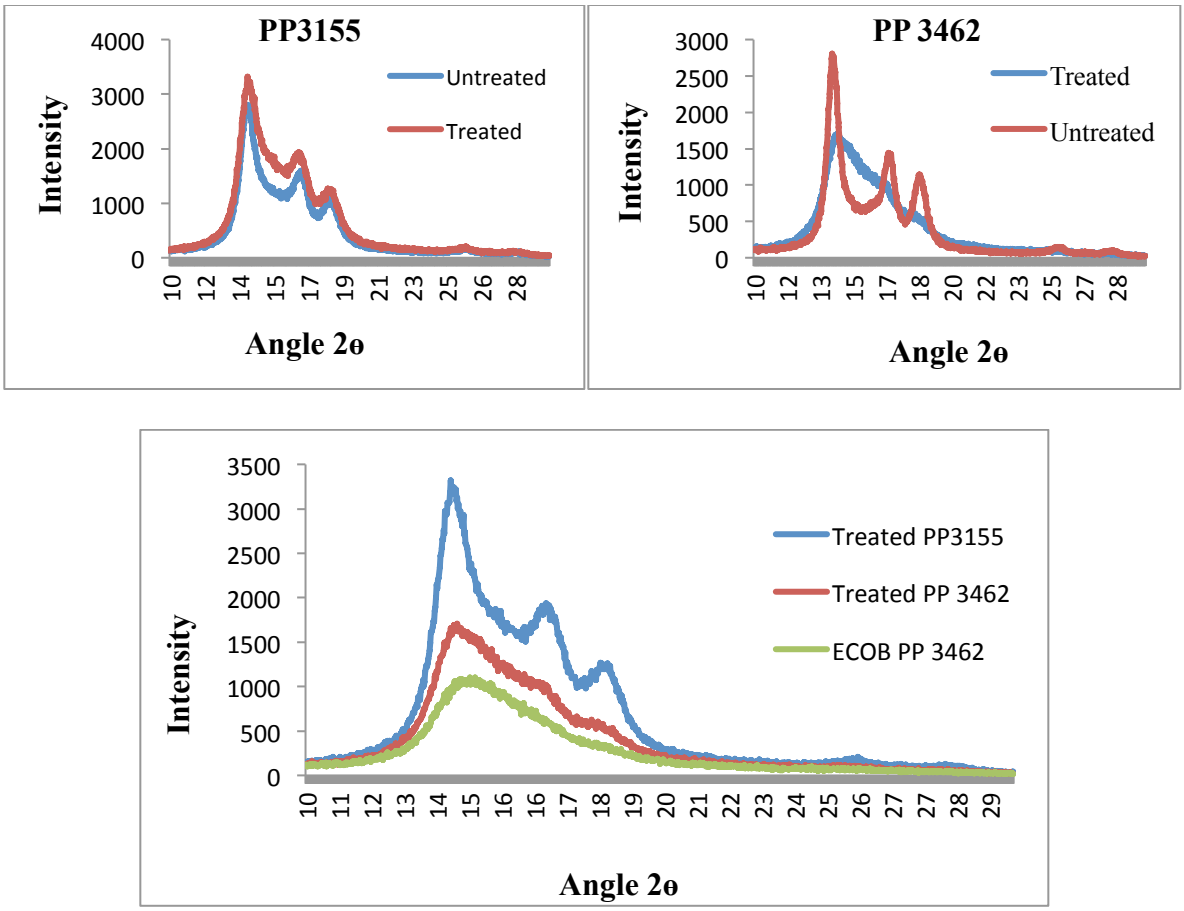

Figure 6. 5 Equatorial X-ray diffraction profiles of PP as-spun fibers spun with and without hIB and ECOB by using different molecular weight polymers.

The azimuthal scans of (110) planes for lower (PP3155) and higher molecular weight (PP 3462) treated PP undrawn fibers are demonstrated in Figure 6.6. It can be seen that treated fibers for both molecular weights demonstrated sharp and strong peaks in azimuthal scans, which indicates well-developed chain orientations for the crystalline phase even if these

fibers showed lower crystallinity percent. As expected, untreated higher molecular weight PP fibers demonstrated a mild and broader peak in azimuthal scan than those of untreated lower molecular weight PP fibers because of the higher level of entanglement. This might suggest that less oriented structure formed at high take-up speed for higher molecular weight untreated fibers.

A more exact investigation of crystalline structure was performed by the detailed analysis in Table 6.4. The primary feature of treated undrawn fibers is highly oriented morphology with lower degree of crystallinity. The degree of crystallinity decreased from 45.72 to 41.50 % for undrawn fibers treated with hIB for lower molecular weight polymer. In addition, the apparent crystal sizes of $L_{110,}$ $L_{040,}$ and L_{130} of the hIB treated fibers are smaller than those of untreated fibers. Although the crystalline orientation factor for untreated fibers, which is about 0.96, is slightly higher than those of hIB treated fibers of 0.94, the amorphous orientation factor is almost double for treated undrawn fibers with the value of 0.63. Relatively higher percentage of crystallinity and crystalline dimensions for the untreated fibers imply a great effect of stress-induced crystallization during the production process.

The structural difference between untreated and treated fibers for higher molecular weight polymer (PP 3462) became more notable when Figure 6.6 and Table 6.4 are examined. The crystal growth process was restricted and the degree of crystallinity decreased from 41.53 to 31.38 % with the treatment by ca. 25 %. The resulting decrease in crystallite size of $L_{110,}$ $L_{040,}$ and L_{130} were observed to almost half of its untreated sizes (Table 6.4). Furthermore, the

unique high amorphous orientation factor of approximately 0.71 is higher than that of untreated fibers of 0.28 by ca. 154 % with observation of improving crystalline orientation factor from 0.93 to 0.95. It indicates that the noncrystalline chains are highly extended for the hIB filaments. The high amorphous orientation factor with a low degree of crystallinity and higher mechanical performance for undrawn treated fibers implies the evidence for the existence of a taut–tie noncrystalline phase. The effects of the higher number of tie molecules and the high amorphous orientation factor on the mechanical properties have been studied by researchers. They concluded a strong relationship exists between the tie molecules and mechanical properties[27-28].

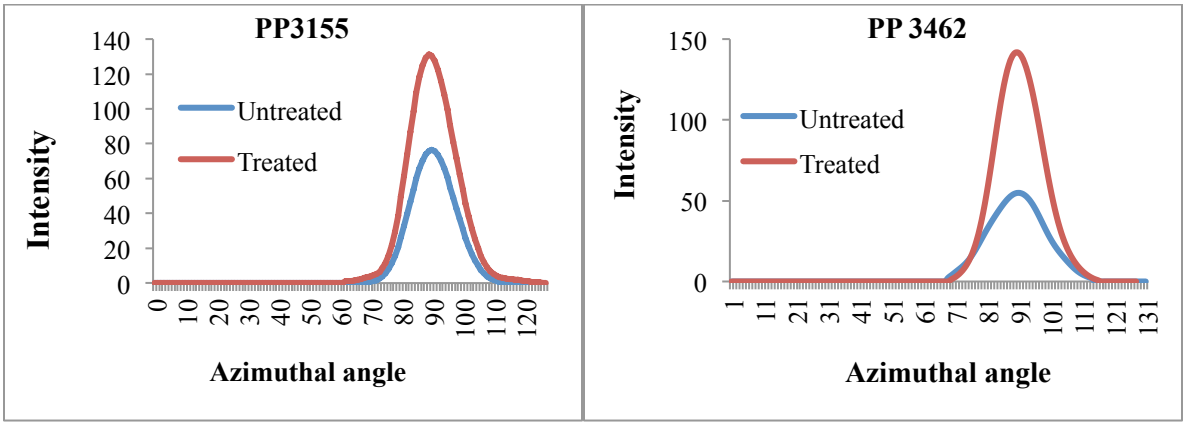

Figure 6. 6 Azimuthal X-ray diffraction profiles of undrawn lower (PP3155) and higher (PP 3462) molecular weight polypropylene fibers spun with and without hIB.

Table 6. 4 Degree of crystallinity, crystalline and amorphous orientation factor, and crystalline dimensions of lower and higher molecular weight PP as-spun fibers with and without hIB.

				Crystallite size (Å)		
Sample	**Crystallinity (%)**	f_c	f_a	L_{110}	L_{040}	L_{130}
PP3155 (U)	45.72	0.96	0.32	83	67	83
PP3155 (T)	41.50	0.94	0.63	76	64	78
PP 3462 (U)	41.53	0.93	0.28	132	135	122
PP 3462 (T)	31.38	0.95	0.71	74	47	65

*U represents untreated and T is abbreviation for treated fibers.

The as-spun treated fibers were drawn mainly to the near-maximum draw ratio in order to investigate the possible structural changes and the improvement for mechanical properties. Figure 6.7 and Table 6.5 illustrate X-ray diffraction profiles of drawn lower (PP3155) and higher (PP 3462) molecular weight polypropylene fibers with their structural parameters after 1.49 draw ratio at the drawing temperature of 120 ^{o}C. In general, after the drawing process, the apparent crystal sizes and degree of crystallinity of fibers increased for both hIB and without hIB fibers. In addition, the peaks of hIB fibers spun at about 2500 m/min changed drastically from unresolved peak(s) to resolved sharp peaks with very high intensities after

just 1.34 draw ratio for lower and higher molecular weight polymers (Figure 6.7). This indicates a well-developed chain orientation and crystalline structures, as determined by detail in degrees of crystallinity of fibers spun with hIB, which are greater than that of fibers without hIB treatment, as illustrated in Table 6.5. Degree of crystallinity increased from 54.92 to 66.61 % and from 55.97 to 61.28 % at draw ratio of 1.49 by increasing ca. 21 and 10 % for lower and higher molecular weight polymers, respectively, with hIB spinning system. The crystallite sizes of treated lower molecular weight polymer (PP3155) were relatively higher than those of untreated fibers. The structural improvement level for degree of crystallinity and crystallite dimensions for fibers which were produced from lower molecular weight polymer spun with hIB implies that the hIB process is more beneficial for lower molecular weight polymers. The crystalline orientation factor for the control, untreated fibers, slightly decreased from 0.96 to 0.95 after the drawing because control fibers were not stable and started to degrade at the drawing temperature of 120 ^{o}C. It was difficult to obtain drawn control fibers at the temperature of 120 ^{o}C due to the low thermal stability of the fibers. However, for treated fibers (PP3155), the crystalline orientation factor slightly increased from 0.94 to 0.95 through the hot drawing process potentially due to the thermally stable phase. As expected, the significant improvement was observed for amorphous orientation factor for treated fibers after the drawing process. The amorphous orientation factor increased from 0.57 to 0.94 by ca. 65 % for treated lower molecular weight polymer fibers, resulting in a highly oriented amorphous and crystalline phase.

Table 6.5 also demonstrates that the effect of liquid is not same as for higher molecular weight polymer fibers even if a highly oriented crystalline and amorphous phase were achieved. The crystalline and amorphous orientation factor increased when the values of control and treated fibers are compared from 0.92 to 0.96 and 0.59 to 0.89, respectively. However, the crystallite sizes did not increase, as the control fibers had the larger sizes (Table 6.5). Increasing the crystallinity but at the same time decreasing the crystallite size phenomenon can interestingly be observed for UHMWPE after irradiating with γ-rays or other high-energy electronic beams[29]. This explains the recrystallization process with the taut-tie chain scission. The changing crystalline orientation factor is negligible, as observed for our treated fibers. The taut-tie chain scission can induce reorganization of the crystalline phase with increasing its perfection because of the relaxation of strained regions of the crystal. During this arrangement, secondary crystallization can be started with increasing the melting temperature by improving lamellae perfection and/or lamellae thickening[30]. The similar effects of radiation on the crystal structure and melting behavior can be observed via irradiation of oriented isotactic polypropylene[31]. However, increasing the absorbed dose could decrease the melting temperature and the perfection of the crystals. The recrystallization process with the taut-tie chain scission might be a reason for hIB treated fibers, which were produced from higher molecular weight polymer. An evidence for the recrystallization process is discussed during the DSC data analysis. Another possible explanation is that undrawn treated fibers (PP 3462 (T)) already had very small crystalline dimensions (Table 6.4), and therefore hot drawing with low draw ratio was only able to

increase the sizes with limited growth. Hence, an appropriate annealing process can be applied to the drawn treated fibers to increase the crystallite sizes which probably yield much higher mechanical properties. In addition, high crystallinity with small crystal dimensions indicates a higher number of crystals and shorter distance between the crystals which cause shorter noncrystalline chains. This unique feature, in addition to a very high value of amorphous orientation factors, confirms highly extended noncrystalline chains and a large number of taut-tie molecules.

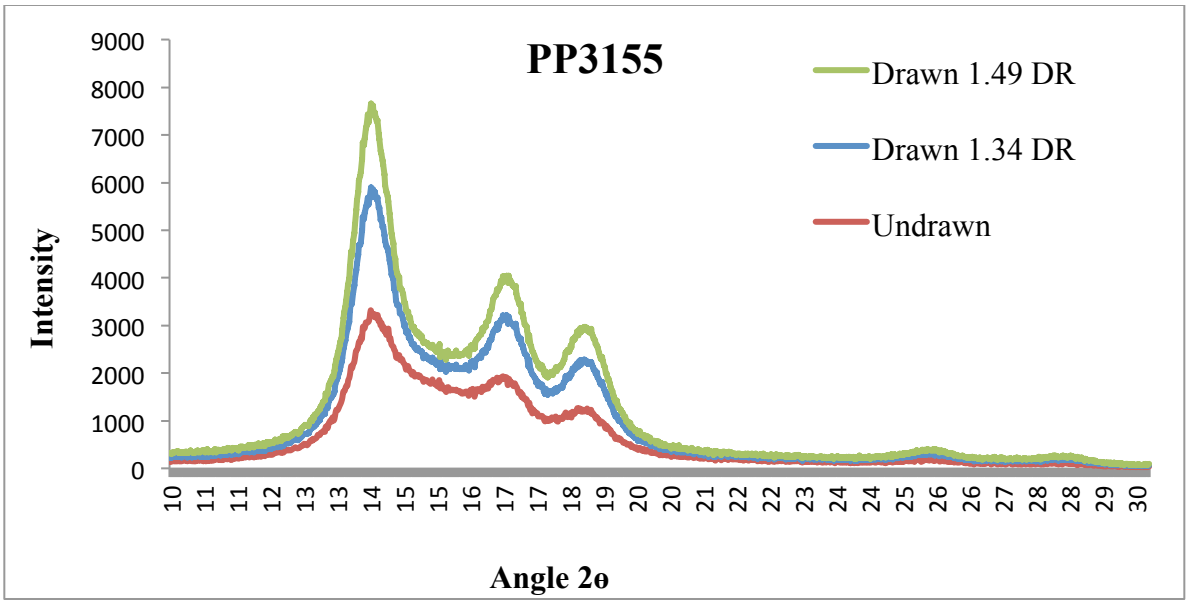

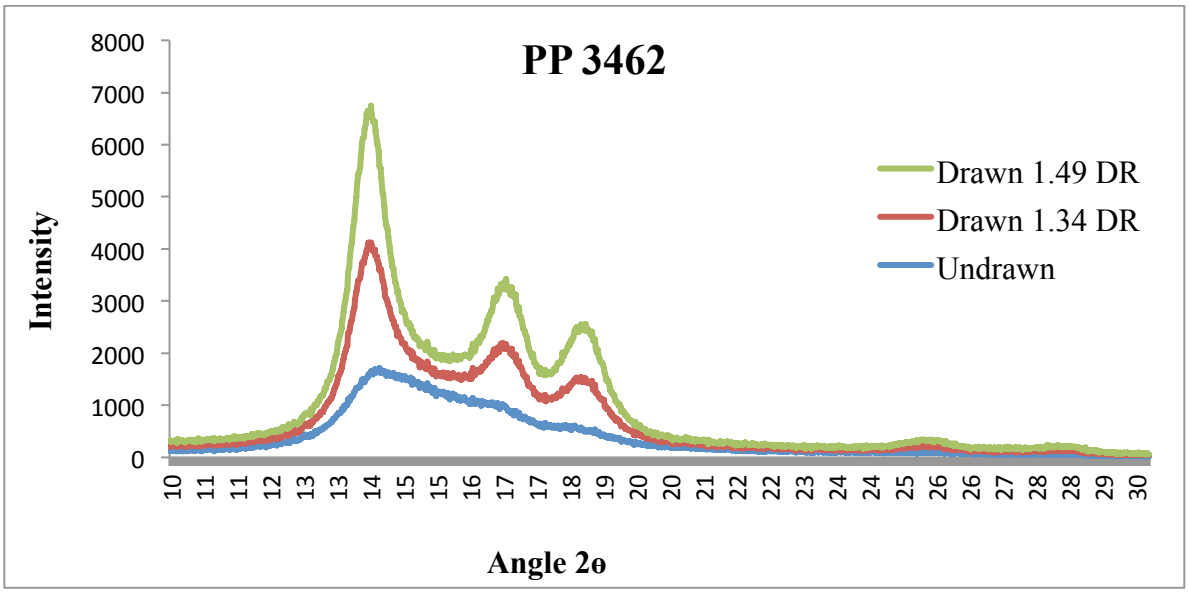

Figure 6. 7 Azimuthal X-ray diffraction profiles of drawn lower (PP3155) and higher (PP 3462) molecular weight polypropylene fibers spun with hIB at different draw ratios.

Table 6. 5 Degree of crystallinity, crystalline and amorphous orientation factor, and crystalline dimensions of lower and higher molecular weight PP drawn fibers with and without hIB at 1.49 draw ratios.

				Crystallite size (Å)		
Sample	**Crystallinity (%)**	f_c	f_a	L_{110}	L_{040}	L_{130}
PP3155 (U)	54.92	0.95	0.57	94	80	85
PP3155 (T)	66.61	0.95	0.94	109	95	84
PP 3462 (U)	55.97	0.92	0.59	142	141	111
PP 3462 (T)	61.28	0.96	0.89	116	97	89

*U represents untreated and T is abbreviation for treated fibers.

6.4.4 Thermal Properties of Untreated and Treated Fibers

The structural changes occurring during the crystallization process can be investigated using differential scanning calorimetry (DSC). However, it is important to mention that new DSC exothermic peaks can be formed during the analysis[32]. This is due to the fact that crystallites formed at low temperatures are subjected to partial melting and recrystallization to yield a perfection process. An increase in the overall crystallinity can be observed as a result of the perfection process. On the other hand, the DSC curve can have multiple endotherms in the melting region for *i*-PP during the scanning process. The first peak temperature is a range between 150-170 ^{o}C, which demonstrates the melting of less ordered (α_1) unoriented spherulites consisting of folded chain crystal lamellae of original fibrillar crystals. The temperature range for the second peak is between 170-185 ^{o}C, which corresponds to the more oriented and ordered (α_2) monoclinic crystal phase[33-34]. The second temperature peak of crystals corresponds to the melting of recrystallization of first peak crystals and shows a thermodynamically more stable phase.

Figure 6.8 shows DSC curves of lower molecular weight PP (PP3155) fibers spun without hIB spinning system at various draw ratios. The first and second peaks are relatively broader for undrawn, untreated fibers. These peaks became sharper after a drawing process at 1.30 and 1.49 draw ratios at the drawing temperature of 120 ^{o}C. At the draw ratio of 1.49, the second peak became sharper and more pronounced, which represents a more ordered crystalline structure. As observed in Table 6.6, the temperature for first melting peaks slightly

decreased from 155.56 to 153.08 ^{o}C, even though the draw ratio increased to 1.49 DR. However, the second melting peaks increased from 168.88 to 172.39 ^{o}C by increasing the draw ratios. Furthermore, the degree of crystallinity increased from 41.75 to 48.32 % by increasing draw ratios for untreated lower molecular weight PP (PP3155) fibers.

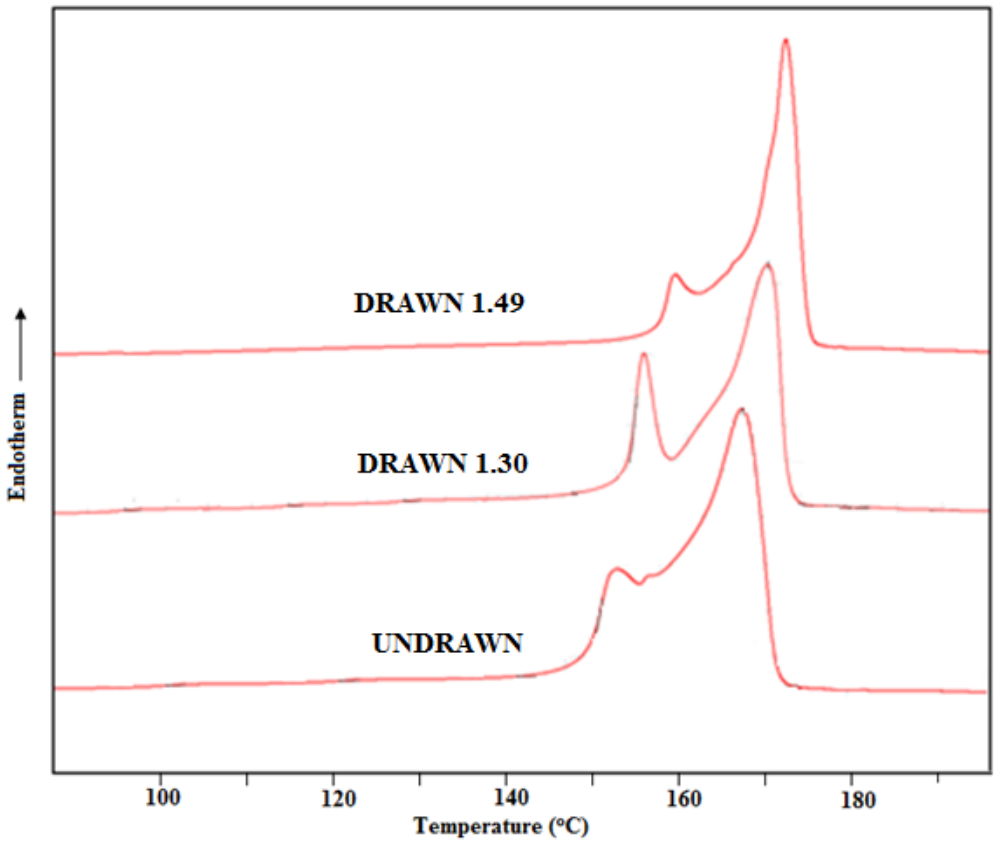

Figure 6. 8 DSC curves of polypropylene (PP3155) fibers spun without hIB at various draw ratios at the drawing temperature of 120 ^{o}C.

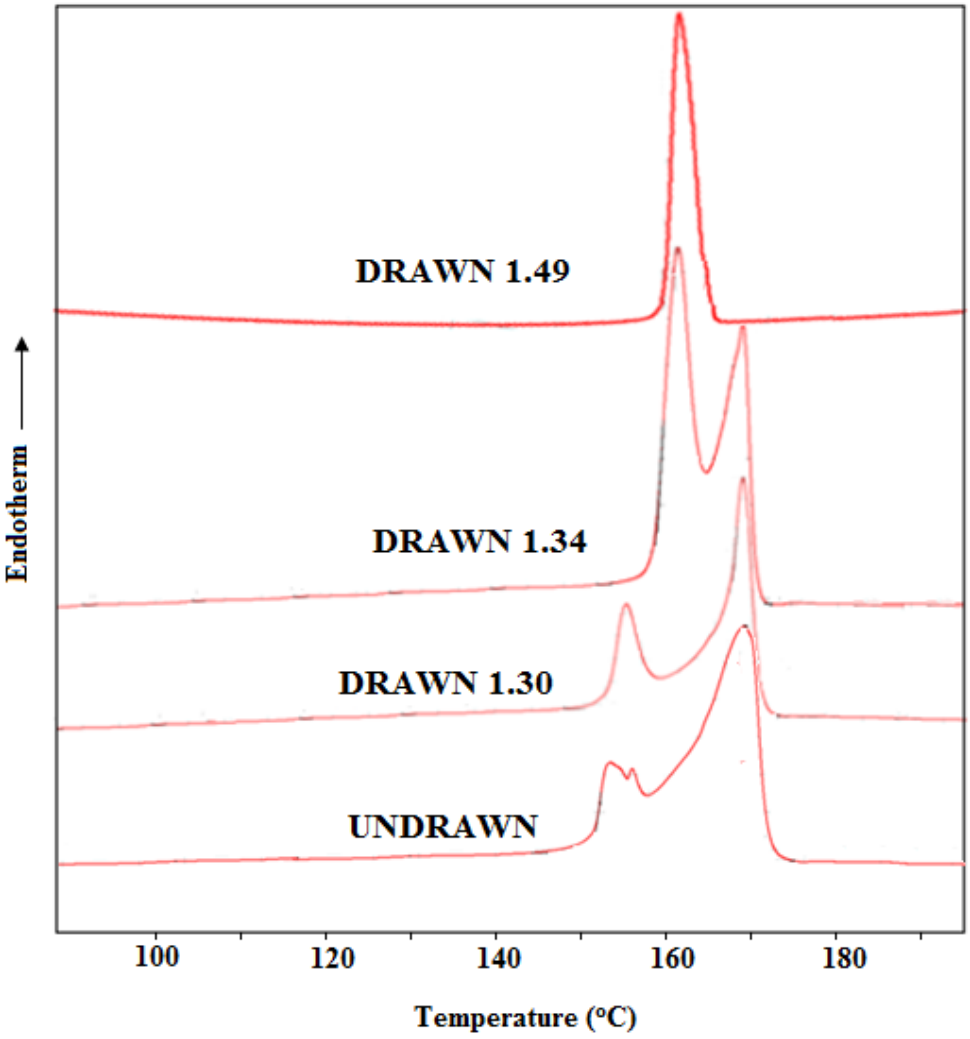

Figure 6. 9 DSC curves of polypropylene (PP3155) fibers spun with hIB at various draw ratios at the drawing temperature of 120 ^{o}C.

Figure 6.9 illustrates the DSC curves of treated polypropylene (PP3155) fibers at various draw ratios up to 1.49 DR at the drawing temperature of 120 ^{o}C. The broader melting peaks for undrawn fibers changed to sharp for first and second melting peaks when the drawing process was carried out. DSC curves of lower molecular weight treated PP filaments acted differently when compared with untreated fibers after 1.34 draw ratios. Up to draw ration of 1.49, the first melting peak is related to the less ordered (α_1) crystalline form and that the second one is related to the more ordered (α_2) monoclinic crystal phase. Increasing the draw ratios resulted in a shift of the peaks towards the higher temperature for the treated fibers. Interestingly, the first peak of DSC curve at 1.34 draw ratios is more dominant than that of second peak. The most interesting fact is that the drawing process did not generate the appearance of double-peak melting endotherms; instead, it generated only a narrow peak almost between the two peaks of undrawn treated fibers at 1.49 draw ratios at the drawing temperature of 120 ^{o}C. Moreover, the highest onset of melting point at the highest degree of crystallinity of 62 % was observed at 1.49 draw ratio. In this case, probably nearly perfect crystals were formed. A single melting endotherm was observed after the annealing process after a certain temperature and processing time[34-35]. Guerra et al.[35] have proposed "continuum" of intermediate modifications in which modification from the limiting disordered α_1 to the limiting ordered α_2. In this regard, the transition from a disordered to a more ordered α form occurred through the recrystallization process to more perfect crystal morphology by melting and renewing crystallization of metastable crystals. In addition, the degree of crystallinity increased from 48.32 to 62.01 % by ca. 28 % at 1.49 draw ratios when

untreated and treated fibers with hIB spinning system were compared. After the drawing process at only 1.49 draw ratio, the degree of crystallinity increased from 44.72 to 62.01 % by ca. 39 % for treated lower molecular weight PP fibers. The increasing peak temperature and degree of crystallinity, coupled with the increasing draw ratio, strongly indicates a higher level of molecular ordering and crystallinity for treated drawn fibers.

Table 6. 6 Thermal properties of polypropylene (PP3155) as-spun and drawn fibers with and without hIB at various draw ratios.

Sample	Onset Melting Point (^{o}C)	Peak Melting Point (^{o}C) (1^{st} peak)	(2^{nd} peak)	ΔH^{o}_{f} (J/g)	Crystallinity (%)
Untreated-undrawn PP	152.27	155.56	168.88	87.260	41.75
Treated-undrawn PP	152.63	154.90	172.27	93.464	44.72
Untreated PP at 1.30 DR	151.44	153.85	171.53	95.794	45.83
Treated PP at 1.30 DR	155.66	157.93	173.79	107.648	51.51
Untreated PP at 1.49 DR	150.23	153.08	172.39	100.996	48.32
Treated PP at 1.49 DR	160.46	164.55		129.598	62.01

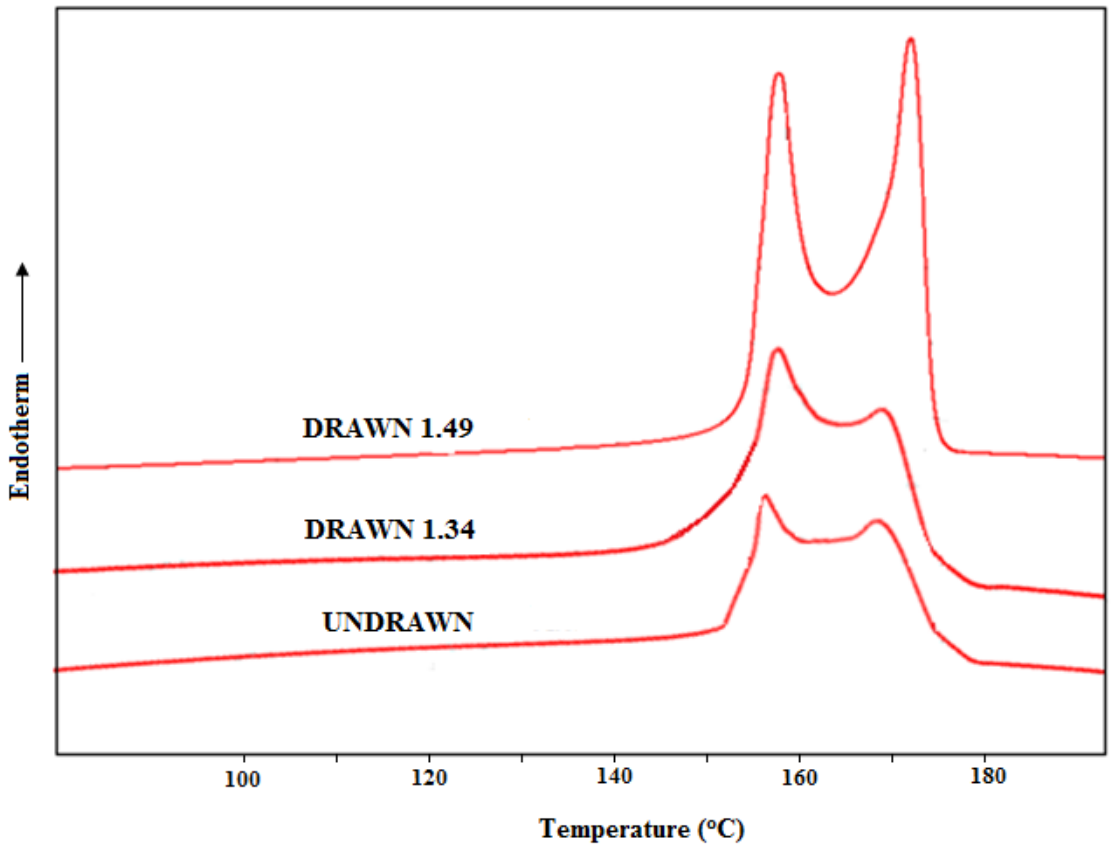

Figure 6. 10 DSC curves of polypropylene (PP 3462) fibers spun without hIB at various draw ratios at the drawing temperature of 120 ^{o}C.

Figure 6.10 presents DSC curves of as-spun and drawn untreated higher molecular weight PP (PP 3462) fibers were made at the take-up velocity of about 2500 m/min at 170 cm production distance. The DSC curves show double endotherms in the melting region for *i*-PP during the scanning process as observed for lower molecular weight untreated PP fibers. In

this case, the second peak was also formed by crystal melting and recrystallization. It represents the more ordered (α_2) monoclinic crystal phase with the thermodynamically more stable phase. As investigated in detail in Table 6.7, the temperatures for first and second peaks increased from 155.64 to 158.85 ^{o}C and from 170.65 to 174.64 ^{o}C, respectively, by increasing the draw ratios to 1.49. Additionally, the degree of crystallinity increased from 38.68 to 51.44 % by increasing the draw ratios.

It can be realized that there is a significant difference between lower and higher molecular weight untreated PP fibers for their DSC curves when Figure 6.8 and 6.10 are compared. For all lower molecular weight fibers, the second peaks are more dominant, whereas the first peaks are more pronounced for higher molecular fibers, even though all the fibers were produced almost with the same production parameters. Despite the fact that the second peak for higher molecular weight untreated fibers appears more dominant, there is no tremendous difference between first and second peaks at 1.49 draw ratios (Figure 6.10). At the draw ratio of 1.49, the area of second peak increased that lead to the formation of more ordered crystalline structures. This phenomenon implies the lower molecular weight untreated fibers possess a more ordered (α_2) monoclinic crystal phase than that compared to higher molecular weight fibers. Moreover, as seen in Figure 6.10, the first peaks for undrawn and drawn untreated fibers show a narrow melting range, which demonstrates that more uniform structures for (α_1) crystalline form exists other than that of the more ordered (α_2) monoclinic crystal phase. Hence, the DSC curves for untreated higher molecular weight fibers suggest that a higher draw ratio of more than 1.49 can be applied to the fibers to obtain a more

oriented, ordered crystal phase with a higher crystallinity and improved mechanical properties.

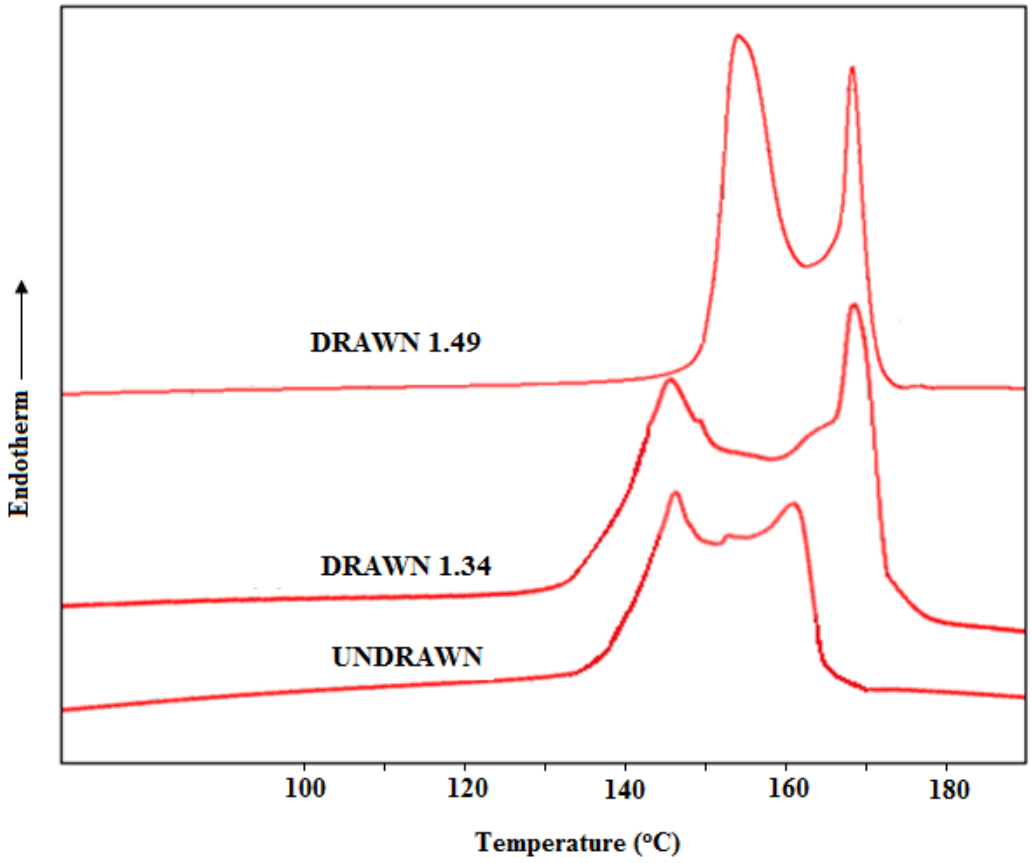

Figure 6. 11 DSC curves of polypropylene (PP 3462) fibers spun with hIB at various draw ratios at the drawing temperature of 120 ^{o}C.

On the other hand, DSC curves for treated higher molecular weight fibers are quite different than those of untreated fibers, as shown in Figure 6.11 for as-spun and drawn filament. After the drawing process of 1.34 and 1.49 draw ratios, the second melting peaks demonstrate a narrow melting range becoming clear and sharp, corresponding to extended and oriented macromolecular crystals for the treated fibers. Although the onset and first peak melting temperature for the treated fibers increased from 151.05 to 158.83 ^{o}C and from 153.85 to 161.68 ^{o}C, respectively, the second melting peak temperature initially increased and then decreased after 1.34 draw ratio from 178.70 to 174.74 ^{o}C at the draw ratios of 1.49 (see Table 6.7). At 1.49 draw ratios, the low-temperature crystallization peak became larger and shifted to a higher temperature; however, for control fibers, it was observed that the second peak had larger areas than the first peak. Further, the degree of crystallinity increased from 44.57 to 56.17 % by increasing draw ratios up to 1.49. Interestingly, these peak melting temperatures and degree of crystallinity for treated higher molecular weight fibers suggest the similar structural developments as those for treated lower molecular weight fibers shown in Figure 6.9. However, the modification from the limiting disordered α_1 to the limiting ordered α_2 was not completed for higher molecular weight fibers, although the near maximum draw ratio of 1.49 was performed for the fibers. Many trials for the liquid and spinning conditions were attempted for these fibers (PP 3462), but the results showed that the optimum process conditions, which were found till now, can be improved to obtain more oriented and fine structural development. This possible development after the optimization can bring the fibers

performance close to its theoretical performance, even if more than 12 g/d and 190 g/d were manufactured so far for tenacity and modulus performances, respectively.

In addition to the structural development of treated higher molecular weight fibers, another interesting phenomenon is that DSC scan display more than double melting endotherms when Figure 6.11 is carefully examined, as observed for ECOB treated fibers (please see our related study's chapter). This additional peak is located between 160-165 ^{o}C for hIB as-spun fibers, then shifted to between 170-175 ^{o}C for drawn hIB fibers at 1.34 draw ratios. Finally, the peak maxima became 174.74 ^{o}C for drawn hIB fibers at the draw ratio of 1.49. It can be thought that some different type of crystals in the second peak have been co-existing in the hIB as-spun fibers and this intermediate-temperature peak, which became obvious at 1.49 draw ratios. Another evidence of this different type of crystal is that, when draw ratios increased from 1.34 to 1.49, the second melting endotherm decreased from 178.7 to 174.7 ^{o}C. In general, the second peak temperature should increase by increasing the number of draw ratios by hot drawing processes. Therefore, the second peak at 1.49 draw ratios was most likely formed from the additional intermediate peak of hIB treated fibers. X-ray analysis also confirmed that a different type of crystal possibly existed for the treated fibers because of the observation of higher degree of crystallinity with smaller crystallite sizes. All these behaviors suggest that the limiting disordered α_1 to the limiting ordered α_2 was not completed for the crystals in the intermediate-temperature peak. Hence, double melting peaks have been observed instead of single ones, as were observed for the treated drawn lower molecular

weight PP fibers (Figure 6.9). This additional peak appears very narrow and sharp at 1.49 draw ratio, whereas the first peak is much broader at the same draw ratio.

Table 6. 7 Thermal properties of polypropylene (PP 3462) as-spun and drawn fibers with and without hIB at various draw ratios.

Sample	Onset Melting Point (^{o}C)	Peak Melting Point (^{o}C) (1^{st} peak)	(2^{nd} peak)	ΔH^{o}_{f} (J/g)	Crystallinity (%)
Untreated-undrawn PP	152.67	155.64	170.65	80.850	38.68
Treated-undrawn PP	151.05	153.85	171.04	93.161	44.57
Untreated PP at 1.34 DR	153.21	157.04	170.03	88.705	42.44
Treated PP at 1.34 DR	154.55	156.07	178.70	110.485	52.86
Untreated PP at 1.49 DR	155.65	158.85	174.64	107.520	51.44
Treated PP at 1.49 DR	158.53	161.68	174.74	117.401	56.17

Figure 6.12 clearly shows the effect of liquid type and molecular weight of polypropylene on the structural development of treated fibers at 1.49 draw ratio at the drawing temperature of

120 ^{o}C. The DSC curve for LMW PP fibers (PP3155) spun with hIB indicates the structural development of ultra-high strength fibers is significant because it has only a single, narrow, sharp peak. When the effect of the bath type considered, the hIB process is more beneficial than ECOB's for the structural development to come close at the 'continuum' of intermediate modifications. Further, the improvement of the internal structure for treated PP 3462 is much closer than that of ECOB PP 3462 to the treated drawn PP 3155 when Figure 6.12 was carefully examined with some other discussion points which have already been presented. However, in the terms of the tenacity and modulus performance, there is no significant difference between all these three drawn fibers, except the modulus value of ECOB PP 3462 fibers, which is lower than others.

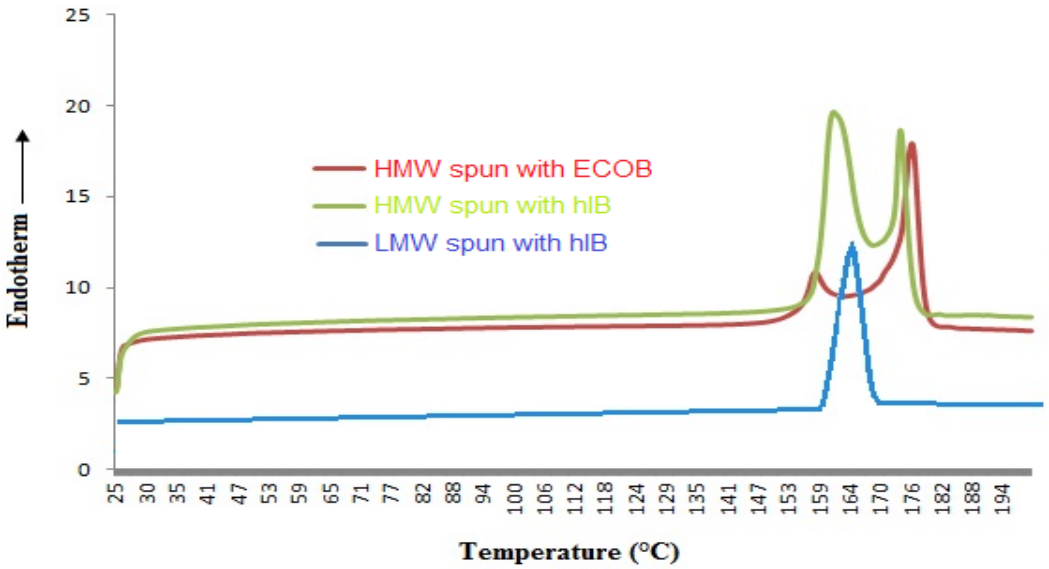

Figure 6. 12 The effect of liquid type and molecular weight of polypropylene on the DSC curves of the treated fibers after drawing at 1.49 draw ratios.

6.4.5 Effect of hIB on Birefringence of Treated Fibers

In general, birefringence of semi-crystalline isotactic polypropylene fiber is considered an orientation measure of the amorphous and crystalline regions. Increasing of birefringence implies that the molecular chains are oriented or aligned in parallel direction more than that of a perpendicular one via any type of processing. However, the crystalline orientations for the fibers are usually higher, hence the degree of amorphous orientation is more dominant on the overall orientation to determine the birefringence. The take-up speed and drawing process are two important parameters for the traditional melt spinning process to increase birefringence. Furthermore, increasing both take-up velocity and draw ratio lead to an increase in the overall orientation by the increasing the alignment of molecules along the drawing direction. In fact, the birefringence values for as-spun and drawn fibers, which are produced by the traditional (high speed) melt spinning process, are lower because of limited structural development. However, the hIB spinning system gives a unique improvement for the birefringence when compared with the traditional high speed melt spinning method, as seen in Figure 6.13. It can be observed that the birefringence increased from 0.023 to 0.033 and from 0.021 to 0.036 by ca. 43 and 71 % by using lower (PP3155) and higher (PP 3462) molecular weight polymer via hIB method, respectively. While all untreated and treated of lower and higher molecular weight fibers are compared, there is not any tremendous difference either before or after drawing processes (see Figure 6.13). In the hIB spinning system, both stress (the drag force) and the temperature profiles were modified after the

setting of the optimum process conditions, which improves the birefringence dramatically. Unlike the untreated fibers, the unique properties of undrawn treated fibers of low crystallinity and high birefringence indicate decreasing of the occurrence of folded chains and the formation of extended chains. In addition to low crystallinity and higher birefringence for treated as-spun fibers, higher tenacity and modulus performance verify the existence of higher fraction of taut–tie molecular chains for treated fibers than those of untreated fibers.

After the drawing process of 1.34 draw ratio at the drawing temperature of 120 ^{o}C, the overall orientation increased for all treated and untreated fibers (Figure 6.13). Birefringence increased by ca. 42 and 70 % from 0.026 to 0.037 and from 0.023 to 0.039 by using hIB spinning system after the drawing process. Interestingly, the improvement between hIB and without hIB fibers for undrawn and drawn fibers is almost the same, which indicates the importance of the overall orientation before the drawing process. The sharp increase in the degree of crystallinity after just 1.34 draw ratio with high birefringence for treated fibers induced what was probably orientational crystallinity, in which taut–tie molecular chains were developed and transformed into crystals.

The highest values for birefringence were observed for the higher molecular weight fibers (PP 3462) than those of lower molecular weight ones (PP3155) for undrawn and drawn fibers. Hence, it can be suggested that the level of birefringence for treated lower molecular weight fibers implies believably that a saturated level of molecular orientation has been reached. In addition, the degree of crystallinity is always higher for hIB fibers when the lower

molecular weight polymers were used. The amorphous orientation factor is very close to each other when the drawing process's values of both before and after are considered for treated lower and higher molecular weight fibers. All of these parameters (birefringence, degree of crystallinity, and amorphous orientation factor) are clearly indicating that the process conditions, especially for higher molecular weight fibers (PP 3462), could be improved. Hence, higher orientation for molecular chains for those fibers can be transformed into taut-tie molecular chains and/or crystals, which causes a higher degree of crystallinity and even more fiber performance for the tenacity and modulus performances.

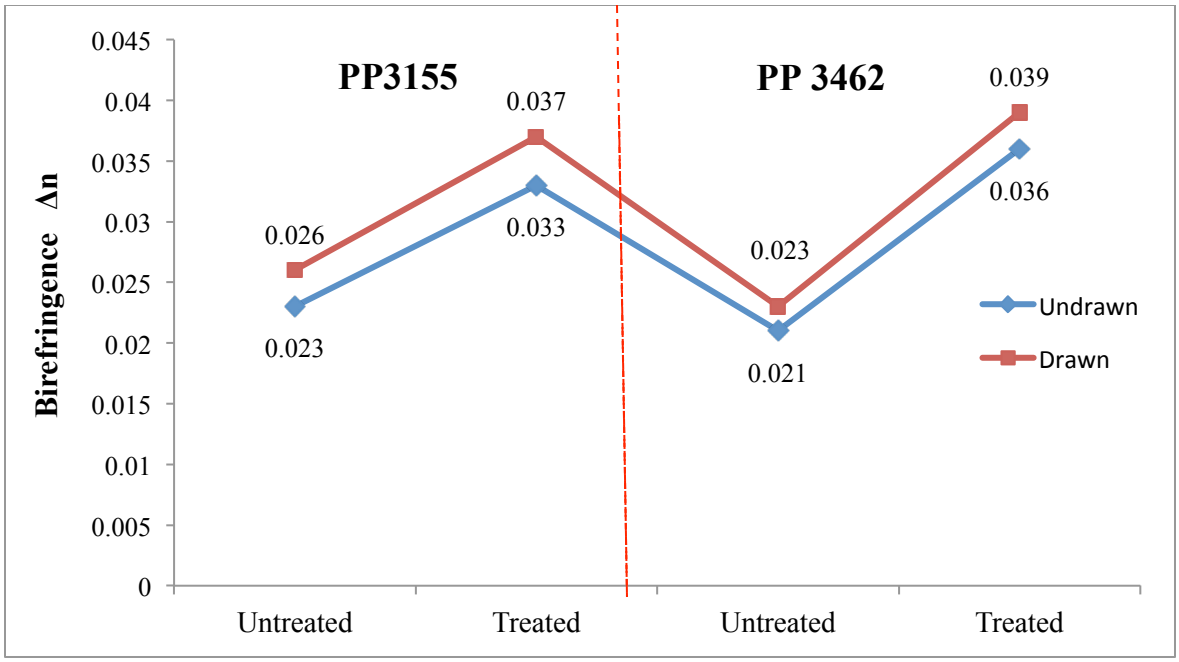

Figure 6. 13 The relation between birefringence of untreated and treated with hIB of *i*-PP fibers by using lower (PP3155) and higher (PP 3462) molecular weight polymers (draw ratio = 1.34).

The second prominent feature is a very strong correlation between the birefringence and tenacity values for all untreated and treated fibers. Increasing birefringence for fibers yields improvements in tenacity, as seen in Figure 6.14. A polynomial trendline was observed between the birefringence and fiber's tenacity for undrawn fibers with R^2 of 0.892. The equation for this correlation is as follows:

$$y = -14190x^2 + 974.6x - 9.558 \qquad (7)$$

where: y is the fiber tenacity (g/d), and x is the birefringence (Δn).

In addition, there was a significant increase in the relationship between tenacity and birefringence after the drawing process was observed for all fibers, even if the same trendline of polynomial with $R^2 = 0.990$ was determined (see eq 8).

$$y = 6754.5x^2 - 112.41x + 6.1354 \quad (8)$$

where: y is the fiber tenacity (g/d), and x is the birefringence (Δn).

Prediction of tenacity is more difficult than initial modulus. Tenacity could be low because of cracks or because of weak points within the fiber. After the drawing process, the higher the crystallinity, the larger the crystal sizes, increasing the amorphous and crystalline orientation factors presumably to inhibit the effects of weak points during the tensile tests. Hence, R-squared values for the trendline increased after the drawing process. In addition, the prediction of the tenacity from the birefringence by a linear or direct correlation is very challenging and almost impossible. For instance, after the drawing process, the lower molecular weight fibers showed the birefringence of 0.037 and 11.50 g/d for the tenacity; however, at the similar value of birefringence of 0.036 for untreated, undrawn higher molecular weight, fibers only demonstrated the tenacity performance of 6.91 g/d.

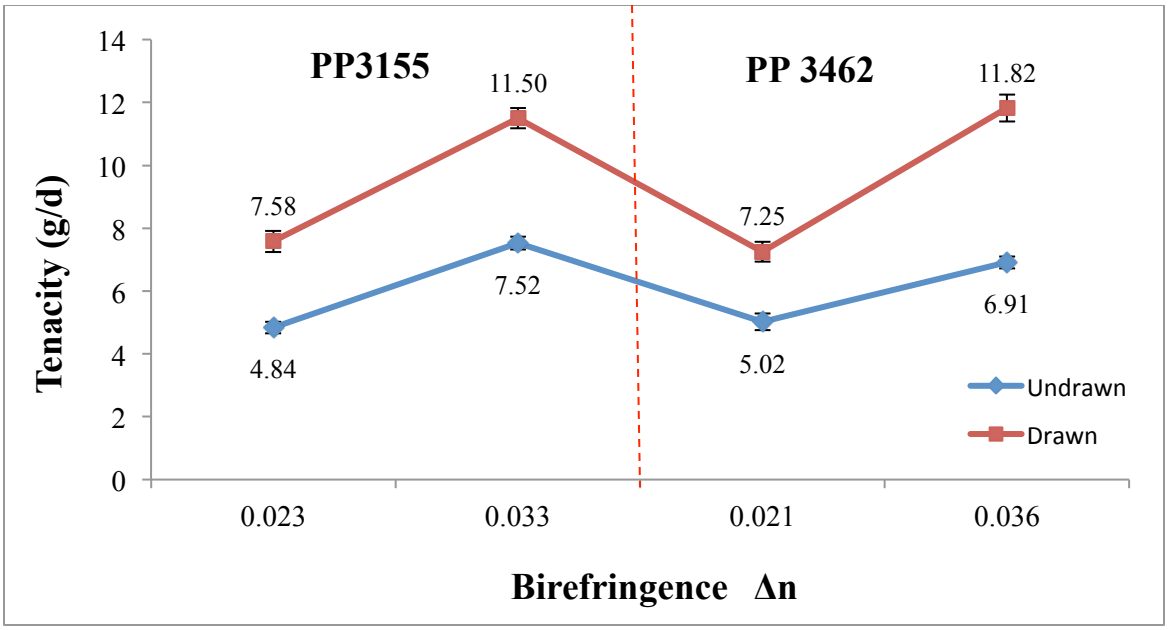

Figure 6. 14 The relation between birefringence and tenacity of untreated and treated with hIB of *i*-PP fibers by using lower (PP3155) and higher (PP 3462) molecular weight polymers (draw ratio = 1.34).

An unexpected display of fibers between the drawn untreated and drawn treated fibers was observed when the fibers were examined by a Nikon Eclipse polarizing microscope with water immersion, as demonstrated in Figure 6.15. These dark-banded structures on the treated fibers were also exactly observed for the ECOB treated fibers after the drawing process. The formation of the void structure[36] could be a reason for these dark transverse lines. Further, this similar structure can be observed for etched Kevlar fibers[37].

Interestingly, the dark-banded morphology is significantly different for drawn treated lower molecular weight fibers, as shown in Figure 6.15. These fibers only showed some dark spots, although all drawn treated fibers with hIB and ECOB are white in color with outstanding performance; untreated ones are transparent to the naked eye. The difference between the molecular weights of PP 3462 and PP3155 is a strong evidence for the morphological changes in drawn fibers. This interesting phenomenon could be explained primarily due to the occurrence of homogeneous and continuous structures for lower molecular weight polymers during the drawing process because of a substantially smaller number of entanglements. In the drawing process, smaller number of entanglements seem to experience more homogeneous deformation which, in this case, leads to more uniform structures for the given draw ratio. After the drawing process, treated PP3155 fibers showed a higher amorphous orientation factor of 0.94 than those of PP 3461 filaments of 0.89. Hence, the transparent morphology is more dominant for drawn treated lower molecular weight fibers when compared with drawn treated higher molecular weight ones (Figure 6.15). These observations can be also attributed to the fact that the strain-induced crystallization (during the drawing process) mainly occurred by the high molecular weight tail. Therefore, the molecular weight differences between these fibers have most likely revealed that the distinct strain-induced crystallization behaves differently under the microscope.

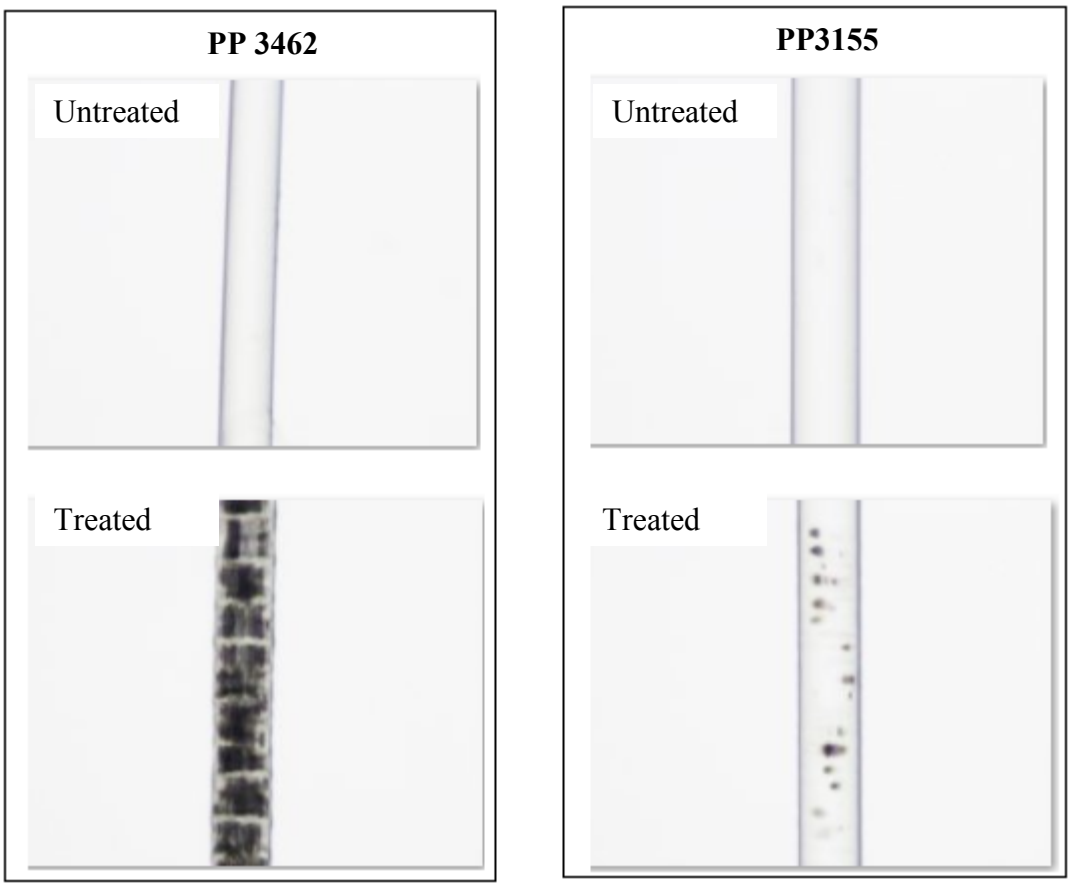

Figure 6. 15 Microscope images of untreated, and treated fibers by using higher (PP 3462) and lower (PP3155) molecular weight polymer after the drawing of 1.49 draw ratios.

6.5 Conclusions

Ultra-high performance and different types of precursors morphology polypropylene fibers were obtained by using lower (PP3155) and higher (PP 3462) molecular weight polymers via hIB spinning system. The mean value of the highest tenacity and modulus of treated lower molecular weight fibers are 7.52 g/d and 75.51 g/d for as-spun and 12.21 g/d with 196.66 g/d for drawn fibers after only 1.49 draw ratios, respectively. The similar performance was also observed for treated higher molecular weight fibers. The theoretical modulus of PP is 35–42 GPa[19], 275-330 g/d, which shows the hIB fiber's modulus performance is approaching its theoretical maximum values.

It should be noted that the optimum process conditions, such as liquid temperature and liquid depth, and the precursors for crystallization, are different and depend upon the molecular weight of polymers to obtain high-tenacity and high-modulus fibers. Another crucial result from this study is that higher elongation at break (probably more than 100 %) is one of the disadvantages of wanted precursor morphology for crystallization, even if the treated undrawn fibers show high tenacity. This was confirmed during the tensile test measurements for the drawn fibers.

The production distance between the spinneret and hIB tank for both polymers were the same and adjusted 170 cm, which was the highest production distance in our laboratory conditions. In our another study focusing on PET fibers spun with hIB, the optimum distance for PET fibers was determined to be 90 cm, which was the shortest production distance. This

difference can be explained as the huge difference between the glass transition temperature of PP and PET; additionally, PP fiber needs about double the time for PET fibers to solidify at the same conditions. However, these different types of precursors for crystallization demonstrated the common feature being highly oriented, yet noncrystallized or showing the first stage of crystallization, as seen in X-ray analysis. After the drawing process to low draw ratio of 1.34, the treated fibers showed a well-developed chain orientation and highly crystallized structures with superior mechanical performance.

Even if the hIB spinning system with the higher molecular weight polymer gave more opportunity for study at different liquid temperatures and other working conditions, hIB spinning system is more beneficial for low molecular weight polypropylene (melt flow rate of 36 g/10 min), as we concluded also for PET fibers. It is well recognized that from the combined analysis of SEM, X-ray and DSC for treated fibers that the optimum fine crystallization and molecular orientation were developed for the low molecular weight PP fibers. For example, only low molecular weight undrawn treated fibers (PP3155) showed the fibrils in their cross-section, in which the fibers not only had highly oriented structures, but also demonstrated separation of lamellae in blocks to evolve into a fibrillar structure. After the drawing process, the fracture mechanism of the PP fibers (PP3155) is closer to Kevlar and Spectra than those of higher molecular weight drawn treated PP fibers (PP 3462). The DSC analysis indicated that low molecular weight PP fibers (PP3155) were spun with hIB showed a tremendous structural development for ultra-high strength fibers by generating a single, narrow, sharp peak after just 1.49 draw ratios. Another evidence of this unique improvement

can be seen in Figure 6.5, which shows that the highest overall intensity was observed for the low molecular weight PP fibers when compared with PP fibers (PP 3462) spun with hIB and ECOB spinning system.

As a result, this study contributes for the first time that the hIB spinning system has the capability of manufacturing ultra-high performance PP fibers even before the drawing processes. The structure developments and the precursor morphology in the resulting hIB as-spun and drawn filaments were significantly affected by the process conditions. The optimum process conditions varied and changed according to the polymer and liquid types, and molecular weights of polymers.

6.6 References

1. Market Study: Polypropylene. As viewed on line at (November 25th, 2012): http://www.ceresana.com/en/market-studies/plastics/polypropylene/

2. Somani, R. H., Young, L., Hsiao, B. H., Agarwal, P. K., Fruitwala, H. A., & Tsuo, A. H. (2002). Shear-induced precursor structures in isotactic polypropylene melt by in-situ rheo-SAXS and rheo-WAXD studies. *Macromolecules*, 35, 9096-9104.

3. Kumaraswamy, G., Kornfield, J. A., Yeh, F., & Hsiao, B. (2002). Shear-enhanced crystallization in isotactic polypropylene. 3. Evidence for a kinetic pathway to nucleation. *Macromolecules*, 35, 1762 -1769.

4. Coppola, S., Balzano, L., Gioffredi, E., Maffettone, P. L., & Grizzuti, N. (2004). Effects of the degree of undercooling on flow induced crystallization in polymer melts. *Polymer*, 45, 3249–3256.

5. Seki, M., Thurman, D. W., Oberhauser, J. P., & Kornfield, J. A. (2002). Shear-mediated crystallization of isotactic polypropylene: The role of long chain-long chain overlap. *Macromolecules*, 35, 2583–2594.

6. Ziabicki, A. (1996). Crystallization of polymers in variable external conditions 1. General equations. *Colloid and Polymer Science*, 274(3), 209-217.

7. Ziabicki A. Crystallization of polymers in variable external conditions. II. Effects of cooling in the absence of stress and orientation. *Colloid and Polymer Science,* 274, 705-716.

8. Balzano, L., Rastogi, S., & Peters, G. W. M. (2009). Crystallization and precursors during fast short-term shear. *Macromolecules*, 42, 2088-2092.

9. Kanaya, T., Takayama, Y., Ogino, Y., Matsuba, G., & Nishida, K. (2007). Precursor of primary nucleation in isotactic polystyrene induced by shear flow. *Lecture Notes in Physics*, 714, 87–96.

10. Balzano, L., Rastogi, S., & Peters, G. W. M. (2009). Crystallization and precursors during fast short-term shear. *Macromolecules*, 42 (6), 2088-2092.

11. White, E. E. B., Winter, H. H., & Rothstein, J. P. (2012). Extensional-flow-induced crystallization of isotactic polypropylene. *Rheologica Acta*, 51(4), 303-314.

12. Lin, C. Y., Tucker, P. A., & Cuculo, John, A. (1992). Poly(ethylene terephthalate) melt spinning via controlled threadline dynamics. Journal of Applied Polymer Science, 46, 531-552.

13. Hotter, J. F., Cuculo, J. A., Tucker, P. A., & Annis B. K. (1998). Effect of liquid isothermal bath position in modified poly (ethylene terephthalate) PET melt spinning process on properties and structure of as-spun and annealed filaments. Journal of Applied Polymer Science. 69, 2051–2068.

14. Lin, C. Y., Tucker, P. A., & Cuculo, John, A. (1992). Poly(ethylene terephthalate) melt spinning via controlled threadline dynamics. Journal of Applied Polymer Science, 46, 531-552.

15. Bhuvanesh, Y. C., & Gupta V. B. (1995). Interaction between viscoelastic and structural relaxation in drawn polypropylene yarn. *Polymer*, 36(19) 3669-3674.

16. Lin, K. Y., Xanthos, M., & Sirkar, K. K. (2009). Novel polypropylene microporous membranes via spherulitic deformation – Processing perspectives. *Polymer*, 50, 4671–4682.

17. Samuels, R. J. (1968). Quantitative characterization of deformation in drawn polypropylene films. *Journal of Polymer Science Part A*, 6, 1101-1139.

18. Brandrup J., & Immergut E. H. (1999). *Polymer Handbook*. New York: Willey 2nd Ed.

19. Mukhopadhyay, S., Deopura, B. L., & Alagirusamy, R. (2004). Production and properties of high-modulus--high-tenacity polypropylene filaments. *Journal of Industrial* Textiles, 33 (4), 245-268.

20. Chen, P., Afshari, M., Cuculo, J. A., & Kotek, R. (2009). Direct formation and characterization of a unique precursor morphology in the melt-spinning of polyesters. *Macromolecules*, 42, 5437–5441.

21. Sheehan, W. C., & Cole, T. B. (1964). Production of super-tenacity polypropylene filaments. *Journal of Applied Polymer Science*, 8, 2359-2388.

22. Hautojärvi, J., & Leijala, A. A. (1999). Morphological study of melt-spun polypropylene filaments by atomic force microscopy. *Journal of Applied Polymer Science*, 74, 1242-1249.

23. Hearle, J. W. S., Lomas, B., & Cooke W. D. *Atlas of Fibre Fracture and Damage to Textiles*. Boca Raton, FL: CRC Press. 1998; 2nd Ed.

24. Peterlin, A. (1971). Molecular model of drawing polyethylene and polypropylene. *Journal of Materials Science*, 6, 490-508.

25. Ottone, M. L., Peirotti, M. B., & Deiber, J. A. (2002). Modeling melt spinning with stress induced crystallization at high take up velocities. Numerical results for the PET melt. *Mecanica Computacional*, 21, 67-85.

26. Chen, J. Y., Tucker, P. A., & Cuculo, J. A. (1997). High-performance PET fibers via liquid isothermal bath high-speed spinning: Fiber properties and structure resulting from threadline modification and posttreatment. *Journal of Applied Polymer Science*, 66, 2441–2455.

27. Rim, P. B., & Nelson, C. J. (1991). Properties of PET fibers with high modulus and low shrinkage (HMLS). I. Yarn properties and morphology. *Journal of Applied Polymer Science*, 42, 1807-1813.

28. Kunugi, T., Ito, T., Hashimoto, M., & Ooishi M. (1983). Preparation of high-modulus and high-strength isotactic polypropylene fiber by zone- annealing method. *Journal of Applied Polymer Science*, 28, 179-189.

29. Zhang, H., Shi, M., Zhang, J., & Wang, S. (2003). Effects of sunshine UV irradiation on the tensile properties and structure of ultrahigh molecular weight polyethylene fiber. *Journal of Applied Polymer Science*, 89, 2757–2763.

30. Dudic, D., Kostoski, D., Djokovic, V., & Stojanovic Z. (2000). Recrystallization processes induced by accelerated ageing in isotactic polypropylene of different morphologies. *Polymer Degradation and Stability*, 67, 233-237.

31. Kostoski, D., & Stojanovic, Z. (1995). Radiation-induced crystallinity changes and melting behavior of drawn isotactic polypropylene. *Polymer Degradation and Stability*, 47, 353-356.

32. Holdsworth, P. J., & Turner-Jones, A. (1971). The melting behaviour of heat crystallized poly(ethylene terephthalate). *Polymer*, 12, 195-208.

33. Somani, R. H., Yang, L., Sics, I., Hsiao, B. S., Pogodina, N., Winter, H. H., Agarwal, P., Fruitwala, H., & Tsou, A. Orientation-induced crystallization in isotactic polypropylene melt by step-shear deformation. As viewed on line at (November 25th, 2012): http://rheology.tripod.com/z09.13.pdf

34. Caldas, V., Brown, G. R., Nohr, R. S., & Macdonald, J. G. (1996). 13C CP/MAS NMR studies of morphological changes in polypropylene: 2. The double melting

endotherm of spunbonded fabrics. *Journal of Polymer Science: Part B: Polymer Physics*, 34, 2085-2098.

35. Guerra, G., Petraccone, V., Corradini, P., De Rosa, C., Napolitano, R., Pirozzi, B., & Giunchi, G. (1984). Crystalline order and melting behavior of isotactic polypropylene (α form). *Journal of Polymer Science: Polymer Physics Edition*, 22(6), 1029–1039.

36. Farrow, B., & Ford, J. E. (1964). Transverse markings in strained fibres. *Nature*. 201 (4951), 183-184.

37. Shahin, M. M. (2003). Optical microscopy study on poly(p-phenylene terephthalamide) fibers. *Journal of Applied Polymer Science*. 90, 360–369.

38. Andreassen, E., & Myher, O. J. (1993). Infrared spectroscopy measurements of residual stresses in polypropylene fibers. *Journal of Applied Polymer Science,* 50, 1715–1721.

39. Huo, H., Jiang, S., An L., & Jiachun, F. (2004). Influence of shear on crystallization behavior of the *β* phase in isotactic polypropylene with *β*-nucleating agent. *Macromolecules*, 37, 2478-2483.

40. Arvidson, S. A., Khan, S. A., & Gorga, R. E. (2010). Mesomorphic-r-monoclinic phase transition in isotactic polypropylene: a study of processing effects on structure and mechanical properties. *Macromolecules*, 43, 2916–2924.

41. Karacan, I., & Benli, H. (2011). The influence of annealing treatment on the molecular structure and the mechanical properties of isotactic polypropylene fibers. *Journal of Applied Polymer Science*, 122, 3322–3338.

42. Cuculo J. A. et al. (1992). US patent: US005149480A. Melt spinning of ultra-oriented crystalline polyester filaments.

43. Cuculo J. A. et al. (1998). US patent: US005733653A. Ultra-oriented crystalline filaments and method of making same.

44. Exxon MobilPP3155 Homopolymer Grade. As viewed on line at (June 17th 2011): http://www.matweb.com/search/datasheet.aspx?matguid=d32d7bd5f1ed4c1dbd86e2b7f6b63297

45. Total Polypropylene 3462. As viewed on line at (17th 2011): http://www.lonestarchemical.com/datasheets/polypropylene/72-total-polypropylene-3462

CHAPTER VII

An Unusual Structure Development for High Performance Poly(ethylene terephthalate) Fibers using A Low Molecular Weight Polymer: Developing a Rare Formation of Precursor for Crystallization

Keywords: high performance, high throughputs, polyester fiber, economical, unique structure, horizontal isothermal bath (hIB).

7.1 Abstract

High performance poly(ethylene terephthalate) fibers (PET) were obtained using a low molecular weight polymer via horizontal isothermal bath (hIB), followed by a postdrawing process. We investigated a unique formation of a precursor for crystallization which differentiated in its molecular orientation and crystalline structures from traditional high speed spinning PET fibers. A sharp increase in crystallinity for treated fiber was observed after drawing process even though the fibers showed a very low or almost no any crystallinity before the drawing process. Filament properties of as-spun and drawn hIB and control filaments of each different process conditions were compared by utilizing a scanning electron microscope (SEM), birefringence, wide angle X-ray diffraction (WAXD), tensile testing, and differential scanning calorimetry (DSC). As would be expected, the performances of resulted treated undrawn and drawn fibers have dramatically improved with a developing unique morphology. The tenacity values more than 8 g/d for as-spun and 10 g/d for drawn treated fibers after just drawn at 1.279 draw ratio (DR) were observed. These performance values are considerably higher than that of the control PET fiber. An explanation of the structural development of high performance fibers using low molecular weight polymer spun with hIB is proposed by structural characterization.

7.2 Introduction

High performance polyester fibers are widely used in industry and our daily lives. Hence, studies on structural improvement of filament and its relation to production conditions have been examined carefully by researchers for many years. This resulted in 60 % of the world's total polyester production having been consumed as fiber in 2010[1]. In general, zone drawing / zone annealing, microwave heating, 1 or 2 step drawing high-speed spinning, vibrational hot drawing, two-step spin draw processes, solution spinning, and solid-state extrusion are the most important production methods to manufacture high performance polyester fibers[2-3]. Structural development of fibers in one step high speed spinning process is limited even if it appears promising in the case of economical and high throughputs. Therefore, two-step spin-draw and multi-step drawing processes are widely accepted and utilized to obtain high modulus and tenacity polyester filaments[2,4]. On the other hand, the solution spinning techniques is one of the crucial methods by using ultra-high molecular weight polymers to produce high performance PET fibers, but the use some organic solvents raise questions about their toxicity[5, 6]. This method is expensive and the production speed is slow. Sometimes more than one bath is required in the production lines and a very high draw ratio is needed to manufacture high performance fibers.

Full understanding of precursors for crystallization and crystallization in polyester fibers is limited because of fast crystallization kinetic and the different formation of precursors. According to process conditions and polymer properties, a number of precursor models have

been proposed. These precursors can be nematic, smectic, other less unidentified structures, and sometimes microvoids and/or banded structure can be associated with these forms[7]. In addition, all these forms have some common structural properties, as they are highly oriented but have noncrystallized molecular chains or chain segments. Nicholson et al.[8] have observed mesophase formation by drawing at the drawing temperature of 110 °C with the draw ratio of 4 using a very low oriented as-spun yarn. After the drawing process, the fibers were rapidly cooled to inhibit the crystallization, which showed a different usual form of triclinic and were described as 'mesophase' form. However, this mesophase form, yet still exhibiting spatial order, was not very stable, and the annealing process could easily destroy it. In addition, Carr et al.[9] have produced nematic phase by drawing PEN films uniaxially at 120 ^{o}C at the draw ratios range from 3.5 to 5.5 with observing long-range noncrystalline order when the drawing temperature increased to 140 ^{o}C for the films which showed a partially crystalline morphology. Generally, the mesophase forms when the sample is cooled rapidly after the processing to inhibit any crystallization. Afterwards, the drawing process can be applied at the temperature close to the glass transition temperature (T_g) or between glass transition and crystal melting temperature[10]. The critical draw ratio is also very important because it sets up the onset of the crystallization. As seen in the past, the effect of temperature and draw ratios is significant for crystallization in the polymers. Higher draw ratios for PET increase the rate of strain-induced crystallization; however, the higher temperature will lead to an increase in molecular mobility to promote relaxation and crystallization.

Commonly, strain-induced crystallization occurs for PET materials, which are mechanically drawn close to the glass transition temperature within the temperature range between 20 and 80 ^{o}C[11]. Alfonso and co-workers[12] studied the crystallization kinetics in the orientated state for PET filaments. They showed that the orientation of the amorphous phase is very important and has a very strong relationship with crystallization and the rate of crystallization. A higher orientation for amorphous phase leads to improved crystallization. In addition, increasing the temperature to a certain point causes an increase in the crystallinity.

On the other hand, Smith et al.[13] investigated the rate of crystallization by carefully drawing different oriented non-crystalline PET fibers at 100, 120 and 150 °C. Prior to the extrusion process, the polymer melt stayed at 295°C for 10 minutes to avoid any nuclei remaining from the previous history and crystallization. Afterwards, the produced fibers were quenched rapidly to prevent any crystalline formation. The crystallization kinetics was observed by using density measurement and boiling water shrinkage of the fibers; the samples were held at constant length during the density measurements. It has been demonstrated that the degree of orientation had a great influence on the rate of crystallization. The resulting fibers showed the nucleation and initial growth of crystallites as a very rapid process for oriented PET at 120°C, which is about the order of milliseconds. However, when unoriented fibers were used, the crystallization time was several minutes. Moreover, Lu and Hay[14] observed that the crystallization rate for a strain-induced mechanism was much higher than a thermally induced mechanism at the same temperature. It was explained that the entropy of extension is

the main factor, which increases the driving force for crystallization while reducing the free energies for nucleation and crystal growth. During the drawing process, unoriented molecular chains start to align in the amorphous regions, which resulted in higher orientation levels. The molecular chains mobility in the amorphous regions decreases after the crystallization process is induced by orientation. They[14] have also observed the lower degree of orientation and crystallinity after increasing the temperature at a certain point of strain rate and elongation because of increasing molecular chain relaxation.

As a result, many researchers have investigated many structural developments to understand and make a better correlation between internal structure and material performance. Consequently, the researchers have developed numerous production techniques to improve the material's mechanical and thermal properties. One of the most important methods was revealed in the 1990s, a novel melt-spinning process with the liquid isothermal bath (LIB) [6, 7, 15, 31-32]. In this method, the resulted as-spun fibers had a very high degree of orientation and low and/or no crystallinity but had a high tenacity and modulus. Superior fiber mechanical properties were observed by drawing the fibers spun with LIB to a low draw ratio. The synthetic melt spun fibers were extruded into a liquid isothermal bath, which should be at least 30 ^{o}C above the glass transition temperature of the polymer with the take-up speed between 3000-7000 m/min. Numerous attempts have been performed by varying the liquid's temperature, liquid dept, distance between the spinneret and the tank, take-up speed, etc. to observe and make correlation between the resulted fibers' performance and process conditions. These works have concluded that the high level of threadline stress, which

occurred during the fibers moving through the liquid, hindered molecular chains and segments mobility to form a very high orientation level and effectively prevent crystal growth for undrawn filaments. This method was eventually modified by the utilization of a horizontal liquid isothermal bath (hIB)[7], to reduce energy consumption. It requires less capital equipment and can be used in large-scale production setting. As a result, hIB technique is simpler, safer, and can be applied to many different types of thermoplastic polymers.

Almost all researchers have been using higher molecular weight polymers for their studies to produce high performance fibers, also for the hIB method as well. For this study, we will present, for the first time, the spinning of high performance PET fibers by using a low molecular weight polymer via hIB method with an unusual structural development.

7.3 Experimental

7.3.1 Materials and Production Methodology

Fiber forming PET chips having intrinsic viscosity (IV) of 0.65 dL/g was used in this study. The PET chips were vacuum-dried at 140 ^{o}C for 16 hours. As-spun PET fibers with and without hIB were produced by using a Fourne single-screw extruder, which had a single-hole with a hyperbolic spinneret with 0.6 mm exit diameter with the take-up speeds around 3000 m/min. Figure 7.1 shows that the production parameters which we used during the fiber production.

Modified Instron tensile testing equipment with a 60 cm long heating tube was used to draw fibers with the draw speed of 50 mm/min, and the draw temperature of 220 ^{o}C.

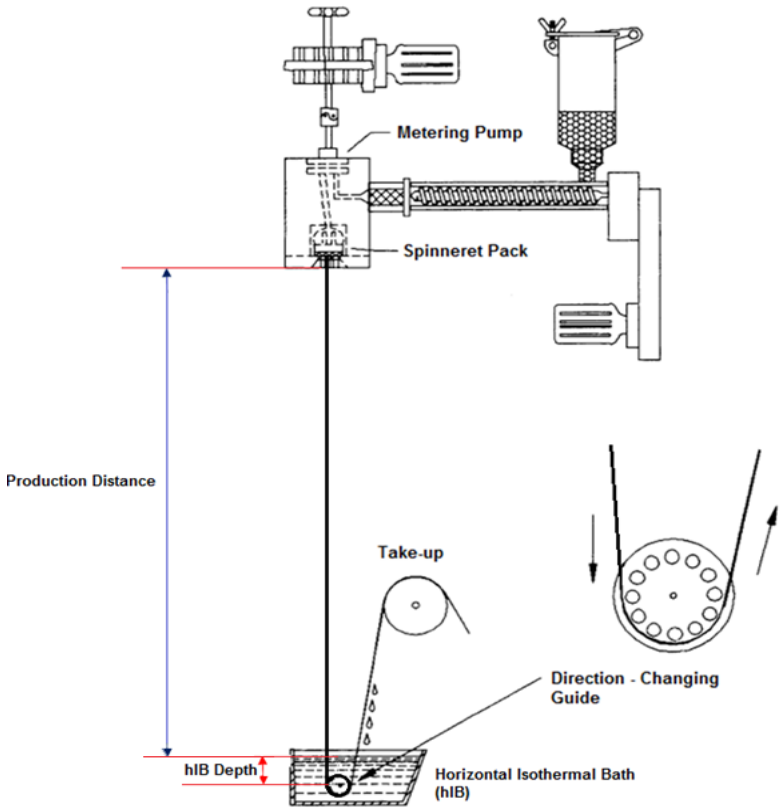

Figure 7. 1 Melt spinning process with hIB spinning system[28].

7.3.2 Experiments and Characterization

Vibromat ME Tester equipment was used to determine denier of the monofilaments. The measurements are based on the resonance frequency principle. The fiber modulus and tenacity (gf/denier), in addition to the percentage strain at break, were observed via a MTS Q-test/5 universal testing machine using TestWorks 4EM V4.11B software according to ASTM D3822.

Fiber surface and cross-section morphology were investigated using JEOL 6400 model of a Cold Field Emission Scanning Electron microscope after fiber coating with a layer of Au/Pd at 0.5-30keV accelerating voltage. The fiber cross-section was obtained to put the fibers into the liquid nitrogen and then broken apart in it.

The X-ray generator that is Rigaku SmartLab X-ray Diffractometer (XRD) equipped with CuK_{α} radiation source, λ=1.542 Å, was operated at the power of 40 kV and 44 mA. The diffracting intensities were determined every 0.02^{o} from 2θ scans in the range of $5 - 40^{o}$. Crystallites sizes were determined by using the Scherrer equation[17]:

$$L_{hkl} = \frac{K\lambda}{\beta cos\Theta} \qquad (1)$$

where β is the peak half width, K is taken to be unity, λ is the radiation wavelength (1.542 Å), and ɵ is the Bragg angle.

DSC measurements were performed on a Perkin Elmer Diamond DSC Model 7 with Pyris software version 5. A small amount of 3 to 5 mg of the fibers were used for the DSC measurements with the heating rate of 20 ^{o}C /min under a flow of nitrogen gas up to 280 ^{o}C. The degree of crystallinity of PET fibers was calculated[25] from equaiton (2) :

$$\text{Degree of crystallinity (\%)} = \frac{\Delta H_f x 100}{\Delta H_f^0} \qquad (2)$$

where ΔH_f is the heat of fusion of PET fibers. ΔH_f^0 is heat of fusion of 100 % crystalline PET which is 140 J/g[18].

Density measurements for all untreated and treated fibers were carried out by using ASTM D1505-10 standard. The experiment was run at 23 °C by using a density gradient column containing sodium bromide solution (NaBr) in the density range of 1.335 – 1.415 g/cm³. The volume fraction crystallinity (X_v) was determined from eq. 3[19]:

$$X_v = \frac{p - p_a}{p_c - p_a} \qquad (3)$$

where p is the determined fiber density, p_a and p_c are the density of the amorphous and crystalline phases with the values of 1.335 and 1.455 g/cm^3, respectively.

Birefringence for the fibers was observed by using a Nikon polarizing microscope. At least three individual sample measurements were done for each fiber sample. A series of mineral oil refractive index liquids were used as an immersion liquid. The mean birefringence values were determined with the equation 4[15]:

$$\Delta n = n_{II} - n_{\perp} \qquad (4)$$

where n_{II} and $n_{\perp}$ are parallel and perpendicular refractive index of the sample, respectively.

7.4 Results and Discussion

7.4.1 Mechanical Properties of the PET Fibers Spun with and without hIB

In general, polymer chips having a high intrinsic viscosity (IV) close to 1 are used to produce high tenacity PET fibers by achieving a high degree of the orientation for the undrawn fibers and the formation of tie-chains connecting to the crystals. Hence, high tenacity and modulus fiber products can be obtained. However, it is known that the threadline dynamics of the fibers can be controlled with a liquid isothermal bath (hIB) spinning followed by a hot drawing process to improve the morphology of the fibers. Therefore, different set of as-spun fibers with a lower IV of 0.65 dL/g PET chips were spun with the hIB technology at take-up speed in the range of 2900–3000 m/min. Fiber properties of the as-spun fibers and control fibers of each process were compared. Unlike PET control samples, the hIB as-spun and drawn fibers showed unique structural development with demonstration of high tenacity and high modulus. The spinning conditions and comparison of the mechanical fiber properties of the hIB as-spun, control fibers and the fibers after hot drawing process are listed in Table 7.1, Table 7.2 and Table 7.3, respectively.

Table 7. 1 Spinning conditions of PET fibers spun with and without hIB.

Sample ID	Take-up speed (m/min)	Liquid temp. (^{o}C)	Liquid depth (cm)	Distance (cm)	Denier
PET0	2910			90	9.20±0.25
PET00	2910	CONTROL FIBERS		120	10.93±0.39
PET000	2910			150	10.14±0.18
PET1	2880			90	10.86±0.15
PET11	2885	60	20	120	10.30±0.15
PET111	2900			150	11.12±0.22
PET2	2913			90	10.29±0.08
PET22	2913	100	20	120	10.98±0.18
PET222	2913			150	12.13±0.36
PET3	2923			90	10.44±0.10
PET33	2931	125	20	120	10.61±0.32
PET333	2919			150	11.02±0.40
PET4	2921			90	10.35±0.07
PET44	2909	140	20	120	10.08±0.21
PET444	2909			150	9.77±0.13

As can be seen from Table 7.2, the results indicated that the fibers' tenacity significantly increased with hIB technology. PET fibers tenacity increased by ca. 58, 95, 88, and 90 %

from 4.19±0.10 g/d to 6.60±0.26, 8.19±0.09, 7.87±0.12, and 7.97±0.13 g/d for undrawn fibers at 90 cm distance between the spinneret and tank with the bath temperature of 60, 100, 125 and 140 ^{o}C, respectively. At the same time, the modulus tremendously increased by ca. 70, 80, 58, and 86 % from 64.62±3.83 g/d to 109.54±6.39, 116.52±9.19, 102.40±4.93, and 120.14±4.05 g/d at the same production parameters. In addition, the percentage of elongation decreased from 73.50±6.74 to 33.38±4.23, 24.55±2.79, 28.57±2.57, 25.50±1.35 % for the undrawn hIB fibers with the bath temperature of 60, 100, 125 and 140 ^{o}C by ca. 55, 67, 61, 65 % respectively.

Table 7. 2 Mechanical properties of PET as-spun fibers spun with and without hIB.

Sample ID	Tenacity (g/d)	Modulus (g/d)	Elongation (%)
PET0	4.19±0.10	64.62±3.83	73.50±6.74
PET00	2.17±0.08	38.23±3.20	137.47±10.29
PET000	2.05±0.04	27.22±5.80	160.14±26.84
PET1	6.60±0.26	109.54±6.39	33.38±4.23
PET11	6.26±0.31	105.72±5.69	39.21±5.87
PET111	6.05±0.24	103.33±5.35	51.45±5.17
PET2	8.19±0.09	116.52±9.19	24.55±2.79
PET22	7.85±0.14	116.94±6.55	22.13±2.88
PET222	7.41±0.21	103.59±6.06	24.97±4.44
PET3	7.87±0.12	102.40±4.93	28.57±2.57
PET33	7.91±0.13	108.36±5.04	27.14±2.68
PET333	7.66±0.19	103.53±5.21	24.49±4.57
PET4	7.97±0.13	120.14±4.05	25.50±1.35
PET44	8.04±0.14	120.52±4.33	28.14±3.68
PET444	8.07±0.12	118.05±6.50	26.00±2.51

It is obvious that the hIB fibers have not only a higher initial modulus and higher strength but also have a lower percent elongation at break than those of the control fibers. In the study,

the effect of changes in the mechanical properties of PET fibers was assessed in terms of its tenacity, modulus, and elongation at break for different distances between the spinneret and hIB bath. The highest tenacity and modulus of 8.04±0.14 g/d (1.02 GPa) and 120.52±4.33 g/d (15.32 GPa) by the increasing ca. 270.51 and 215.25 % from the control sample without hIB, respectively, were obtained by using the hIB technology at the bath temperature of 140 ^{o}C with 120 cm distance (see Table 7.1 and 7.2) for the undrawn fibers. This performance for the treated as-spun fibers is very surprising and tremendous because the traditional PET fibers can show this performance after very high draw ratios and more than two step drawing processes by using high molecular weight polymers. In the case of 150 cm production distance, the significant effect of the hIB spinning system on fiber tenacity and modulus was observed. As shown in Table 7.2, a positive improvement is found between the hIB bath temperature and tenacity values of PET fibers spun with hIB at 150 cm production distance between the spin pack and the tank.

Associated with this matter, an interesting point of data shows which of the modulus values for the bath temperature of 60, 100, and 125 ^{o}C of the as-spun fibers are very close to each other at about 103 g/d. The modulus value has reached approximately 118 g/d for the undrawn fibers spun with hIB when the liquid temperature was set to 140 ^{o}C. The tenacity value increased from 2.05±0.04 g/d to 8.07±0.12 g/d, with increasing the modulus values from 27.22±5.80 g/d to 118.05±6.50 g/d by ca. 294 %, and 334 % respectively, while the sample ID's of PET000 and PET444 are compared.

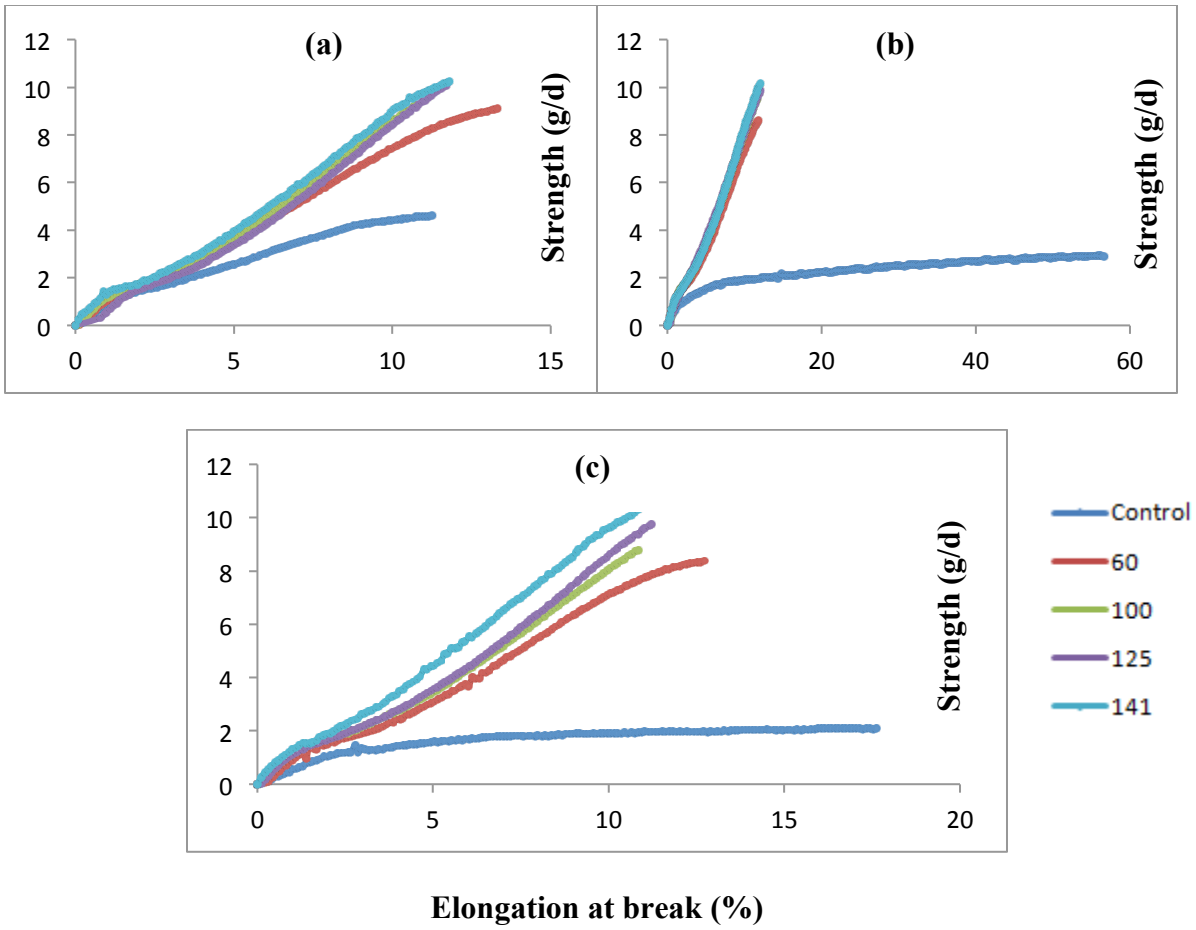

Figure 7. 2 Comparison of the strength of drawn fibers at 1.279 DR with the drawing temperature of 220 ^{o}C at (a) 90, (b) 120 and (c) 150 cm production distance.

After the drawing process, as expected, the hIB fibers with a draw ratio of 1.279 had an increased tenacity and modulus with a lower elongation, as seen in Figure 7.2. All samples were drawn at the same temperature of 220 ^{o}C with the same draw ratio, which is near to the

maximum draw ratios for the treated fibers at this temperature. It was noted that the mean value of tenacity increased with an increasing of the hIB temperature, but there was no significiant difference between tenacity values at different hIB bath temperatures when standard deviation are considered for tretaed PET filaments. Interestingly, the modulus values for PET fibers produced with hIB were similar after the hot drawing for the bath temperature of 60, 100 and 125 ^{o}C. The mean value for modulus relatively increased for the bath temperature of 140 ^{o}C and reached 145.27±9.27 g/d at the distance of 90 cm. At the production distance of 90 cm between the spin pack and the hIB tank, the difference in tenacity between the hIB and control fibers is 4.41, 4.54, 5.31 and 5.56 g/d for 60, 100, 125, and 140 ^{o}C, respectively, in which it is clear that the differences increased by increasing the liquid temperature. The highest improvement for the tenacity is ca. 121 % from 4.67±0.13 g/d to 10.30±0.27 g/d for tretaed fibers at the liquid temperature of 140 ^{o}C. In addition, the initial modulus increased by ca. 25, 36, 28 and 48 % from 98.17±9.46 g/d to 123.09±5.60, 133.64±4.40, 125.61±7.99 and 145.27±9.27 g/d for the same hIB temperature range, respectively. The elongation percentage has similar values and remains essentially constant for the different process conditions, which are approximately between 11 and 13 %.

On the contrary, an increase in tenacity became more prominent at the distance of 120 and 150 cm for the drawn control and treated fibers (see Figure 7.2). In addition, many fibers' breaks occurred during the drawing process for the control sample at 220 ^{o}C because the control fibers were not stable at high temperature, hence easily degraded and finally broke. After many trials, a few samples were obtained, and these fibers have unusual and very low

elongation at break percentage, which was about 19.28 % with tenacity value of 2.06 g/d for 150 ^{o}C production distance.

It lends credence to the statement that the hIB technology has the potential to produce high tenacity and high modulus filaments at a low draw ratio (1.279 DR), even if a low IV PET (0.65 dL/g) polymer was used. In addition, the comparison of performance analysis for the low (0.65 dL/g) and high (0.90 and 0.97 dL/g) molecular weight PET fibers spun with hIB method show no any significant difference for the undrawn and drawn fibers. Therefore, it can be concluded that the hIB method is more beneficial for the low molecular weight PET polymers. The fine structural development for the low molecular weight fibers is provided in the next sections.

7.4.2 Scanning Electron Microscopic Analysis

As demonstrated in previous studies and our work, the banded morphology is one of the most crucial parameters for hIB polyester fibers. It represents a precursor for crystallization that has highly oriented amorphous structures[7]. High molecular weight PET (0.97 dL/g) filaments were spun with hIB, and then drawn at 132 ^{o}C with 1.279 draw ratios. The resulted fibers showed the banded structure for drawn and also undrawn fibers, as seen in Figure 7.5. The ordering process is one of the most dominant factors to form the banded structure[7, 20]. Hence, lower molecular weight PET (0.65 dL/g) fibers were analyzed based on this point. The fibers were marked in three zones to observe any possible structural changes during the drawing process. A section outside the heating tube was unheated; the second zone was the transit zone between the outside and inside drawn zone, and the third zone was the drawn zone in the tube in which the filaments was fully heated and drawn. All control and treated fibers were drawn at1.279 DR with the drawing temperature of 220 ^{o}C.

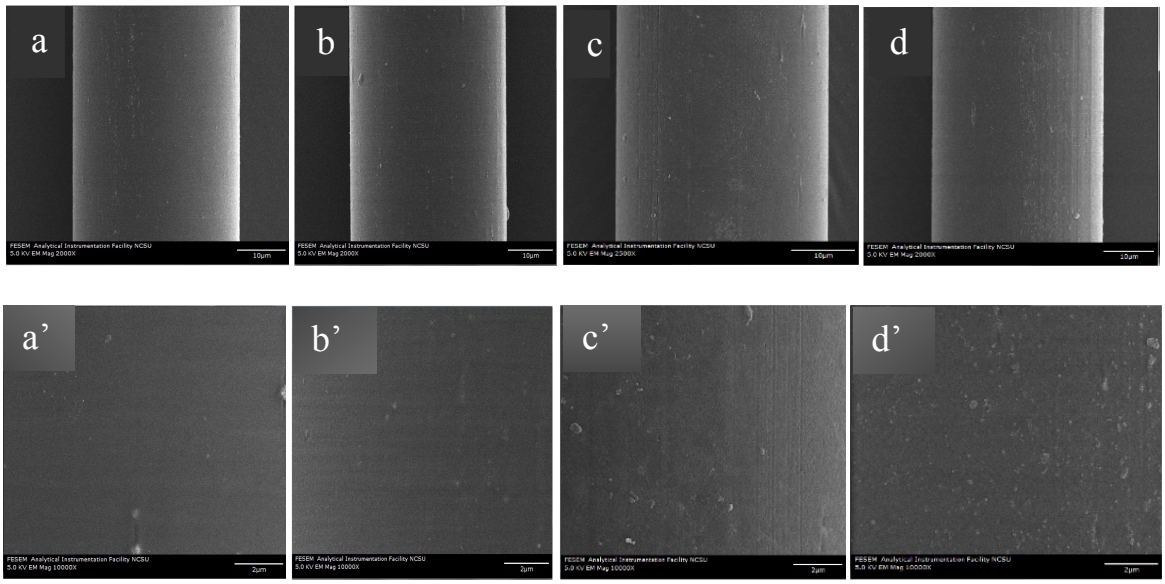

Figure 7. 3 Low and high (letter with apostrophe) magnification of SEM images for PET as-spun fibers treated with hIB at (a) 60, (b) 100, (c) 125, and (d) 140 ^{o}C liquid temperatures. (Scale bar = 10 and 2 μm for low and high magnifications, respectively)

Firstly, there is no any significant difference for hIB and control fibers for surface analysis before and after the drawing process. As Figure 7.3 and 7.4 show, interestingly, there is not any banded structure either perpendicular or along the fiber axis on the hIB fiber surface for low molecular weight PET (0.65 dL/g) fibers; however, the banded structure was observed for high molecular weight fibers produced from 0.97 dL/g (Figure 7.5). Even if the low molecular weight fibers demonstrated superior mechanical performance for both as-spun and

drawn fibers, the banded morphology was unexpectedly not observed. The formation of the banded structure can be related to the skin and core structure[21] when the skin layer has higher molecular orientation and birefringence. The molecular orientation difference between skin and core structure also should be more than a certain value. In addition, the banded morphology contains highly oriented, amorphous, crystalline, or just newly developed, less ordered crystallites with some highly entangled polymer chains[15, 22]. These conclusions are coming from the structural observation of copolyester type materials[21, 22]. Furthermore, the banded structure was also observed for LIB treated polyester fibers in which the fibers also showed the smaller crystal size[15]. Firstly, the effects of the process conditions on low and high molecular weight PET might be different. Therefore, more studies with different process conditions should be done to document the development of the banded structure. However, in our case, we observed higher crystal sizes after LMW PET filaments with hIB than HMW PET fibers produced by LIB method in the past. Secondly, the difference of molecular orientation for skin-core structure might be less than a certain value which leads to the banded structure. Thirdly, the low molecular weight PET may cause less "highly entangled polymer chains" to form when compared to the high molecular weight PET. A combination of these reason(s) might possibly account for the absence of the banded morphology for the low molecular weight PET fibers spun with hIB before and after the drawing processes.

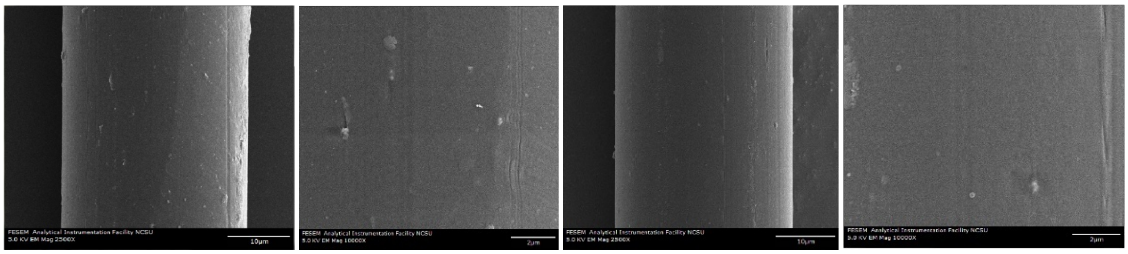

outside drawn zone transit drawn zone

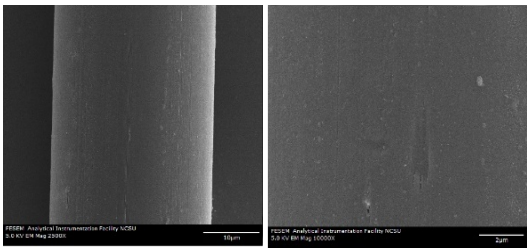

inside drawn zone

Figure 7. 4 SEM images of drawn PET fibers spun with hIB at the temperature of 125 ^{o}C. (Scale bar = 10 and 2 μm for low and high magnifications, respectively)

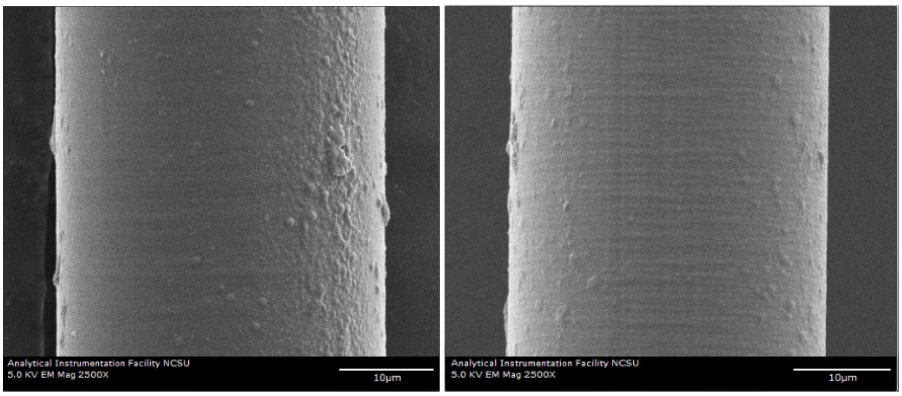

Figure 7. 5 SEM images of PET (0.97 dL/g) fibers spun with hIB for undrawn (left), and outside drawn zone (right) fibers. (Scale bar = 10 μm)

To further investigate, the fiber samples were broken in the liquid nitrogen, and the cross-section was observed via a field emission scanning electron microscope to study the inner morphology. Figure 7.6 shows the fractured surface of the undrawn treated fibers. There is significant effect of the temperature of the hIB spinning system on the formation of fibrillar structures. Fibrillar structure did not form for fibers spun with hIB at the temperature of 60 and 100 ºC, although they showed ultrahigh performance. This result further supports the hindrance of crystal growth under high levels of stress and appropriate temperatures in which lamellar slip can lead to *c*-axis orientation until obtaining a fully oriented structure[33]. On the other hand, fibrillar structures have been observed in fibers spun with hIB spinning systems

at the temperature of 125 and 140 ºC for as-spun fibers. This is very interesting and showed the dependence of crystallinity on the liquid temperature. In this experiment, it can be speculated that the mechanism for the formation of the fibrillar morphology was formed after fully oriented structure was reached and an additional extension caused a new type of deformation mechanism, which is called crystal cleavage[33]. Hence, the fibers show separation of lamellae in blocks and become more oriented to evolve into a fibrillar structure at the liquid temperature of 125 and 140 ºC. X-ray data for undrawn fibers clearly supported this relationship between the fibrillar structure and the liquid temperature, which will be given in the next section. A higher hIB temperature probably increased the chains mobility to form three dimensional arrangements of the crystals to evolve into the fibrillar structure. These fibers performed an outstanding performance with a higher degree of crystallinity and crystal size.

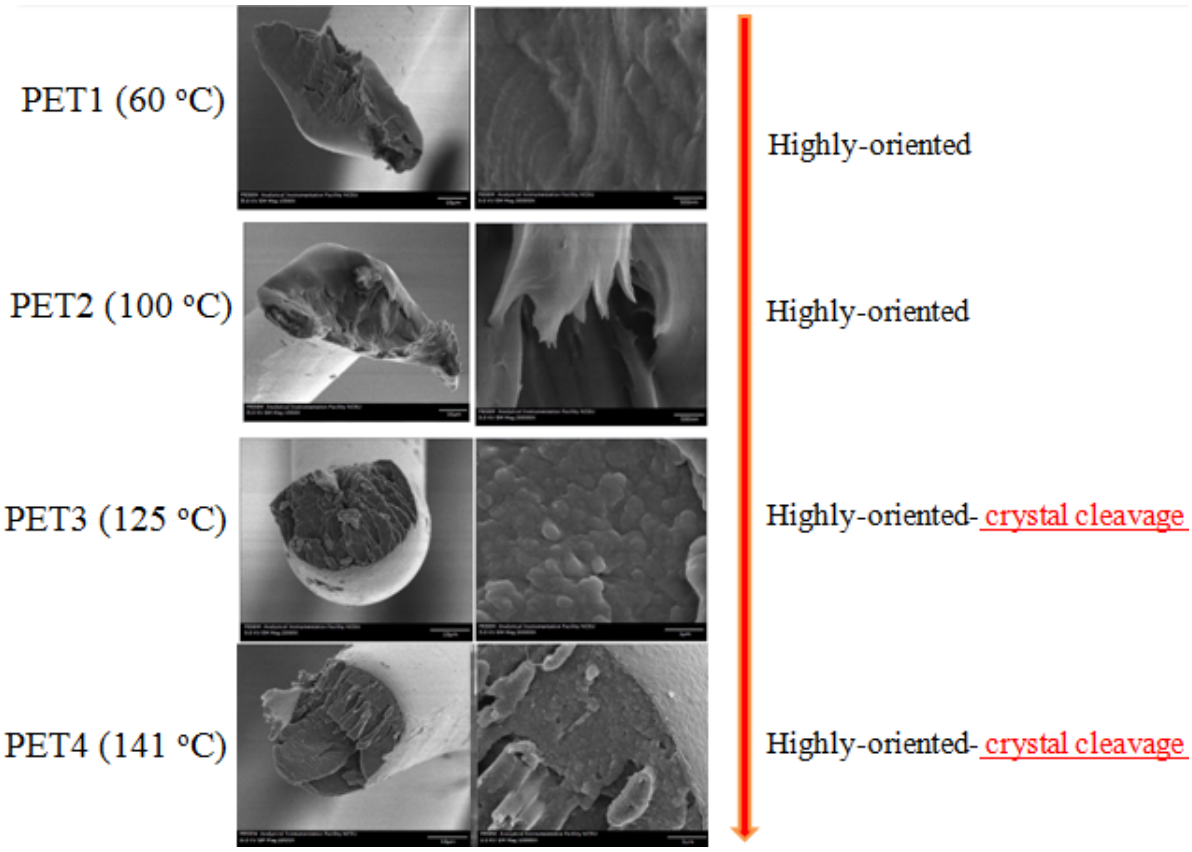

Figure 7. 6 SEM Images of cross section of undrawn PET fibers spun with hIB spinning system at different liquid temperatures.

(Scale bar = 10 and 2 μm for low and high magnifications for 60, 100, and 140 ^{o}C respectively. Scale bar = 1 μm for high magnifications for 125 ^{o}C)

Figure 7.7 demonstrates the fractured surface of the drawn PET fibers. It is clear that the drawn and transparent fiber had a smooth surface with stretched fibrils inside in which the diameter is decreasing from the sheath to the core of the fibers. This is a strong evidence to demonstrate a highly crystallized fibrillar structure. The as-spun hIB fibers had highly ordered structures, which can be transformed into fibrillar crystals via a little hot drawing to produce high performance filaments; this could potentially increase the fraction of taut tie molecules in amorphous regions and lead to the formation of higher orientation after the drawing processes. It has been generally accepted that polymers normally undergo chain-folding during crystallization, and microfibrils which consist of alternating chain-folded lamellae and amorphous regions to make the conventional fibers[23]. Stacked lamellae are the main reason to form the fibrils, and they are typically about 10 nm in diameter with approximately 50 nm lengths along the fiber axis[24].

It can be seen that in Figure 7.7 that the cross section of the drawn PET control without hIB fiber has poorly developed, sparse fibrillar morphology after drawing at 1.279 DR with the drawing temperature of 220 ^{o}C. This phenomenon is related to the fact that the traditional process produces the fibers with low strength and relatively poor occurrence of fibrillar structure. This is a weak point and is undesirable in industrial end-use applications for high performance fibers.

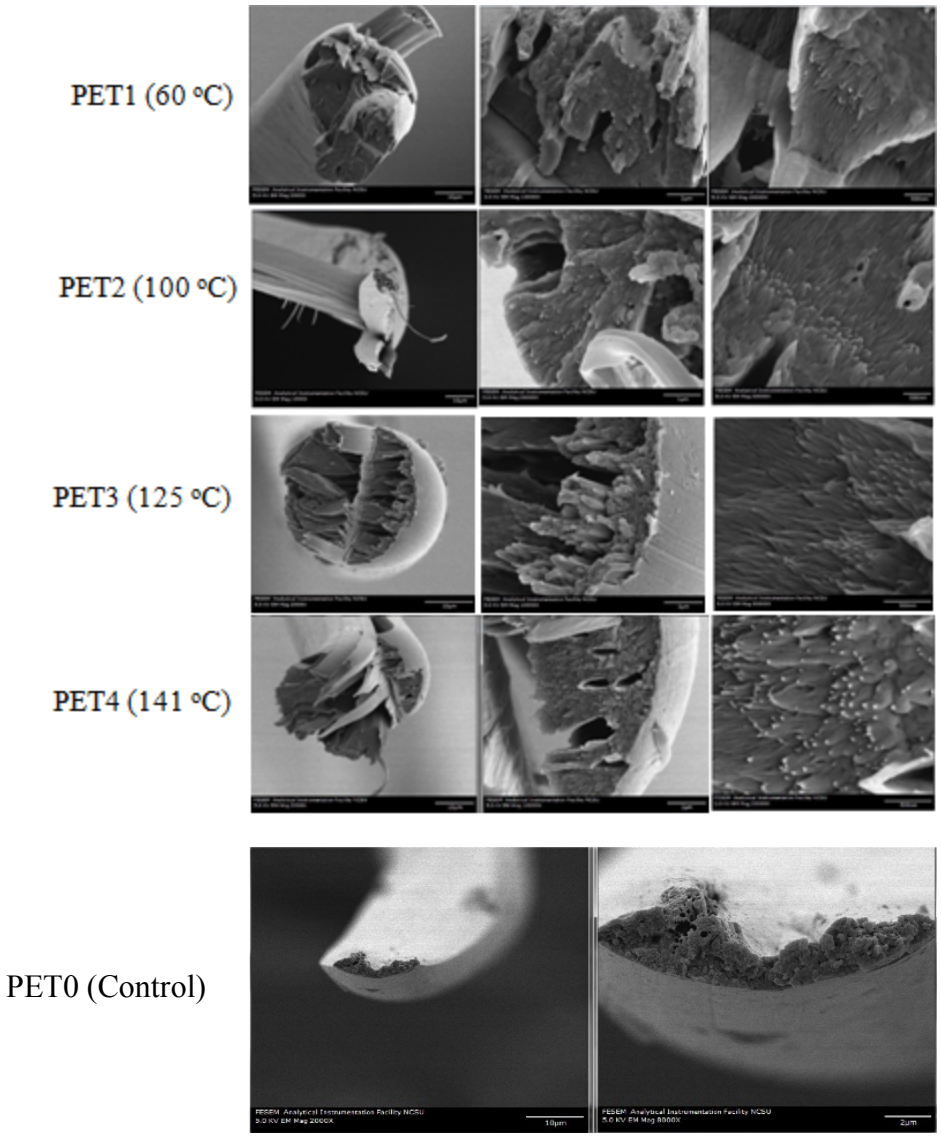

Figure 7. 7 SEM Images of cross section of drawn PET fibers spun with hIB spinning system at different liquid temperatures with control sample.

(Scale bar range between 10 μm and 500 nm for low and high magnifications, respectively)

The further investigation of the fibril diameters are shown in Table 7.3 for control and treated fibers before and after the drawing processes. As stated previously, some poorly developed fibrils were observed for drawn control fibers with the mean diameters of more than 400 nm, but there was not any fibril for undrawn control filaments. The fibers were produced at the liquid temperature of 125 and 140 ^{o}C and had the similar fibril diameters for undrawn fibers, in which the diameters are about 350 nm. However, after the drawing process, the mean value of fibrils for PET4 is smaller than PET3. There are two distinct populations of microfibrils which are 'coarse' fibril at about ~ 200 nm, and 'fine' fibril at about ~ 38 nm in diameters for drawn fibers. The fibers which have been produced at the liquid temperature of 100, 125 and 140 ^{o}C showed the similar 'coarse' and 'fine' fibrils diameters, but the 60 ^{o}C liquid temperature one has a little higher mean value for the diameters, as demonstrated by Table 7.3.

It might be speculated that we were able to demonstrate just a group of lamellae for the 'fine' fibrils, which were obtained by hIB method. As Murthy et al.[25] have stated, the typical lamellae diameter is about 10 nm.

Table 7. 3 Fibril diameters for control and hIB treated fibers.

	Fibril diameters (nm)		
	Undrawn	**Drawn**	
	Coarse	Coarse	Fine
PET0 (Control)	-	418.39±88.27	-
PET1 (60 ^{o}C)	-	215.15±75.80	45.10±17.10
PET2 (100 ^{o}C)	-	181.94±44.17	36.84±11.34
PET3 (125 ^{o}C)	344.44±56.34	210.37±39.28	37.65±8.18
PET4 (140 ^{o}C)	341.18±83.78	196.08±57.41	33.93±10.78

7.4.3 Wide Angle X-Ray Data Analysis

Figure 7.8, 7.9 and 7.10 show the wide angle X-ray diffraction (WAXD) patterns of the PET filaments spun without hIB and with hIB at different liquid temperatures with the distance of 90 cm. The equatorial diffraction profile was fitted using PDXL with ICDD PDF file software program. Murthy et al.[26] have shown at least two amorphous peaks, which are 17.5 and 23.5^{o}, observed for the most 'amorphous' sample.

In Figure 7.8, as expected, a noisy, weak diffraction of X-ray pattern was collected for undrawn control samples. However, as seen in Figure 7.9, using hIB method even at different process conditions demonstrated a great influence on as-spun fiber morphology. It can be seen in Figure 7.9 that, until the bath temperature is 125 ^{o}C, the first indication is a less developed crystallites phase, which contains highly oriented PET molecules, as supported by demonstrating high tensile performance and the birefringence analysis. The filaments were produced at 60 and 100 ^{o}C, the equatorial X-ray diffraction trace is given for the hIB as-spun fibers, which only gave rise to broad, unresolved traces with high intensity which are not related to the crystals. One of the most important result of this study is that this structural phenomenon was exactly observed by SEM cross-sectional images; as we have described, there was not any fibril formation at these temperatures. In addition, the degree of crystallinity increased from 7.66 to 37.41 % when the temperature of hIB increased from 60 to 140 ºC (Table 7.4).

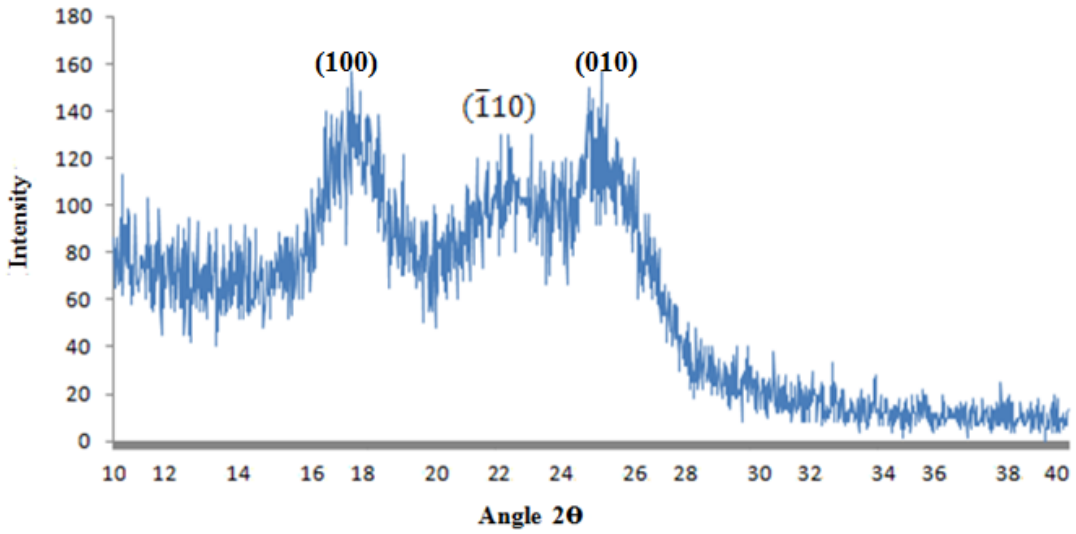

Figure 7. 8 Equatorial X-ray diffraction profiles of PET as-spun fibers spun without hIB spinning system.

It is clear that increasing hIB temperature contributes to crystallization, that is observed at 125 ^{o}C and higher hIB temperatures. The higher hIB temperature would presumably increase the rate of crystallization, as seen in Figure 7.9. Low crystallinity, low elongation, and high tenacity and modulus for hIB fibers might be looked upon as the first evidence that the mostly noncrystalline chains of the hIB as-spun fibers with poorly developed crystalline are highly ordered or oriented. In addition, the amorphous phase can be divided in two-component systems, the oriented (anisotropic) and the unoriented (isotropic) components[30]. Different weak peaks in the amorphous phase can be explained as the order of different

crystallographic directions and/or evidence for incipient crystalline order in samples[26]. Table 7.4 demonstrates the crystal growth of these fibers was significantly suppressed, hence smaller apparent crystal sizes range from 13 to 27 Å at the hIB temperature of 60 and 100 ^{o}C when they were formed. The percent crystallinity for the control and treated fibers at the liquid temperature of 100 ^{o}C is comparable; hence, it can be concluded that the treated one has a higher number of crystals because of smaller crystal sizes as demonstrated in Table 7.4. The highest crystallinity and crystal size were observed at 140 ^{o}C liquid temperature. These prominent features of the as-spun treated filaments at the temperature of 140 ºC promoted crystal growth, possibly because of the increasing of local molecular mobility. Furthermore, the sharp peaks in the Figure 7.9 might have occurred due to the undrawn polycrystalline precursor.

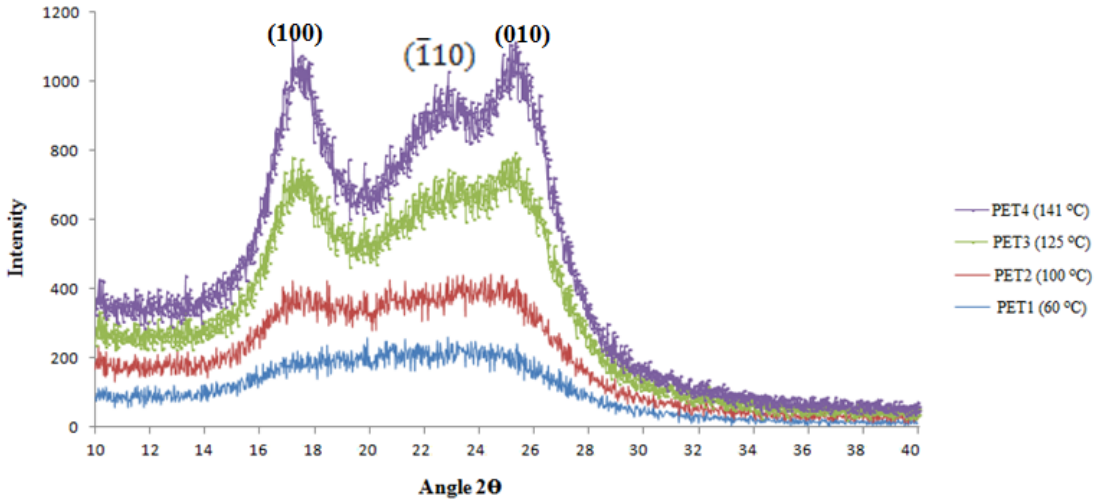

Figure 7. 9 Equatorial X-ray diffraction profiles of PET as-spun fibers spun with hIB spinning system.

Table 7. 4 Degree of crystallinity and crystalline dimensions of PET as-spun fibers under various hIB temperatures.

		Crystallite size (Å)		
hIB Temperature (°C)	**Crystallinity (%)**	**L_{100}**	**$L_{\bar{1}10}$**	**L_{010}**
-	28.92	29	25	36
60	7.66	13	17	13
100	26.51	23	20	27
125	32.37	31	25	33
140	37.41	40	28	34

After the hot drawing at 1.279 DR at the temperature of 220 °C, the treated and untreated fibers show distinct crystal peaks, as observed in Figure 7.10. The treated fibers have gained the fibrillar structures, hence well-developed crystals were detected at a low draw ratio. The crystallinity and crystallite sizes were calculated by using WAXD data and are shown in Table 7.5. After the drawing process, the equatorial diffraction scan demonstrated better resolved peaks, indicating a more highly developed crystalline structure in which the crystal growth was significant. However, the data for untreated fibers are still noisy and weak, which points out that less developed and unoriented parts are more dominant in the morphology.

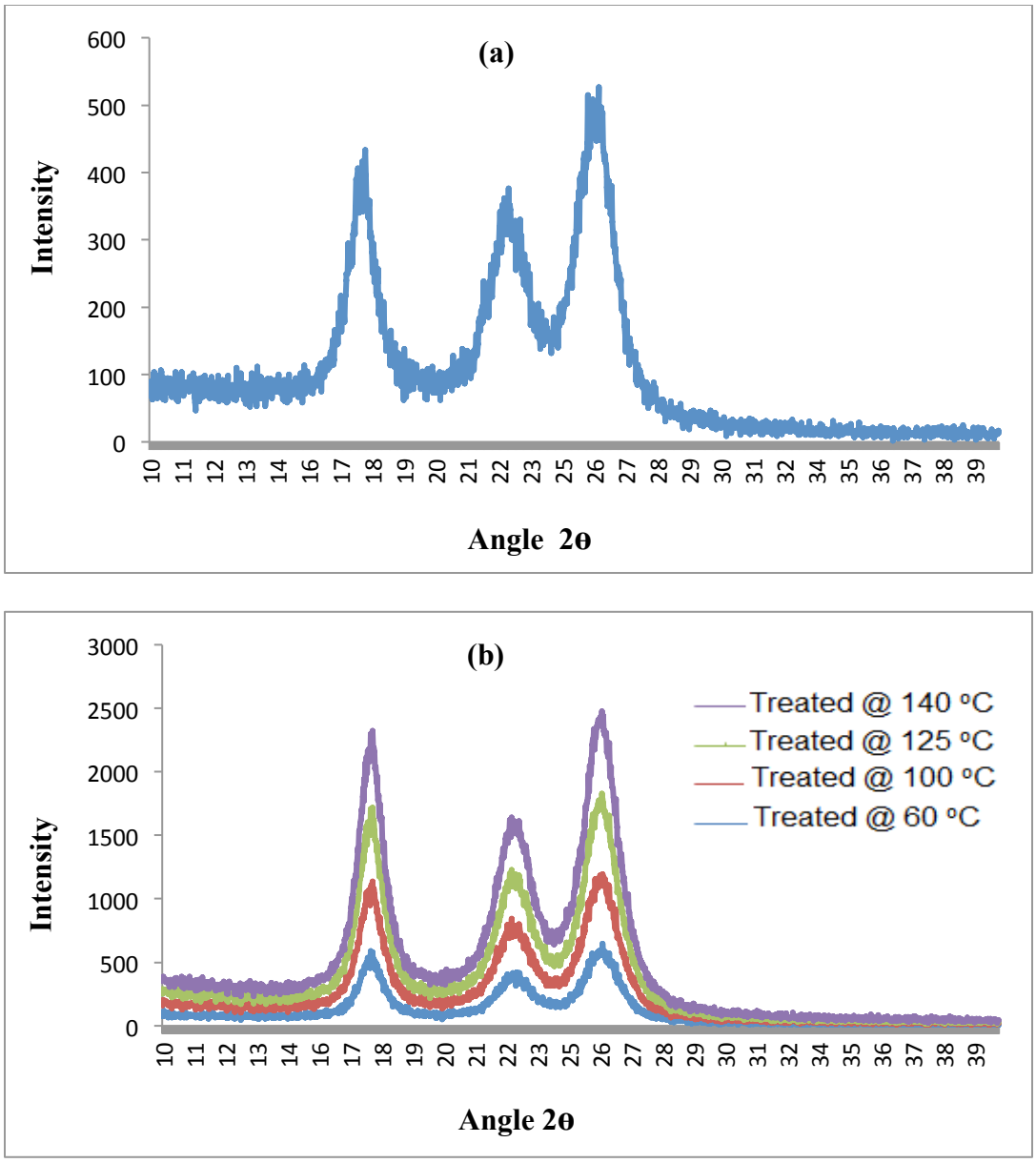

Figure 7. 10 Equatorial X-ray diffraction profiles of drawn PET fibers (a) spun without hIB, and (b) with hIB.

Table 7.5 demonstrates degree of crystallinity and crystalline dimensions for the drawn fibers. After the drawing, the apparent crystal sizes and degree of crystallinity of fibers increased for both hIB and without hIB fibers. In general, degree of crystallinity and crystallite sizes of fibers spun using hIB are greater than those of fibers without the hIB treatment. After the drawing process, the degree of crystallinity has increased approximately 14 % from 39.56 to 45.06 % when the liquid temperature was set to 140 ^{o}C. However, when the liquid temperature increased from 60 to 140 ºC, the degree of crystallinity increased from 39.78 to 45.06 % by ca. 13 %. Despite the fact that the crystallinity for control and the fibers, which were obtained at the liquid temperature of 60 ^{o}C, are close to each other, the tenacity and modulus value differences are about 94 and 25 %, respectively, higher for the treated one. The occurrence of this difference is considered to be at least partially the result of the hot liquid that presumably caused the formation of higher crystal size, higher orientation, and the higher number of taut-tie molecules. Fibers spun with hIB at 60 ºC and without hIB have almost the same crystallinity level as that of the small crystal sizes for the control fibers, implying that the number of crystals is higher than that of hIB treated fibers. Furthermore, the degree of crystallinity and crystallite size of fibers spun with hIB at the temperature of 100, 125 and 140 ºC has essentially the similar value as seen in Table 7.5.

Table 7. 5 Degree of crystallinity and crystalline dimensions of drawn PET spun fibers under various hIB temperatures.

		Crystallite size (Å)		
hIB Temperature (^{o}C)	**Crystallinity (%)**	**L_{100}**	**$L_{\bar{1}10}$**	**L_{010}**
-	39.56	73	51	57
60	39.78	83	58	62
100	44.23	82	56	59
125	44.32	83	60	58
140	45.06	85	59	59

7.4.4 Differential Scanning Calorimetry Data Analysis

It has been found that DSC curves do not show the state of a direct reflection of the material at room temperature[27]. During the heating process, crystallites, which are formed at low temperatures, undergo a continuous perfection process, hence partial melting and recrystallization can occur during the scan before the polymer is totally melted, which leads to an increase in the overall crystallinity.

Table 7.6 and Figure 7.11 present thermal properties and DSC curves of as-spun control and its respective hIB treated fibers made at a spinning speed of about 3000 m/min. Glass transition temperature (Tg) was not observed for both fibers probably because of the presence of a relatively rigid amorphous phase[15]. However, it might be observed for fibers spun at a lower take-up speed and heating rate for DSC analysis, and also for fibers with a lower degree of crystallinity. Moreover, the dual melting peak can be observed for the fibers. The first melting peak represents less developed and less ordered crystals. More order with greater perfection crystals for the higher temperature peak is observed with extended chain segments.

On the other hand, it can be seen that the as-spun control and treated fibers have a broad melting range from initial melting to final melting, as shown in Figure 7.11, which indicates a typical semi-crystalline polymer.

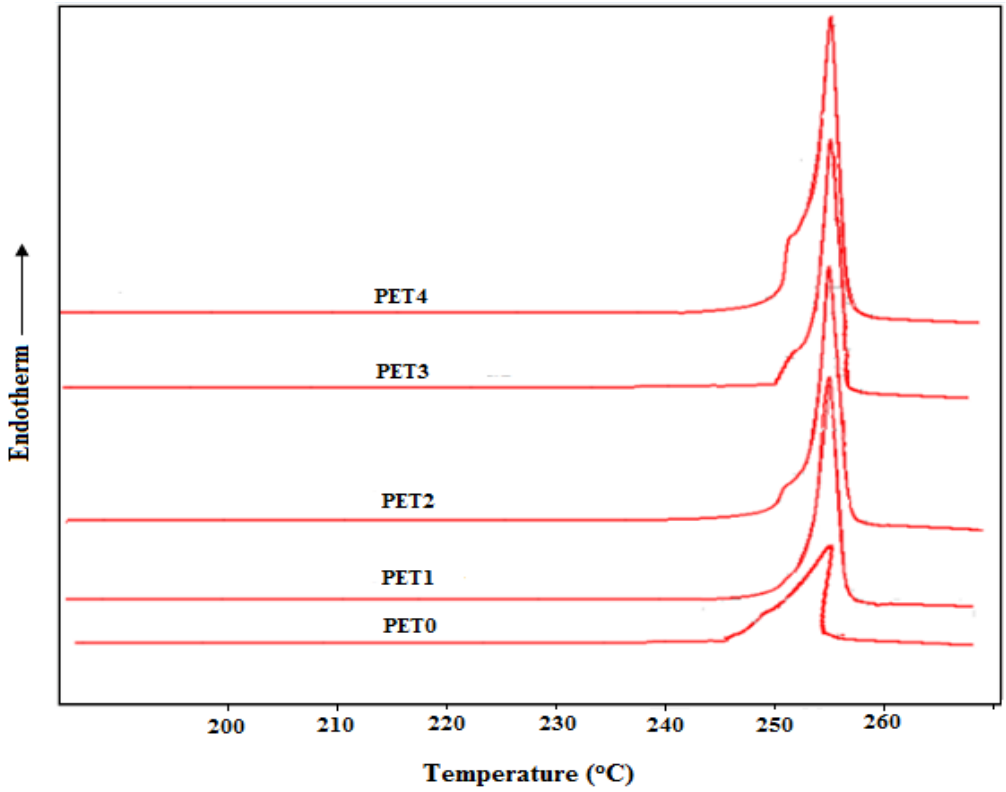

Figure 7. 11 DSC curves of PET as-spun fibers spun with and without hIB under different liquid temperatures.

Table 7.6 also shows the thermal properties of PET as-spun fibers with and without using the hIB spinning system. Note that no significant increase for melting points were observed when compared with treated and control fibers, which are between 253 and 255 ^{o}C. However, the percent crystallinity has increased from 28.54 to 36.69 % by ca. 29 % using hIB technology at the liquid temperature of 140 ^{o}C. It is beneficial in developing extended

macromolecular chains to gain improvement in fiber performance. In addition, the percent of crystallinity increased from 33.65 to 36.69 % by increasing the liquid temperature from 60 to 140 ^{o}C for the treated fibers.

Table 7. 6 Thermal properties of PET as-spun fibers spun with and without LIB*.

Sample ID	Onset Melting Point (^{o}C)	Peak Melting Point (^{o}C)	ΔH^{o}_{f} (J/g)	Crystallinity (%)
PET0	248.31	253.16	39.950	28.54
PET1	250.11	253.29	47.105	33.65
PET2	251.39	253.86	49.457	35.33
PET3	251.08	255.10	50.523	36.09
PET4	250.95	254.86	51.359	36.69

* The data was provided from the first heating curve.

The most prominent feature of the drawn treated fiber is the increased degree of crystallinity and melting points, as shown in Figure 7.12a. The narrow melting peaks with lower melting points represent a low degree of crystallinity and small crystallite size present in the filaments[28], which was also confirmed by our X-ray analysis. After the drawing process with

1.279 DR at 220 ^{o}C, the treated fibers demonstrated higher temperature peaks and crystallinity. These results clearly support the transformation from a highly oriented amorphous phase to the formation of highly developed crystallites that lead to a larger portion of extended chain segments. Figure 7.12b shows the fibers which were produced at the liquid temperature of 140 ^{o}C for as-spun and drawn samples. The highest fiber performance was observed at this temperature; therefore, the effect of production distance on fibers at the same temperature was investigated. As observed, PET fibers at the production distance of 90 cm showed the highest crystallinity and melting temperature.

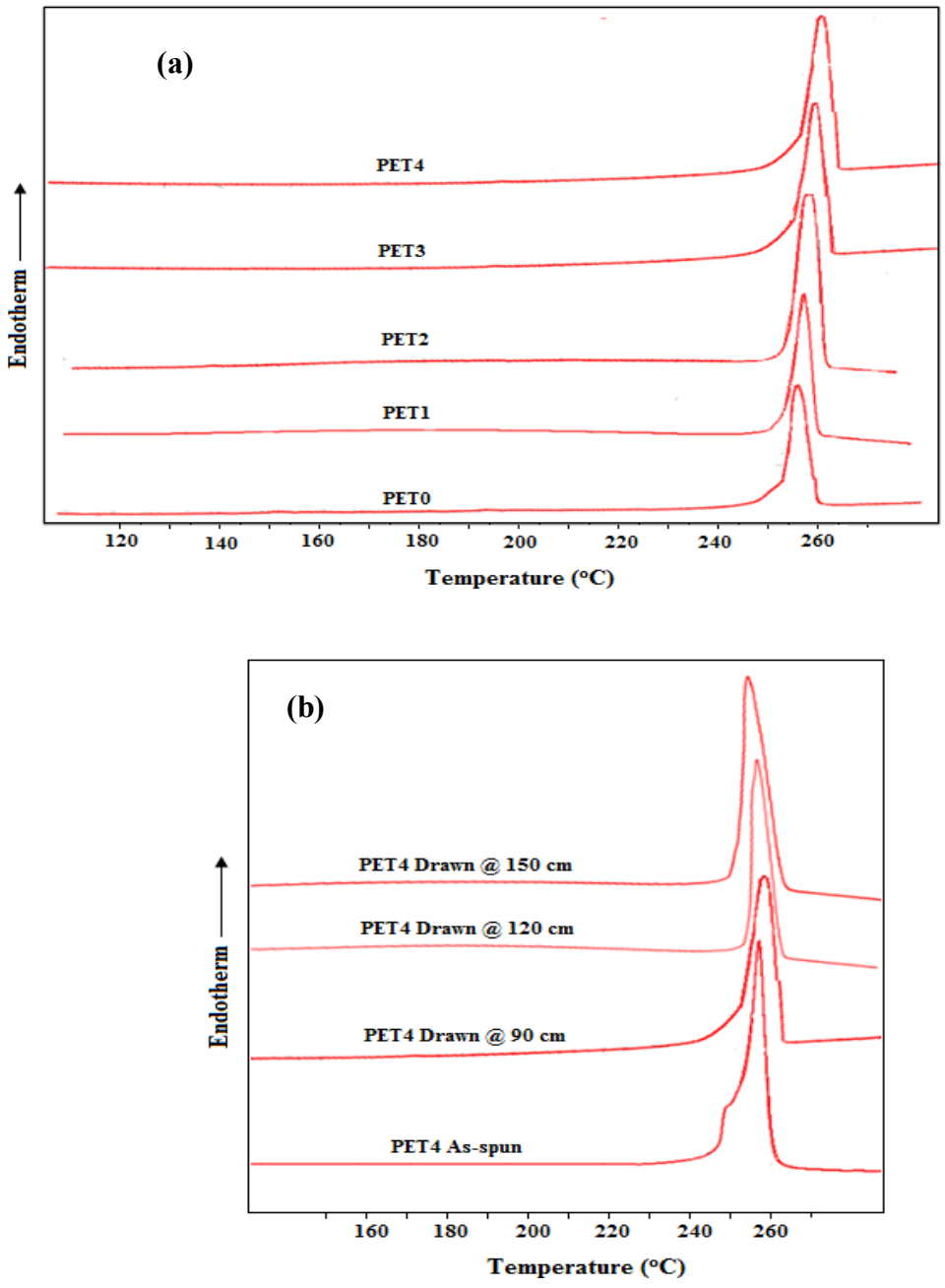

Figure 7. 12 DSC curves of drawn PET fibers spun (a) with and without hIB under different liquid temperatures, and (b) PET4 as-spun and drawn fibers spun with hIB at 140 ^{o}C at different production distance.

Table 7.7 demonstrates that the fibers can be classified into two groups according to their onset melting temperature. The first group includes the control; the fibers were produced at 60 and 100 ^{o}C liquid temperatures with about 250 ^{o}C onset temperature. The second group consists of 125 and 140 ^{o}C liquid temperatures for fibers with approximately the onset temperature of 256 ^{o}C. Interestingly, these two families of fibers were exactly observed for undrawn SEM and X-ray data analysis. Peak melting temperatures increased by increasing the liquid temperature at the same production distance of 90 cm, although control and PET1 (the liquid temperature of 60 ^{o}C) showed the similar temperature of about 254 ^{o}C. The highest peak melting temperature was observed for 262.56 ^{o}C at the liquid temperature of 140 ^{o}C after just drawing with 1.279 DR at 220 ^{o}C. It can be noted that the onset and melting temperature increased from 249.37 to 256.35 ^{o}C and from 254.05 to 262.56 ^{o}C by increasing of 6.98 and 8.51 ^{o}C, respectively, when control and the hIB treated fibers were compared. This illustrates that both the control and treated fibers have a different recrystallization rate during the DSC scan. The percent of crystallinity increased from 37.29 to 45.13 % by ca. 21 % by using hIB technology at 140 ^{o}C. In addition, the different liquid temperatures strongly influenced the percentage of crystallinity in which the percent of crystallinity increased from 39.95 to 45.13 % by increasing the liquid temperature from 60 to 140 ^{o}C.

Table 7. 7 Thermal properties of drawn PET fibers spun with and without hIB*.

Sample ID	Onset Melting Point (^{o}C)	Peak Melting Point (^{o}C)	ΔH^{o}_{f} (J/g)	Crystallinity (%)
PET0	249.37	254.05	52.210	37.29
PET1	249.74	253.75	55.930	39.95
PET2	252.46	257.88	61.172	43.69
PET3	256.76	261.38	59.727	42.66
PET4	256.35	262.56	63.178	45.13

* The data was provided from the first heating curve.

As stated previously, increasing the production distance between the spinneret and tank caused a decrease in the onset and peak melting points and the percent crystallinity at the same liquid temperature, as demonstrated in Table 7.8 for the treated fibers. There is a 4.35 and 5.04 ^{o}C difference between the onset and peak melting points when the production distance increased from 90 cm to 150 cm, respectively. In addition, the percentage of crystallinity decreased by ca. 8.4 % from 45.13 to 41.65 % by increasing the production distances.

Table 7. 8 Thermal properties of as-spun and drawn PET fibers spun with hIB at 140 ^{o}C*.

Sample ID	**Onset Melting Point (^{o}C)**	**Peak Melting Point (^{o}C)**	**ΔH^{o}_{f} (J/g)**	**Crystallinity (%)**
PET4	250.95	254.86	51.359	36.69
PET4 Drawn @ 90 cm	256.35	262.56	63.178	45.13
PET4 drawn @ 120 cm	253.53	259.37	60.627	43.31
PET4 drawn @ 150 cm	252.00	257.52	58.312	41.65

* The data was provided from the first heating curve.

7.4.5 Birefringence and Density Data Analysis

The degree of molecular orientation and the extent of crystallization are two important parameters for polymer morphology, which has a strong relationship with its fiber application areas. WAXS patterns of undrawn and drawn hIB treated and untreated samples, shown in Figure 7.8, 7.9, and 7.10, demonstrate significantly different crystalline structure and orientation, as shown by the intensity and sharpness of the equatorial reflections. The determination of birefringence and the indication of overall orientation is another pathway that can be employed to predict the orientation of these fibers. It is also known that the orientation has an impact on fiber modulus performance. In general, the overall orientation is affected by crystalline and the amorphous orientation factor, and the crystalline orientation factor is usually high for semi-crystalline polymeric fibers. In this case, the amorphous orientation factor is a key factor for overall orientation. In the industry, different levels of orientation can be obtained, which depends on the operating speeds[29]. If the speed is between 500 to 1500 m/min, it will yield low oriented, whereas partially oriented yarn can be produced at the speed range of 2500 and 4000 m/min. The roller and/or winder speed should be more than 6000 m/min to manufacture fully oriented materials. As mentioned before, the degree of alignment of chains along the fiber axis has a significant relation with the operation speed.

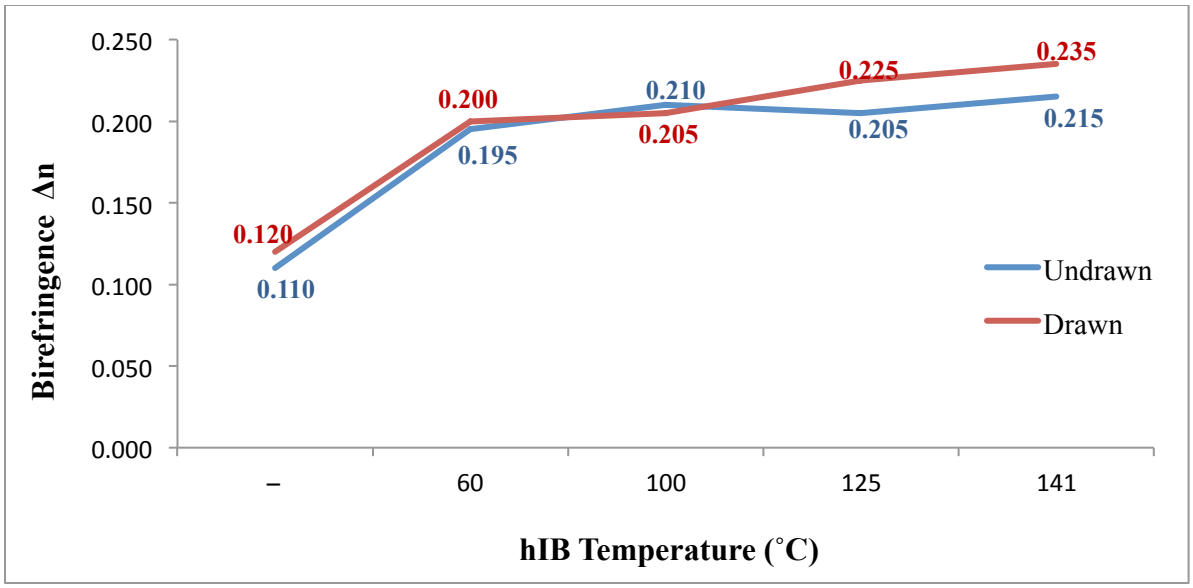

Figure 7. 13 The relation between birefringence of treated and untreated PET fibers at various hIB temperatures for undrawn and drawn fibers.

Figure 7.13 shows the birefringence of treated and untreated fibers at the production distance of 90 cm at about 3000 m/min take-up speed. At first glance, there is not any significant difference for the birefringence value between treated fibers at different liquid temperatures, although an increasing trend was observed with the increasing liquid temperatures. The birefringence increased from 0.195 to 0.215 and from 0.200 to 0.235 for treated as-spun and drawn fibers, respectively, by increasing the liquid temperature from 60 to 140 ^{o}C. The highest birefringence were observed for the fibers produced at the liquid temperature of 140

^{o}C for as-spun and drawn fibers (1.279 DR) at a value of 0.215 and 0.235, respectively. The lowest birefringence was always observed for the control samples for both undrawn and drawn filaments at the value of 0.110 and 0.120, respectively. Birefringence values for as-spun and drawn control fibers are in the range as expected for the traditional melt spinning production method. At the 90 cm of production distance, the birefringence for the treated fibers with 140 ^{o}C almost doubled that of the control samples for undrawn and drawn fibers. This indicates the molecular orientation level for the treated fiber is probably coming close to the highest level, as demonstrated by cross-section SEM images and X-ray data. Moreover, the effect of hot liquid with its drag force allowed us to obtain improved molecular chain orientation for lower molecular weight PET fibers during the treatment. Therefore, this highly oriented precursor hindered a poorly developed structure, which was rapidly formed during the traditional melt spinning process.

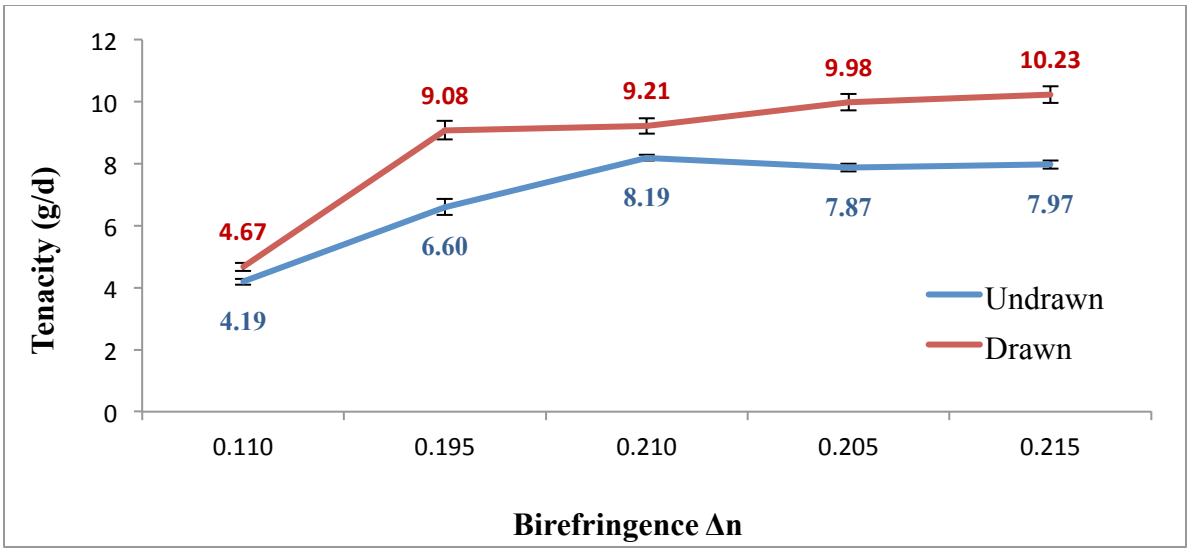

Figure 7. 14 The relation between birefringence and tenacity of treated and untreated PET fibers at various hIB temperatures for undrawn and drawn fibers (draw ratio = 1.279) (Exponential (undrawn) $R^2 = 0.9703$, and Polynomial (drawn) $R^2 = 0.9998$).

Amorphous region in the semi-crystalline polymers is divided into two main groups, namely anisotropic (oriented) and isotropic (unoriented) phases[30]. Hence, the orientation factor is strongly related with orientation degree of anisotropic phase and, in general, isotropic phase does not contribute to the overall birefringence and orientation factor. As seen in Figure 7.14, there is a strong correlation between the tenacity and birefringence values for undrawn and drawn fibers. The correlation for undrawn fibers of $R^2 = 0.9703$ is an exponential trendline as shown in the equation 5.

$$y = 2.067e^{6.3434x} \quad (5)$$

where: y is tenacity (g/d) and x is birefringence.

In addition, the correlation for drawn fibers of $R^2 = 0.9998$ is a well fit for polynomial trendline in the equation 6.

$$y = -180.51x^2 + 112.56x - 6.2384 \quad (6)$$

where: y is tenacity (g/d) and x is birefringence.

Figure 7.14 also demonstrates increased birefringence from 0.110 to 0.215 for undrawn fibers that correlates with improvement of tenacity from 4.19 to 7.97 g/d by ca. 96 and 90 %, respectively. Even if the highest mean tenacity for undrawn fibers was observed at the value of 8.19 g/d with the bath temperature of 100 ^{o}C, when the standard deviation is considered, tenacity for fibers that were produced at 100 and 140 ^{o}C are almost the same. Another interesting point from Figure 7.14 is that the undrawn fibers produced at 100 ^{o}C and higher bath temperature till 140 ^{o}C demonstrated almost the same performance in the terms of tenacity values and had the similar birefringence of around 0.2. Although the fibers were

produced at the bath temperature of 60 ^{o}C and showed the birefringence value of 0.195, these fibers demonstrated relatively lower tenacity than that of other treated as-spun fibers. It strongly indicates the birefringence value of 0.2 is an important threshold to obtain ultra-high performance PET fibers. It is also supported by the similar tenacity values for all drawn treated fibers which showed birefringence greater than 0.2 (as seen in Figure 7.14). The highest jump was observed for the tenacity values from undrawn to drawn fibers by ca. 38 %, which were produced at the bath temperature of 60 ^{o}C. This is due to the fact that the drawn fibers were obtained at this bath temperature, which shows the birefringence of 0.2.

It can be concluded that the bath temperature should be at least 100 ^{o}C to obtain birefringence values higher than 0.2 to obtain ultra-high tenacity for the as-spun fibers. Figure 7.14 indicates that after the drawing process with only 1.279 DR, the fiber tenacity increased from 4.67 to 10.23 by increasing birefringence from 0.120 to 0.235 by ca. 119 and 96 %, respectively. Increasing bath temperature from 60 to 140 ^{o}C caused tenacity values to improve from 9.08 to 10.23 g/d. In this case, birefringence varied from 0.200 to 0.235 by ca. 13 and 18 %, respectively.

Another curious phenomenon is that the overall orientation (birefringence) has a strong influence on the fiber tenacity. The orientation is sometimes more important than the crystals' growth and crystallinity for semi crystalline polymers until a certain value of crystallinity. For example, even if the treated fibers showed the close tenacity values to each other, which were manufactured at the liquid temperature of 100, 125 and 140 ^{o}C, the only

fibers, which have some crystalline morphology, were observed at the bath temperature of 125 and 140 ^{o}C when Figure 7.9 is checked.

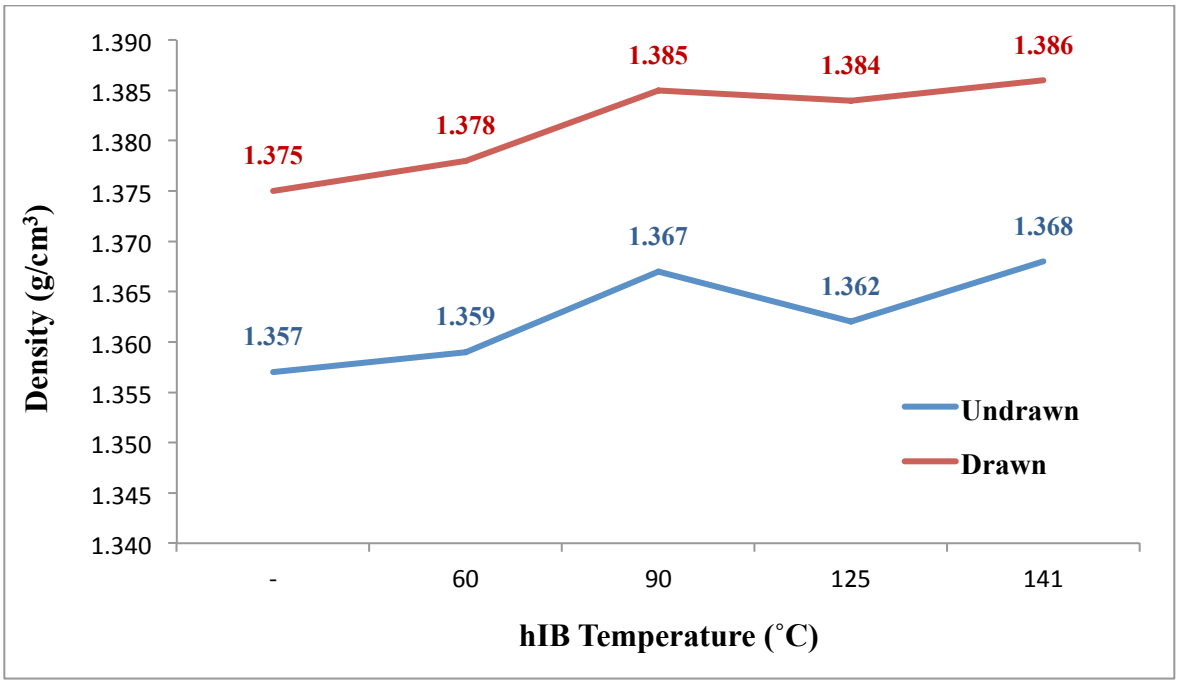

Figure 7. 15 Fibers density of untreated and treated fibers by hIB before and after drawing process (draw ratio = 1.279).

Figure 7.15 demonstrates the fibers density before and after the drawing process as a function of hIB liquid temperature at the same production distance of 90 cm and similar take-up speed of around 3000 m/min. Even if the trend for the density values was improved for as-spun fibers as the liquid temperature increased, it is hard to make a correlation between the density values and liquid temperature. On the other hand, an exponential trendline was well fitted between the fibers' density and hIB liquid temperature for drawn fibers of $R^2 = 0.9138$. The equation 7 for this correlation is shown below:

$$y = 1.3747e^{6E-05x} \quad (7)$$

where: y is fiber density (g/cm^3), and x is liquid temperature (^oC).

As seen in Figure 7.15, the as-spun fibers density increased from 1.357 to 1.368 g/cm^3 when the fibers were spun with hIB at 140 ^oC. As the liquid temperature increased from 60 to 140 ^oC, the density raised from 1.359 to 1.368 g/cm^3. It is quite clear that monotonical increase in density over the range investigated for drawn fibers is an exponential trendline. The density of 1.385 g/cm^3 for the hIB spun drawn fibers at the liquid temperature of 100, 125 and 140 ^oC was not changed significantly with the increasing liquid temperature. After drawing process, the lowest density was observed for the control sample at the value of 1.375 g/cm^3. However,

the highest density value of 1.386 g/cm^3 has been demonstrated as the liquid temperature increased further to 140 ^oC.

It is known that if a fiber has a lower crystallinity after production with a traditional high speed spinning method, usually this fiber can be more extended than that of a fiber with a higher crystallinity. As demonstrated in Table 7.9, the volume fraction crystallinity for untreated control sample (PET0) is lower than that of all treated fibers before and after drawing process. Thus, as expected, control fibers were able to be drawn to higher draw rations than that of all treated fibers.

Demonstrating a low extensibility, higher birefringence, higher tenacity and modulus show that all hIB fibers most probably have taut–tie noncrystalline chains and highly ordered amorphous phase structures. On the other hand, when the degree of crystallinity, which was obtained by X-ray (Table 7.4) and determined by density measurement (Table 7.9), were compared, the volume fraction crystallinity for as-spun PET1 (the liquid temperature of 60 ^oC) changed drastically and became higher than that of the values for PET0 (control) fibers. These differences at least suggest that there is less formation of a void structure and higher orientation of chains for treated fibers, which were formed during the hIB processes. A reason for the formation of void structure is generally associated with the use of much higher take-up speeds for the melt spinning methods. In Table 7.9, the volume fraction crystallinity increased from 18.33 to 27.50 % when the fibers were treated at the liquid temperature of 140 ^oC by ca. 50 % for as-spun fibers. For the drawn fibers, the crystallinity improved by ca.

28 % from 33.33 to 42.50 % at a draw ratio of 1.279 with the drawing temperature of 220 ^{o}C when the fibers spun with hIB at the temperature of 140 ^{o}C. The effect of the liquid temperature on the volume fraction crystallinity for treated fibers is also significant and increased from 20.00 to 27.50 % and from 35.83 to 42.50 by increasing the liquid temperature from 60 to 140 ^{o}C for as-spun and drawn fibers, respectively. Despite the fact that the crystallinity for drawn PET2, PET3, and PET4 are close to each other, it cannot be stated that these fibers should have also similar crystallinity before the drawing process (see Table 7.9).

Table 7. 9 Volume fraction crystallinity of untreated and treated fibers by hIB before and after drawing process (draw ratio = 1.279).

Sample ID	**Undrawn volume fraction crystallinity (%)**	**Drawn volume fraction crystallinity (%)**
PET0	18.33	33.33
PET1	20.00	35.83
PET2	26.67	41.67
PET3	22.50	40.83
PET4	27.50	42.50

7.5 Conclusions

Ultra-high performance as-spun and drawn PET fibers with unique properties were produced by using a horizontal isothermal bath (hIB). This study is the first known report of a production of high performance PET filament from a lower molecular weight polymer having intrinsic viscosity (IV) of 0.65 dL/g. The highest tenacity was observed more than 8 and 10 g/d for as-spun and drawn fibers, respectively.

At the liquid temperature of 60 and 100 ^{o}C and the production distance of 90 cm, the fibers demonstrated relatively higher tenacity and modulus values than that of the distance of 120 and 150 cm. However, when the liquid temperatures were fixed to 125 and 140 ^{o}C, the tenacity and modulus values came close to each other at three different production distances for undrawn fibers. The effects of production distances became a more prominent feature for the drawn fibers for their mean modulus performance at different liquid temperatures. Increasing production distance caused a decrease in the modulus of fibers for each liquid temperature. Therefore, almost all other characterization methods for the fibers which were presented in this study were obtained from the production distance of 90 cm.

SEM analysis indicates that there was not any banded structure either perpendicular or along the fiber axis on the hIB treated fiber surface for PET fibers. In addition, the significant effect of the temperature of the hIB spinning system on fibrillar structure was demonstrated. The fibrillar structure has not been observed for fibers spun with hIB at the temperature of 60 and 100 ºC, although the fibrillar structures was formed at the liquid temperature of 125 and 140

^{o}C for the as-spun fibers. The fibrillar morphology can be formed after a fully oriented structure was reached but, interestingly, we probably obtained this unique structure for undrawn fibers at the liquid temperature of 125 and 140 ^{o}C with the liquid depth and production distance of 20 and 90 cm, respectively. Strong similarities were found when SEM images of cross-section and X-ray diffraction for the as-spun treated fibers were compared. If the equatorial X-ray diffraction profile showed clear crystalline peaks that caused us to observe the fibrillar structure in the cross-section for the same fiber.

Other characterization methods in this work, such as DSC, X-ray, birefringence, etc., demonstrated that the resulted as-spun fibers developed a rare formation of precursors for crystallization with a highly oriented structure which transformed into a highly crystallized fibrillar structure after only drawing at 1.279 draw ratios at the drawing temperature of 220 ^{o}C.

Depending on the process conditions for the PET fibers, the precursor for the crystallization can be formed during the drawing process at the drawing temperature higher or closer to its glass transition temperature at a very high draw ratio and strain rate. However, the precursor can be developed, as we observed during the hIB melt spinning process where certain conditions are satisfied. As clearly demonstrated by cross-section of SEM images and X-ray data for the undrawn treated fibers, the type of precursor can be different according to the liquid temperatures. The effects of a higher level threadline tension and the lower liquid temperatures, while cooling at a very slow rate, restricted for the fibers the formation and

growth of crystallites; however, this probably increased the residual frozen-in orientation and the higher rate of motion of neighboring chain segments, which promoted the occurrence of tree-dimensional structure when fibers were treated at higher liquid temperatures. This phenomenon may also lead to a higher molecular orientation. Furthermore, at a higher liquid temperature, the threadline temperature is much higher than the glass transition temperature of the polymer. Hence, there is a greater probability to form tree-dimensional arrangements and obtain more developed crystals for the as-spun fibers (Figure 7.9).

Finally, this study contributes a further understanding of the structure development of lower molecular weight PET fibers spun via hIB with highly improved mechanical and thermal properties.

7.6 References

1. Lina, W., Yanwei, Wang, Z. D., Xuelian, X., Wentao, L., Suqin, H., & Chengshen, Z. (2011). Discussion on production of flat cross-section industry polyester filament. *Advanced Materials Research.* 332-334, 526-529.

2. Wu, G., Zhou, Q., Chen, J. Y., Hotter, J. F., Tucker, P. A., & Cuculo J. A. (1995). The effect of a liquid isothermal bath in the threadline on the structure and properties of poly(ethylene terephthalate) fibers. *Journal of Applied Polymer Science,* 55, 1275-1289.

3. Hobbs, T., & Lesser, A. J. (2000). Preparation of high performance poly(ethylene terephthalate) fibers: two-stage drawing using high pressure CO2. *Polymer*, 41, 6223–6230.

4. Wu, G., Jiang, J. D., Tucker, P. A., & Cuculo J. A. (1996). Oriented noncrystalline structure in PET fibers prepared with threadline modification process. *Journal of Polymer Science: Part B: Polymer Physics*, 34(12), 2035-2047.

5. Ito, M., Takahashi, K., & Kanamoto, T (1990). Preparation of high-modulus and high- strength fibers from high molecular weight poly (ethylene terephthalate). *Journal of Applied Polymer Science,* 40, 1257-1263.

6. Wu, G, & Cuculo, J. A. (1995). Preparation of high performance pet fiber by solution spinning technique. *Journal of Applied Polymer Science,* 56, 869-875.

7. Chen, P., Afshari, M., Cuculo, J. A., & Kotek R. (2009). Direct formation and characterization of a unique precursor morphology in the melt-spinning of polyesters. *Macromolecules,* 42, 5437–5441.

8. Nicholson, T. M., Davies, G. R., & Ward, I. M. (1994). Conformations in poly(ethylene terephthalate): a molecular modelling study. *Polymer,* 35, 4259-4262.

9. Carr, P. L., Nicholson, T. M., & Ward, I. M. (1997). Mesophase structures in poly(ethylene terephthalate), poly(ethylene naphthalate) and poly(ethylene naphthalate bibenzoate). *Polymers for Advanced Technologies,* 8, 592-600.

10. Welsh, G. E., Blundell, D. J., & Windle, A. H. (2000). A transient mesophase on drawing polymers based on polyethylene terephthalate (PET) and polyethylene naphthoate (PEN). *Journal of Materials Science*, 35, 5225-5240.

11. Lu, X. F., & Hay, J. N. (2001). Crystallization orientation and relaxation in uniaxially drawn poly(ethylene terephthalate). *Polymer*, 42(19), 8055–8067.

12. Alfonso, G. C., Verdona, M. R., & Wasiak, A. (1978). Crystallization kinetics of oriented poly (ethylene terephthalate) from the glassy state. *Polymer*, 19, 711-716.

13. Smith, F., & Steward, R. (1974). The crystallization of oriented poly(ethylene terephthalate). *Polymer*, 15, 283-286.

14. Lu, X. F, & Hay, J. N. (2001). Crystallization orientation and relaxation in uniaxially drawn poly(ethylene terephthalate). *Polymer*, 42(19), 8055–8067.

15. Hotter, J. F., Cuculo, J. A., Tucker, P. A., & Annis, B. K. (1998). Effect of liquid isothermal bath position in modified poly (ethylene terephthalate) PET melt spinning process on properties and structure of as-spun and annealed filaments. *Journal of Applied Polymer Science,* 69, 2051–2068.

16. Wang, I. C., Dobb, M. G., & Tomka, J. G. (1996). Polypropylene fibres: exploration of conditions resulting in high tenacity. *Journal of the Textile Institute,* 87, 1-12.

17. Wang, I. C., Dobb, M. G., & Tomka, J. G. (1995). Polypropylene fibres: an industrially feasible pathway to high tenacity. *Journal of the Textile Institute,* 86, 383-392.

18. Duhovic, M., Bhattacharyya, D., & Fakirov, S. (2010). Nanofibrillar single polymer composites of poly(ethylene terephthalate). *Macromolecular Materials and Engineering,* 295, 95–99.

19. Chen, J. Y., Tucker, P. A., & Cuculo, J. A. (1997). High-performance PET fibers via liquid isothermal bath high-speed spinning: fiber properties and structure resulting from threadline modification and posttreatment. *Journal of Applied Polymer Science*, 66, 2441–2455.

20. Abou-Kandil, A. I., & Windle, A. H. (2007). The morphology of 50% PET/PEN random copolymer as revealed by high resolution scanning electron microscopy and X-ray diffraction. *Polymer,* 48, 4824-4836.

21. Takeuchi, Y., Shuto, Y., & Yamamoto, F. Band pattern development in shear-oriented thermotropic copolyester extrudates. *Polymer*, 29, 605-612.

22. Abou-Kandil, A., & Windle, A. H. (2007). The morphology of 50% PET/PEN random copolymer as revealed by high resolution scanning electron microscopy and X-ray diffraction. *Polymer*, 48, 4824-4836.

23. Mukhopadhyay, S., Deopura, B. L., & Alagirusamy, R. (2004). Production and properties of high-modulus–high-tenacity polypropylene filaments. *Journal of Industrial Textiles*, 33(4), 245-268.

24. Murthy, N. S., & Grubb, D. T. (2003). Deformation in lamellar and crystalline structures: in situ simultaneous small-angle X-ray scattering and wide-angle X-ray

diffraction measurements on polyethylene terephthalate fibers. *Journal of Polymer Science: Part B: Polymer Physics*, 41, 1538–1553.

25. Avci H. (2010). Novel Approaches to the Development and Characterization of Antimicrobial Conventional and Nanostructured Materials. MS thesis. *North Carolina State University*.

26. Murthy, N. S., Correale, S. T., & Minor H. (1991). Structure of the amorphous phase in crystallizable polymers: poly(ethylene terephthalate). *Macromolecules*, 24, 1185-1189.

27. Holdsworth, P. J., & Turner-Jones, A. (1971). The melting behaviour of heat crystallized poly(ethylene terephthalate). *Polymer*, 12, 195-208.

28. Lin, C. Y., Tucker, P. A., & Cuculo, John, A. (1992). Poly(ethylene terephthalate) melt spinning via controlled threadline dynamics. *Journal of Applied Polymer Science*, 46, 531-552.

29. Karacan, I. (2005). An in depth study of crystallinity, crystallite size and orientation measurements of a selection of poly(ethylene terephthalate) fibers. *Fibers and Polymers*, 6,(3), 186-199.

30. Harget, P. J., & Oswald H. J. (1979). Birefringence in amorphous polyethylene terephthalate fibers. *Journal of Polymer Science: Polymer Physics Edition,* 17(3), 531–534.

31. Cuculo J. A. et al. (1992). US patent: US005149480A. Melt spinning of ultra-oriented crystalline polyester filaments.

32. Cuculo J. A. et al. (1998). US patent: US005733653A. Ultra-oriented crystalline filaments and method of making same.

33. Ohta, T. (1983). Review on processing ultra high tenacity fibers from flexible polymer. *Polymer Engineering and Science*, 23(13), 697-703.